CHARLES UNIVERSITY IN PRAGUE

Faculty of Science

Study program:

Molecular and Cellular Biology, Genetics and Virology

Mgr. Andrea Beňová

Vliv obesity a metabolických onemocnění na molekulární vlastnosti kmenových buněk kostní dřeně ve vztahu k metabolismu kosti a tukové tkáně

Effect of obesity and metabolic complications on molecular characteristics of bone marrow skeletal stem cells in relation to bone and adipose tissue metabolism

Doctoral Thesis

Supervisor: Mgr. Michaela Tencerová, PhD.

Laboratory of Molecular Physiology of Bone, Institute of Physiology, Czech Academy of Science

Prague, 2024

Declaration

Prohlašuji, že předložená disertační práce je mou původní prací, vypracovanou pod vedením Mgr. Michaely Tencerové, PhD. a všechny zdroje literatury byly náležitě citovány. Tato práce nebyla dříve předložena, ať už celá nebo částečně, za účelem získání jiné akademické kvalifikace.

I declare that the submitted doctoral thesis is my original work, conducted under the supervision of Mgr. Michaela Tencerová, PhD., and all sources of literature have been appropriately cited. This thesis has not been previously submitted, in whole or in part, to obtain any other academic qualification.

In Prague, March 2024 …….

Acknowledgement

First of all, I would like to express my biggest gratitude to my supervisor Mgr. Michaela Tencerova, PhD., for her never-ending help, positive energy, kindness and for so many opportunities she gave me during my PhD. I would like to also thank to my dearest colleagues from Laboratory of Molecular Physiology of Bone, to both Miskas for so many eppendorf tubes prepared every time I needed and for their good mood and smile every day. Very special thanks belong to my dearest Miska F and Mata for always being there for me during the best but also hardest times. I will miss you so much.

I would also like to thank to my parents to be the best role models I could ever imagine. Special thanks belong to my power women trio- my mum, sister and grandma, for their prayers and never ending support. I really appreciate that you have always been with me even on long distance.

Very special thanks belong to my beloved Filip. Thank you for being proud of me, encouraging me, for taking care of me and helping me every day I needed.

Abstract

Obesity and diabetes are metabolic complications associated with higher accumulation of fat in periphery and bones leading to higher fracture risk. Several approaches have been introduced in the treatment of obesity and diabetes - non-pharmacological (e.g. dietary intervention or physical activity) and pharmacological (e.g. metformin, thiazolidinediones (TZDs)) to improve metabolic complications.

Dietary intervention including omega-3 polyunsaturated fatty acid (PUFA) supplementation showed multiple beneficial effects on bone parameters and bone marrow skeletal stem cells (BMSC) properties in animal and clinical studies. However, this was not well studied in obesogenic conditions. Further, TZDs (e.g. pioglitazone, rosiglitazone) are very effective insulin sensitizers but with several side effects (increased bone marrow adiposity (BMA) with higher fracture risk) due to their mechanism of action. MSDC-0602K, a novel TZD analog, has been developed to minimize side effects on fat metabolism. However, its impact on bone phenotype and bone marrow skeletal stem cells BMSCs in relation to obesity has not been intensively studied.

Thus, in my PhD thesis I investigated both approaches using high-fat diet (HFD)-induced obesity mouse model. 8 weeks old male mice were fed with HFD or HFD supplemented with omega-3 PUFA, MSDC-0602K or pioglitazone for 2 months to investigate their effects on metabolic, bone parameters and stem cell properties using several methods including μCT, histology, analysis of osteoclast differentiation from bone marrow (BM) cells isolated from treated mice (in study using omega-3 PUFA treatment), cultivation of primary BMSCs and their cellular and metabolic characterization.

In dietary interventional study, omega-3 PUFA treatment showed robust changes in bone microstructure and mechanical properties characterized by low cortical porosity and BMA in tibia, and increased bone strength of femur compared to HFD. These changes were also manifested on cellular level, by decreased osteoclastogenesis of BM cells, increased osteoblast differentiation of BMSCs coupled with decreased cellular respiration and lower senescent phenotype with omega-3 PUFAs. Further, pharmacological approach comparing classical TZD pioglitazone with MSDC-0602K showed less detrimental effect of new analog on bone microstructure compared to pioglitazone group, which was accompanied with higher distribution of smaller BM adipocytes. Cellular analysis revealed increased osteoblast differentiation of primary BMSCs in MSDC-0602K treated mice. However, cellular respiration

as well as glycolysis were increased in MSDC-0602K BMSCs compared to pioglitazone group suggesting different utilization of nutrients by these drugs. These unexpected results led us to compare effect of these drugs on bone and peripheral AT metabolism using BMSC cell line and adipose derived stem cell line (AT-MSCs) 3T3-L1, where we observed decreased respiration with MSDC-0602K compared to pioglitazone, suggesting also different mechanism of action in bone and in periphery. To further understand the TZD actions on cellular metabolism in periphery and bones, we measured nutrient utilization in BMSC cell line and AT-MSCs. We observed increased utilization of glutamine by MSDC-0602K in BMSCs compared to pioglitazone, while in AT-MSCs MSDC-0602K preferred glucose over glutamine. Thus, we performed fluxomic analysis of ^{13}C labelled glucose and glutamine in BMSC treated with MSDC-0602K and pioglitazone and we observed increased glutamine and decreased glucose utilisation with MSDC-0602K compared to pioglitazone. These results are supporting our hypothesis that increased glutamine metabolism in BMSCs by MSDC-0602K treatment can contribute to lower senescence, increased osteoblastogenesis of BMSCs and improved mechanical properties of bones.

Taken together, our findings using non-pharmacological treatment in obesity showed pronounced beneficial effects of omega-3 PUFA supplementation of HFD-treated mice on bone microstructure, bone mechanical properties and cellular homeostasis. Further, pharmacological approach showed decreased side effect of treatment on bone and BMSC properties with MSDC-0602K compared to pioglitazone by activation of glutamine metabolism. Thus, this thesis brings two potential strategies of preventing negative effect of metabolic diseases but also opens a new perspective for further research of synergistic effect of these molecules in clinical practice.

Keywords: Obesity-induced bone fragility; Omega-3 polyunsaturated fatty acids, Thiazolidinedione analog MSDC-0602K; Bone marrow stromal cells; Cellular metabolism; Bone marrow adipose tissue; Bone microstructure

Abstrakt

Obezita a diabetes jsou metabolické komplikace spojené s vyšší akumulací tuku v periferii a kostech, mající za následek zvýšené riziko fraktury. Při léčbě obezity a diabetu bylo zavedeno několik přístupů - nefarmakologických (např. dietní intervence nebo fyzická aktivita) a farmakologických (např. metformin, tiazolidindiony (TZD)) ke snížení metabolických komplikací.

Dietní intervence včetně suplementace omega-3 polynenasycenými mastnými kyselinami (PUFA) ve studiích na zvířatech a v klinických studiích prokázala mnohonásobné příznivé účinky na kostní parametry a vlastnosti kmenových buněk kostní dřeně (BMSC). To však nebylo dobře prozkoumáno v obezogenních podmínkách. Dále jsou TZD (např. pioglitazon, rosiglitazon) velmi účinnými sensibilizátory inzulinu, ale s několika vedlejšími účinky (zvýšená adipozita kostní dřeně (BMA) s vyšším rizikem fraktur) v důsledku jejich mechanismu účinku. MSDC-0602K, nový analog TZD, byl vyvinut pro minimalizaci vedlejších účinků na metabolismus tuků. Jeho vliv na kostní fenotyp a fenotyp BMSC ve vztahu k obezitě však nebyl intenzivně studován.

V disertační práci jsem zkoumala oba přístupy pomocí myšího modelu dietou indukované obezity (HFD). Samci myší ve věku 8 týdnů byli krmeni HFD nebo HFD doplněným omega-3 PUFA, MSDC-0602K nebo pioglitazonem po dobu 2 měsíců, za účelem prozkoumání účinků na metabolické a kostní parametry a vlastnosti kmenových buněk pomocí několika metod včetně μCT (micro computer tomography) histologie, analýzy osteoklastů diferencovaných z buněk kostní dřeně (BM) izolovaných z léčených myší (ve studii s použitím omega-3 PUFA), kultivace primárních BMSC a jejich buněčná a metabolická charakterizace.

V dietní intervenční studii ukázalo použití omega-3 PUFA významné změny v mikrostruktuře kosti a mechanických vlastnostech charakterizovaných nízkou kortikální porozitou a BMA v tibii a zvýšenou pevností femuru ve srovnání s HFD. Tyto změny se projevily i na buněčné úrovni, sníženou osteoklastogenezí BM buněk, zvýšenou diferenciací BMSC na osteoblasty spolu se sníženou buněčnou respirací a nižším senescentním fenotypem s omega-3 PUFA. Dále ukázal farmakologický přístup porovnávající klasický TZD pioglitazon s MSDC-0602K méně škodlivý účinek nového analogu na mikrostrukturu kosti ve srovnání s pioglitazonem, což bylo doprovázeno vyšší distribucí menších adipocytů BM. Buněčná analýza odhalila zvýšenou osteoblastovou diferenciaci primárních BMSC u myší léčených MSDC-0602K. Nicméně, buněčná respirace a glykolýza byly u MSDC-0602K BMSC ve

srovnání s pioglitazonem zvýšené. Což naznačuje odlišné využití živin těmito léky. Překvapivé výsledky nás vedly k porovnání účinku těchto léků na kostní a periferní metabolismus AT pomocí buněčné linie BMSC a linie kmenových buněk odvozených z tukové tkáně (AT-MSC) 3T3-L1, kde bylo pozorována snížená respirace s MSDC-0602K ve srovnání s pioglitazonem, což také naznačuje odlišný mechanismus účinku v kosti a v periferii. Pro lepší porozumění účinků TZD na buněčný metabolismus v periferii a v kostech, bylo měřeno využití živin v buněčné linii BMSC a AT-MSC. Bylo pozorováno zvýšené využití glutaminu pomocí MSDC-0602K v BMSC ve srovnání s pioglitazonem, zatímco v AT-MSC MSDC-0602K byla preferována glukóza před glutaminem. Byla provedena fluxomická analýza ^{13}C označené glukózy a glutaminu v BMSC ošetřeném MSDC-0602K a pioglitazonem a byla pozorována zvýšena utilizace glutaminu a snížená utilizace glukózy u MSDC-0602K ve srovnání s pioglitazonem. Výsledky podporují naši hypotézu, že zvýšený metabolismus glutaminu v BMSC ošetřením MSDC-0602K může přispět ke snížení stárnutí, zvýšené osteoblastogenezi BMSC a zlepšení mechanických vlastností kostí.

Celkově vzato, naše zjištění využívající nefarmakologickou léčbu obezity prokázala výrazné příznivé účinky suplementace omega-3 PUFA u myší léčených HFD na kostní mikrostrukturu, mechanické vlastnosti kostí a buněčnou homeostázi. Dále farmakologický přístup ukázal snížený vedlejší účinek léčby MSDC-0603K na vlastnosti kostí a BMSC ve srovnání s pioglitazonem pomocí aktivace metabolismu glutaminu. Práce přináší dvě potenciální strategie prevence negativního vlivu metabolických onemocnění a zároveň otevírá novou perspektivu pro další výzkum synergického efektu těchto molekul v klinické praxi.

Klíčová slova: Obezitou indukovaná křehkost kostí; Omega-3 polynenasycené mastné kyseliny, Analog thiazolidindionu MSDC-0602K; Kmenové buňky kostní dřeně; Buněčný metabolismus; Tuková tkáň kostní dřeně; Mikrostruktura kosti

Abbreviations

α- KG- α- ketoglutaric acid

Acc- Acetyl-CoA carboxylase

AcCoA- Acetyl-Coenzyme A

ACLY- ATP-citrate synthase

ADIPOQ- Adiponectin

AGE- Advanced Glycation End Products

Akt- Protein kinase B

ALP- Alkaline phosphatase

AMPK- AMP-activated protein kinase

AT- adipose tissue

ATGL- Adipose tissue triglyceride lipase

AT-MSC- Adipose derived stem cell

BAT- Brown adipose tissue

BM- Bone marrow

BMA- Bone marrow adiposity

BMAd- Bone marrow adipocyte

cBMAd- Constitutive bone marrow adipocytes

rBMAd- Regulated bone marrow adipocytes

BMAT- Bone marrow adipose tissue

BMD- Bone mineral density

BMI- Body mass index

BMP- Bone morphogenetic protein

BMSC- Bone marrow skeletal cell

C/EBPA- CCAAT-enhancer binding protein family

Cit- Citrate

Col1a1- Collagen 1 type a 1

CR- Caloric restriction

CS- Citrate synthase

CXCL12- (C-X-C motif) ligand 12

DAG- Diacylglycerol

Dgat- Diacylglycerol acyltransferase

DHA- Docosahexaenoic acid

DKK1- Dickkopf-1

DPP4- Dipeptidyl peptidase-4

DXA- dual-energy X-ray absorptiometry

Elovl6- Elongase of long chain FA family 6

EPA- Eicosapentaenoic acid

ER- Endoplasmic reticulum

ESC- Embryonic stem cell

FA- Fatty acid

Fas- Fatty acid synthase

FFA- Free fatty acid

FASN- Fatty acid synthase

FDA- Food and Drug Administration

FGF- Fibroblast growth factor

G3P- Glycerol-3-phosphate

GH- Growth hormone

Gln- Glutamine

Glu- Glucose

GLP-1- Glucagon-like peptide-1

GLS- Glutaminase

HFD- High fat diet

HIF-1α- Hypoxia-inducible factor 1α

hMSC- Human mesenchymal stem cell

HSC- Hematopoietic stem cells

HSL- Hormone-sensitive lipase

IGF-1- Insulin like growth factor 1

IL-6- Interleukin-6

iPSC- Induced pluripotent stem cell

IR- Insulin receptor

LCN2- Lipocalin 2

Lpl- Lipoprotein lipase

MAG- Monoacylglycerol

MD- Mediterranean diet

MGL- Monoacylglycerol lipase

mitoNEET- Mitochondrial membrane-associated protein (mito) containing the amino acid sequence Asn-Glu-Glu-Thr (NEET)

MMP9- Metalloproteinase 9

MPC- Mitochondrial pyruvate carrier

MSC- Multipotent stem cell

mTOR- Mammalian target of rapamycin

NKT- Natural killer T cells

Oac- oxaloacetate

OCN- Osteocalcin

OGDH- alpha-ketoglutarate dehydrogenase

OPG- Osteoprotegerin

OPN- Osteopontin

OXPHOS- Oxidative phospohorylation

PEPCK- Phosphoenolpyruvate carboxykinase

PET/CT- Positron emission tomography and computerized tomography

PPARγ - Peroxisome proliferator-activated receptor γ

PSC- Pluripotent stem cell

PTH- Parathyroid hormone

PUFA- Polyunsaturated fatty acids

Pyr- Pyruvate

RANK- Receptor Activator of Nuclear κB

RANKL- Receptor Activator of Nuclear κB Ligand

ROS- Reactive oxygen species

RUNX2- Runt-related transcription factor 2

SAT- Subcutaneous adipose tissue

Scd- Stearoyl-CoA desaturase

SCF- Stem cell factor

SGLT2- Sodium-glucose cotransporter-2

SOST- Sclerostin

Suc- Succinate

SVF- Stromal vascular fraction

T3- Triiodothyronine

T4- Thyroxine

T2D- Type 2 diabetes

TAG- Trigliceride

TCA- Tricarboxylic acid

TGF-ß- Transforming growth factor-beta

TNF-α- Tumor necrosis factor-α

TSH- Thyroid-stimulating hormone

TZD- Thiazolidinedion

UCP1- Uncoupling protein 1

WAT- White adipose tissue

WHO- World Health Organization

Wnt- Wingless-type mouse mammary virus integration site

Content

1. Introduction

1.1. Bone physiology

1.1.1. Bone microstructure

Bone tissue, an essential component of the skeleton, provides a mechanical support for the body and protects vital organs. It is characterized by its unique combination of mechanical strength, durability, and its remarkable ability to regenerate and adapt [1, 2].

The human skeleton primarily consists of two types of osseous structures: cortical and trabecular bone. Cortical bone, characterized by its high density and reduced surface area, envelopes the bone marrow (BM) cavity. This type of bone is organized into Haversian systems, which are constituted by concentric lamellae of osseous tissue encircling a central canal, housing blood vessels [3]. Conversely, trabecular bone, also referred to as cancellous or spongy bone, has a lower density and an expanded surface area compared to the cortical bone. It predominantly occupies the central regions of long bones, flat bones, and vertebrae. This bone type is formed by an interconnected network of bone trabeculae, separated by cavities filled within the BM [4]. Major structural parts of cortical and trabecular bone are depicted in Figure 1.

Cortical bone accounts approximately 80% of the skeletal mass and the distribution of cortical and trabecular bone varies across different skeletal regions [5]. For instance, regions such as the distal part of long bones, vertebral bodies, and the calcaneus are predominantly trabecular, while the shafts of long bones and the femoral neck consist mainly of cortical bone. This distribution has a high clinical relevance because trabecular bone, with its extensive surface area, undergoes more rapid remodeling than cortical bone. Consequently, in conditions of increased bone turnover, bone loss is more pronounced in areas abundant in trabecular bone [4].

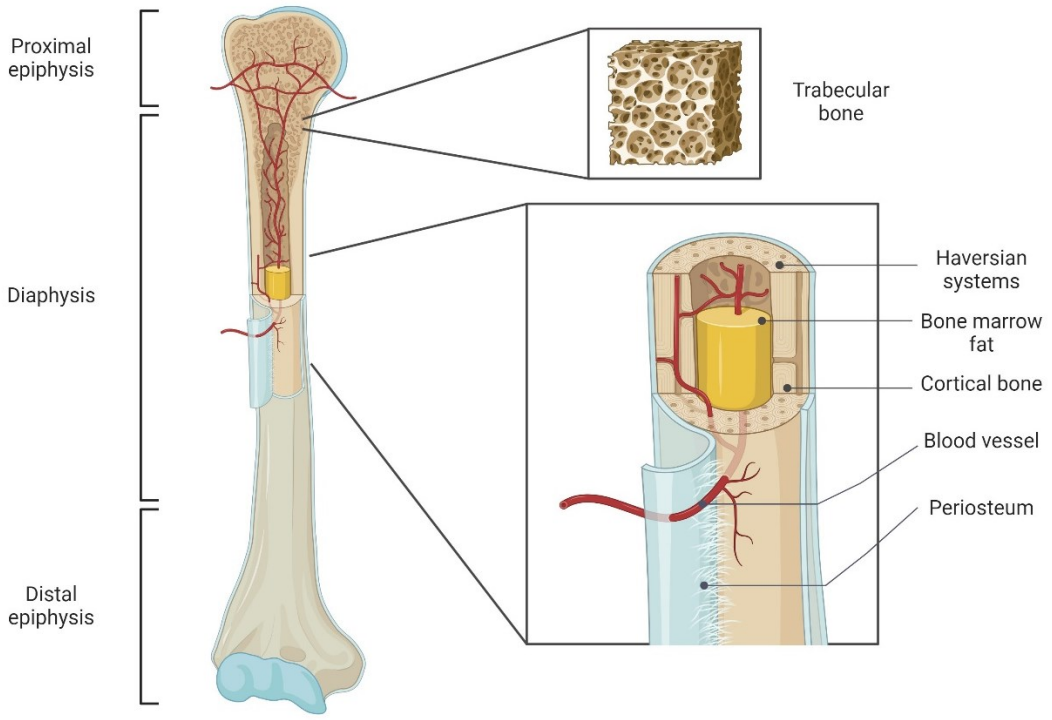

Figure 1. Cross-section structure of femur. The figure depicts a cross-section of the human femur, showing the proximal epiphysis at the hip joint, the diaphysis as the central shaft, and the distal epiphysis at the knee joint. Enhanced views detail the trabecular bone with its honeycombed structure in the epiphysis, the dense cortical bone along the diaphysis, and the Haversian systems within the cortical bone. Bone marrow fat central to hematopoiesis is also illustrated, alongside the blood vessels that supply the bone and the surrounding periosteum, a connective tissue layer that facilitates growth and repair. The image clearly distinguishes the robust cortical bone of the shaft from the supportive trabecular bone at the ends. (Figure created in Biorender.com)

Bone is a diverse organ with a mineralized matrix housing BM, which is vital for recruiting bone cells and its immune properties [6]. BM is composed of various cell populations, including hematopoietic stem cells (HSCs) that develop into blood and immune cells, and bone marrow stromal cells (BMSCs), which differentiate into bone-forming cells (osteoblasts), bone marrow adipocytes (BMAds) and chondrocytes [7] through activation of different transcriptional programs and secreted factors [7].

Bone processes are intricately linked to the composition of the bone matrix, where type I collagen plays a pivotal role. As the primary organic both cortical and trabecular bone matrices, type I collagen consists of two alpha1 (I) and one alpha2 (I) peptide chains, forming a triple helix [8]. After being synthesized as a pro-peptide, collagen undergoes critical post-

secretion modifications, including the cleaving of its terminal fragments by proteolytic enzymes. The remaining triple helix domains align in a staggered formation to form collagen fibrils. These fibrils are further stabilized by pyridinium cross-links, which are essential for bone's tensile strength. Bone degradation releases these cross-links into the extracellular fluid, making them measurable as markers of bone resorption [9].

The bone matrix also contains smaller amounts of other collagens, non-collagenous proteins, and growth factors. While some proteins like osteocalcin are specific to bone, others such as fibronectin and various growth factors are also found in other connective tissues [10]. Non-collagenous proteins, including fibronectin, are crucial for attaching bone cells to the matrix, and growth factors like transforming growth factor-beta (TGF-ß) embedded in the bone matrix play a vital role in regulating bone cell activities and promoting bone formation [11].

The organic framework of bone is essential for mineralization, which gives mechanical rigidity to the bone, complementing the tensile strength and elasticity from collagen. Bone minerals, primarily calcium and phosphate, form hydroxyapatite crystals. Defects in bone mineralization, as seen in conditions like rickets, osteomalacia, and hypophosphatasia, can lead to a significant impairment of skeletal tissue [4].

1.1.2. Bone remodeling cycles

Bones constantly undergo remodeling, a process when old bone is removed and replaced by the new one. Bone remodeling depends on the proper functions of two primary cell types in bone: osteoclasts (originating from myeloid stem cell lineage) and osteoblasts [12, 13]. Osteoclasts are multinucleated cells derived from monocytes, responsible for bone resorption, i.e. breaking down old bone matrix, while osteoblasts, which possess osteogenic capabilities, are involved in forming new bone tissue, a bone formation [14]. Additionally, osteocytes, which develop from osteoblasts, play a significant role in the remodeling process through their mechano-sensory functions [15]. Maintaining a constant bone mass requires a balance between bone resorption and bone formation [16, 17]. These processes are in balance under normal physiological condition, while aging, osteoporosis, diabetes impair bone homeostasis in the favor of bone loss [18, 19].

Bone remodeling cycle is divided into several phases: i) activation phase, ii) remodeling phase, iii) reversal phase, and iv) formation phase. The whole process is summarized in Figure

2. Activation of bone resorption cycle is usually initiated by various stimuli such as micro-fracture, a change in mechanical load detected by osteocytes, or the release of factors like tumor necrosis factor-α (TNF-α), parathyroid hormone (PTH), and interleukin-6 (IL-6) in the bone microenvironment [20]. These triggers activate lining cells, which are dormant osteoblasts, leading to an increased expression of Receptor Activator of Nuclear κB Ligand (RANKL) on their surface. RANKL then interacts with Receptor Activator of Nuclear κB (RANK) on pre-osteoclasts, prompting their fusion and differentiation into multinucleated osteoclasts [20].

During resorption phase osteoclasts adhere to the bone surface and begin to dissolve the bone. This involves two steps: firstly, acidification of the bone matrix to dissolve its inorganic component, and secondly, the release of lysosomal enzymes like cathepsin K and metalloproteinase 9 (MMP9), which break down the organic component. Once their task is complete, osteoclasts undergo apoptosis to prevent excessive bone resorption [21]. Recent research of McDonald et al. showed an alternative fate for RANKL-stimulated osteoclasts, where they split into daughter cells named osteomorphs [22]. Blocking RANKL prevented this process, leading to osteomorph accumulation. Moreover, single-cell RNA sequencing revealed that osteomorphs are transcriptionally unique from osteoclasts and macrophages, exhibiting distinct non-canonical osteoclast genes linked to specific bone structural and functional phenotypes in mice when these genes are removed [22].

The reversal phase in bone remodeling plays a crucial role in coupling bone resorption with bone formation by creating an osteogenic environment at the remodeling sites. This phase involves novel cellular elements such as canopies, capillaries and osteoblast-lineage reversal cells [23-25]. This phase is characterized by dynamic changes in cell interactions; bone-lining cells and BM envelope cells become active, and reversal cells engage with osteoclasts and canopies. These interactions prompt the activation of osteogenic activity in the reversal and canopy cells. Reversal cells also modify the bone surface as they develop into mature osteoblasts. Critical for the initiation of bone formation, this phase relies on the proliferation and differentiation of canopies and reversal cells. However, in bone diseases like osteoporosis, the disruption of canopies impairs the supply of osteoprogenitors, affecting the healing process. Thus, the availability of local osteoprogenitors, along with osteogenic molecules, is crucial for effective bone remodeling [26, 27].

In the formation phase, the resorption of the bone matrix releases various growth factors, such as bone morphogenetic proteins (BMPs), fibroblast growth factors (FGFs), and

TGF β. These factors are believed to recruit osteoblasts to the resorbed area. The osteoblasts then produce a new, initially uncalcified bone matrix (osteoid) and subsequently promote its mineralization, completing the remodeling process. An imbalance between the resorption and formation phases indicates improper bone remodeling, affecting bone mass and potentially leading to pathological conditions in bone homeostasis (reviewed in [28]).

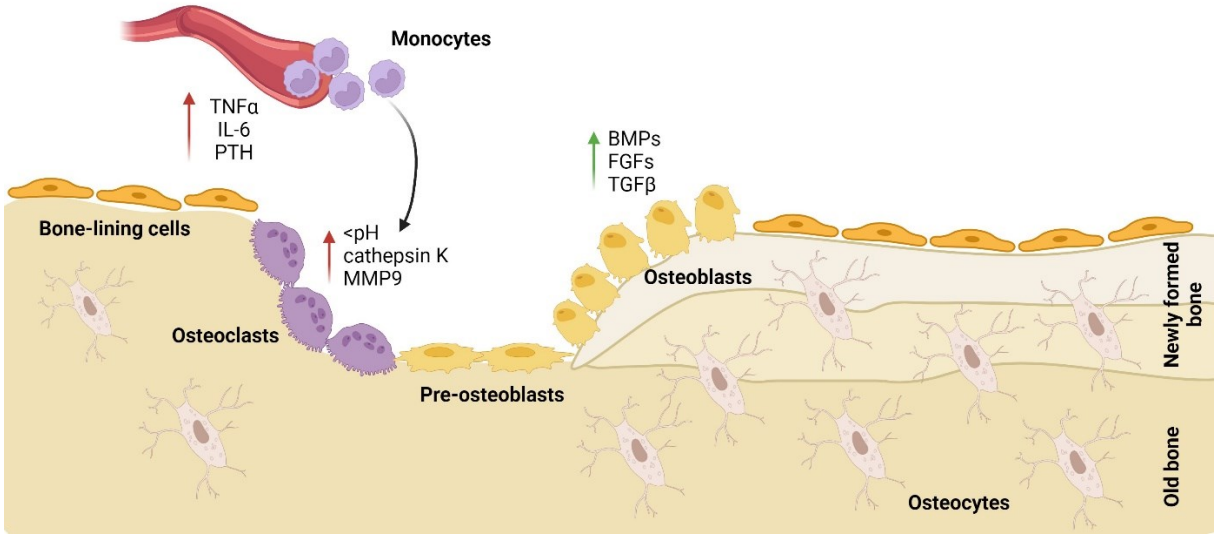

Figure 2. Phases of bone remodeling. The process initiates by releasing of cytokines like TNFα (Tumor necrosis factor alpha), IL-6 (Interleukin 6), and PTH (Parathyroid hormone), leading to the recruitment of monocytes. These monocytes transition into osteoclasts, which commence the resorption phase by decreasing the local pH and releasing lytic enzymes such as cathepsin K and MMP9 (Metalloproteinase 9), resulting in the breakdown of old bone. Subsequently, signaling molecules like BMPs (Bone morphogenic proteins), FGFs (Fibroblast growth factors), and TGFβ (Transforming growth factor beta) promote the differentiation of pre-osteoblasts into osteoblasts during the bone formation phase. These osteoblasts are responsible for synthesizing new bone matrix, culminating in the development of newly formed bone. Osteocytes, which are mature bone cells embedded within the bone matrix, emerge from osteoblasts that have completed their bone-forming activity. (Figure created in Biorender.com)

1.1.3. Regulation of bone remodeling

In the previous chapter we characterized complex process of bone remodeling, however, it is crucial to know, how this process is regulated on molecular level. Bone remodeling can be

regulated ether by hormonal regulation or by different peptides that impact bone remodeling and function of bone cells.

One of the main hormonal regulators of bone remodeling is PTH. PTH plays a crucial role in calcium homeostasis, maintaining serum calcium levels by stimulating bone resorption, increasing calcium reabsorption in the kidneys, and boosting renal calcitriol production [29]. PTH has a dual effect on bone, promoting formation when intermittently released and resorption when continuously secreted [30]. The growth hormone (GH)/IGF-1 (insulin like growth factor 1) system are key hormones for skeletal growth, stimulating cell proliferation, function and survival of osteoblasts. GH deficiency in animal and human studies showed reduced longitudinal bone growth [31, 32]. GH regulates growth directly through its receptor or indirectly via liver and skeletal IGF-1 expression [33]. Further, IGF-1 is present in both, osteoblast and osteoclasts suggesting involvement in regulation of both bone formation and resorption [34]. During bone remodeling, IGF-1 plays an essential role in maintaining of bone mass and skeletal homeostasis [35]. Moreover, deficiency of this hormone in mouse showed impairment of bone formation and deficit in bone mineral density (BMD) [36]. However, IGF-1 regulates also osteoclast differentiation which was documented by experiments using IGH-1 null mice. They showed increased bone formation and impaired bone resorption [37]. IGF-1 regulates gene expression of RANK and RANKL, and maintain normal physiological interaction between the osteoclasts and osteoblasts [37]. Calcitonin is hormone released by thyroid glands responsible for regulation of calcium level in blood by decreasing it [38]. In relation to bone health, calcitonin support osteoblast proliferation and inhibit osteoclast by removing their ruffled border, stopping their motility, and inhibiting proteolytic enzyme secretion [39]. Glucocorticoids have also mixed impact on bone cells, essential for osteoblast maturation but reducing their activity and enhancing osteoclast recruitment [40]. From positive regulators of bone remodeling, insulin acts as an anabolic hormone in bone remodeling, promoting osteoblast differentiation and function, which enhances bone formation. It influences the proliferation of osteoblasts, collagen synthesis, and mineral deposition, contributing positively to bone density and strength [41]. Primary calvarial osteoblasts and osteoblast-like cell lines express numerous insulin receptors (IRs) [42], showing high insulin binding capacity. Insulin at physiological doses increases osteoblast proliferation [43], collagen synthesis [44], alkaline phosphatase (ALP) production [6], and glucose uptake [45], highlighting insulin's significant role in osteoblast function and bone metabolism. Thyroid-stimulating hormone (TSH), thyroxine (T4), and triiodothyronine (T3) enhance osteoblastic

activity and contribute to bone elongation at the epiphyseal plates in long bones, primarily through the proliferation of chondrocytes. In conditions of hypothyroidism, bone turnover is reduced, while in hyperthyroidism, it is elevated [46]. This variation in bone turnover results from the effects of T3 and T4 on the quantity and activity of osteoblasts and osteoclasts. For instance, the heightened metabolic state in thyrotoxicosis leads to increased function in osteoblasts and a rise in both the number and activity of osteoclasts, resulting in increased bone turnover [46]. Other regulators of bone remodeling are adipokines adiponectin and leptin. Adiponectin is mainly from bone marrow adipose tissue (BMAT) [47] and it is secreted by adipocytes derived from BMSCs [48]. It is bound by receptors on osteoblast and osteoclast. In general, this adipokine promotes osteoblastogenesis and inhibits osteoclastogenesis [49, 50]. However, during metabolic changes like menopause or obesity, changes in adiponectin signaling take place which leads to increased bone resorption [51]. Furthermore, leptin signaling is one of the crucial pathways affecting satiety and thus energy metabolism in humans. Leptin has dual effect on bone tissue. If the leptin is bound by receptors on hypothalamus, it centrally inhibits osteoblast differentiation [52]. However, leptin can locally promote bone formation and inhibit bone resorption by binding to the expressed receptors on the osteoblasts [53].

Other factors, including steroid hormones play important role in the regulation of bone homeostasis. Estrogen significantly impacts bone metabolism through direct and indirect mechanisms on the skeleton. It influences osteoblastic cell expression by increasing osteoprotegerin (OPG) levels and decreasing the expression of RANKL and TNF-α. This hormonal effect leads to a reduction in bone resorption, showcasing estrogen's pivotal role in maintaining bone health [54]. Estrogen deficiency (typical for postmenopausal osteoporosis) results in increased bone remodeling, characterized by bone resorption surpassing bone formation, leading to reduced bone mass [55]. Animal studies suggest that estrogen may affect local factors regulating the precursors of osteoblasts and osteoclasts. Estrogen appears to inhibit the production and action of IL-6, a factor involved in bone resorption. Additionally, in the absence of estrogen, osteoclast survival is believed to increase, contributing to a more significant degree of bone turnover [56]. Moreover, several studies showed negative effect of testosterone deficiency on bone quality in healthy older man [57, 58]. On the other hand, intramuscular testosterone administration was associated with 8% increase of lumbar BMD compared to placebo group in older men [59].

Calcitriol, active form of vitamin D3, is essential for enhancing intestinal calcium and phosphorus absorption, thereby aiding bone mineralization. Additionally, vitamin D3 has significant anabolic effects on bone, influencing bone turnover [60]. A key element in regulation of bone homeostasis plays Wingless-type mouse mammary virus integration site (Wnt) signaling. This signaling pathway is crucial for embryogenesis, postnatal development, and adult tissue homeostasis [61], however it has gained attention also for its role in bone formation and regeneration [62].

Wnt signaling pathways, divided into canonical and non-canonical categories, play critical roles in various biological processes, including bone health. The canonical pathway operates through β-catenin stabilization and is significant in bone disorders [63]. Wnt ligands, which are glycoproteins, initiate this pathway by binding to co-receptors on osteoblast cells, leading to a series of intracellular events that activate β-catenin. This activation results in the nuclear translocation of β-catenin, interaction with transcriptional factors, and the upregulation of target genes crucial for bone formation and repair. Sclerostin and Dickkopf-1 (DKK1) are negative regulatory molecules of Wnt signaling bone remodeling. Sclerostin binding to osteoblast cell surface Wnt signaling co-receptors leads to inhibition of this signaling pathway [64-66]. *Dkk1* expression increases temporarily during human adipogenesis, inhibiting canonical Wnt signaling [67]. Overexpressing *Dkk1* induces adipogenesis [67], while Dkk1 knockdown via siRNA inhibits it [68]. In mouse models of diet-induced obesity, *Dkk1* knockout decreased BMAT and prevented cortical bone loss caused by high-fat diets [69]. Similarly, eliminating SOST (protein product of sclerostin) globally or treating with SOST antibodies enhanced trabecular bone volume, and reduced both the number and size of BMAds, indicating a significant role of these pathways in bone and fat tissue regulation [70]. This suggests that modulating Wnt signaling could be advantageous for treating skeletal disorders, including osteoporosis, by potentially enhancing bone density and reducing fracture risks [62, 71].

FGF superfamily consist of 22 proteins involved in multiple biological function such as growth, development and metabolism. Positive effect of FGF-2 and FGF-18 on osteoblastogenesis are well known [72, 73]. Further, FGF23 is bone-derived endocrine factor regulating vitamin D and phosphate homeostasis [74]. In vitro research on mouse osteoblasts linked elevated FGF23 protein levels with increased osteoblastic activity and ALP bone nodules, alongside higher osteopontin (OPN) expression. However, increased calcitriol levels were found to upregulate FGF23 and inhibit matrix mineralization in a dose-dependent manner,

suggesting FGF23 might regulate bone mineralization through OPN expression control [75]. Another study demonstrated that physiological concentration of FGF23 enhances osteoblast differentiation and activity in mouse BMSCs by up-regulating of osteocalcin (OCN), ALP and OPG in dose dependent manner [76]. On the other hand, relationship between bone and FGF21 remains only partially understood. Animal studies suggest FGF21 indirectly impacts bone by boosting peroxisome proliferator-activated receptor γ (PPARγ) activity, leading to bone resorption [77, 78]. In Fgf21 transgenic mice, high FGF21 levels drove lipogenesis in bone marrow precursors, reduced osteoblast activity, and heightened osteoclast activity via PPARγ in BMSCs. This led to lower BMD, significant bone loss, and increased fragility due to reduced bone formation and elevated resorption [78]. Elevated FGF21 levels are linked to adverse effects on bone metabolism, while Fgf21-knockout mice show increased bone formation and decreased resorption, leading to a high bone mass phenotype [78].

Another protein regulators affecting bone remodelling are dipeptidyl peptidase-4 (DPP4) and lipocalin 2 (LCN2). Both of these proteins are known as negative regulators of bone remodelling and their role in musculoskeletal framework is not fully understood [79, 80]. DPP4, secreted from mature adipocytes including those in BM, plays a complex role in bone metabolism with several potential mechanism: a) DPP4 influences bone remodelling indirectly by interacting with peptide substrates on bone cells, such as glucagon-like peptide-1, glucagon-like peptide-2, glucose-dependent insulinotropic polypeptide and others. This interaction modulates signaling pathways crucial for bone health; b) it also acts in the immune system, serving as a receptor or co-stimulatory protein affecting signaling in various immune cells, including CD4+ T cells, CD8+ T cells, B cells, and macrophages, linking immune responses to bone metabolism; c) through its enzymatic activity, DPP4 hydrolyses sites on chemokines, interleukins, and cytokines, playing a role in the regulation of inflammatory processes that are key to bone remodelling [79]. Further, LCN2, a secretory glycoprotein frequently classified as an adipokine [81]. LCN2 exhibits a responsive behavior to diminished mechanical stimuli across both skeletal and muscular tissues, showing elevated levels during mechanical inactivity in both murine models and human subjects [82, 83]. Intriguingly, the deficiency of LCN2 emerges as a detrimental factor for bone integrity, indirectly influencing osteoblast activity by altering metabolic energy processes [84]. Importantly, an upregulation of LCN2 induces the synthesis of RANKL and IL-6, culminating in enhanced osteoclast formation and a decline in osteoblast maturation [82].

As it was showed, regulation of bone homeostasis is very complex process involving many factors of different kind and different origin (summarized in Figure 3). Many factors were classified as adipokines originating in adipose tissue. Therefore, for the purpose of this work it is important to understand also the biology of adipose tissue (AT) and its interplay with bone homeostasis.

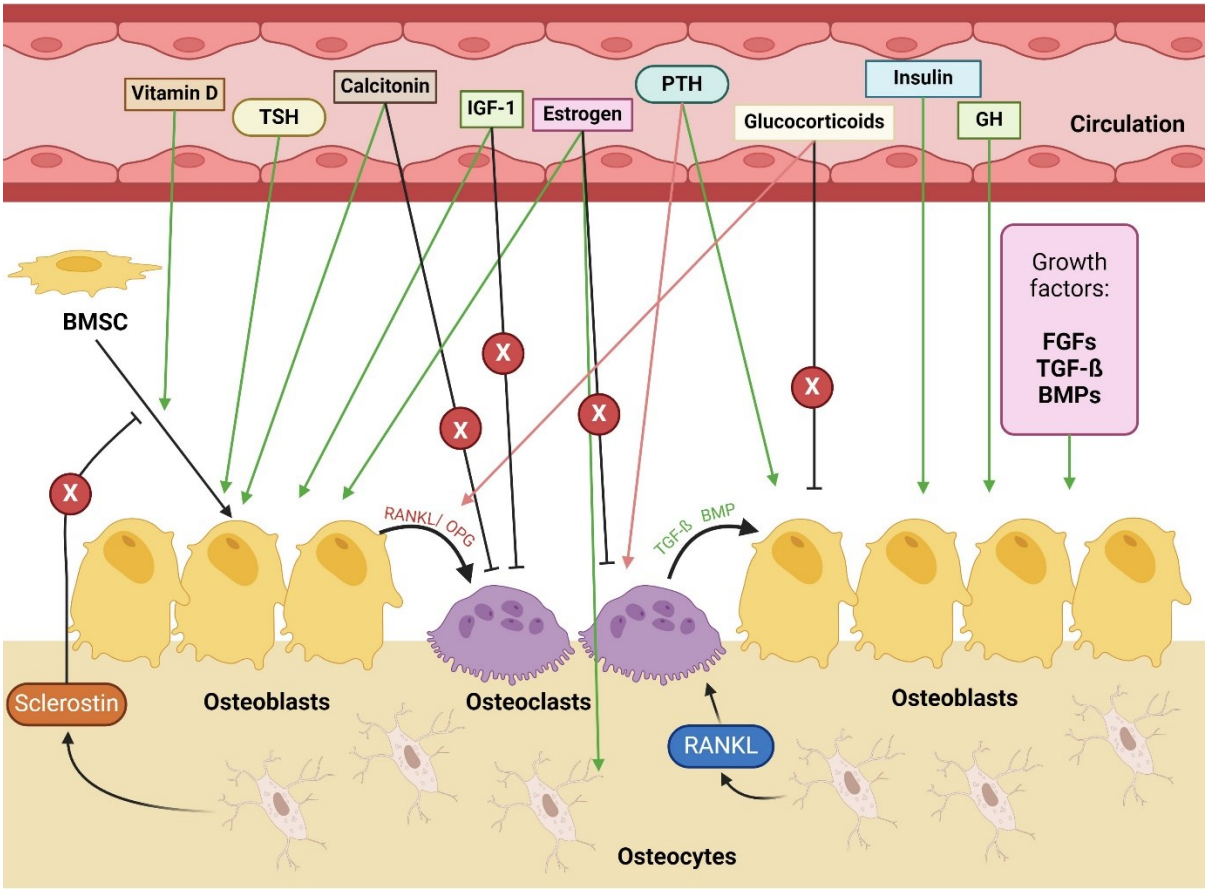

Figure 3. Regulation of bone remodeling. This scheme displays different regulatory molecules and hormones released from circulation promoting bone formation by stimulating osteoblasts (green arrows) or inhibiting osteoclasts, or promoting bone resorption by stimulating osteoclasts (red arrow) or inhibiting osteoblasts. (Abbreviations: BMPs, Bone morphogenic proteins; BMSC, Bone marrow skeletal cells; FGFs, Fibroblast growth factors; IGF-1, Insulin growth factor 1; GH, Growth hormone; OPG, Osteoprotegerin; PTH, Parathyroid hormone; RANKL, Receptor activator of nuclear factor-kβ ligand; TGF-β, Transforming growth factor beta; TSH, Thyroid-stimulating hormone) (Figure created in Biorender.com)

1.2. Adipose tissue biology

1.2.1. Types of adipose tissue and characteristics

AT is a complex and dynamic connective tissue that plays a pivotal role in energy storage, thermoregulation, and endocrine function [85]. Body fat percentage differs among genders, in healthy adult men it is between 12-20% while in women it is between 20-30% of total body mass [86]. There are two main types of AT: white adipose tissue (WAT) and brown adipose tissue (BAT), each with distinct functions and cellular characteristics. WAT is primarily involved in energy storage and metabolic regulation. It stores energy in the form of triglycerides (TAGs) within large, unilocular lipid droplets. Adipocytes in WAT also secrete a variety of bioactive molecules, known as adipokines (including, adiponectin, leptin), which play significant roles in metabolic homeostasis [87]. BAT plays a crucial role in energy expenditure and thermogenesis, a process of heat production in the body. Unlike WAT, BAT contains smaller, multilocular lipid droplets and a high density of mitochondria, giving it a brown appearance. The thermogenic activity of BAT is primarily mediated by the uncoupling protein 1 (UCP1), which dissipates the proton gradient in mitochondria to generate heat [88]. Distinct roles of BAT and WAT is evident from their different origin, as they originate from different precursor cells [89]. Recent animal and human studies reported a unique secretory profile of BAT, known as batokines (e.g. Slit homolog 2 protein and Ependymin related protein1), which are involved in the thermogenic program of AT and lipid metabolism [90].

Additionally, AT is present within bones, forming a crucial part of the BM microenvironment, known as BMAT. BMAT located within the BM, changes its volume throughout life [91]. At birth, BM primarily contains hematopoietic cells, which in adulthood (around age 25) are replaced by yellow BM rich in BMAT, especially in distal bones, constituting about 70% of total BM volume [92] and 10% of total AT volume in adult humans [93]. Human BMAds share similar morphology with subcutaneous adipocytes (SAT), characterized by a unilocular lipid droplet and a peripheral nucleus. BMAds share the characteristics of both WAT and BAT adipocytes in terms of adipocyte morphology and secretion of adipokines. However, BMAd function and its precursors seems to be different from peripheral adipocytes in the context of bone homeostasis and BM microenvironment [94]. Further differences between BMAT and peripheral AT are discussed in chapter 2.3 BMAT-characterization in comparison to peripheral AT.

Moreover, two additional types of adipocytes, beige and pink, have been recently identified. Beige adipocytes exhibit features of both brown and white fat cells and are typically found within subcutaneous WAT. They originate either from a unique subset of preadipocytes or through the transformation of existing white adipocytes. Gene expression studies suggest that

beige fat cells are a unique type of thermogenic fat cell initially observed in rodents exposed to cold [95, 96]. However, "beiging" or "browning" can be also induced in response to various stimuli such as diet, exercise, drug treatment, plant-based bioactive molecules, and adipokines [97-99]. This phenomenon may offer protective effects against obesity and metabolic disorders and is inducible in both mice and humans [100], but is more prominent in mice.

Pink adipocytes, discovered in 2014, emerge in the subcutaneous WAT of female mice during late pregnancy and continue through lactation. These cells, which originate from white adipocytes, acquire epithelial-like characteristics, forming milk-secreting alveoli and giving the tissue a pink appearance [101]. Pink adipocytes have distinct features such as compartmentalized lipid droplets and cytoplasmic projections, resembling epithelial cells more than typical adipocytes. The transformation and reversion of these cells during pregnancy, lactation, and post-lactation in rodents [102] suggest a reversible process, although it's unclear if this occurs in humans. The absence of a crucial adipogenic transcription factor in the mammary secretory epithelium can lead to a pro-breast tumorigenic environment, hinting that the white-to-pink transition could provide insights into breast cancer biology [101, 103]. Further research into adipocyte plasticity may reveal new therapeutic strategies for obesity and related complications, as well as cancer. The major AT characteristics are summarized in the Figure 4.

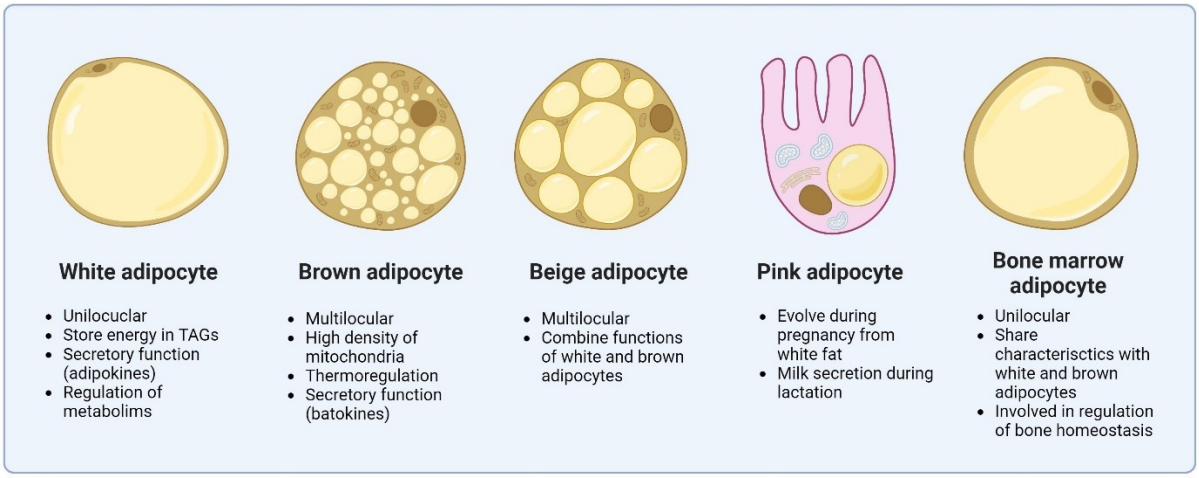

Figure 4. Main differences between adipose tissues types. This scheme depicts basic morphological and functional differences between AT types. (Figure created in Biorender.com)

1.2.2. Regulation of AT biology

AT plays a pivotal role in regulating energy balance and insulin sensitivity in vertebrates, orchestrating the flow of energy depending on metabolic demands. Disruptions in AT function due to genetic factors, diet, disease, or aging contribute significantly to the widespread prevalence of metabolic disorders such as obesity and type 2 diabetes (T2D) [104]. This tissue operates through a sophisticated network of transcription factors that manage adipocyte development, function, and aging. Among these, PPARγ stands out for its critical and irreplaceable role in adipogenesis, lipid management, and maintaining insulin sensitivity, highlighting its key position in AT physiology [104].

First of all, different AT like WAT and BAT play distinct roles in the body as they originate from distinct precursor cells. WAT is derived from multipotent mesenchymal stem cells which give rise also to fibroblasts, osteoblasts, and other cell types, such as muscle cells and chondrocytes [105]. Moreover, AT is in general considered as ideal source of multipotent mesenchymal stem cells (MSCs) as SAT is easily accessible [106]. Fat aspirate is source of adipose-derived stromal/stem cells which can be effectively isolated and expanded in cell culture. The freshly isolated stromal vascular fraction (SVF) from AT typically contains up to 3% stem and precursor cells, a concentration that is about 2,500 times higher than the frequency of stem cells found in BM, which is up to 0.002% [107].

Further BAT is believed to emerge from the mesoderm, one of the three primary germ layers in early embryonic development. This common origin links them closely with other mesoderm-derived tissues such as skeletal muscle, bone, white adipocytes, and connective tissues, indicating a shared early developmental pathway among these diverse cell types and tissues [108-111]. Even though the origin of WAT and BAT is different, all of them undergo process of differentiation before they become fully matured ready to fulfil their roles in the metabolism [112, 113]. Then, mature adipocytes respond to different metabolic stimuli which decide if the energy will be stored or utilized [114]. As the time pass, cells undergo senescence which leads to loss of differentiation and thermogenic capacity [115]. PPARγ is recognized as a central regulator throughout the different phases of an adipocyte life, playing a crucial role in coordinating numbers of molecular processes that ensure the normal physiological functions of white, brown, and beige adipocytes [116].

PPARγ is most abundantly expressed in AT and can be significantly induced in other tissues when subjected to a high-fat diet (HFD) [117]. It functions by forming unique transcription complexes with various interacting partners or through epigenetic modifications, thus

executing essential and wide-ranging roles in AT. These functions include: a) promoting adipocyte differentiation and lipid storage, b) facilitating the acquisition of brown/beige adipocyte identity, c) maintaining the thermogenic capacity of brown/beige adipocytes, d) overseeing the functional decline of brown/beige adipocytes during aging, and e) regulating the gene program associated with diabetes [118]. PPARγ is considered as a master regulator of adipogenesis, as its ectopic expression alone in fibroblasts can initiate the adipogenic program, a feature that cannot be achieved by any other factors in the absence of PPARγ [119, 120]. Further reinforcing its importance, studies in adult mice showed that targeted deletion of PPARγ in AT using a tamoxifen-dependent Cre-ER(T2) recombination system results in adipocyte death followed by their renewal, highlighting PPARγ necessity for the survival of mature adipocytes [121, 122]. Clinically, individuals carrying heterozygous mutations in PPARg exhibit partial lipodystrophy and insulin resistance, emphasizing the gene's pivotal role in adipocyte function and metabolic regulation [123]. Additionally, PPARγ acts as a key thrifty gene, orchestrating gene programs that favor energy storage, predominantly in WAT [124].

Moreover, more hormones and molecules are involved in regulation of WAT biology like insulin, glucagon, catecholamines, sex hormones and other paracrine and endocrine factors. On the other hand, BAT is mostly regulated by sympathetic nervous system [88, 125]. In general, lipolysis, process of TAG release from AT, is induced by glucagon, catecholamins while insulin has antilipolytic activity. Moreover, dietary components like caffeine, ethanol and calcium may also induce this process [126]. On the contrary, lipogenesis, process which is opposite to lipolysis, is induced by carbohydrate diet which leads to elevated plasmatic level of TAG. Glucose affects lipogenesis indirectly by metabolic intermediate acetyl-CoA, which stimulates FA synthesis [127]. Moreover, glucose support insulin stimulated activity of lipogenic enzymes like fatty acid synthase (FASN) [128]. On the other hand, glucagon decrease activity of FASN and leptin during the regulation of food intake downregulate genes involved in FA and TAG synthesis which limits fat storage [127]. Sex hormones like estrogen and androgens influence fat distribution, with estrogens promoting SAT accumulation and androgens favoring VAT deposition [129].

Previous chapters summarize regulation of AT and bone metabolism with some molecules involved in both processes but often with distinct roles. All together it represents introduction to better understanding of unique characteristics of bone marrow adiposity which is one of the central topics of this thesis.

1.2.3. BMAT- characterization in comparison to peripheral AT

As it was already mentioned in chapter 2.1, BMAT has common morphological features of WAT and BAT, however functionally it is a distinct AT as it was proposed in the study by Suchacki et al. [94] where they showed differences in transcriptomic profile and marker genes between WAT, BAT and BMAT in rabbits and humans leading to different response of BMAT to insulin and cold exposure. Moreover, further analysis using ^{18}F-FDG PET/CT (Positron emission tomography and computerized tomography) insulin stimulated glucose uptake in mouse and humans showed decreased insulin responsiveness of BMAT compared to peripheral AT in normal conditions and cold exposed animals and human subjects. These finding are consistent with findings that BMAT do not express UCP1 protein and thus it misses regulation of thermogenesis similar to BAT [130].

Recent studies in mice and humans [131] identified two types of BMAT: 'regulated' marrow adipocytes (rBMAds) and 'constitutive' marrow adipocytes (cBMAds). rBMAds exist as individual adipocytes dispersed throughout the skeleton, playing a role in the process of hematopoiesis. On the other hand, cBMAds form large, contiguous groups of adipocytes located in the distal parts of the skeleton and do not have a regulatory function in hematopoiesis [131]. BMAds can be smaller or comparable in size to WAT adipocytes, with cBMAds generally larger than rBMAds.

Further, compared to WAT and BAT, role of BMAT in whole body metabolism is poorly understood. There are well known bioactive molecules like adiponectin, DPP4 and LCN2 secreted by BMAT which play important role in inflammation and metabolism [47, 132]. Recent study by Li et al. tested BMAT function as energy source for BM environment by creating a BMAd-*Pnpla2*$^{-/-}$ mice with impaired BMAd lipolysis [133]. This model highlighted importance of BMAT lipolysis in bone homeostasis under conditions of caloric restriction. Under these stress condition, BMAT of control mice increased lipid uptake, lipogenesis and lipolysis however in BMAd-*Pnpla2*$^{-/-}$ mice with caloric restriction (CR) this induction of adipocyte genes was impaired which led to decrease of energy supply and HSC and osteoblast dysfunction. Moreover, RNA seq analysis of BMAT has shown that caloric restriction significantly increases the expression of genes involved in extracellular matrix organization and skeletal development and that energy from BMAd is essential for facilitating these adaptive changes. Proliferation and differentiation of myeloid cell progenitors was also decreased with

CR and impaired BMAd lipolysis suggesting important role of BMAT as energy supplier for myeloid cells [133]. This unique BMAd-specific knock-out model brought new perspective to study the role of BMAT.

Also, BMAT plays a role in regeneration of HSCs after irradiation by releasing stem cell factor in mice [134] showing important role of BMAT for hematopoietic maintenance. Irradiation is usually followed by BM transplantation and co-transplantation of HSC together with BM preadipocytes showed to be a great approach to cure hematopoietic impairment [135]. However, the physiological importance of metabolic roles of BMAT in different conditions is still under investigation of several research groups including ours [136, 137].

1.2.4. AT metabolism and its regulation

In general, AT metabolism represents a critical aspect in the regulation of energy utilization and whole-body energy homeostasis because of its primary function to utilize the excess calories in the form of TAGs. Similar to peripheral AT, besides a small volume of BMAT in the whole body, it has been shown that BMAT also contributes to the energy metabolism, particularly in lipid synthesis, storage, and release, involving intricate processes like fatty acid (FA) esterification into TAGs [138]. This lipid synthesis is a tightly controlled process, essential for maintaining energy homeostasis through ongoing interactions with peripheral organs, including extramedullary AT. The process involves FA esterification into TAG, where free FA (FFA) are activated into acetyl-CoA, subsequently forming monacylglycerol (MAG) and diacylglycerol (DAG) through reactions with glycerol-3-phosphate (G3P) [138]. Adipocytes are the primary site for TAG storage in healthy individuals. Notably, reduced adipocyte capacity to increase TAG deposition, as seen in conditions like human lipodystrophies and obesity, leads to systemic lipid excess and 'lipotoxicity', disrupting overall glucose tolerance [139]. Additionally, glucose plays a role in enhancing lipogenesis, both by stimulating insulin secretion and upregulating lipogenic genes such as FA synthase (*Fas),* lipoprotein lipase *(Lpl),* acetyl-CoA carboxylase *(Acc),* elongase of long chain FA family 6 *(Elovl6),* stearoyl-CoA desaturase 1 *(Scd-1),* stearoyl-CoA desaturase 2 *(Scd-2)*, and diacylglycerol acyltransferase (*Dgat*) [91].

In contrast, AT lipolysis involves the breakdown of stored TAGs, releasing FFAs and glycerol, with key enzymes like adipose tissue triglyceride lipase (ATGL), hormone-sensitive lipase (HSL), and monoacylglycerol lipase (MGL) playing crucial roles [140] in lipid

metabolism. Two lipolytic pathways in human adipocytes involve catecholamines and natriuretic peptides, promoting lipolysis via β-adrenoreceptors and natriuretic peptide receptor A [141]. These proteins involved in lipolysis are potential drug targets for treating metabolic syndrome and obesity.

Recent proteomic and metabolomic/lipidomic studies [142] found that human BMAds express a range of proteins involved in cholesterol metabolism, but display lower levels of lipolytic enzymes, particularly MGL, ATGL, and HSL, compared to subcutaneous adipocytes. This suggests a unique lipolytic activity in BMAds and some degree of resistance to lipolytic stimuli [142]. Additionally, BMAds have been observed to have higher TAG and MAG levels, both saturated and unsaturated, than subcutaneous adipocytes [142], indicating less effective MAG hydrolysis. BMAds also exhibit increased free cholesterol content, pointing out a distinct lipid composition which may be significant for their role in BMSC differentiation and bone homeostasis [142]. However, the study by Scheller et al. using male Sprague-Dawley rats indicates that lipolysis in BMAT is both treatment and site-specific. Rodent rBMAds respond to nutrient deprivation and β3-adrenergic receptor agonist treatments by undergoing lipolysis, while cBMAds are resistant to these stimuli. Interestingly, forskolin, an adenylyl cyclase activator, has been shown to activate lipolysis in both rBMAds and cBMAds in rodents [137]. Moreover, Scheller et al. discovered a differential lipid utilization pattern between rBMAds and cBMAds, noting that cBMAds have a higher content of unsaturated lipids compared to rBMAds. This is consistent with the increased levels of unsaturated FA, particularly oleate and palmitoleate, in cBMAds. Additionally, there was a higher expression of other desaturases, including Fads1 and Fads2, in both genders. A gender-specific variation was observed, with increased Scd2 levels in male mice and higher Fads3 levels in females [131].

Lipogenesis and lipolysis in adipocytes are regulated by metabolic pathways, including insulin signaling, AMP-activated protein kinase (AMPK) activation, and beta-adrenergic signaling. While the modulation of insulin signaling in peripheral AT has been extensively studied, research into insulin signaling in BMAds is emerging. Experiments involving the ablation of the insulin receptor (IR) in aP2-Cre mice have shown significant effects, such as a marked reduction in AT mass and protection against obesity [143] and associated glucose metabolism dysfunction [144]. However, a study by Qiang et al. found that Adipoq-Cre-mediated IR knockout in mice led to lipodystrophy and metabolic dysfunction, also confirming IR deletion in BMAds [145]. They observed a reduction in the volume of cBMAds in the distal tibia of fat-specific IR^{FKO} mice, attributable to decreased adipocyte size rather than number

[145]. This suggests that IR loss does not affect the development of BMAds but is essential for lipid accumulation in these cells. PET/CT scanning with radiolabeled glucose tracers indicated insulin-induced glucose uptake in BM in animals (mouse and pigs), pointing out the insulin responsiveness [146, 147]. However, Suchacki et al. reported that BMAT, in both rabbits and humans, is resistant (less responsive) to insulin-stimulated glucose uptake compared to peripheral WAT. Their studies showed decreased levels of phosphorylated Akt S473 and T308 in tibial distal BMAT compared to gonadal WAT, with insulin stimulating phosphorylation of Akt S473 but not T308 in distal BMAT. This indicates a resistance of BMAT to insulin-stimulated phosphorylation of Akt at T308 [94].

These findings highlight the need for further studies to understand BMAT direct role in whole-body metabolism. Additionally, the relevance of these findings to human physiology needs to be investigated. Further emphasizing the metabolic activity of BM, in vivo tracing studies using radiolabeled glucose and lipid tracers in mice have shown that postprandial glucose and lipid uptake in the skeleton are comparable to those in other metabolically active organs such as the liver, muscle, or AT. These findings highlight BM as an actively participating organ in the utilization of energy coming from nutrition, demonstrating its significant role in overall metabolic processes.

1.3. Cellular composition of bone marrow

1.3.1. Stem cells- general overview

Stem cells are unspecialized cells within the body (AT, BM, brain, blood vessels, skin, teeth and heart) characterized by their ability to differentiate into any cell type and their capacity for self-renewal. Present in both embryonic and adult stages, stem cells undergo various levels of specialization starting as totipotent stem cells heading toward unipotent stage with each step reducing their developmental potency. This means a unipotent stem cell has a more limited differentiation range compared to a totipotent one [148, 149].

Totipotent stem cells possess the most extensive differentiation potential, capable of dividing and differentiating into all cells of an organism, including both embryonic and extra-embryonic structures. The zygote, formed post-fertilization, is a prime example of a totipotent cell, with the potential to develop into any of the three germ layers or extra-embryonic structures like the placenta. Approximately four days post-fertilization, the inner cell mass of

the blastocyst attains pluripotency. This specific part of the blastocyst serves as the origin for pluripotent stem cells (PSCs) [148, 149].

PSCs can form cells of all germ layers but are incapable of creating extraembryonic structures (e.g. placenta). Examples include embryonic stem cells (ESCs), derived from the inner cell mass of preimplantation embryos, and induced pluripotent stem cells (iPSCs), derived from the epiblast layer of implanted embryos. The spectrum of pluripotency ranges from fully pluripotent cells, like ESCs and iPSCs, to cells with reduced potency, such as multi-, oligo-, or unipotent cells [149].

Multipotent stem cells in general, with a more limited differentiation scope than PSCs, specialize in specific cell lineages. For instance, HSCs can develop into various blood cell types. Upon differentiation, these cells become oligopotent, restricted to cells within their lineage [149]. Further, oligopotent stem cells differentiate into a few cell types. An example is the myeloid stem cell, capable of dividing into several types of white blood cells but not red blood cells [149]. Unipotent stem cells, with the most limited differentiation capacity, possess a unique ability to divide repeatedly, making them promising for therapeutic applications in regenerative medicine. These cells can only form one cell type, such as dermatocytes, but their persistent division enhances their therapeutic potential [150, 151].

1.3.2. Characterization of cellular microenvironment in bones

BM is a soft tissue located within bones, constituting about 5% of an adult total body mass [152]. It is primarily known as a hematopoietic organ, crucial for the production of new blood cells. Besides its hematopoietic role, BM also represents mechanical and immune functions. It contains two major cellular types: a) BMSCs, which are key components for bone formation, and b) HSCs, responsible for generating various immune cells important for immune responses and myeloid precursors giving rise to osteoclasts, important for bone resorption [7, 153] and c) other cell types including nerve cells and endothelial cells important for innervation and vascularization of BM microenvironment (summarized in Figure 5) [154, 155]. BMSCs facilitate bone tissue regeneration through osteoblast differentiation and neovascularization, supporting the growth of new tissue [156, 157]. In contrast, HSCs are typically quiescent but can become mobilized in response to external stimuli. A significant proportion of HSCs resides in BM, with only about 0.01% capable of migrating into the circulation [158]. These circulating

HSCs in the peripheral blood are drawn to specific sites by cytokines like SCF (stem cell factor), CXCL12 ((C-X-C motif) ligand 12), or IL-8 [159].

Hematopoiesis begins in the fetal liver, where HSCs proliferate and then migrate to the BM. In adulthood, this migration continues from BM to peripheral blood, ensuring consistent hematopoiesis [160]. During HSC migration from BM, the stem cells move from proliferative niches to regions within the BM that are more oxygenated and vascularized [161]. In situations of stress, injury, or pharmacological intervention, changes in HSC niche formation and interactions with BMSCs can lead to increased HSC mobilization and egress. These processes are influenced by the metabolic status of the organism, which can be altered by factors like CR, obesity, and T2D [162]. However, the impact of metabolic complications on the composition of BM, the interactions between HSCs and BMSCs, and the inflammatory status within the BM remains insufficiently documented.

BM is a diverse immune organ, comprising various cell types that perform distinct immune functions. HSCs responsible for the production of myeloid and lymphoid precursors, and BMSCs known for their immunosuppressive properties [7, 153, 163]. Studies have shown that 8–20% of BM mononuclear cells are part of the lymphocyte lineage, which includes T cells, B cells, and Tregs [164], while approximately 1% represent plasma cells that contribute to antibody production [165]. BM also houses natural killer T cells (NKT) (approximately 0.4–4%) [166], dendritic cells (1–2%) [167], myeloid progenitor cells (which give rise to osteoclasts), megakaryocytes essential for platelet production through thrombopoietin (1%) [168], as well as neutrophils (8–15%), eosinophils (0.5–2%), and basophils (0.01–2%). BM is a crucial reservoir for neutrophils, facilitating their migration into circulation as an initial defense against infection and stress [169]. Additionally, senescent neutrophils are phagocytosed by stromal BM macrophages [170]. The composition of immune and progenitor cells in BM undergoes changes influenced by age, metabolic status, or inflammatory conditions.

BM vascularization, including blood vessels and sinusoids, creates a barrier between BM and peripheral circulation [171]. This microvasculature system allows the release of proliferating progenitor cells and secreted molecules from BM into the bloodstream, responding to stimulatory signals or physiological conditions that modulate the local microenvironment of target tissues [172].

Early in life, many bones contain red BM, rich in hematopoietic activity, which gradually decreases with age and turns into yellow “fatty” BM [173]. In adults, red BM is limited to a few bones like the sternum, vertebrae, ribs, or pelvic bones, which contribute to hematopoiesis [174]. Therefore, the maintenance of bone homeostasis at various locations within the body is influenced by the composition of BM, specifically the balance of HSCs and BMSCs. These cells collectively contribute to the structural integrity of bones, as well as their mechanical strength and immune functionalities [7, 175]. The interaction between these cells activates processes such as proliferation, migration, and differentiation of stem cells, coupled with the production of various bioactive molecules that create the BM microenvironment [7, 153, 173]. The maintenance of this environment is crucial for healthy cell development, immune system functionality, and bone homeostasis and whole-body metabolism.

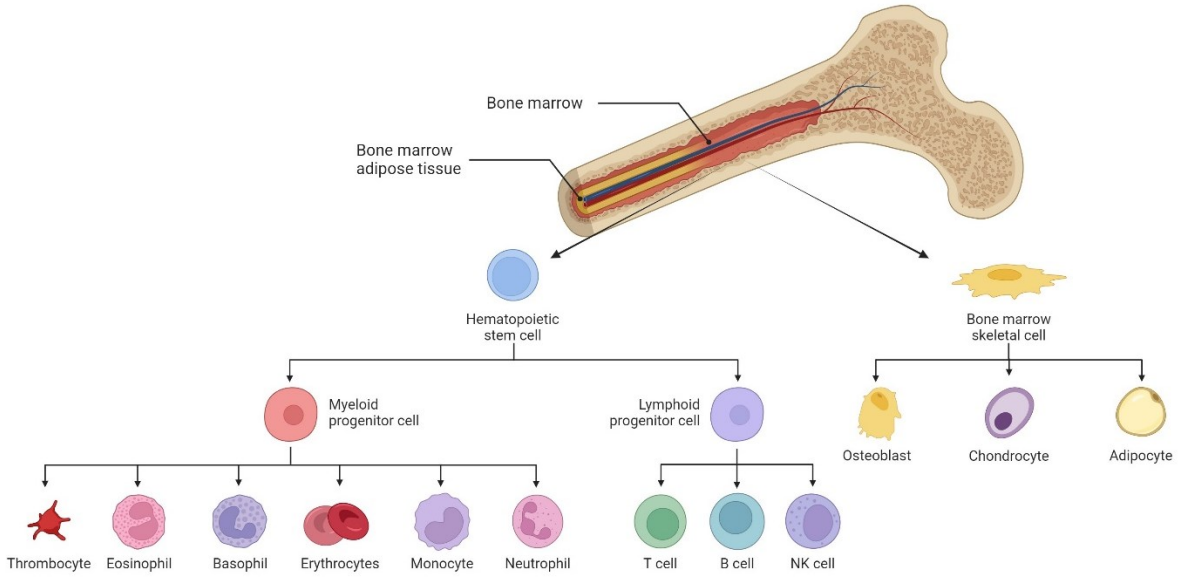

Figure 5. Cellular composition of healthy BM. The composition of different cell types with HSC and BMSC origin within the bone marrow. Figure adapted from [6] and created in Biorender.com.

1.3.3. BMSCs and their differentiation properties

BMSCs constituting about 0.01–0.1% of total BM cells in adults, have the remarkable ability to differentiate into various cell types. These include osteoblasts, adipocytes and chondrocytes, all of them important in maintaining bone homeostasis [7, 163]. Additionally,

BMSCs support hematopoiesis and play immunoregulatory function [176]. The BMSC differentiation process is governed by both intrinsic mechanisms, such as transcription factors, cofactors, posttranscriptional, and posttranslational modifications, and extrinsic factors like secretory molecules, the BM microenvironment, and metabolic cues both described further [6].

Several strategies have been implemented to identify the factors and pathways that govern the lineage-specific differentiation of BMSCs towards adipogenesis and osteogenesis. It is important to note that BMSCs contain progenitor cells capable of differentiating into both adipocytes and osteoblasts [177]. Both, *in vitro* and *in vivo* studies have indicated an inverse relationship between the osteogenic and adipogenic differentiation pathways in BMSCs. Specifically, osteogenic differentiation is associated with a suppression of adipogenesis [178]. Moreover, the reduced bone mass typical characteristic trait during aging, obesity or osteoporosis is often associated with an increase in BMAT [179-182]. This suggests that the signaling pathways activated during osteogenic or adipogenic differentiation might function as molecular "switches" [183]. These switches are critical in determining the lineage-specific differentiation pathway chosen by BMSCs. Understanding and manipulating these molecular switches could be crucial in development of therapeutic interventions for metabolic bone diseases, such as aging, obesity, and osteoporosis, where BMSC function is compromised [184].

Differentiation of BMSCs is driven by many factors and regulatory molecules. One of the most relevant are transcriptional factors from CCAAT-enhancer binding protein family (C/EBP) including C/EBPα, C/EBPβ, C/EBPγ and C/EBPδ. C/EBPβ, in cooperation with ATF4, plays a pivotal role in promoting osteogenic differentiation [185, 186]. On the other hand, C/EBPα is a key regulatory factor in adipogenic differentiation. The early induction of both C/EBPβ and C/EBPδ leads to the expression of C/EBPα, which then interacts with PPARγ during the early stages of adipogenesis [120, 187]. C/EBPα and PPARγ act synergistically as crucial transcriptional factors to induce the expression of adipocyte-specific genes, such as AP2 and ADIPOQ, thereby driving the development of a mature adipocytic differentiation phenotype [188].

PPARγ, a member of the nuclear receptor superfamily, is a critical factor in initiating adipogenic differentiation and sustaining the mature state of adipocytes [189]. *In vitro* experiments involving the silencing of PPARγ through siRNA in mature 3T3-L1 adipocytes led to a decrease in the expression of adipocyte-specific gene markers, a reduction in lipid

accumulation, and diminished insulin responsiveness [190]. Similarly, *in vivo* experiments using a mouse model deficient in PPARγ revealed a decrease in adipogenic differentiation and an increase in bone mass [190]. This finding underscores the role of PPARγ in targeting bone marrow adiposity (BMA) and enhancing bone formation *in vivo*. This enhancement in bone formation is potentially mediated through the endogenous inhibition of mammalian target of rapamycin (mTOR) activity, which in turn inhibits osteoblastic differentiation [191, 192].

Osteoblast differentiation of BMSCs is regulated by many factors responsible for whole process of extracellular matrix maturation and mineralization of BMSCs [193]. Runt-related transcription factor 2 (RUNX2) is a central regulator of osteoblast differentiation and bone formation [194, 195]. Regulation of RUNX2 gene expression is crucial regulatory step of BMSC differentiation because mutation in this gene leads to downregulation of osteoblastogenesis [195]. Moreover, coordinated activity between RUNX2 and the TGF-β/ BMP signaling pathways plays an important role in BMSC differentiation. Specifically, Smad proteins, which are activated by TGF-β/BMP signaling, are crucial for maintaining osteoblastic differentiation in BMSCs. The Smad proteins regulate the expression of various transcription factors that are essential for osteoblast development and function (e.g. RUNX2, osterix) [196].

In addition, as it was already mentioned in chapter 1.3 about regulation of bone remodeling, important regulator of BMSC differentiation represents also Wnt/β-catenin signaling pathway which promotes osteogenic differentiation [62, 63]. Moreover, osterix is another important regulator of osteoblastogenesis. It is a transcriptional factor which functions downstream of RUNX2 and it plays an essential role in bone formation [197]. Moreover, osterix is important activator of ALP, collagen type 1 and osteocalcin, that are important osteogenic markers for mineralization and osteoblast maturation [197, 198]. Further, ALP plays important role in matrix mineralization via its phosphatase enzymatic activity [199]. However, there are also negative regulators like OPN, DKK1(inhibitor of Wnt signaling) and sclerostin [64-66] involved in the regulation of bone resorption via mediating of osteoclast attachment to the bone [200, 201].

Epigenetic modifications, such as histone deacetylation, play a role in BMSC differentiation, with increased acetylation during osteoblast differentiation leading to enhanced expression of genes like Runx2, BMP-2, osterix, and OPN [202, 203]. Addison et al. identified Zfp521 as a critical regulator of lineage specification in progenitor cells, regulating BMP-induced MSC differentiation coupled with histone modification at the Zfp423 promoter [204].

Recent work of Rauch et al. [205] highlights that, regardless of their origin from BM or AT, MSCs differentiating towards adipocytes undergo far more significant transcriptional changes and genome remodeling compared to those differentiating into osteoblasts. This finding builds upon previous research that showed cultured mouse BMSCs are more closely related to osteoblasts than to adipocytes, suggesting a niche-dependent preprograming of these cells towards a bone-forming lineage [206]. The study underscores the fact that MSCs, in general, necessitate substantial alterations in their transcriptional programming to differentiate into adipocytes than to osteoblasts, highlighting the complexity of adipogenic differentiation [205].

All these molecules mentioned above (listed in Table 1) represent a part of whole regulatory processes of BMSC differentiation. However, cellular metabolism and lifestyle changes in the life of individuals may also play a crucial role in bone homeostasis and BMSC fate, which may affect bone and whole-body metabolism.

Table 1. Major regulators of BMSC differentiation. Adapted from [6].

Regulator Type	**Regulator**	**Role in Adipogenic Differentiation**	**Role in Osteogenic Differentiation**
Transcription Factors	C/EBP	Key regulatory factor in adipogenesis. Early induction leads to expression of adipocyte-specific genes.	-
	PPARγ	Critical in initiating adipogenic differentiation and maintaining mature adipocyte state.	
	RUNX2	-	Central regulator of osteoblast differentiation and bone formation.
	Osterix	-	Essential for bone formation, downstream

			of RUNX2, activates osteogenic markers.
Signaling Pathways	Wnt/β-catenin	-	Promotes osteogenic differentiation.
	TGF-β/BMP-2	-	Activates Smad proteins, crucial for osteoblast development.
Enzymes	ALP	-	Important in matrix mineralization and osteoblast maturation.
Epigenetic factors	Histone deacetylation	-	Increased acetylation enhances expression of osteogenic genes.
Others	Zfp521	-	Regulates lineage specification and BMP-induced MSC differentiation.

1.3.4. BMSC metabolism

The skeletal system is highly multifunctional, playing roles in mechanical support, enabling movement, producing blood cells, storing minerals, and regulating endocrine functions. This wide array of functions is orchestrated through a complex interplay of various cell types, including osteoblasts, chondrocytes, BMAds and stromal cells, all of which originate from BMSC. Each type of skeletal cells has unique metabolic needs that align with its specific functions and are affected by the constraints of their microenvironment. Specific metabolites are essential for maintaining skeletal stem cells, directing lineage allocation, and facilitating cellular communication, thereby playing a pivotal role in the overall functioning and health of the skeletal system [207-209].

In various stem cell models, including pluripotent embryonic stem cells, hematopoietic, muscle stem cells, and immune cells, cellular functions and differentiation are significantly influenced by the cell metabolic and bioenergetics state [210]. Pluripotent embryonic stem

cells, for instance, favor anabolic glycolysis, a trait shared with rapidly proliferating cells [211]. Hematopoietic progenitor cells show a differentiation-dependent preference for either glycolysis or oxidative phosphorylation (OXPHOS) [212]. However, cultured human BMSCs exhibit a highly glycolytic nature [213]. Glycolysis provides not only a source of energy in the form of ATP but also carbon for the generation of biomass in proliferating cells [214]. Glucose can also contribute to different pathways like pentose phosphate pathway which contributes to nucleotide synthesis and reducing molecules for anabolism and oxidative stress mitigation, or serine-synthesis pathway to contribute to the biosynthesis of nucleotides, amino acids, and lipids [214]. However, the specific roles of these pathways in skeletal stem cells have not been extensively studied yet.

The low oxygen tensions (1–2%) prevalent in the BM [215] may promote a glycolytic phenotype [213]. This is suggested by observations that the *in vitro* expansion of BMSCs under ambient oxygen levels (20–21%) progressively increases mitochondrial glucose oxidation, a process associated with increased oxidative stress and cellular senescence [213]. In BMSCs the transcription factor hypoxia-inducible factor 1α (HIF-1α) plays a crucial role in regulating this glycolytic phenotype [216, 217]. Furthermore, the loss of HIF-1α showed negative effect on cell survival in bone highlighting the importance of HIF-1α for BM microenvironment functionality in conditions of oxygen and nutrient deficiency [217]. Intriguingly, skeletal progenitors are often located in perivascular areas within both the BM and periosteum under normal conditions [218, 219], raising questions about their potential dependence on HIF-1α stabilization and glycolysis in their native niches. Moreover, the exact role of glucose oxidation in skeletal stem cells, especially in *in vivo* environments, remains to be clarified.

When glucose is predominantly utilized in glycolysis for bioenergetics or biosynthesis, other nutrients can support the mitochondrial tricarboxylic acid (TCA) cycle to satisfy cellular demands. The TCA cycle not only provides reducing equivalents (NADH and FADH2) for oxidative phosphorylation but also supplies metabolic intermediates for biosynthesis and cellular signaling [220]. Apart from glucose-derived pyruvate, several other metabolites can fuel the TCA cycle by providing acetyl-CoA for oxidation (e.g. FA or ketone bodies) or acting as anaplerotic substrates (e.g. glutamine or odd-chain FAs) [220]. There is still a lack of information about role of FA oxidation in skeletal stem cells. This pathway does not contribute heavily to cellular ATP production in human BMSCs (approximately 0.5 %) [221]. However, recent studies deleting important enzymes involved in FA oxidation like palmitoyltransferase

1a in mouse skeletal stem cells and periosteal stem cells showed no significant changes in cell viability, suggesting that their metabolism does not heavily depend on FAs [222].

Amino acid metabolism is critically important for cellular energetics and biosynthesis, especially in proliferating cells [223]. Human and mouse BMSCs actively take up glutamine in culture [224]. The depletion of extracellular glutamine, inhibition of glutaminase (GLS) - the enzyme that converts glutamine to glutamate while releasing ammonia - or inhibition of glutamate transaminases, which connect glutamine catabolism to both the TCA cycle and amino acid synthesis, significantly reduces colony formation and proliferation of mouse BMSCs [224]. In culture, BMSCs utilize glutamine for fueling the mitochondrial TCA cycle, amino acid synthesis, and glutathione biosynthesis [224, 225].

Later, during the differentiation, cells change their metabolic demands according to the cell type they change into. As it was already mentioned, glucose is very important metabolite for bone cells preserving the “stemness” of proliferating BMSCs [226]. However, there are some studies indicating the importance of glucose metabolism as energy source for BMSC differentiation [227, 228]. These studies have shown that inhibition of glycolysis has been found to significantly suppress osteogenesis in primary BMSCs [227]. Similarly, when glycolysis pathways are diminished in BMSC-like ST2 cells, there is a noticeable decrease in osteogenesis and mineralization [228]. This highlights the critical role of glycolysis in the osteogenic differentiation and function of BMSCs. On the other hand, another study has suggested that the osteogenic differentiation of BMSCs requires a metabolic transition from glycolysis to an enhanced reliance on mitochondrial OXPHOS [229]. This shift is thought to be crucial for ensuring an adequate energy supply required for the osteogenic differentiation process. This finding implies that the metabolic requirements of BMSCs may vary significantly during their differentiation into specific cell lineages, such as osteoblasts.

Furthermore, research findings regarding the role of OXPHOS in the osteogenic differentiation of BMSCs vary. Some studies have indicated that OXPHOS is activated in BMSCs during osteogenic differentiation, potentially through mechanisms such as the downregulation of HIF-1 expression or by promoting β-catenin acetylation in C3H10T1/2 cells [230]. Inhibition of OXPHOS has been shown to reduce the osteogenic potential of these cells [230]. However, opposite results have been reported by Pattappa et al., who found no significant change in OXPHOS activity during human MSCs (hMSCs) cell line [231]. Similar findings were reported by Esen et al. in ST2 osteoblastic cells [232]. On the other hand,

Hofmann et al. observed that OXPHOS supercomplexes are indicative of adipogenic, but not osteogenic, differentiation in hMSCs [233].

These diverse findings suggest that while OXPHOS is crucial in regulating the osteogenic differentiation of C3H10T1/2 cells through mechanisms like intracellular β-catenin signaling pathways or HIF1α level modulation, it may not be necessary for the osteogenic differentiation of human MSCs and ST2 cells. However, OXPHOS appears to contribute to the adipogenic differentiation supporting the cells with energy for histon acetylation and activation of adipogenic programs [234]. These differences of BMSC metabolism between adipo and osteo pre-commited BMSC were also documented in recent paper by Tencerova et al. [207] where they also observed these metabolic differences which may be a consequence of different metabolic demands of organism. They also compared metabolic response of immortalized BMSC cell line with adipose-derived stem cell line 3T3-L1 which showed that during adipogenic conditions pre-committed BMSC responds in the same trend to insulin stimulation as 3T3-L1 cells in terms of analysis of lipid content within the cells [207]. Moreover, the similarity in metabolic difference of osteoblast-like cells and 3T3-L1 cells was documented by Guntur et al. [235], where they showed preference of OXPHOS as energy source by 3T3-L1 cells compared to glycolysis preference by osteoblast-like cells.

FA and amino acid metabolism play crucial roles in the differentiation of BMSCs. For FA metabolism, it has been established that they serve as a significant energy source for skeletal progenitor cells, second only to glucose [236]. Studies have shown that long-chain saturated FAs like palmitate can inhibit osteogenic differentiation in hMSCs [237, 238], a process that can be mitigated by oleate [238, 239]. Conversely, arachidonic acid tends to favor adipogenic differentiation while inhibiting osteogenic differentiation [240]. Enhancing FA oxidation promotes osteogenic differentiation, whereas its suppression can favor chondrogenic differentiation [222]. FA-specific receptor GPR120 is present in BMSCs and increases during osteogenic induction, indicating FA role in facilitating bone formation [241].

Regarding amino acid metabolism, glutamine is pivotal in BMSC differentiation [242]. It serves not only as an energy source but also as a donor for various biosynthetic processes. Glutamine metabolism, particularly through the TCA cycle, provides ATP necessary for BMSC energetic and synthetic demands during osteogenic differentiation [224, 243]. The enzyme GLS and glutamine metabolite α-ketoglutaric acid (αKG) also enhance the osteogenic

potential of BMSCs, with the latter reducing histone methylations [224, 244]. These insights into glutamine metabolism could offer new therapeutic avenues for bone loss treatments.

1.4. Obesity and metabolic complications in relation to bone homeostasis

1.4.1. Characterization of obesity and T2D

Obesity is a global epidemic affecting millions of people of all ages and socioeconomic statuses. According to the World Health Organization (WHO), the prevalence of obesity nearly tripled between 1975 and 2016, indicating a disturbing upward trend (https://www.who.int/news-room/fact-sheets/detail/obesity-and-overweight). Obesity is characterized as a complexed metabolic disease caused by imbalance between energy intake and energy expenditure [245]. From medical point of view, Body Mass Index (BMI) is used to define whether your body weight is healthy based on your weight and height [246]. The health implications of obesity are extensive and multifaceted. It is a major risk factor for numerous chronic diseases, including cardiovascular diseases (like heart disease and stroke), which are leading causes of death worldwide. Obesity is also linked to a higher incidence of certain cancers, musculoskeletal disorders like osteoarthritis, osteoporosis and respiratory problems such as sleep apnea [247].

One of the most significant health concerns associated with obesity is its link to T2D, a chronic condition characterized by insulin resistance and high fasting blood glucose levels. The relationship between obesity and T2D is well-established, with the former being a major risk factor for the development of the latter [248]. Obesity leads to increased circulating lipid levels and inflammation, which contribute to insulin resistance. When the body cells become resistant to the action of insulin, blood sugar levels rise, paving the way for T2D [248].

T2D is a metabolic disorder that results in high blood sugar, insulin resistance, and a relative lack of insulin- at the beginning there is a high insulin level, which with longer chronic prevalence of T2D leads to impairment of insulin production [249], which is opposite to type 1 diabetes characterized by inability of beta cells to produce insulin. The failure of β-cells, losing approximately 80% of their functionality, coupled with insulin resistance in muscle tissues and the liver, forms a detrimental trio at the heart of T2D physiological aberrations [250]. The onset of T2D is often gradual and can develop over many years. Symptoms may include increased thirst, frequent urination, hunger, fatigue, blurred vision, and slow-healing

sores or frequent infections. Risk factors for T2D include obesity, physical inactivity, genetics, age, increased VAT and certain health problems such as high blood pressure [248].

However, it is well known, that obesity and T2D cause AT dysfunction characterized by increased size of adipocytes, adipokine secretion from AT and ectopic fat accumulation [251]. Ectopic fat refers to the accumulation of TAGs within organs not primarily designed for fat storage, such as the liver, skeletal muscle, heart, pancreas [252], and notably, bones [135]. This abnormal fat deposition can disrupt the normal function of cellular microenvironment within the organs, leading to complications like osteogenic and hematopoietic regeneration, which is a common precursor to various metabolic disorders [135].

1.4.2. Obesity and impact on bone homeostasis

Obesity can lead to a systemic inflammatory state that disrupts the balance of bone remodeling, resulting in dysregulated bone homeostasis and subsequent bone loss. This disruption is driven by two primary mechanisms: (i) obese AT releases pro-inflammatory mediators that diminish osteoblast activity while promoting osteoclast differentiation and bone resorption; and (ii) during obesity, the differentiation of BMSCs towards the osteogenic lineage is inhibited, whereas adipogenic differentiation is favored [253, 254]. The hypertrophic AT enhances the expression and secretion of cytokines like TNF-α, IL-1β, IL-6 and the infiltration of M1-like macrophages and other immune cells [255]. Whether acting independently or synergistically, these cytokines can activate intracellular signaling pathways leading to bone degradation.

TNF-α is well known for its pro-osteoclastic effect, enhancing the formation of multinucleated TRAP-positive cells alongside RANKL [256, 257]. Previous studies have demonstrated that TNF-α stimulates osteoclast precursors in obese mice fed a HFD and increases RANKL expression in BM macrophages [258, 259]. Additionally, HFD-fed mice exhibit lower trabecular numbers and thickness and reduced trabecular bone volume compared to their lean counterparts [260]. Conversely, TNF-α knockout mice fed with HFD experienced less bone loss, fewer femoral osteoclasts, and increased RUNX2 expression in BMSCs than HFD-fed wild-type mice [260]. The upregulation of RANKL by TNF-α in stimulated osteocytes further promotes osteoclast differentiation, both *in vitro* and *in vivo* [261]. TNF-α also affects osteoblast activity; it reduces the expression of osteogenic transcription factors RUNX2 and osterix in osteoblasts or BMSCs undergoing osteogenic differentiation, leading to

decreased mineralization and expression of bone markers such as OCN and ALP [259, 262]. Moreover, TNF-α induces the upregulation of miR-150-3p in osteoblasts, which in turn decreases β-catenin expression, a crucial transcription factor for osteogenesis [263]. TNF-β similarly exerts a harmful effect on bone by reducing the expression of RUNX2, collagen type I, OCN, and diminishing mineralization during BMSC osteoblastic differentiation [264].

Elevated levels of IL-1β in the bloodstream are indicative of the chronic, low-grade inflammation typical of obesity and its related conditions [265]. Moreover, IL-1β is recognized for its ability to promote osteoclast migration and bone resorption [266-268]. When combined with RANKL, IL-1β significantly boosts osteoclast formation *in vitro* by increased TRAP staining and the upregulation of osteoclast-specific markers such as cathepsin K, OSCAR, NFATC1, Cfos, and DC-STAMP [267-271].

While osteoblasts are primarily known for synthesizing the extracellular matrix, IL-1β has been found to increase the production of metalloproteases by these cells [272]. Yang et al. demonstrated that IL-1β elevates the expression of MMP-9 and MMP-13 in osteoblasts [273], further exacerbating bone degradation in the context of inflammatory conditions. Additionally, IL-1β can disrupt the production of hormonal factors by bone tissue, including FGF23, which plays a crucial role in regulating serum levels of vitamin D and phosphate [274, 275]. An overactive FGF23 response can lead to disrupted mineralization processes, contributing to bone fragility [276].

In vivo model of bone loss using the application of neutralizing IL-6 antibodies demonstrated a protective effect against osteoporosis, indicated by improvements in bone mineral density, trabecular number, and thickness [277]. The inhibition of IL-6 resulted in a decreased ratio of RANKL/OPG in osteoblasts and reduced osteoclast differentiation within a microgravity model [277]. Additionally, IL-6 was found to suppress osteoblast activity through the downregulation of the osteogenic transcription factor RUNX2 [277, 278]. Osteoblasts lacking IL-6 showed increased activity of ALP and higher expression of RUNX2 compared to wild-type. Furthermore, these IL-6 knockout mice fed with HFD displayed a significant increase in trabecular bone volume, number, and thickness compared to HFD-fed wild-type mice, highlighting critical role of IL-6 in bone metabolism and its potential as a therapeutic target for enhancing bone health in obesity-related osteoporosis [279].

Hyperglycemia and HFD lead not only to increased osteoclast activity but it also contributes to alterations in BM and immune function stimulating neutrophil activation [181, 280, 281].

Morbid obesity increases circulating neutrophils, enhancing their inflammatory potential [282]. High glucose conditions also promote thrombocyte maturation in the liver and BM, impacting megakaryocyte activation [283]. Furthermore, obesity increases eosinophil number in BM of mouse model of allergic asthma, affecting their ability to move to the site of the allergic reaction [284]. Study by Liu et al. [285] highlighted the impact of obesity on BMSC mobilization and the selective migration of specific immune cells.

However, recent works by Tencerova et al. [180, 181] have reported that obesity does not necessarily lead to increased inflammatory responses in the BMSCs and HSCs of HFD male mice or obese men, compared to their lean controls. Further, Trotter et al, showed no changes of inflammatory genes in BM of HFD mice compared to lean [286]. However, another study using 5-week-old male mice on HFD, showed not only higher rates of osteoclast precursors but also increased osteoclast formation, bone resorption activity, and elevated expression of factors critical for osteoclastogenesis such as RANKL, TNFα, and TRAP [258]. Moreover, acute exposure to dietary FAs increased osteoclastogenic activity in circulating monocytes and cytokine secretion [287]. However, study by Tencerova et al. using HFD in 12-week-old C57BL/6 male mice [181] showed no significant changes in osteoclast activity or number. Conversely, a clinical study in obese subjects indicated a reduction in both bone resorption and formation, suggesting a decrease in bone turnover [180].

As we described in previous chapters, BMSC differentiation may function as molecular switch between osteoblast and adipocyte differentiation. However, during obesity, differentiation capacity of BMSCs is altered in favor of adipocyte formation over osteoblast and chondrocyte differentiation [181]. This shift impairs bone homeostasis and affects the production of secretory factors that influence neighboring cell functions in the BM [135, 288]. Recent studies have showed negative effect of increased BMA on bone homeostasis in both mouse and humans [180, 181, 289-291]. Results from experiments using C57BL/6J mice and 12 or 20 weeks long HFD intervention showed deleterious effect of the HFD on bone microstructure and increased BMAT compared to control diet [181]. Moreover, differentiation potential of BMSC was shifted toward adipocyte differentiation after HFD intervention compared to control. Similar results were observed in the human study using obese male individuals with increased insulin signaling and adipocyte progenitors in BM microenvironment suggesting mechanism of obesity-associated bone fractures [180]. From the metabolic point of view, these changes increased use of glucose and OXPHOS by BMSC which leads to increased production of reactive oxygen species (ROS) and cellular exhaustion

resulting in increased senescent phenotype of cells in obese individuals compared to lean controls. Moreover, the senescent cellular phenotype is typical also for AT-MSCs of obese individuals [292] which highlights importance of studying of BMSC in context of treatment of T2D and obesity [180].

In context of effect of obesity on whole bones, there are evidences of negative impact of HFD on bone mechanical properties and bone microstructure. Several *in vivo* studies are showing decreased bone strength, stiffness and fracture toughness using 3-point bending test of femurs [293], reduced bone mass [294-296], trabecular density [297], trabecular bone volume, bone mineral content and quality [298] by HFD in male mice. Studies are also reporting smaller effect of HFD on cortical bone caused by strengthening of this bone part by increased body weight load and by the fact that trabecular bone exhibits higher bone surface to volume ration then cortical. However, decreased bone mechanical properties together with increased BMA are two major factors contributing to increased fracture risk in obese and T2D patients [180, 181].

To sum up, obesity has a negative effect on bone homeostasis, considering its impact on structural, mechanical properties and cellular changes, differentiation capacity and their molecular functions (summarized in Figure 6), which need to be studied in more details in connection to interventional studies.

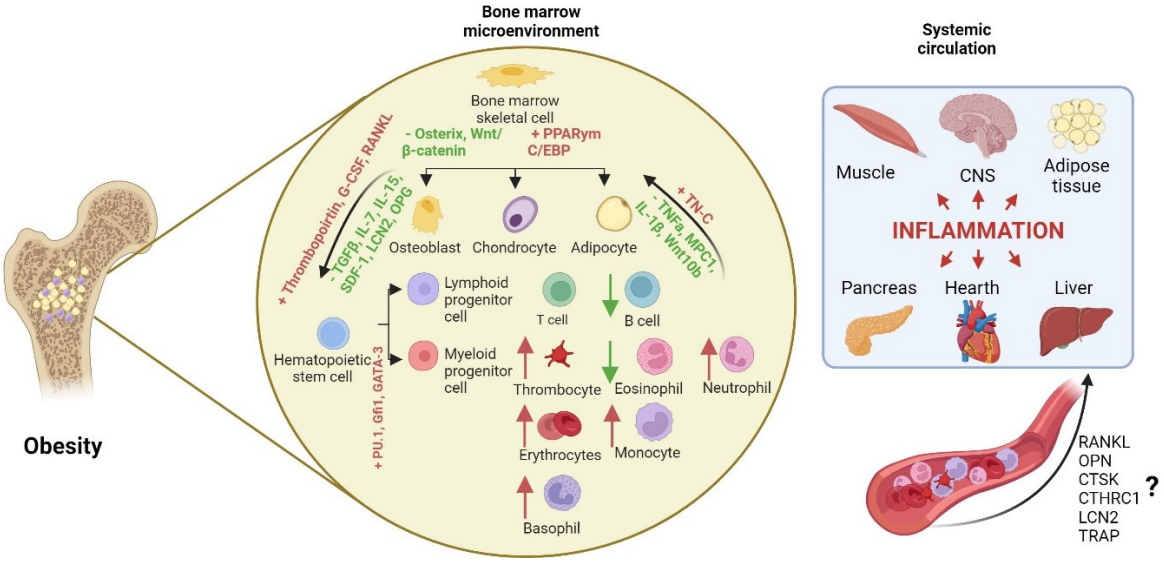

Figure 6. The impact of obesity on bone structure and differentiation fate of BMSC and HSC. Changes in BM homeostasis due to obesity involve alterations in the cellular composition and the profile of bioactive molecules secreted by HSCs and BMSCs. These modifications are linked to broader systemic effects that influence whole-body metabolism and inflammation. Figure adapted from [6] and created in Biorender.com.

1.4.3. Comparison of peripheral adipose tissue and BMAT in response to metabolic complications

In the previous chapter, we summarized the effect of obesity on BMAT biology and bone health describing increased adiposity within BM and decreased inflammatory response. Thus, it indicates that there are some metabolic differences between BMAT and peripheral fat in response to obesity.

Peripheral AT reacts on increased caloric intake related to obesity by hyperplasia (increased number) and hypertrophy (increased size) of adipocytes. Even though, hyperplasia is typical also for "healthy" fat expansion, however hypertrophy usually leads to lipid dysfunction associated with increased cell death, inflammation and other pathologies [299]. This pro-inflammatory phenotype of obesity is caused by ectopic storage of FFAs in non-adipose organs like liver or muscle [300]. These toxic lipids can disrupt the function of several critical cellular organelles, including mitochondria, the endoplasmic reticulum (ER), and lysosomes [301-303].

Chronic obesity and excessive nutrition lead these organelles into a state of dysfunction, creating a domino effect where the malfunctioning of one organelle adversely impacts the others, resulting in cellular damage, systemic dysfunction, and ultimately, cellular apoptosis. The resulting systemic inflammation and increased ROS production exacerbate the situation. Immune cells are recruited to the inflamed regions in an attempt to mitigate the damage, yet these cells can also contribute to the inflammation originating from the affected sites. The inflammation, fueled by ER stress and lysosomal dysfunction, relies on overloaded calcium (Ca2+) and ROS as signaling messengers [302, 303]. This inflammatory environment is a key factor in the development of insulin resistance, highlighting the intricate link between cellular stress, systemic inflammation, and metabolic disease [304].

On the other hand, the expansion of BMAT associated with obesity does not impair insulin sensitivity in BMAds, pointing to an important contrast to the reduced insulin sensitivity observed in peripheral AT under similar conditions, but without pro-inflammatory condition in BM, even though hyperplasia and hypertrophy occur in BMAT under obesogenic conditions too [120, 305]. Notably, adults with morbid obesity and T2D, characterized by elevated serum insulin levels, show increased BMAT volume at critical skeletal sites like the lumbar spine and femoral metaphysis, compared to non-diabetic individuals [306].

This set of evidence suggests that changes in insulin receptor functionality or insulin levels play a significant role in regulating BMAT development, however, there are huge differences between response of peripheral and bone adipocytes to obesogenic conditions.

1.5. Treatment of obesity and T2D in relation to bone health

1.5.1. Classification of obesity and T2D treatment

When obesity and T2D is diagnosed in patients, first line treatment is mainly based on reduction of accumulated fat by healthy lifestyle changes like physical activity, diet intervention or lifestyle changes [307, 308]. In line with this treatment, pharmacological treatment is used to enhance overall well-being of individuals with obesity and T2D targeting specific metabolic or inflammatory pathways impaired in these disorders, indicating that multifaceted approach is necessary to tackle the complexities of this metabolic disorder [309].

In addition, huge global incidence of obesity has created a constant need for new drugs for this disease. There are several approaches in development of new pharmacological treatments for this disease which will be discussed in the following chapter.

1.5.2. Non-pharmacological and pharmacological interventions

Optimal management of obesity and diabetes focuses on maintaining plasma glucose levels and weight gain within the normal physiological range to a healthy, non-diabetic individual, while avoiding the risk of hypoglycemia. In a healthy person, normal weight gain and plasma glucose levels are influenced by dietary nutrient intake, physical activity, and hormones that regulate glucose homeostasis (insulin) and satiety (leptin) which should be consequently taken to account during obesity and diabetes management [310, 311]. Moreover, these strategies lead also to improve negative impact of obesity on bone metabolism and obesity-induced bone fragility [312-314].

To reduce the load of increased caloric intake, exercise is often used to protect against obesity [313]. Exercise has been shown to effectively normalize body weight, decrease body fat, enhance glucose metabolism, and reduce markers of systemic inflammation in mouse models of diet-induced obesity [315, 316] because of mechanical stimulation induced by exercise to promote bone remodeling and healthy bone homeostasis. Recent studies using 12 or 14 week-long voluntary exercise (running wheels) C57BL/6 male mouse model of obesity showed improved bone volume in tibia and vertebra, trabecular parameters (BMD, trabecular number, trabecular thickness) in tibia, bone mechanical and material properties and decreased BMAT-induced by obesity [317, 318].

Further, many modifications in the diet have been made to reveal potential dietary supplements which can positively affect whole body metabolism and decrease negative side effects of obesity also on bones [224, 319]. Glutamine, a nonessential amino acid, plays a crucial role in regulating oxidoreductase activity and inflammation [320]. Among the components of a protein-enriched diet, the inclusion of glutamine has shown to have beneficially impact on bone metabolism, underscoring its significance in nutritional strategies aimed to improve bone health [224]. Glutamine metabolism is fundamental in controlling the proliferation of BMSCs, their allocation to specific lineages, and the differentiation of osteoblasts [224]. Previous studies showed improved BMD, trabecular and cortical architecture of bones of Balb/C female mouse using monosodium glutamate [321].

Further, changing composition of diet in terms of fat content (i.e. enrichment of omega-3 polyunsaturated FAs (omega 3- PUFAs) showed positive effect on whole-body metabolism and bone. Emerging evidence highlights that the promotion of a "healthy adipocyte" phenotype can be influenced by several natural factors, including physical activity, calorie restriction, and particular dietary constituents, notably omega-3 PUFAs. Long-chain omega-3 PUFAs, such as eicosapentaenoic acid (EPA; 20:5n-3) and docosahexaenoic acid (DHA; 22:6n-3), have been shown to offer broad health benefits [322]. These include acting as natural hypolipidemics, reducing hepatic lipid accumulation [323], increasing plasma levels of adiponectin [324], ameliorating low-grade inflammation in obesity [325], and enhancing intestinal FA oxidation [326]. Furthermore, omega-3 PUFAs reduced adiposity which one and limit adipocyte proliferation in male rodent obesity models [327, 328], and similar effects on obesity reduction have been observed in human studies [329, 330].

Additionally, both animal and human studies have shown that omega-3 PUFAs positively influence bone health in various pathological conditions, including osteoporosis, obesity, and aging [183, 331]. Previous studies showed inhibitory effect of omega-3 PUFAs on osteoclastogenesis and thus positive impact on bone remodeling [332, 333]. This body of research underscores the potential of dietary interventions, especially those involving omega-3 PUFAs, in managing and preventing diseases related to lifestyle factors. However, there is still lack of studies showing effect of omega-3 PUFA on BMAT phenotype which can help to better understand if this dietary intervention helps also reduce negative effects of obesity or metabolic complications.

From the clinical perspective, weigh reduction is considered as key step to revers metabolic abnormalities caused by obesity and T2D [334, 335]. However, the increasing body of evidence showed that using CR to reduce weight is often coupled with negative side effects on skeletal system such as decreased BMD and increased BMAT [336-339]. Therefore, using the approaches with slower weight reduction needs to be considered to avoid these side effects, Thus, lifestyle modifications including diet intervention and exercise showed to have a positive effect on bone turnover markers [340] and BMD [341] in patients with T2D. From the nutritional interventions eating of food with low glycemic index is often used [342, 343], as well as different kinds of diets like Mediterranean diet (MD), primarily plant-based, is known for its health benefits, particularly in cardiovascular diseases and cancer [344]. Moreover, positive effects of MD on BMD were showed, however these results might be due to composition of the diet consisting olive oil, fruits, vegetable and fish rich in anti-inflammatory and antioxidant nutrients [334, 345, 346].

In this chapter we showed positive effects of non-pharmacological approach in obesity and T2D management in animals and humans. However, in many cases, lifestyle interventions are not enough to achieve weight loss and improved glucose and bone metabolism, thus alternative options as pharmacological treatment have to be considered.

1.5.3. Classical treatment of metabolic disorders and its side effects on bone

The management and treatment of obesity and diabetes typically start with lifestyle modifications which are combined with pharmacological treatment. In T2D is primarily managed with drugs that enhance insulin secretion or its activity. Conventional first-line therapies for T2D include biguanides, such as metformin, which increase insulin sensitivity, and sulfonylureas, which boost insulin secretion [347]. Sulfonylureas were also among the first classes developed for T2D management. Their insulin sensitizing effect is mediated directly by stimulation of pancreatic β-cells [348]. They represent second-line of treatment of T2D.

Further, thiazolidinediones (TZDs) target multiple intracellular metabolic pathways to enhance insulin action and improve insulin sensitivity. They function both as nuclear transcription regulators and insulin sensitizers, illustrating their dual role in diabetes management [349]. The use of TZDs as PPARγ agonists is indicated for their ability to enhance insulin sensitivity, thereby aiding in the control of blood sugar levels in patients with T2D. Moreover, TZDs are able to affect metabolic processes through binding of mitochondrial proteins, particularly mitochondrial pyruvate carrier (MPC) (pyruvate transport via MPC is summarized in Figure 7) [350, 351]. Although the effectiveness of TZDs through PPARγ is known [352-354], there are also studies on PPARγ-independent effects of TZDs in which PPARγ KO mice were used [355, 356]. These studies confirm inhibition of MPC, resulting in inhibition of complex I of the respiratory chain, which uses pyruvate as a substrate. Divakaruni et al. also found that two classical TZDs, pioglitazone and rosiglitazone, affect the ADP/O2 ratio in human myocytes and mouse primary myoblasts, which may lead to a shift toward anaerobic metabolism [356]. Research by Colco et al. additionally demonstrated that pioglitazone is also able to bind to the mitochondrial protein mitoNEET (mitochondrial membrane-associated protein (mito) containing the amino acid sequence Asn-Glu-Glu-Thr (NEET)), which is associated with complex I of the respiratory chain. It follows that this TZD is capable of inhibiting mitochondrial metabolism not only through MPC but also through the protein mitoNEET [357]. On the contrary, the study by Rabøl et al. showed a different effect

of pioglitazone and rosiglitazone on mitochondrial metabolism, where pioglitazone increased the level of respiration and rosiglitazone decreased it in muscle cells [358].

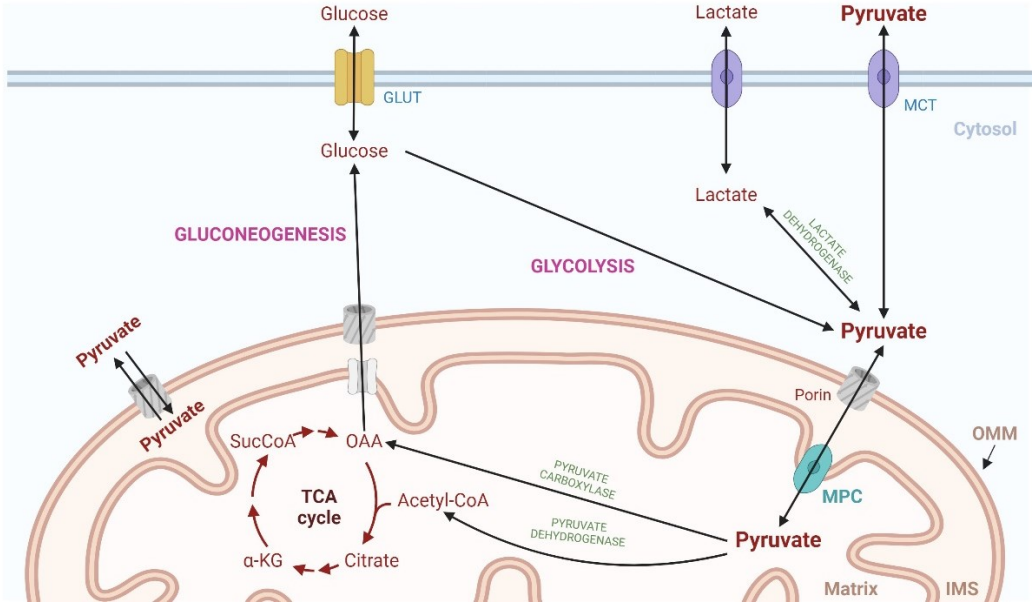

Figure 7. Pyruvate transport to mitochondria. Schematic figure showing how pyruvate is transported into the mitochondrial matrix via MPC protein in the inner mitochondrial membrane (Figure created in Biorender). (Abbreviations: α-KG, alpha keto-glutarate; GLUT, glucose transporter; IMS, inner mitochondrial membrane; MCT, monocarboxylate transporter; MPC, mitochondrial pyruvate carrier; OAA, oxaloacetate; OMM, outer mitochondrial membrane; SucCoA, succinyl-coenzyme A)

These two TZDs were approved as monotherapy drugs in conjugation with lifestyle modification like exercise, diet or weight reduction. However, rosiglitazone went through critical examination and The US Food and Drug Administration (FDA) highlighted cardiovascular risks coupled with using of this drug (http://wayback.archive-it.org/7993/20161022203147/http://www.fda.gov/NewsEvents/Newsroom/PressAnnouncements/2007/ucm109026.htm.). Even though all the restrictions have been withdrawn in 2013 (https://www.fda.gov/drugs/drug-safety-and-availability/fda-drug-safety-communication-fda-requires-removal-some-prescribing-and-dispensing-restrictions) the use of rosiglitazone remained controversial and its usage declined significantly [359].

TZDs as insulin sensitizers act primarily by targeting intracellular metabolic pathways to enhance insulin action and increase insulin sensitivity in critical tissues such as muscle and fat [360]. These drugs function by increasing adiponectin levels, which is a cytokine secreted by fat tissue known for its role in improving insulin sensitivity and promoting FA oxidation and improving adipogenic potential of fat cells. Additionally, TZDs reduce hepatic gluconeogenesis and facilitate insulin-dependent glucose uptake in muscle and fat tissues [349, 361]. The primary mechanism through which TZDs achieve their effects is by binding PPARγ [361]. The binding of TZDs to PPARγ induces a conformational change that alters the expression of various genes involved in the regulation of metabolism, including lipoprotein lipase, glucokinase, and fatty acyl-CoA synthase [362]. In addition to their role in glycemic control and the improvement of insulin sensitivity, TZDs have potential anti-inflammatory and anti-cancer properties. Research has shown that these drugs may slow the progression of medial intimal thickening and decrease coronary intimal hyperplasia. They also exhibit beneficial effects on endothelial function, atherogenesis, fibrinolysis, and ovarian steroidogenesis [349]. Some studies have suggested that activation of PPARγ receptors might induce apoptosis in cancer cells. However, these additional mechanisms of TZDs are still under investigation due to contradictory results and the presence of potential confounders [349].

Unfortunately, TZDs have several side effects, particularly when used for a long time. One of the significant side effects of TZDs is dose-related fluid retention, which can occur in up to 20% of patients [349, 360]. There have also been reports indicating that TZDs can cause an increase in intravascular volume, potentially leading to congestive heart failure [363]. Notably, the risk of heart failure and associated mortality is higher with rosiglitazone compared to pioglitazone. This difference in risk profiles further emphasizes the need for careful consideration and monitoring when prescribing TZDs, especially in patients with existing cardiovascular concerns [363].

Another notable side effect associated with TZD treatment is weight gain, which can be attributed to several mechanisms. Adipocytes, which have the highest concentration of PPARγ receptors in the body, are significantly affected by TZDs. Firstly, TZDs upregulate PPARγ receptors in the central nervous system, which can lead to increased feeding behavior [364, 365]. Additionally, TZD agents contribute to the expansion of AT mass by promoting the maturation of preadipocytes into mature adipocytes [366] and by increasing fat storage through the enhanced movement of free FAs into cells. This is connected also with increased

cardiovascular risk of this treatment [367]. Fluid retention associated with TZD use also contributes to weight increase [353].

Another side effect caused by TZD treatment is increased fracture risk [368-370]. The underlying mechanisms for this increased fracture risk and bone density reduction are thought to involve the PPARγ activation and the down-regulation of insulin-like growth factor. Also, it has been shown that TZD increase accumulation of Advanced Glycation End Products (AGEs), compounds that are the products of non-enzymatic reactions between reducing sugars and proteins, lipids, or nucleic acids [371], which leads to impaired bone increased bone fracture risk [372]. These processes can divert the differentiation pathway of osteoblasts towards adipocytes instead of bone-forming cells, leading to bone loss [368, 373]. Interestingly, the fractures associated with TZD use are more commonly observed in the distal extremities, such as the forearm, wrist, ankle, foot, and tibia, rather than in the axial skeleton, which includes the hip, pelvis, and femur. These include postmenopausal females and patients who are concurrently taking medications such as glucocorticoids or proton pump inhibitors. This increased risk necessitates careful consideration and monitoring of bone health in patients undergoing TZD treatment, especially those with additional risk factors for fractures [370, 374, 375].

1.5.4. Modern approaches in treatment of obesity and diabetes in consideration to bone metabolism

Obesity and diabetes, particularly T2D, is indeed a complex chronic endocrine disorder that has become a significant global health challenge [376]. Currently, main pharmacological treatment for T2D includes the administration of insulin or insulin-like agents for those who require it, and oral hypoglycemic agents [377, 378].

There are many different classes of pharmacological treatment currently on the market using different approaches like nano-technology, stem cell therapy or novel lifestyle modifications [379]. Alpha-glucosidase inhibitors work in the gastrointestinal tract to reduce glucose absorption, thus lowering blood glucose levels [380]. Drugs affecting the incretin system have recently increased attention of the clinicians and scientists, including glucagon-like peptide-1 (GLP-1) analogues, which promote early insulin release from the pancreas in the treatment not only T2D but also obesity. GLP-1 are a class of drugs used for the treatment of T2D [381]. They mimic the effects of the GLP-1 hormone, which stimulates insulin secretion after eating,

helping to regulate blood sugar levels, reducing body weight and promote satiety. In T2D, the natural release and response of this hormone can be impaired. There are several drugs approved by FDA from this class, which differ in dosage and administration [381-384]. However, effect of this class of drug is still under the examinations in context of cardiovascular and fracture risk, and the impact on bone metabolism. Previous studies of GIP effect on bones showed promising results showing decreased osteoclastogenesis using human osteoclastic cells [385]. Another relatively novel class of antidiabetic drugs is the sodium-glucose cotransporter-2 (SGLT2) inhibitors [386]. SGLT2 is crucial in glucose reabsorption in the kidneys. Inhibiting this transporter leads to glucosuria, which can help reduce hyperglycemia in diabetes patients [387]. However, studies have shown controversial results of SGLT2 on bone fracture risk. There are studies showing, that SGLT2 may promote osteoclastogenesis via secondary PTH increase [388] and cause mineral structure damage. On the other hand, there are studies showing decreased risk of major osteoporotic fractures (0,3%) with SGLT2 compared to GLP-1 treatment [389].

Indeed, while the development of novel treatments for T2D is essential, it is also crucial to refine existing therapies to enhance their safety and efficacy. First generation of TZDs, including pioglitazone and rosiglitazone, are known for their high insulin-sensitizing effects and direct inhibiting of MPC in mitochondria, however, these drugs vary in their ability to bind and activate the PPARγ transcription factor, a mechanism associated with significant side effects that have constrained the development of new treatments. As a result, one strategic approach in T2D treatment development involves improving these existing medications [390]. The goal is to retain their beneficial insulin-sensitizing effects while minimizing their adverse side effects.

Thus, “second generation” of TZDs shows promise in modulating MPC activity with reduced direct interaction with PPARγ, aiming to retain beneficial effects while minimizing adverse outcomes. MSDC-0160, also known as PNU-91325, is a pioneering modulator of mitochondria target of TZDs (mTOT) [391, 392] referred to as "PPARγ-sparing." As a member of “second generation” of TZDs, MSDC-0160 demonstrates significantly reduced potency in activating PPARγ—about 20 times less than pioglitazone [393]. In a Phase 2 clinical trial, MSDC-0160 doses of 100–150mg achieved reduction of hemoglobin A1c comparable to 45mg of pioglitazone over 12 weeks [392]. Despite its "PPARγ-sparing" label, MSDC-0160 at these doses still induced typical PPARγ activation effects, including fluid retention, weight gain, and elevated adiponectin levels, but these effects were approximately half as pronounced as those

observed with pioglitazone. MSDC-0160 is now being developed for neurodegenerative diseases rather than T2D [394, 395].

Meanwhile, a related compound, MSDC-0602K, showed promise as an effective insulin sensitizer in rodent studies and demonstrated positive outcomes in an unpublished phase 2 diabetes trial (NCT01280695). MSDC-0602K, a novel TZD analog with minimal PPARγ activation, was studied for its effect on insulin resistance in obese mice by Chen et al. [396]. This study showed, that treatment significantly enhanced multi organ insulin sensitivity, reduced adipose tissue inflammation, and corrected hepatic metabolic issues, notably by decreasing hepatic lipogenesis and gluconeogenesis. The beneficial outcomes of MSDC-0602K in reducing insulin resistance pathways were observed even in liver-specific PPARγ knockout mice. This suggests the drug's effects on hepatocytes and metabolic processes like lipogenesis and gluconeogenesis are independent of PPARγ activation, highlighting a PPARγ-independent mechanism of action for MSDC-0602K's therapeutic effects [396]. Further, Fukunaga and colleagues compared effect of MSDC-0602K and rosiglitazone on skeletal homeostasis in BM isolated macrophages and 6 months old male C57BL/6 mice. This study showed reduced osteoclast induction and no effect on bone microstructure and BMAT with MSDC-0602K compared to rosiglitazone [397]. Moreover, recent study by Bardova et al. [398] showed additive positive effect using omega-3 PUFAs and MSDC-0602K in C57BL/6N male obese mice. The study highlighted the synergistic effects of omega-3 PUFA and MSDC-0602K on the metabolism of diet-induced obese mice, emphasizing the importance of TAG/FA cycling in WAT. It also revealed that the two TZDs differentially affected WAT gene expression and metabolism, with these effects being influenced by the presence of omega-3 PUFAs, suggesting a nuanced interaction between dietary components and pharmacological interventions in modulating AT function and overall metabolic health [398].

To sum up, omega-3 PUFAs together with second generation TZD MSDC-0602K showed significant positive effect in treatment of diet induced negative effects on whole-body metabolism and bones. However, there is still missing knowledge about the effect of these treatments on bone and BMAT metabolism under the obesogenic conditions. Thus, the main focus of this thesis would be to bring novel insights in this area of research comparing first and second generation of TZDs together with non-pharmacological treatment with omega-3 PUFAs on bone metabolism and effect on BMAT *in vitro* and *in vivo*.

2. Hypothesis and specific aims

Obesity and T2D are characterized by multiorgan complications, including reduction of bone density/quality and abnormal accumulation of fat in the periphery as well as in the BM. These changes are caused by disruption of bone homeostasis by increased bone resorption and adipogenic differentiation of BMSC over osteoblastogenesis.

Several approaches have been applied in treatment of metabolic diseases, like non-pharmacological (dietary intervention or physical activity) and pharmacological (e.g. insulin, metformin, TZD etc.). Dietary intervention using omega-3 PUFAs as non-pharmacological treatment showed multiple beneficial effect on whole body metabolism as well as on bone and BMSC properties in animal and clinical studies. However, this was also not well studied in obesogenic conditions. Further, TZDs are antidiabetic drugs that bind to PPARγ promotor which leads to improved insulin sensitivity, on the other hand, it also causes side effects by undesired increased fat accumulation in periphery and in the bones contributing to bone fragility and fracture risk. Thus, novel analog of TZDs, MSDC-0602K has been developed with the same insulin sensitizing effect but with lower affinity to PPARγ. This drug is already in phase 2 of clinical trials (NCT01280695), however there is still lack information about effect of this drug on bone and bone marrow adiposity in obesity.

Thus, in this thesis, we tested both approaches, non-pharmacological and pharmacological, using HFD-induced obesity mouse model to investigate the effect of omega-3 PUFA and MSDC-0602K supplementation in HFD diet on obesity-induced bone impairment and fragility risk.

The objectives of the thesis were divided in 3 main aims:

- **AIM 1: To study the effect of dietary interventions on bone and fat metabolism in obese mice.**

- **AIM2: To investigate the effect of novel TZD analog MSDC-0602K on bone and BMAT metabolism in mouse model of obesity**

- **AIM 3: To study potential differences in the mechanism of action of classical TZDs and new analog MSDC-0602K in BMSCs**

3. Results

3.1. AIM 1: To study the effect of dietary interventions on bone and fat metabolism in obese mice.

Reference: *Benova A*, Ferencakova M, Bardova K, Funda J, Prochazka J, Spoutil F, Cajka T, Dzubanova M, Balcaen T, Kerckhofs G, Willekens W, van Lenthe GH, Charyyeva A, Alquicer G, Pecinova A, Mracek T, Horakova O, Coupeau R, Hansen MS, Rossmeisl M, Kopecky J, Tencerova M. Omega-3 PUFAs prevent bone impairment and bone marrow adiposity in mouse model of obesity. Commun Biol. 2023 Oct 14;6(1):1043. doi: 10.1038/s42003-023-05407-8. PMID: 37833362; PMCID: PMC10575870.

Summary: One of the complications of obesity includes an increased accumulation of fat within the bones, leading to an increased risk of fractures. The primary causes of obesity are excessive caloric intake or a diet enriched in saturated and trans-unsaturated FAs, which are associated with an increased BMI and negatively affect bone and fat metabolism. Previous research by Tencerova et al. [181], along with other previous studies [298, 399], have shown that obesity compromises bone quality and alters the phenotype of BMSCs due to enhanced adipogenesis and a senescent microenvironment, resulting in increased bone fragility. Addressing obesity, T2D, and the associated risk of bone fractures presents a significant challenge to healthcare systems, typically requiring lifestyle modifications such as dietary changes or increased exercise.

Omega-3 PUFAs, including DHA and EPA, are essential dietary components due to their numerous health benefits. Both animal and human studies have revealed omega-3 PUFAs positive effects on bone health under various conditions such as osteoporosis, obesity, and aging. Nonetheless, the influence of omega-3 PUFAs on BMSC metabolism and BMA in obesity has yet to be fully explored.

Thus, in the present part of the thesis we showed a positive effect of 2-month long omega-3 PUFA supplementation in HFD on cortical and trabecular bone microstructure of tibia and L5 vertebra, mechanical bone strength of femur and BMAT composition in proximal tibia in male C57BL/6N mice compared to the HFD group. Moreover, *in vitro* experiments with primary BMSCs isolated from mice fed with HFD supplemented with omega-3 PUFAs exhibited a reduction in adipocyte differentiation but an increase in osteoblast differentiation. This shift

was accompanied by a less senescent phenotype and a decrease in osteoclast formation, and bioenergetic phenotype indicating a more favorable BM microenvironment that supports bone formation. Our findings emphasize the positive impact of an omega-3 PUFA-enriched diet on bone and cellular metabolism, suggesting its potential applicability in the treatment of metabolic bone disorders.

Author's contribution: The author of this thesis was mainly involved in the design of *in vivo* and *in vitro* experiments, discussion of the results with the rest of the authors of manuscript, writing of the manuscript and performing following experiments: analysis of the μCT data, isolation of primary BMSCs, assays related to measurement of BMSC differentiation phenotype, measurement of cellular metabolism by Seahorse, isolation, differentiation and TRAP staining of osteoclast and *in vitro* experiments with omega-3 PUFA treatment on BMSCs.

communications biology

ARTICLE

https://doi.org/10.1038/s42003-023-05407-8 OPEN

Omega-3 PUFAs prevent bone impairment and bone marrow adiposity in mouse model of obesity

Andrea Benova[1,2], Michaela Ferencakova[1], Kristina Bardova[3], Jiri Funda[3], Jan Prochazka[4], Frantisek Spoutil[4], Tomas Cajka[5], Martina Dzubanova[1,2], Tim Balcaen[6,7,8], Greet Kerckhofs[6,7,9,10], Wouter Willekens[11], G. Harry van Lenthe[12], Arzuv Charyyeva[1], Glenda Alquicer[1], Alena Pecinova[13], Tomas Mracek[13], Olga Horakova[3], Roman Coupeau[1], Morten Svarer Hansen[14], Martin Rossmeisl[3], Jan Kopecky[3] & Michaela Tencerova[1]✉

Obesity adversely affects bone and fat metabolism in mice and humans. Omega-3 polyunsaturated fatty acids (omega-3 PUFAs) have been shown to improve glucose metabolism and bone homeostasis in obesity. However, the impact of omega-3 PUFAs on bone marrow adipose tissue (BMAT) and bone marrow stromal cell (BMSC) metabolism has not been intensively studied yet. In the present study we demonstrated that omega-3 PUFA supplementation in high fat diet (HFD + F) improved bone parameters, mechanical properties along with decreased BMAT in obese mice when compared to the HFD group. Primary BMSCs isolated from HFD + F mice showed decreased adipocyte and higher osteoblast differentiation with lower senescent phenotype along with decreased osteoclast formation suggesting improved bone marrow microenvironment promoting bone formation in mice. Thus, our study highlights the beneficial effects of omega-3 PUFA-enriched diet on bone and cellular metabolism and its potential use in the treatment of metabolic bone diseases.

[1] Laboratory of Molecular Physiology of Bone, Institute of Physiology of the Czech Academy of Sciences, Prague, Czech Republic. [2] Faculty of Science, Charles University, Prague, Czech Republic. [3] Laboratory of Adipose Tissue Biology, Institute of Physiology of the Czech Academy of Sciences, Prague, Czech Republic. [4] Czech Centre for Phenogenomics & Laboratory of Transgenic Models of Diseases, Institute of Molecular Genetics of the Czech Academy of Sciences, Prague, Czech Republic. [5] Laboratory of Translational Metabolism, Institute of Physiology of the Czech Academy of Sciences, Prague, Czech Republic. [6] Biomechanics lab, Institute of Mechanics, Materials, and Civil Engineering, UCLouvain, Louvain-la-Neuve, Belgium. [7] Pole of Morphology, Institute for Experimental and Clinical Research, UCLouvain, Brussels, Belgium. [8] Department of Chemistry, Molecular Design and Synthesis, KU Leuven, Leuven, Belgium. [9] Department of Materials Engineering, KU Leuven, Leuven, Belgium. [10] Prometheus, Division of Skeletal Tissue Engineering, Katholieke Universiteit Leuven, Leuven, Belgium. [11] FIBEr, KU Leuven, Leuven, Belgium. [12] Department of Mechanical Engineering, KU Leuven, Leuven, Belgium. [13] Laboratory of Bioenergetics, Institute of Physiology of the Czech Academy of Sciences, Prague, Czech Republic. [14] Molecular Endocrinology Laboratory (KMEB), Department of Endocrinology, Odense University Hospital, Odense C DK-5000, Denmark. ✉email: michaela.tencerova@fgu.cas.cz

Obesity is a worldwide health problem associated with metabolic complications affecting whole body metabolism[1]. The higher accumulation of fat in the bones is one of the metabolic complications leading to high fracture risk[2]. Obesity is mainly caused by excess caloric intake or an unbalanced diet, usually consisting of saturated and *trans*-unsaturated fatty acids (FAs) linked with higher body mass index (BMI) and complications affecting bone and fat metabolism[3]. Previous studies, including our findings, documented[4–7] that obesity negatively affects bone quality and phenotype of bone marrow stromal cells (BMSCs) due to increased adipogenesis and senescent microenvironment, which leads to higher bone fragility. Treatment of obesity, type 2 diabetes, and bone fracture risk is challenging for healthcare systems. It usually includes lifestyle changes such as dietary intervention or increased physical activity (reviewed in[8,9]). Omega-3 polyunsaturated fatty acids (omega-3 PUFAs), namely docosahexenoic acid (DHA; 22:6n-3) and eicosapentaenoic acid (EPA; 20:5n-3), are fatty acids (FAs) that cannot be synthesized in sufficient amounts in the body. Therefore, they represent essential diet components with multiple beneficial effects on health (reviewed in[10]). EPA and DHA play a role as natural hypolipidemics, which reduce the accumulation of hepatic fat[11], ameliorate low-grade inflammation caused by obesity[12], increase adiponectin plasma levels[13] and enhance intestinal FA oxidation[14,15]. Moreover, several animal[16,17] and human[18] studies have also shown a positive effect of omega-3 PUFAs on bone health in different pathological conditions, including osteoporosis, obesity, or aging. However, the effect of omega-3 PUFAs on BMSC metabolism and bone marrow adiposity (BMA) under obesogenic conditions has not yet been thoroughly investigated.

Recent animal studies using high fat diet (HFD) supplemented with omega-3 PUFAs in aging osteoporotic models showed a diminished negative impact on bone loss, osteoclastogenesis and BMA[19,20]. Further, Cao et al.[21] reported positive effects of omega-3 PUFAs supplementation on bone parameters in HFD-fed C57BL/6 male mice over 6 months of dietary intervention. However, these studies did not focus their investigation on the early timepoint of dietary intervention with omega-3 PUFAs in younger animals, along with obesogenic conditions corresponding to the early impact of metabolic disturbances on bone homeostasis and stem cell properties in the bone microenvironment.

Previous in vitro studies documented that omega-3 PUFAs induce changes in BMSC plasma membrane composition, which leads to higher osteoblastic differentiation of these cells[22]. In addition, a study by Cugno et al.[23] showed that omega-3 PUFA supplementation of C3H10T1/2 cells could restore its osteoblastic differentiation capacity and inhibit the up-regulation of osteoclast (OC) differentiation of RAW264.7 cells. However, the exact molecular mechanism behind the omega-3 PUFA effect on bone cells and BMA in vivo is unknown.

Thus, the present study aimed to investigate whether omega-3 PUFA supplementation in HFD diet may prevent a detrimental effect on bone microstructure, bone marrow adipose tissue (BMAT), and molecular characteristics of BMSCs and OCs in an animal model of diet-induced obesity using young C57BL/6N male mice.

Results

Omega-3 PUFAs improve bone parameters in obese mice. To investigate the effect of omega-3 PUFAs on metabolic and bone parameters in a HFD-induced animal model of obesity, 12-week-old C57BL/6N male mice were randomly assigned to 8-week-feeding with HFD or HFD supplemented with omega-3 PUFAs (HFD + F) and chow diet (ND) as a control. As a result, metabolic parameters, including body weight gain, glucose tolerance, and fasting insulinemia were worsened by HFD as shown in our previous studies[6,24], which were improved in HFD + F compared to the HFD group without any effect on food intake (Supplementary Fig. 1a–e).

As an extension of the interventional studies mentioned above[6,24], the impact of omega-3 PUFA supplementation in HFD on bone physiology was investigated. μCT analyses of the proximal tibia and L5 vertebrae were performed in treated mice. HFD did not affect bone microstructure in the proximal tibia compared to the ND group (Fig. 1a, b; Supplementary Fig. 2a–d), while omega-3 PUFA supplementation (i.e., HFD + F diet) increased trabecular bone volume (Tb.BV/TV) and trabecular number (Tb.N) in proximal tibia compared to the HFD group (Fig. 1a, b) with no change in other cortical and trabecular parameters measured in the tibia (Supplementary Fig. 2a–d). Further, in L5 vertebrae, trabecular number (Tb.N), trabecular thickness (Tb.Th.) and trabecular separation (Tb.Sp) were not changed in treated mice (Supplementary Fig. 2e–g). However, HFD increased L5 cortical porosity (Ct.Po.) and decreased cortical thickness (Ct.Th.), when compared to the ND group (Fig. 1c, d), while omega-3 PUFA-enriched diet improved L5 Ct.Po (HFD vs. HFD + F, $p = 0.0101$), Ct.Th. (HFD vs. HFD + F, $p = 0.0384$) and cortical bone volume (Ct.BV/TV) (HFD vs. HFD + F, $p = 0.0465$) and cortical area fraction (B.Ar/T.Ar) (HFD vs. HFD + F, $p = 0.0465$) (Fig. 1c–f) compared to the HFD group, reaching more improved results than ND group (Fig. 1c, d). These changes are depicted in the 3D representative pictures of cortical bone with highlighted pores in the cortex (Fig. 1g). Further, measurement of mechanical properties using a three-point bending test showed stronger femora in HFD + F mice compared to HFD and ND group (Fig. 1h). Moreover, assessment of the ratio of circulating levels of bone formation marker procollagen type 1 N-terminal propeptide (P1NP) and bone resorption marker tartrate-resistant acid phosphatase (TRAP) (P1NP/TRAP) revealed a increased bone formation rate in the HFD + F vs. ND group (ND vs. HFD + F, $p = 0.0038$) (Fig. 1i; Supplementary Fig. 2h, i).

Thus, these findings demonstrated that omega-3 PUFAs supplemented for 8 weeks diminished the negative impact of HFD feeding on bone microstructure and bone strength in obese mice.

Omega-3 PUFAs decrease BMAT volume in obese mice. To further examine the impact of omega-3 PUFA treatment on BMA, BMAT volume was analyzed using contrast-enhanced X-ray microfocus computed tomography (CECT). In order to visualize BMAT in mouse bones, we used a contrast-enhancing staining agent (CESA), Hexabrix, which has been previously shown to visualize the adipocytes in the bone marrow (BM) cavity[6] and allowed faster tissue staining as it is a smaller molecule compared to other used CESA 1:2 Hafnium-substituted Wells-Dawson polyoxometalate (POM)[25].

CECT analysis of Hexabrix-stained bone marrow adipocytes (BMAds) showed increased BMAd number in HFD compared to the ND group, as previously published using OsO_4[4,5]. This increase was prevented by omega-3 PUFAs in HFD + F mice (HFD vs. HFD + F, $p = 0.0005$) (Fig. 2a, b). Further image analysis revealed that the differences in BMAd number across the three groups correlated with both BMAT volume (Fig. 2c) and diameter of adipocytes (Fig. 2d). Interestingly, in response to omega-3 PUFAs, both parameters were normalized to the level of the ND group. These changes in BMAT volume measured by CECT were also confirmed by histomorphometric analysis of H&E-stained sections of the proximal tibia (Fig. 2e–g).

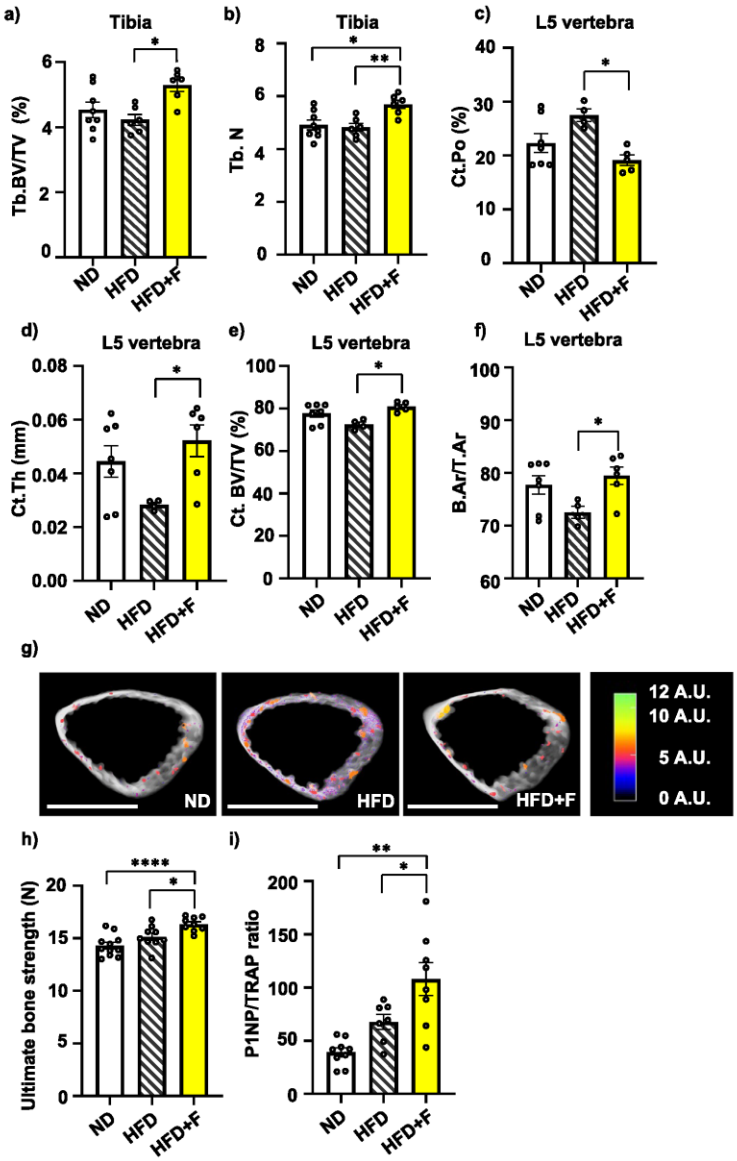

In summary, this data shows the impressive impact of omega-3 PUFAs in terms of BMAT volume reduction in the bones of obese mice, which reached the values of ND mice.

Omega-3 PUFAs improve the lipidome and metabolome of circulating plasma and BM in obese mice. To further characterize the impact of omega-3 PUFAs on plasma levels and bone microenvironment in obese mice, a global lipidomic and metabolomic analysis was conducted using liquid chromatography-mass spectrometry (LC-MS) on samples from plasma, BM, and bone powder (BP) obtained from treated mice. The analysis revealed a total of 905 metabolites, including polar metabolites and several simple and complex lipids across these three biological matrices with an overlap of 83%. Furthermore, the dataset was subjected to partial least-squares discriminant analysis (PLS-DA). The PLS-DA results demonstrated a distinct separation of HFD and HFD + F groups from ND in all matrices based on individual lipid species, while less separation using polar metabolites was observed (Supplementary Fig. 3a–c).

Fig. 1 Omega-3 PUFAs protect bones from the detrimental effect of HFD in obese mice. a, **b** µCT analysis of trabecular bone in proximal tibia in treated mice. Trabecular parameters were calculated as (**a**) trabecular bone volume per total volume of trabecular space (Tb.BV/TV) and (**b**) trabecular number (Tb.N). µCT analysis of cortical parameters of L5 vertebrae was calculated as (**c**) relative amount of pore space in the volume of cortical bone (cortical porosity (Ct. Po)), (**d**) mean cortical thickness (Ct. Th), and (**e**) cortical bone volume per total volume (Ct. BV/TV). **f** cortical area fraction (B.Ar/T.Ar) ($n = 4$–8 per group; one-way ANOVA, Tukey's multiple comparison test with $^{*}p \leq 0.05$, $^{**}p \leq 0.01$). **g** Representative pictures of 3D reconstructed µCT images from cortical bone analysis of L5 vertebrae (scale bar 1000 µm) with the colorimetric scale of pore size (scale bar 0–12 A.U.: shades of pseudocolors represent size of pores divided into categories according to their volume). Pictures were created using CTvox. **h** The ultimate bone strength of femurs was evaluated as the first point of the plateau of the load-displacement curve measured during a three-point bending test ($n = 9$–11 per group; one-way ANOVA, Tukey's multiple comparison test, with * $p \leq 0.05$, **** $p \leq 0.0001$). **i** Analysis of the ratio of circulating markers of bone resorption (P1NP) and bone formation (TRAP) in murine plasma samples after 8 weeks of dietary intervention ($n = 8$-10 per group; one-way ANOVA, Tukey's multiple comparison test with * $p \leq 0.05$, ** $p \leq 0.01$). Data are presented as mean ± SEM (groups coding: white column-ND, black line shading-HFD, yellow column-HFD + F).

From a broader perspective, using the sum of the abundances of unique lipid species for each lipid class, 24 out of 32 were significantly decreased in plasma, especially triglycerides (TG), diacylglycerols (DG), cholesterol, ceramides (CER), and phosphatidylcholines (PC) in HFD + F compared to HFD group (Fig. 3a). On the other hand, only three lipid classes (lysophosphatidylglycerol (LPG), *N*-acyl ethanolamines (NAE), and ether-linked phosphatidylinositol (EtherPI)) were altered in BM (Fig. 3b), and four lipid classes (fatty acid ester of hydroxy fatty acid (FAHFA), EtherPI, ether-linked triacylglycerol (EtherTG), and cholesteryl ester (CE)) in BP (Fig. 3c). Further detailed analysis of the abundance of individual lipid species and polar metabolites revealed interesting changes in circulating metabolites in plasma compared to BM and BP (Supplementary Fig. 4, 5, 6). Specifically, the significant enrichment of DHA (22:6n-3) and EPA (20:5n-3) in both plasma and BM in the HFD + F group vs. HFD group (Supplementary Fig. 4, 5) suggests their contribution to the beneficial effect on improving metabolism and local BM microenvironment in obese mice. Furthermore, these findings showed that dietary supplementation of omega-3 PUFAs in HFD has a positive impact on decreasing circulating levels of lipids in HFD mice along with increased levels of DHA and EPA in BM, thus confirming data from µCT evaluation on different BMAT compositions in individual groups.

Omega-3 PUFAs improve the differentiation capacity of BMSCs in obese mice. To evaluate the impact of omega-3 PUFAs treatment on cellular characteristics of BMSCs, primary BMSCs were isolated from mice subjected to different dietary interventions to evaluate their molecular phenotype. While a short-term proliferation rate of primary cultures did not differ between the groups (Supplementary Fig. 7a), the colony-forming units-fibroblast (CFU-f), a marker of stem cell properties, showed an increased number in the HFD + F compared to the HFD group (Fig. 4a, b).

Further, HFD increased adipocyte (AD) differentiation of primary BMSCs after 8-week treatment in mice compared to cells isolated from ND mice, which was visualized by Oil Red O (ORO) staining (Fig. 4c). This impact of HFD on BMSCs was prevented by omega-3 PUFA supplementation as primary cultures of BMSCs from HFD + F mice showed less ORO-positive AD (Fig. 4c). These changes were also confirmed by gene expression profile of adipogenic markers (*Ppary2, Cebpa, Adipoq, Cd36, Fsp27, Vcam*), which were decreased in BMSCs from the HFD + F compared to HFD or ND group (Fig. 4d). Moreover, expression of oxidative stress (*Hmox1*) and inflammatory markers (*TNFα*) was decreased in the HFD + F compared to the HFD group, and the expression of senescence marker (*p53*) was downregulated in HFD + F compared to ND (Fig. 4e).

On the other hand, the osteoblast (OB) differentiation potential of primary BMSCs was decreased by HFD measured by Alizarin staining (AZR) and alkaline phosphatase (ALP) activity in comparison to the ND group, which was improved by supplementation with omega-3 PUFAs in obese mice (Fig. 4f±h). Importantly, these changes were further confirmed by gene expression of osteoblastic genes (*Alpl, Oc, Col1a1, Bmp2, Ctnnb1*) (Fig. 4i), which is consistent with the results from µCT analysis of bone and BMAT parameters. Thus, these data demonstrate that omega-3 PUFA supplementation of HFD positively impacts the cellular characteristics of BMSCs and improves their differentiation capacity.

Omega-3 PUFAs affect the differentiation capacity of OCs in obese mice. Previous studies documented an inhibitory effect of omega-3 PUFAs on OC differentiation in vitro and in vivo using OVX or aging mouse model[23,26,27]. Thus, we evaluated OC differentiation capacity with omega-3 PUFA treatment in vitro and in primary BM cells isolated from treated mice after 8 weeks of diet.

In vitro treatment of BM derived cells with 100 µM EPA, DHA or mix EPA and DHA for 5 days induced inhibition of OC differentiation compared to non-treated OCs, which was also confirmed by gene expression of osteoclastic genes (*Trap* and *Ctsk*) (Supplementary Fig. 8a–c).

In primary BM cells isolated from treated mice, TRAP staining revealed increased number of total TRAP + OCs in HFD compared to ND group (ND vs. HFD, $p = 0.0258$), while omega-3 PUFA supplementation decreased OC formation (Fig. 5a, d). Further, we found increased formation of large OCs (cell diameter above 500 µm, more than 30 nuclei) in HFD compared to ND group (ND vs. HFD, $p = 0.038$), which was decreased in HFD + F group (HFD vs. HFD + F, $p = 0.048$) (Fig. 5b, d). However, TRAcP activity measured in primary differentiated OCs showed no differences among groups regardless of the diet (Fig. 5c), which was also confirmed by gene expression of osteoclastic genes (*Trap*, *Ctsk*) (Fig. 5e). However, there was a trend towards decreased gene expression of inflammatory gene *Il1b* (Fig. 5f) in HFD + F compared to HFD group suggesting less inflammatory profile of OCs with lower OC differentiation induced by omega-3 PUFA supplementation in diet.

Omega-3 PUFAs improve insulin and inflammatory responsiveness in HSCs in obese mice. Previous studies applying omega-3 PUFAs in obese mice showed their positive impact on inflammation and insulin signaling pathways in peripheral adipose tissue[24]. Thus, we evaluated AKT and NFκB signaling pathways in HSCs, progenitors of immune cells, derived from treated mice.

Insulin stimulation measured by AKT phosphorylation (pAKT S473/total AKT, and pAKT T308/total AKT) showed that insulin

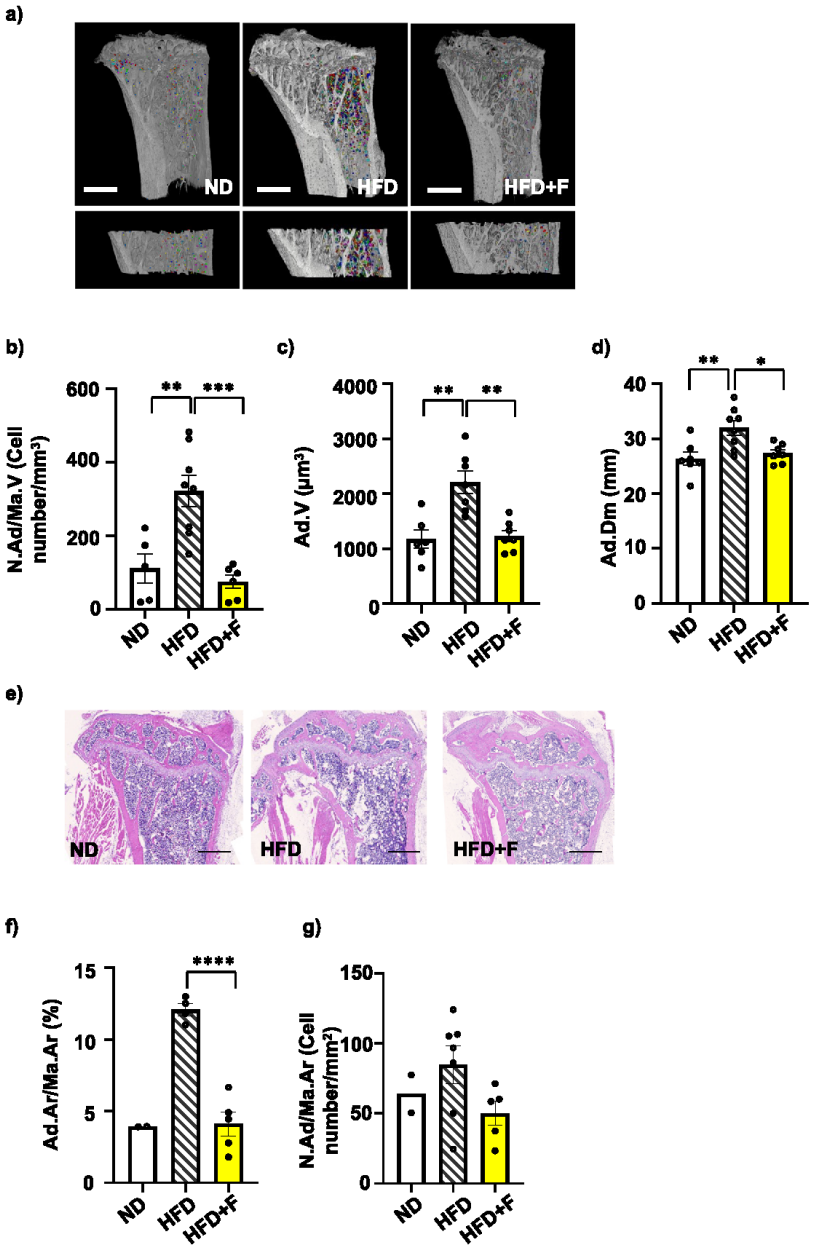

signaling in primary HSCs of HFD mice was not impaired when compared to ND cells (Fig. 6a–d; Supplementary Fig. 9). Interestingly, HFD + F HSCs showed decreased insulin responsiveness compared to HFD HSCs, especially for pAKT T308/total AKT (HFD vs HFD + F, $p = 0.0341$) (Fig. 6c, d; Supplementary Fig. 9).

Further, inflammatory stimulation of primary HSCs by LPS induced activation of NFκB signaling measured by p65 phosphorylation (p-p65/totalp65) in the HFD group, which was decreased in the HFD + F group (HFD vs. HFD + F, $p = 0.0125$) (Fig. 6e, f; Supplementary Fig. 10). Moreover, there was a trend towards decreased expression of bone resorption markers

Fig. 2 Omega-3 PUFAs decrease bone marrow adiposity in obese mice. a Representative pictures of bone marrow adipocytes (BMAds) stained with contrast agent Hexabrix® in the whole proximal tibia and zoomed pictures of BMAds in the selected region of interest in proximal tibia (defined in Material and Methods) of contrast enhanced samples scanned by µCT. Pictures were created using Avizo Software (version 2021.1, ThermoFisher, scale bar 1000 µm). **b** Quantification of BMAd density (N.Ad/Ma.VCell number/mm^3)). **c** Evaluation of BMAT volume (Ad.V (µm^3)) in the selected region of interest in the proximal tibia. (**d**) Quantitative evaluation of the diameter of Hexabrix-stained BMAds in the tibia (Ad.Dm (mm)). (n = 6–8 per group; one-way ANOVA, Tukey's multiple comparison test with $^*p \le 0.05$, $^{**}p \le 0.01$, $^{***}p \le 0.001$). Histomorphometric evaluation of the BMAds showing (**e**) representative pictures from H&E staining of adipocytes from a histological section of the proximal tibia from mice fed with HFD supplemented with omega-3 PUFAs (scale bar 500 µm), (**f**) total adipocyte area (Ad.Ar/Ma.Ar (%)), and (**g**) BMAd density affected by omega-3 supplementation in obese mice (N.Ad/Ma.Ar (Cell number/mm^2)) (n = 2–7 per group; one-way ANOVA, Tukey's multiple comparison test with $^{***}p \le 0.001$, $^{****}p \le 0.0001$. Data are presented as mean ± SEM (groups coding: white column-ND, black line shading-HFD, yellow column-HFD + F).

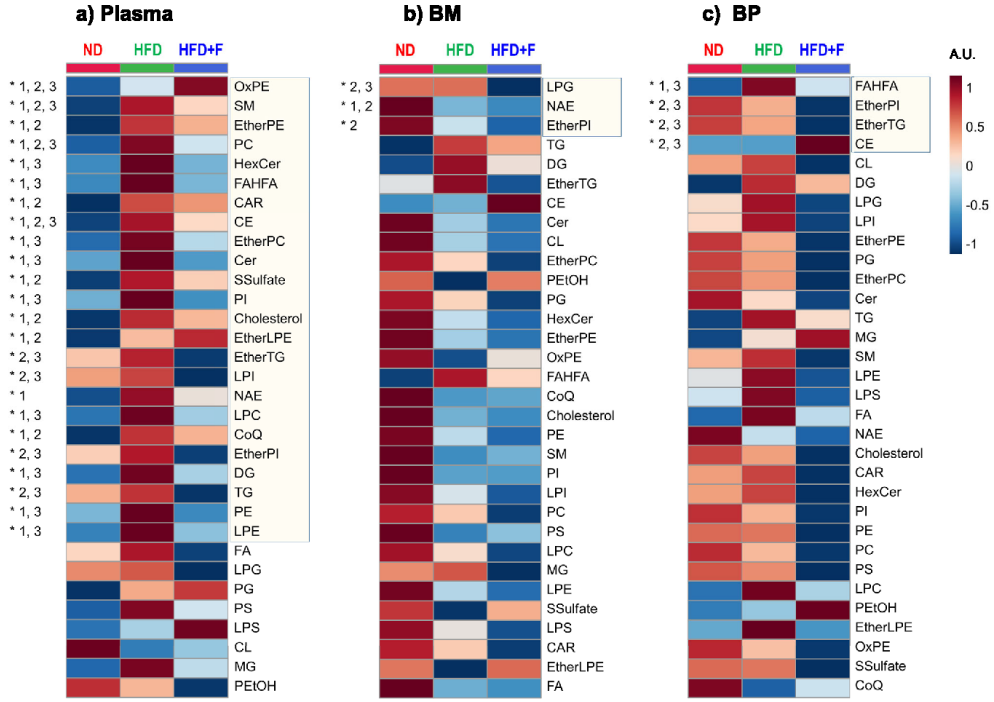

Fig. 3 Lipidomic analysis revealed the effect of omega-3 PUFAs comparing circulating plasma, bone marrow, and bone powder in obese mice. Global lipidomic profiling of plasma (PL), bone marrow (BM), and bone powder (BP) samples obtained from investigated mice using LC-MS. Heatmap of the sum of the abundances of unique lipid species for each lipid class for (**a**) plasma, (**b**) bone marrow, and (**c**) bone powder with group averages (n = 5-10 per group). Lipid classes statistically altered are marked by an asterisk (*) based on ANOVA with p(FDR) < 0.05. Differences between groups are marked as 1 (ND vs. HFD; $p < 0.05$), 2 (ND vs. HFD + F; $p < 0.05$), and 3 (HFD vs. HFD + F; $p < 0.05$) (gradient color keys used in normalized intensity, A.U.). (Lipid class annotation: CAR acylcarnitine, CE cholesteryl ester, CL cardiolipin, Ce, ceramide, CoQ coenzyme Q, DG diacylglycerol, EtherPE ether-linked phosphatidylethanolamine, EtherLPE ether-linked lysophosphatidylethanolamine, EtherPI ether-linked phosphatidylinositol, EtherPC ether-linked phosphatidylcholine, EtherTG ether-linked triacylglycerol, FA free fatty acid, FAHFA fatty acid ester of hydroxy fatty acid, HexCer hexosylceramide, LPC lysophophatidylcholine, LPE lysophosphatidylethanolamine, LPG lysophosphatidylglycero, LPI lysophosphatidylinositol, LPS lysophosphatidylserine, MG monoacylglycerol, NAE *N*-acyl ethanolamines, OxPE oxidized phosphatidylethanolamine, PC phosphatidylcholine, PE phosphatidylethanolamine, PEtOH phosphatidylethanol, PG phosphatidylglycerol, PI phosphatidylinositol, PS phosphatidylserine, SM sphingomyelin, SSulfate sterol sulfate, TG triacylglycerol).

(*Rankl*, *Opg*) in HSCs of the HFD + F vs. HFD group (Fig. 6g). These findings suggest that omega-3 PUFAs decreased insulin and inflammatory signaling in progenitors of immune cells under obesogenic conditions.

Omega-3 PUFAs slow down metabolic activity along with decreased senescence in BMSCs in obese mice. To further evaluate the effect of omega-3 PUFAs on cellular metabolism, we measured the bioenergetic profile in primary BMSCs isolated

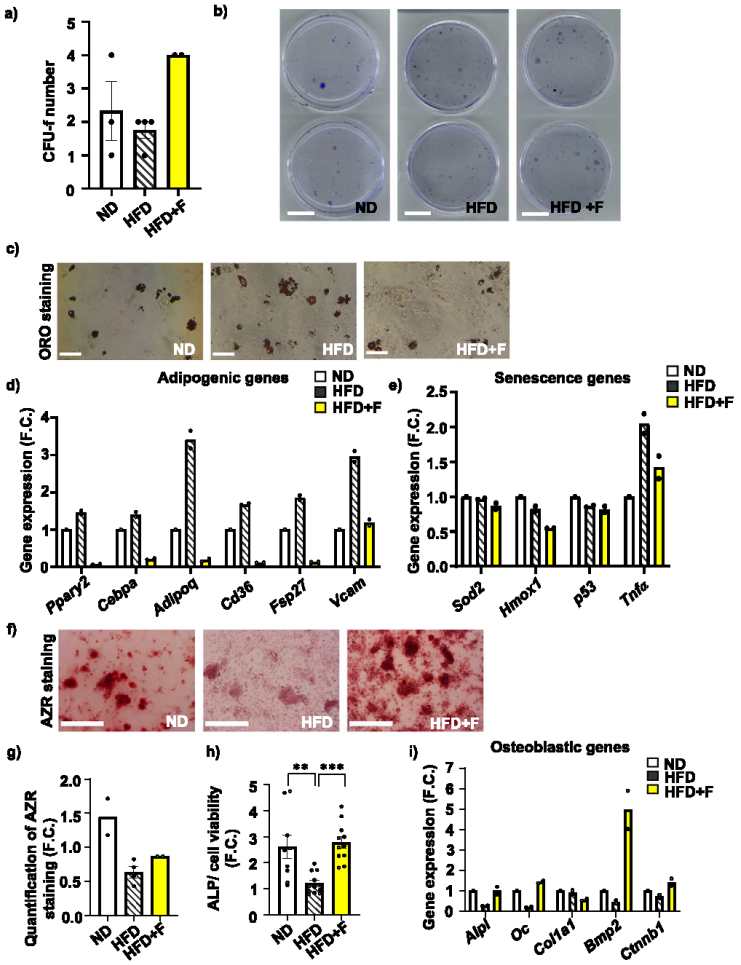

Fig. 4 Effect of omega-3 PUFAs on stem cell properties of primary BMSCs. Analysis of stem cell phenotype by (**a**) colony-forming units-fibroblast (CFU-f) analysis of freshly isolated BMSCs with (**b**) representative pictures of CFU-f analysis (scale bar 20 mm). (n = 2–4 from pooled samples; *t* test $^{*}p \leq 0.05$: HFD vs HFD + F) Data are presented as mean values ± SEM. **c** Representative pictures of Oil red O (ORO) stained lipid droplets in AD differentiated BMSCs (scale bar 500 µm; 10x magnification). **d**, **e** Gene expression profile of BMSCs differentiated towards adipocytes in D10. **d** Gene expression of adipogenic genes (*Ppary2, Cebpa, Adipoq, Cd36, Fsp27, Vcam)* and (**e**) oxidative stress, senescence and inflammatory genes (*Sod2, Hmox1, p53, Tnfα*) (n = 2 from pooled samples). Data are presented as mean fold change (F.C.) of gene expression normalized to BMSCs from ND group ± SEM. **f** Representative pictures of Alizarin Red (AZR) staining for calcified matrix mineralization of OB differentiated BMSCs (scale bar 500 µm; 10x magnification) and (**g**) quantification of eluted AZR staining of mineralized matrix in OB differentiated BMSCs in D10. (n = 2–4; one-way ANOVA, Tukey's multiple comparison test with $^{*}p \leq 0.05$. Data are presented as mean fold change (F.C.) of A_{500} in OB differentiated cells (OB) normalized to BMSCs from ND group ± SEM. **h** Measurement of alkaline phosphatase (ALP) activity normalized to cell viability in OB differentiated BMSCs in D7. (n = 9–11; one-way ANOVA, Tukey's multiple comparison test with $^{**}p \leq 0.01$, $^{***}p \leq 0.001$). Data are presented as mean fold change of ALP activity in OB differentiated cells (OB) from each experimental group ± SEM. **i** Gene expression profile of osteoblastic markers (*Alpl, Oc, Col1a1, Bmp2, Ctnnb1*) in OB differentiated BMSCs in D10 (n = 2 from pooled samples). Data are presented as mean fold change (F.C.) of gene expression normalized to BMSCs from ND group ± SEM (groups coding: white column-ND, black line shading-HFD, yellow column-HFD + F).

from mice at the end of dietary interventions in their undifferentiated state. Using Seahorse technology, measurement of cellular respiration in primary BMSCs showed stimulation of basal respiration and higher maximal respiration rate induced by carbonyl cyanide-4-(trifluoromethoxy) phenylhydrazone (FCCP) in HFD BMSCs compared to ND BMSCs (Fig. 7a). Interestingly, this HFD-induced increased OCR activity was diminished in BMSCs from HFD + F mice. Similarly, glycolysis measurement revealed that HFD + F treatment decreased the glycolytic capacity of the corresponding BMSCs compared to cells from ND or

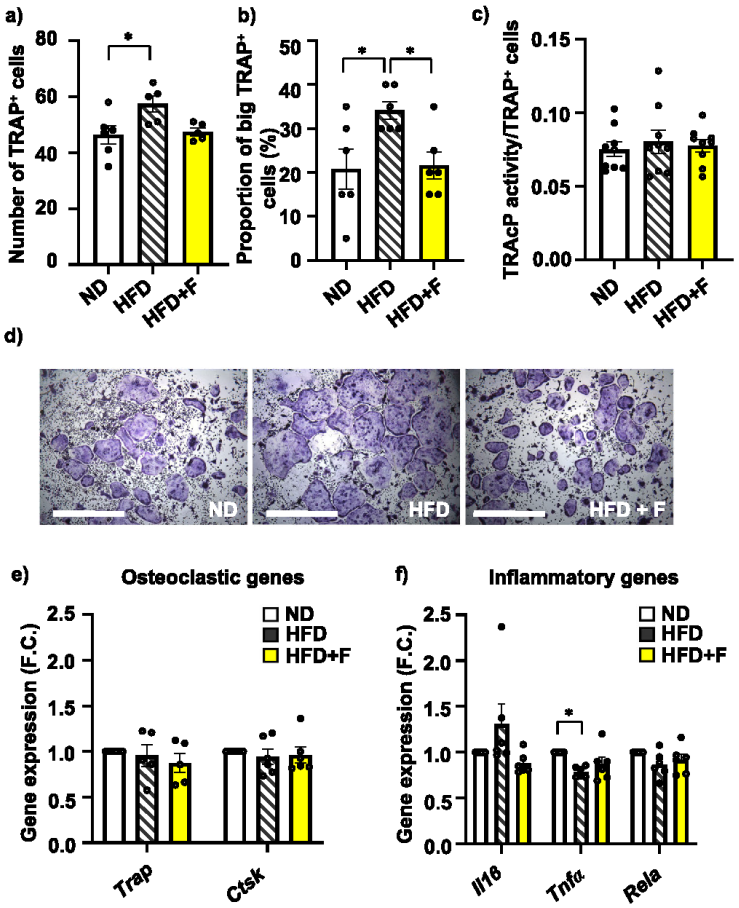

Fig. 5 Omega-3 PUFAs affect the differentiation capacity of OCs in obese mice. a–c Analysis of osteoclast differentiation from BM cells isolated from treated mice. **a** Number of TRAP$^+$ cells, (**b**) Proportion of large TRAP$^+$ OCs from total OCs (cell diameter above 500 µm) and (**c**) measurement of TRAcP activity normalized to number of TRAP$^+$ cells (n = 5–6 per group; one-way ANOVA, Tukey's multiple comparison test with $^*p \leq 0.05$) Data are presented as mean ± SEM. **d** Representative pictures of TRAP$^+$ cells after 5 days of differentiation. Gene expression analysis of (**e**) oscteoclastic genes (*Trap, Ctsk*) and (**f**) inflammatory genes (*Il1β, Tnfα, Rela*) measured in OC differentiated cells after 5 days of differentiation. (n = 5–6 mice per group; one-way ANOVA, Tukey's multiple comparison test with $^* p \leq 0.05$). Data are presented as mean fold change (F.C.) of gene expression normalized to ND group ± SEM (groups coding: white column-ND, black line shading-HFD, yellow column-HFD + F).

HFD mice (Fig. 7b). This is well documented in the energy phenotype profile under basal conditions of BMSCs from HFD + F group showing clear shift towards a quiescent metabolic state, contrasting with rather energetic profile of BMSCs from the HFD and ND groups (Fig. 7c). Further, measurement of β-gal activity and reactive oxygen species (ROS) production in primary BMSCs showed decreased senescent phenotype in the HFD + F compared to the HFD group (HFD vs. HFD + F, $p = 0.0185$; $p = 0.0223$, respectively) (Fig. 7d, e) accompanied by decreased gene expression of senescence-associated secretory phenotype (SASP) markers (e.g., *Fas, Fasgl, Il1β, Vegfa, Vcam, Il10, Il1rn*) in primary BMSCs (Fig. 7f) and HSCs from the HFD + F compared to HFD group (Supplementary Fig. 7b).

These findings demonstrate that omega-3 PUFA treatment in mice slows down the negative effect of HFD on cellular metabolism and senescence in BMSCs and HSCs, thus highlighting their beneficial impact on the BM microenvironment.

Discussion

Non-pharmacological treatments, including dietary restriction and physical activity have been shown to improve metabolic and bone parameters in metabolic diseases such as obesity and osteoporosis. Animal and clinical studies demonstrated that consumption of omega-3 PUFAs can impact bone health by modulating calcium metabolism, prostaglandin synthesis, lipid

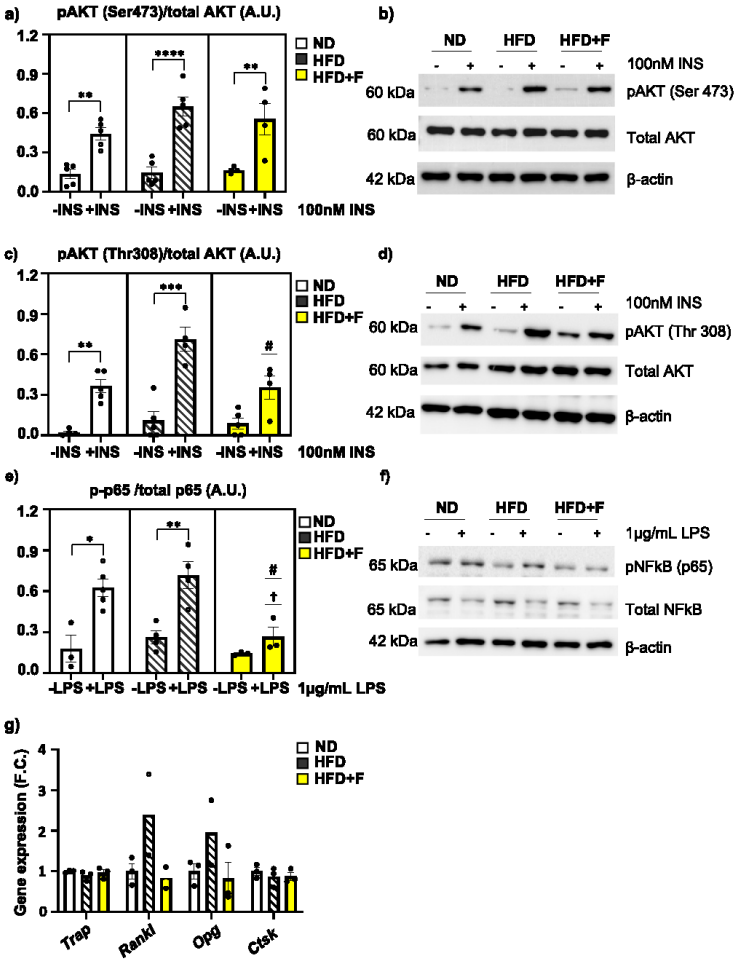

Fig. 6 Omega-3 PUFAs affect insulin and inflammatory signaling and senescence in HSCs of obese mice. a Densitometry evaluation of western blot images representing the results of insulin stimulation (100 nM, 15 min) of p-S473-AKT/total AKT in primary HSCs from the ND, HFD and HFD + F groups (n = 4–5 per group) and (**b**) representative western blot images; (**c**) Densitometry evaluation of western blot images representing the results of insulin stimulation (100 nM, 15 min) of p-T308-AKT/total AKT in primary HSCs from the ND, HFD and HFD + F groups (n = 4–5 per group) and (**d**) representative western blot images. **e** Densitometry evaluation of western blot images representing the results of lipopolysaccharide (LPS) stimulation (1 µg/ml, 15 min) of p-NFκB/totalNFκB in primary HSCs from the ND, HFD and HFD + F groups (n = 3–5 per group) and (**f**) representative western blot images. Data are presented as mean densitometry ± SEM, *t* test, $^{*}p \leq 0.05$, $^{**}p \leq 0.01$, $^{***}p \leq 0.001$, $^{****}p \leq 0.0001$ significant difference between -INS vs. +INS, one-way ANOVA, Tukey's multiple comparison test, †: ND vs. other +INS groups with $p \leq 0.05$, #: HFD vs. other +INS groups with $p \leq 0.05$. **g** Gene expression of bone resorption genes (*Trap, Rankl, Opg, Ctsk*) in primary HSCs (n = 3 per group from pooled samples, one-way ANOVA, Tukey's multiple comparison test. Data are presented as mean fold change (F.C.) of gene expression normalized to HSCs from ND ± SEM (groups coding: white column-ND, black line shading-HFD, yellow column-HFD + F).

oxidation, osteoblast formation, and osteoclastogenesis[28]. However, the underlying mechanisms of how omega-3 PUFAs modulate bone homeostasis in obesity-induced impairment of bone formation are not well documented. In the present study, we report that supplementation with omega-3 PUFAs improved metabolic and bone parameters combined with decreased BMA in obese mice, which were accompanied by increased OB differentiation potential, lower OC differentiation and lowered senescent markers in primary BMSCs. These data support the beneficial effect of omega-3 PUFAs on bone and cellular metabolism of BMSCs and their potential use in the treatment of metabolic bone diseases.

In our study, 8-week-dietary intervention was used to characterize the effect of HFD supplementation with omega-3 PUFAs (enriched with DHA and EPA) on the adverse effects of obesity on bone and fat metabolism in 12-week-old C57BL/6 N male mice.

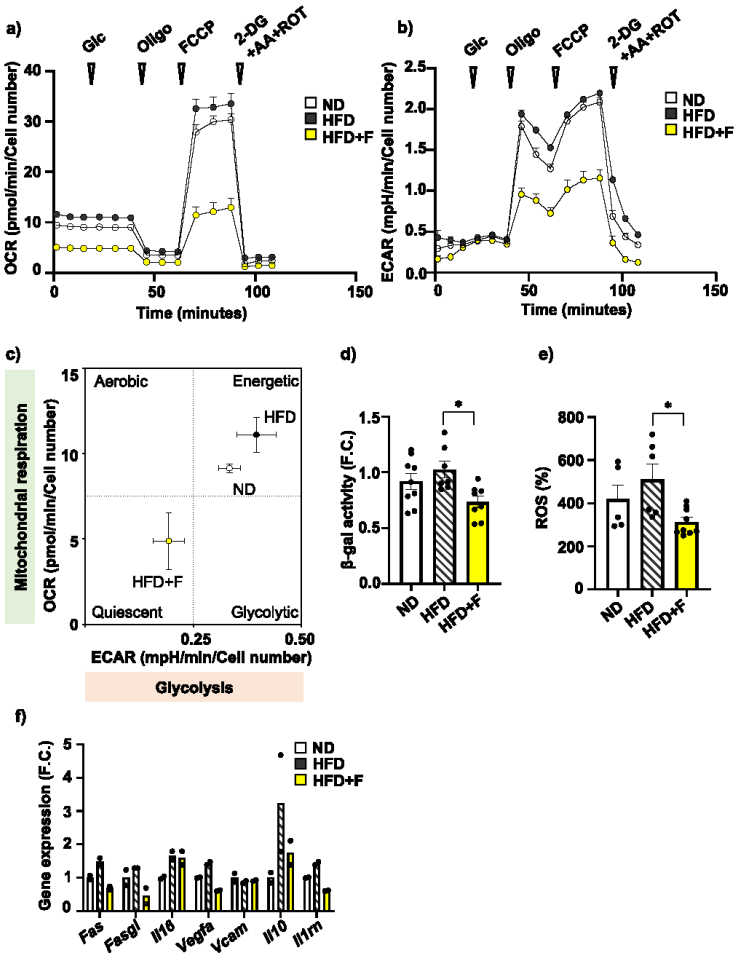

Fig. 7 Omega-3 PUFAs decrease cellular metabolism in BMSCs of obese mice. a Measurement of oxygen consumption rate (OCR) of primary BMSCs isolated from treated mice (n = 2 independent experiments with five replicates per group). **b** Measurement of extracellular acidification rate (ECAR) of primary BMSCs (n = 7–11 per group). Data are presented as mean ± SEM (groups coding: white circle-ND, black circle-HFD, yellow circle-HFD + F), (**c**) XF Energy map visualizing metabolic phenotype profile of cultivated BMSCs. The Energy map was calculated from basal OCR and ECAR mean values (n = 7–11 per group). **d** Analysis of senescence of cultivated mouse BMSCs using β-galactosidase activity measurement. **e** Measurement of ROS production in cultivated mouse BMSCs (n = 7–9 per group, one-way ANOVA, Tukey's multiple comparison test with * $p \leq 0.05$). Data are presented as mean ± SEM. **f** Gene expression analysis of SASP markers in primary BMSCs obtained from treated mice exposed to 50 µM H_2O_2 for 6 h (*Fas, Fasgl, Il1β, Vegfa, Il10, Il1rn*) (n = 2 per group from pooled samples). Data are presented as mean fold change (F.C.) of gene expression normalized to ND group ± SEM (groups coding: white column-ND, black line shading-HFD, yellow column-HFD + F).

Previous animal studies investigating treatment with omega-3 PUFAs documented different results on bone phenotype, depending on the investigated conditions (growth, osteoporosis, aging, obesity, diabetes), sex (males/females), length of the treatment, and composition of the diet. Farahnak et al.[29] using younger growing animals reported that a 1% DHA-enriched diet increased lumbar bone density and cortical bone volume in 6-week-old female Sprague-Dawley rats after 10 weeks of treatment, which aligns with our study showing improved trabecular and cortical parameters in the proximal tibia and L5 vertebrae measured by µCT, and enhanced bone strength, after 12 weeks of omega-3 PUFA supplementation in male mice. However, similar treatment in 3-week-old C57BL/6 J male and female mice[28] or 6-week-old male diabetic Zucker rats[30] did not induce changes in bone phenotype measured by dual-energy X-ray absorptiometry (DXA), after 9 weeks of treatment, which could be explained by a less sensitive method for evaluation of bone phenotype and different animal model of metabolic diseases.

Other animal studies using longer treatment with omega-3 PUFAs (from twenty to twenty-four weeks of diet) showed a

consistent positive effect of omega-3 supplementation on bone phenotype, emphasizing its importance in diet[19,21,23]. However, in any of these animal studies, the authors did not investigate the effect of omega-3 PUFAs on BMA and primary cells isolated from treated animals.

Recently, Hassan et al., using a murine model of senile osteoporosis (SAMP8 knockout mice), reported that an omega-3 PUFA-enriched diet administered for 10 months prevented age-related bone loss by reducing BMAT expansion (as measured by μCT), thus highlighting the impact of BMAT expansion in the development of metabolic bone diseases[20]. These findings nicely correlate with our observation on reduced BMA induced by an omega-3 PUFA-enriched diet using a shorter intervention period of 2 months. In contrast to the study of Hassan et al., our study used CECT to visualize the BMAds, which allowed a more precise analysis of their structural parameters and distribution in the BM cavity using Hexabrix CESA[31]. Hexabrix is a smaller molecule compared to previously used POM CESA and does not interact with the vasculature inside the BM, allowing faster tissue sample staining[25]. In addition, it is an unharmful compound and is consequently preferred over osmium tetroxide (OsO_4), which is highly toxic[32]. Thus, this contrast agent staining of BMAds is better for detecting the beneficial omega-3 PUFA-induced effects on the size and the number of BMAds. Furthermore, applying CECT allows to choose non-subjective gray value thresholds for segmentation of BMAds.

We also evaluated the molecular phenotype of primary BMSCs isolated from treated mice, which has not been investigated in previous animal studies. We found that the administration of omega-3 PUFA-enriched HFD improved OB differentiation of BMSCs and decreased AD differentiation and senescent phenotype compared to HFD BMSCs. These changes were accompanied by decreased NFκB and insulin signaling in HSCs after omega-3 PUFA treatment compared to the HFD group, suggesting lower inflammatory response and metabolic activity associated with a decreased aging process in immune cells[33]. These findings from primary BM cells support results obtained in vitro using omega-3 PUFAs treatment in C3H10T1/2 and RAW264.7 cells, which showed the inhibition of RANKL and PPARγ signaling pathway[23,34–36]. Furthermore, Levental and colleagues reported that omega-3 PUFAs induced changes in the plasma membrane of BMSCs, which led to higher OB differentiation[22].

In terms of OC differentiation, we observed increased total OC number without any effect on TRAcP activity in HFD compared to ND confirming data from previous animal study using 3-month HFD treatment[26]. This effect was decreased by omega-3 PUFA supplementation in diet. Interestingly, HFD increased formation of bigger OCs compared to ND, which was diminished by omega-3 PUFAs supplementation supporting data from previous in vitro and in vivo studies on inhibitory effect of omega-3 PUFAs on osteoclastogenesis and thus a positive effect of omega-3 PUFAs on bone formation[23,26,27]. However, further studies using single cell RNA seq analysis of OCs might reveal more information about the differences in resorption activity of OCs depends on the number of nuclei or their size. Recent study by McDonald et al.[37] reported interesting phenomenon on OC recycling process via osteomorphs, which affects bone remodeling process. However, it is not known how obesity or diet intervention may affect this process. Future studies are needed to answer these questions.

In our study, we were also interested in the effect of omega-3 PUFAs on cellular metabolism in primary BMSCs, which might explain the local changes in the BM microenvironment. Interestingly, bioenergetic profiling revealed quiescent phenotype (low glycolytic and respiratory activity) in primary BMSCs obtained from HFD + F mice compared to HFD BMSCs with higher energetic profile, which is opposite to response in peripheral adipocytes with increased mitochondrial biogenesis after omega-3 PUFA treatment[38]. The metabolic changes in BMSCs were accompanied by decreased ROS production and senescent activity, suggesting that omega-3 PUFAs protect the BM microenvironment from the harmful effect of obesogenic conditions by reducing the metabolic activity of primary BMSCs, which might support maintenance of the stemness and less epigenetic changes in BMSCs[39].

These beneficial effects on bone metabolism were further confirmed by metabolomic analysis showing a higher concentration of DHA and EPA not only in plasma but also in BM and bone matrix of HFD + F compared to HFD mice, which was associated with a positive impact on bone quality and lower BMA and improved bone microstructural changes. Besides omega-3 PUFAs, omega-6 and omega-9 PUFAs in the diet may benefit bone parameters[20,40]. Thus, it is important to pay more attention to the composition of different PUFAs in experimental diets and their beneficial effects on bone. Further, lipidomic analysis showed decreased levels of prostaglandin in plasma and BM, which correlates with better bone formation also documented in previous studies[30,41,42]. Interestingly, the metabolomic data revealed the different responses to diet in plasma and BM microenvironments, with a strong effect of diet on plasmatic levels of metabolites in comparison to a milder effect in BM or BP metabolite profile under dietary intervention. The metabolomics and cellular data highlight the difference in BM metabolism compared to the periphery and its relative resistance to diet.

The present study is based on the use of several innovative approaches. Firstly, unlike previous studies investigating the effect of omega-3 PUFA treatment on bone, we conducted a comprehensive analysis encompassing both bone and BMAd parameters. Additionally, we thoroughly analyzed the cellular and molecular properties of primary BMSCs and OCs derived from the treated animals. Secondly, we used an interventional study with a preventive design of the treatment to investigate how omega-3 PUFAs impact bone health in obesity. Thirdly, we employed state-of-the-art methods to enhance our understanding of cellular metabolism in BMSCs obtained from the treated mice.

On the other hand, our study has some limitations. We used only 2 months of dietary treatment in C56BL/6 N male mice that did not manifest with a lot of changes in bone and senescent phenotype in BMSCs in HFD condition compared to ND. However, the beneficial effect of HFD + F was already pronounced in comparison to HFD condition. Further, we did not investigate the effects of omega-3 PUFAs in female mice, which is important for future lifestyle recommendations for women with osteoporosis-related metabolic complications.

Taken together, our interventional study using HFD-induced obesity in mice showed that omega-3 PUFA supplementation improved metabolic and bone parameters in obese mice, which was accompanied by reduced BMA and better differentiation potential, and lower senescence in BMSCs. Thus, these data highlight the beneficial effects of omega-3 PUFAs on bone and cellular metabolism and their potential use in the treatment of metabolic bone diseases.

Methods

Animals and dietary interventions. We utilized 10-week-old male C57BL/6 N mice obtained from Charles River Laboratories, Sulzfeld, Germany. The mice were housed at 22 °C with a 12-h light-dark cycle (with light starting from 6:00 a.m.). Upon arrival and prior the beginning of the experiment, all mice had unrestricted access to water and a standard chow diet provided by Ssniff Spezialdieten GmbH, Soest, Germany. At the age of 12 weeks, the

mice were randomly assigned to three groups (n = 8–10, repeated in three independent experiments). The mice were then fed for a duration of 8 weeks as follows: (a) normal diet (ND) with a lipid content of 3.4% wt/wt (Rat/Mouse- Maintenance extrudate; Ssniff Spezialdieten GmbH, Soest, Germany); (b) HFD with lipid content of approximately 35% wt/wt, primarily sourced from corn oil[43]; and (c) HFD supplemented with omega-3 concentrate (HFD + F) (with 46% DHA, 14% EPA, wt/wt; product EPAX 1050 TG; Epax Norway AS, Ålesund, Norway), which replaced 15% wt/wt of dietary lipids to achieve a total EPA and DHA concentration of 30 mg/g diet[24]. The dose of omega-3 PUFAs per mouse was 0.168 g EPAX 1050 concentrate. This dose of omega-3 PUFAs in diet has been shown in the previous animal and clinical studies to prevent HFD-induced obesity complications and improve metabolic parameters[24,43,44]. The macronutrient composition of the experimental diets and fatty acid composition in dietary lipids are presented in Supplementary Tables 1, 2. Body weight and 24-h food intake were assessed weekly throughout the study period. After 8 weeks of dietary interventions, the mice were sacrificed in the fed state by cervical dislocation under diethyl ether anesthesia. Tissue samples and primary mouse BMSCs were collected for subsequent molecular analyses. All experiments were performed according to the Institute of Physiology of the Czech Academy of Sciences guidelines and were approved under protocol 81/2016.

Glucose tolerance test. Intraperitoneal glucose tolerance test (GTT) was performed using 1 mg of glucose/g body weight in overnight fasted mice[24]. Glucose (1 mg/g) was administrated by i.p. injection. Blood glucose levels were measured from the tail vein at the indicated time (0, 15, 30, 60, 90, and 120 min), and glycemia was determined using glucometer (Accu-Chek Performa, Roche).

Biochemical analysis. Blood glucose levels were measured using Accu-Chek Performa glucometers from Roche. Plasma insulin levels were assessed using the Sensitive Rat Insulin RIA Kit (Millipore, Billerica, MA, USA).

Bone histology. Tibias were collected after the dissection and fixed for 48 h in 10% formalin. After formalin fixation, bones were demineralized by EDTA 12% solution for 14 days. Tissues were embedded in paraffin and sections were used for hematoxylin eosin staining, which was further evaluated for BMA[4].

Isolation of BMSCs and hematopoietic stem cells (HSCs). BMSCs were isolated from the bones of the front and hind limbs of C57BL/6 N male mice (after 8 weeks of dietary treatments) following previous protocols with some modifications[4]. Intact bones containing BM were gently cleaned from muscles in the sterile hood. After bone-crushing, collagenase digestion (StemCell, Vancouver, BC, Canada) and negative selection of CD45, CD31 and Ter119 cells (Miltenyi, Bergisch Gladbach, Germany), BMSCs were isolated via several washing steps and centrifugation in order to get cell pellet for the culture. BMSCs were subcultured in growth medium (MEM alpha (Thermo Fisher Scientific, Waltham, MA, USA) + 20% FBS (Thermo Fisher Scientific, Waltham, MA, USA) + 1% penicillin/streptomycin (P/S) (Thermo Fisher Scientific, Waltham, MA, USA) + 0,5% Amphotericin B (Merck, Darmstadt, Germany) + 1% Glutamax (Thermo Fisher Scientific, Waltham, MA, USA) + 1% MEM NEAA (Thermo Fisher Scientific, Waltham, MA, USA) + 1% sodium pyruvate (Thermo Fisher Scientific, Waltham, MA, USA)) and cultivated for further analysis. The positive fraction with HSCs was divided into three samples. One was harvested for mRNA isolation with Tri-Reagent (Merck, Darmstadt, Germany), the second was harvested for proteins, and the rest was seeded and cultivated in a growth medium for further analysis.

In vitro differentiation of BMSCs. Primary BMSCs from passage two were used for analyzing their differentiation capacity.

Osteoblast (OB) differentiation. BMSCs were seeded at a density of 20,000 cells/cm^2. When the cells reached 80% confluence in MEM medium (Thermo Fisher Scientific, Waltham, MA, USA) supplemented with 10% FBS (Thermo Fisher Scientific, Waltham, MA, USA) and 1% P/S (Thermo Fisher Scientific, Waltham, MA, USA) was added to control cells. The rest of the cells were cultivated with osteoblast induction media consisting of 10 mM β-glycerophosphate Merck, Darmstadt, Germany), 10 nM dexamethasone (Merck, Darmstadt, Germany), and 50 µg/ml Vitamin C (Wako Chemicals USA Inc., Richmond, VA, USA). The media was changed every second day for 7 days (ALP activity) and 11 days (Alizarin Red staining).

Alizarin red staining. Mineralization of the cell matrix at day 11 was measured using Alizarin Red S staining. Cells were fixed with 70% ice-cold ethanol for a minimum of 1 h at −20 °C, after which Alizarin Red S solution (Merck, Darmstadt, Germany) was added. Then, the cells were stained for 10 min at room temperature (RT). Excess dye was washed with distilled water, followed by PBS. The amount of mineralized matrix (bound stain) was quantified by elution of the Alizarin red stain, using 20 min of incubation of the cultures in 70% dH2O, 20% ethanol, and 10% methanol solution on a shaker (100 rpm) at RT. The absorbance of the eluted dye was measured at 500 nm using a microplate reader according to the protocol[45].

Alkaline phosphatase (ALP) activity assay. ALP activity and cell viability assay were quantified at day 7 of OB differentiation to normalize the ALP activity data to the number of viable cells.

Cell viability assay was performed using Cell Titer-Blue Assay Reagent (Promega, Madison, WI, USA) at fluorescence intensity ($579_{Ex}/584_{Em}$). ALP activity was determined by absorbance at 405 nm using p-nitrophenyl phosphate (Merck, Darmstadt, Germany) as substrate[46].

Adipocyte (AD) differentiation. Cells were plated at a density of 30,000 cells/cm^2. For AD differentiation, DMEM media (Thermo Fisher Scientific, Waltham, MA, USA) was used, containing 10% FBS (Thermo Fisher Scientific, Waltham, MA, USA), 9% horse serum (Merck, Darmstadt, Germany), 1% P/S (Thermo Fisher Scientific, Waltham, MA, USA), 100 nM dexamethasone (Merck, Darmstadt, Germany), 0.5 uM 3-isobutyl-1-methyxanthine (IBMX) (Merck, Darmstadt, Germany), 1 µM BRL (Merck, Darmstadt, Germany), 3 µg/mL Insulin (Merck, Darmstadt, Germany). The media was changed every three days for 10 days. Horse serum supplementation of media was used for the first three days of induction.

Oil Red O staining. At day 10 of differentiation, cells were rinsed with PBS and fixed in 4% paraformaldehyde (Merck, Darmstadt, Germany) for 10 min at RT. After fixation, cells were briefly rinsed with 3% isopropanol solution (Merck, Darmstadt, Germany), and lipid droplets were stained with Oil Red O solution (Merck, Darmstadt, Germany) for 1 h at RT.

Colony forming units-fibroblast (CFU-f) assay. After BMSC isolation, cells were seeded for CFU 500 cells/60 mm Petri dish and cultivated in growth media. After 14 days in culture, colonies

displaying more than 50 cells were counted using Crystal Violet staining (Merck, Darmstadt, Germany).

Short-time proliferation assay. Isolated BMSCs were plated in a 24-well plate in triplicates at a density of 1000 cells/well in a standard growth medium. Cell number was evaluated after 1, 3, 6, and 9 days. Cells were washed with PBS, detached by trypsinization, and then manually counted using a Bürker-Türk counting chamber.

Insulin and lipopolysaccharide (LPS) responsiveness of HSCs. Primary HSCs were cultured up to passage one and seeded for insulin and LPS stimulation. Cells were plated at a density of 300,000 cells/well in 12 well plates. When they reached the confluence, cells were starved for 4 h in serum-free MEM alpha medium (Thermo Fisher Scientific, Waltham, MA, USA) with 0.5 % BSA, and with 1% P/S then stimulated with 100 nM Insulin or 1 µg/ml LPS for 15 min at 37 °C and harvested for protein used in subsequent analyses.

Osteoclast (OC) differentiation. Primary mouse osteoclasts (OCs) were differentiated from total BM cells isolated from the treated mice at the end of dietary intervention[47]. Briefly, after flushing long bones and lysis of erythrocytes using erythrocyte lysis buffer, the BM cells were seeded in the cell culture plates for the subsequent analysis (96 well plates: 125,000 cell/well for TRAP staining/TRAP activity, 24 well plates: 500,000 cells/well for OC gene expression). The following day, the cells were differentiated with 25 ng/ml RANKL (Peprotech, Cat # 310-01) and 25 ng/ml M-CSF (R&D systems, cat # 216-MC) in alpha MEM media/10 % FBS/1% P/S, and the media was changed every 2nd day up to 5 days. Mature Ocs were defined as multi-nuclei cells with three or more nuclei.

In vitro OC differentiation with short-term treatment with omega-3 PUFAs. BM cells were isolated from C57BL/6 male mice and differentiated to OC[47]. During 5 days of OC differentiation omega-3 PUFAs: 100 µM EPA (Merck, Cat # E2011), 100 µM DHA (Merck, Cat # D2534) or their mix coupled with 0.5 % BSA were added to the differentiation cocktail and changed every 2nd day. After 5 days of OC differentiation TRAP staining and gene expression of OC markers were performed.

TRAcP activity and TRAP staining of mature OCs. Total BM cells were seeded in 96 well plates at the density of 125,000 cells/well and differentiated in OC according to the protocol mentioned above up to 5 days. After day 5, media from the cultured cells was collected and used for the measurement of TRAcP activity according to the manufacture's protocol[47,48]. Then, the cells were fixed with 10% formalin and staining for TRAcP using TRAP kit (Sigma, cat. n. 387A-1KT). Mature OCs were defined as multi-nuclei cells with three or more nuclei. TRAcP activity was normalized to the number of OCs.

Micro-computed Xray tomography (µCT) analysis. Proximal tibias and distal body of the 5th lumbar vertebra (L5) of mice were scanned with a high-resolution µCT SkyScan 1272 (Bruker, Belgium) with resolution 3 µm per voxel (voltage 80 kV, current 125 µA with 1 mm aluminum filter, exposure 1300 ms, 2time averaging, and 0.21° rotation step on 360°scanning). Reconstruction of virtual slices was performed in NRecon 1.7.3.1 (Bruker, Belgium) with InstaRecon 2.0.4.0 reconstruction engine (InstaRecon, Urbana, IL, USA) with 49% beam hardening correction, ring artifact correction = 9, and range of intensities 0–0.09 AU for tibia and 0–0.11 for L5. Reconstructions were reoriented in DataViewer 1.5.6 (Bruker, Belgium). Areas of interest were selected based on the reference section and analyzed in CT Analyzer 1.18.4.0 (Bruker, Belgium) with structure separation based on Otsu's method. Cortical and trabecular bone were analyzed in the same area for structure volume, porosity, density, and connectivity. The analysis region was defined from the first slide under the growth plate to the 230th slide and 3D microarchitecture of trabecular and cortical bone was used for the evaluation of the bone parameters[49].

Contrast-enhanced computed Xray tomography (CECT) workflow

Staining procedure. The staining solution was prepared by mixing commercial Hexabrix® solution (Guerbet, 10 mL, 320 mgI/mL) with 1x PBS (phosphate-buffered saline, 40 mL, 10 mM)[6]. Formalin-fixed proximal tibias (right leg) of the mice were transferred to a 1.5 mL Eppendorf tube containing 1 mL of staining solution. These Eppendorf tubes were placed on a shaker plate (gentle shaking) at ambient temperature. The samples were stained for at least 3 days, after which they were scanned.

µCT image acquisition and reconstruction. For image acquisition, the samples were removed from the Eppendorf tube and wrapped in parafilm to prevent dehydration while exposed to X-rays. Samples were imaged using a Phoenix NanoTom M (GE Measurement and Control Solutions, Boston, MA, USA). A diamond-coated tungsten target was used. The system was operated with the following acquisition parameters: voltage = 60–70 kV, current = 120–140 µA, focal spot size = 1.99 µm, isotropic voxel size = 2 µm^3, exposure time = 500 ms, frame averaging = 1, image skip = 0 and scan time = 20 min. The reconstruction was performed using Datos|x GE Measurement and Control Solutions software (version 2.7.0 – RTM) with a beam hardening correction of 8 and the inline median, ROI CT filter, and Filter volume algorithms implemented in the software. Subsequently, the datasets were normalized using an in-house developed Matlab script, with air and residual Hexabrix solution as references.

CECT image analysis of BMAT. After consistently aligning the datasets (DataViewer 1.5.6, Bruker MicroCT, Belgium), we analyzed the µCT data using CTAn (Bruker MicroCT, Belgium). First, we selected the volume of interest (VOI) in the proximal metaphysis of the tibia, starting 250 slices below the growth plate and covering 500 slices in the distal direction. In this VOI, binarization of the dataset was performed using a global threshold (130–255). This threshold masked both cortical and trabecular bone. Based on this selection, a denoised mask for the bone marrow combined with the trabecular bone was segmented by performing a sequence of VOI shrink-wrap, closing (2–10; increments of 2), and opening (2–10; increments of 2) operations (*i.e.*, everything inside the cortical bone was selected). Next, the newly generated mask was projected on the gray value image, generating a new VOI. In this new VOI, the segmentation of adipocytes was performed using a global threshold (1–59). For the analysis of individual adipocytes, we used the Avizo 3D (version 2021.1, Thermo Fisher Scientific, Waltham, MA, USA) software. First, the adipocytes were binarized and leftover noise was removed using interactive thresholding (1–255) and despeckle (speckle size = 7 µm × 7 µm × 7 µm) module. This was followed by segmenting individual adipocytes using a combination of thickness map computation and the H-extrema watershed module. Next, a border kill module was applied, removing adipocytes cut by the bounding box. Then, a 3D label analysis was performed that allowed the final filtering of the data based on shape (sphericity > 0.5) and volume (>4000 µm^3). Finally,

sphericity, volume (μm^3), area (μm^2), thickness (μm), and the number of adipocytes were computed.

Bone strength analyses. The femora isolated from C57BL/6N male mice after 8-week-long treatment with HFD or HFD supplemented with omega-3 were tested in a three-point bending test using an ElectroForce testing system (TestBench LM1, EnduraTEC Systems Group, Bose Corp., Minnetonka, MN, USA). A standard protocol was used in this experiment[50,51]. The span length and radius of curvature of the supports were 7 mm and 2 mm, respectively. Between dissection and mechanical testing, the bones were fixed in 4% paraformaldehyde at 4 °C for the first 48 h. Then, samples were stored in PBS at 4 °C. The bones were placed with the anterior surface pointing downward and were subjected to a small stabilizing preload (1 N) and two conditioning cycles before loading until failure at a rate of 0.1 mm/s. The following parameters were derived from the load-displacement curve: (1) bone strength (N), determined as the ultimate load during the three-point bending test; (2) work-to-failure (mJ), determined as the area under the load-displacement curve, representing the energy absorbed by the bone before breaking and (3) bone stiffness (N/mm), calculated as the slope of the linear proportion of the loaded-displacement curve, representing the elastic rigidity.

Bioenergetic analysis. Parallel measurement of oxygen consumption rate (OCR) and extracellular acidification rate (ECAR) was performed using the Seahorse XFe24 Analyzer (Agilent, Santa Clara, CA, USA). Primary BMSCs were seeded in a 24-well Agilent Seahorse XF Cell Culture Microplate in 5 plicates at a density of 20,000 cells per well in growth media the day prior to the analysis. The next day, all wells were washed with 1 mL of DMEM (Merck, Darmstadt, Germany) supplemented with 10 mM glucose, 4 mM glutamine, and 2 mM pyruvate (pH 7.4; 37 °C); 500 µL of the same media was pipetted, and the microplate was incubated at 37 °C for 30 min. Meanwhile, an XFe24 sensor cartridge was prepared by injection of substrates according to the protocol[52] to measure metabolic rates with endogenous substrates (basal), and after subsequent additions with a final concentration of 10 mM glucose (Merck, Darmstadt, Germany), 1 µM oligomycin (Oligo) (Merck, Darmstadt, Germany), 2 µM carbonyl cyanide-4-(trifluoromethoxy) phenylhydrazone (FCCP) (Merck, Darmstadt, Germany) and mixture of inhibitors of 1 µM rotenone (Rot) (Merck, Darmstadt, Germany), 1 µg/mL of antimycin A (AA) (Merck, Darmstadt, Germany) and 100 mM 2-deoxyglucose (2DG) (Merck, Darmstadt, Germany) (2DG + AA + Rot). The Seahorse data were analyzed using Wave Software 2.6.1. (Agilent, Santa Clara, CA, USA). The data were normalized by cell number determined by Hoechst 33342 staining of cell nuclei (final concentration 5 µg/mL) (Thermo Fisher Scientific, Waltham, MA, USA), which was performed immediately after the measurement using Cytation 3 Cell Imaging Reader (BioTek, Winooski, VT, USA) and processed by Gen5 software (BioTek, Winooski, VT, USA).

Isolation of mRNA and quantitative RT-PCR. Total RNA exptraction was carried out using TRI Reagent (Merck, Darmstadt, Germany) and the concentration of RNA was deermined using a Nanodrop spectrometer. Subsequently, cDNA synthesis was performed from 1 µg of total RNA using a High-Capacity cDNA Reverse Transcription Kit (Thermo Fisher Scientific, Waltham, MA, USA) according to the manufacturer's protocol. Quantitative real-time PCR was conducted using Light Cycler® 480 SYBR Green I Master (Roche, Basel, Switzerland) with specific primers (GeneriBiotech, Hradec Králové, Czech Republic) as listed in Supplementary Table 3. The RT-PCR data were normalized to the expression of the housekeeping gene (36B4 for mouse).

Western blot. Protein lysates from the cells were prepared using M2 lysis buffer. Protein concentration was measured using BCA assay (Thermo Fisher Scientific, Waltham, MA, USA). Proteins with a final loading concentration of 15 µg/mL were separated in sodium dodecyl sulfate-polyacrylamide gels and transferred onto PVDF (polyvinylidene difluoride) membrane (Imobilon-P) by semi-dry electroblotting. After blotting, membranes were washed for 5 min in TBS (150 mM Tris-HCl, 10 mM NaCl; pH 7,4) and blocked in 5% (*w/v*) fat-free dry milk diluted in TBS-T (TBS with 1% (*v/v*) detergent Tween-20) for 1 h. After blocking, the membranes were washed 5 × 5 min in TBS-T. For immunodetection, the membranes were incubated with primary antibody (diluted in 5% milk) overnight in 4 °C. Next day, membranes were washed 5 × 5 min in TBS-T and then incubated with corresponding HRP-conjugated secondary antibody for 1 h at RT. The list of WB antibodies (Cell Signaling, Danvers, MA, USA) is presented in Supplementary Table 4. Protein detection was performed using ECL Clarity Max detection substrate (Bio-Rad) measured by ChemiDoc imaging system (Bio-Rad, Hercules, CA, USA), and signals were calculated by Image Lab software (Bio-Rad, Hercules, CA, USA). Densitometry analysis was normalized to signals from positive control protein lysates present in each membrane. Uncropped western blot membrane images are shown in Supplementary Fig. 9, 10.

Lipidomics and metabolomics. Global lipidomic and metabolomic profiling of BM, bone powder (BP), and plasma samples was conducted using a combined untargeted and targeted workflow for the lipidome, metabolome, and exposome analysis (LIMeX)[11,53,54] with some modifications. Extraction was performed using a biphasic solvent system of cold methanol, methyl *tert*-butyl ether (MTBE), and 10% methanol. Four different liquid chromatography-mass spectrometry (LC-MS) platforms were used for profiling: (1) lipidomics of complex lipids using reversed-phase liquid chromatography with mass spectrometry (RPLC-MS) in positive ion mode, (2) lipidomics of complex lipids in RPLC-MS in negative ion mode, (3) metabolomics of polar metabolites using hydrophilic interaction chromatography with mass spectrometry (HILIC-MS) in positive ion mode, and (4) metabolomics of polar metabolites using RPLC-MS in negative ion mode.

Sample extraction for metabolomic and lipidomic analyses. BM and BP samples (20–25 mg) were homogenized with 275 µL methanol containing internal standards (PE 17:0/17:0, PG 17:0/17:0, LPC 17:1, Sphingosine d17:1, Cer d18:1/17:0, SM d18:1/17:0, PC 15:0/18:1-d_7, cholesterol-d_7, TG 17:0/17:1/17:0-d_5, DG 12:0/12:0/0:0, DG 18:1/2:0/0:0, LPE 17:1, oleic acid-d_9, PI 15:0/18:1-d_7, MG 17:0/0:0/0:0, PS 17:0/17:0, HexCer d18:1/17:0, DG 18:1/0:0/18:1-d_5, TG 20:0/20:1/20:0-d_5, LPG 17:1, LPS 17:1, cardiolipin 16:0/16:0/16:0/16:0) and 275 µL 10% methanol containing internal standards (caffeine-d_9, acetylcholine-d_4, creatinine-d_3, choline-d_9, TMAO-d_9, *N*-methylnicotinamide-d_4, betaine-d_9, butyrobetaine-d_9, creatine-d_3, cotinine-d_3, glucose-d_7, succinic acid-d_4, metformin-d_6) for 1.5 min using a grinder (MM400, Retsch, Germany). Then, 1 mL of MTBE with internal standard (CE 22:1) was added, and the tubes were shaken for 1 min and centrifuged at 16,000 rpm for 5 min.

Plasma samples (25 µL) were mixed with 765 µL of cold methanol/MTBE mixture (165 µL + 600 µL, respectively) containing the same mixtures of internal standards as before and

shaken for 30 s. Then, 165 µL of 10% MeOH with deuterated polar metabolite internal standards was added, shaken for 30 s, and centrifuged at 16,000 rpm for 5 min.

For lipidomic profiling, 100 µL of the upper organic phase was collected, evaporated and resuspended using 100 µL methanol with internal standard (12-[[(cyclohexylamino)carbonyl]amino]-dodecanoic acid, CUDA), shaken for 30 s, centrifuged at 16,000 rpm for 5 min and used for LC-MS analysis.

For metabolomic profiling, 70 µL of the bottom aqueous phase was collected, evaporated, resuspended in 70 µL of an acetonitrile/water (4:1, *v/v*) mixture with internal standards (CUDA and Val-Tyr-Val), shaken for 30 s, centrifuged at 16,000 rpm for 5 min and analyzed using HILIC metabolomics platform. Another 70 µL aliquote of the bottom aqueous phase was mixed with 210 µL of an isopropanol/acetonitrile (1:1, *v/v*) mixture, shaken for 30 s, centrifuged at 16,000 rpm for 5 min, and the supernatant was evaporated, resuspended in 5% methanol/0.2% formic acid with internal standards (CUDA and Val-Tyr-Val), shaken for 30 s, centrifuged at 16,000 rpm for 5 min and analyzed using RPLC metabolomics platform.

LC-MS-based lipidomics. The LC-MS systems consisted of a Vanquish UHPLC System (Thermo Fisher Scientific, Waltham, MA, USA) coupled to a Q Exactive Plus mass spectrometer (Thermo Fisher Scientific, Waltham, MA, USA).

Lipids were separated on an Acquity UPLC BEH C18 column (50 × 2.1 mm; 1.7 µm) coupled to an Acquity UPLC BEH C18 VanGuard pre-column (5 × 2.1 mm; 1.7 µm) (Waters, Milford, MA, USA). The column was maintained at 65 °C at a flow-rate of 0.6 mL/min. For LC–ESI(+)-MS analysis, the mobile phase consisted of (A) 60:40 (*v/v*) acetonitrile:water with ammonium formate (10 mM) and formic acid (0.1%) and (B) 90:10:0.1 (*v/v/v*) isopropanol:acetonitrile:water with ammonium formate (10 mM) and formic acid (0.1%). For LC–ESI(−)-MS analysis, the composition of the solvent mixtures was the same except for the addition of ammonium acetate (10 mM) and acetic acid (0.1%) as mobile-phase modifiers. Separation was conducted under the following gradient for LC–ESI(+)-MS: 0 min 15% (B); 0–1 min 30% (B); 1–1.3 min from 30% to 48% (B); 1.3–5.5 min from 48% to 82% (B); 5.5–5.8 min from 82% to 99% (B); 5.8–6 min 99% (B); 6–6.1 min from 99% to 15% (B); 6.1–7.5 min 15% (B). For LC–ESI(−)-MS, the following gradient was used: 0 min 15% (B); 0–1 min 30% (B); 1–1.3 min from 30% to 48% (B); 1.3–4.8 min from 48% to 76% (B); 4.8–4.9 min from 76% to 99% (B); 4.9–5.3 min 99% (B); 5.3–5.4 min from 99% to 15% (B); 5.4–6.8 min 15% (B). A sample volume of 0.3 µL, 1.5 µL, and 1.5 µL was used for BM, BP, and plasma extracts, respectively, in ESI(+). A sample volume of 5 µL for all matrices was used in ESI(−). Sample temperature was maintained at 4 °C.

The ESI source and MS parameters were: sheath gas pressure, 60 arbitrary units; aux gas flow, 25 arbitrary units; sweep gas flow, two arbitrary units; capillary temperature, 300 °C; aux gas heater temperature, 370 °C; MS1 mass range, *m/z* 200–1700; MS1 resolving power, 35,000 FWHM (*m/z* 200); number of data-dependent scans per cycle, 3; MS/MS resolving power, 17,500 FWHM (*m/z* 200). For ESI(+), a spray voltage of 3.6 kV and normalized collision energy of 20% was used, while for ESI(−), a spray voltage of −3.0 kV and normalized collision energy of 10, 20, and 30% were set up.

LC-MS-based metabolomics. Polar metabolites were separated on an Acquity UPLC BEH Amide column (50 × 2.1 mm; 1.7 µm) coupled to an Acquity UPLC BEH Amide VanGuard pre-column (5 × 2.1 mm; 1.7 µm) (Waters, Milford, MA, USA). The column was maintained at 45 °C at a flow-rate of 0.4 mL/min. The mobile phase consisted of (A) water with ammonium formate (10 mM) and formic acid (0.125%) and (B) acetonitrile:water (95/5) with ammonium formate (10 mM) and formic acid (0.125%). Separation was conducted under the following gradient: 0 min 100% (B); 0–1 min 100% (B); 1–3.9 min from 100% to 70% (B); 3.9–5.1 min from 70% to 30% (B); 5.1–6.4 min from 30% to 100% (B); 6.4–8.0 min 100% (B). A sample volume of 0.5 µL, 0.5 µL, and 1.5 µL was used for bone marrow, bone powder, and plasma extracts, respectively, in ESI(+). The sample temperature was maintained at 4 °C.

Polar metabolites were also separated on an Acquity UPLC HSS T3 column (50 × 2.1 mm; 1.8 µm) coupled to an Acquity UPLC HSS T3 VanGuard pre-column (5 × 2.1 mm; 1.8 µm) (Waters, Milford, MA, USA). The column was maintained at 45 °C using a ramped flow-rate. The mobile phase consisted of (A) water with formic acid (0.2%) and (B) methanol with formic acid (0.1%). Separation was conducted under the following gradient: 0 min 1% (B) 0.3 mL/min; 0–0.5 min 1% (B) 0.3 mL/min; 0.5–2 min from 1% to 60% (B) 0.3 mL/min; 2–2.3 min from 60% to 95% (B) from 0.3 mL/min to 0.5 mL/min; 2.3–3.0 min 95% (B) 0.5 mL/min; 3.0–3.1 min from 95% to 1% (B) 0.5 mL/min; 3.1–4.5 min 1% (B) 0.5 mL/min; 4.5–4.6 min 1% (B) from 0.5 mL/min to 0.3 mL/min; 4.6–5.5 min 1% (B) 0.3 mL/min. A sample volume of 5 µL was used to inject ESI(−). The sample temperature was maintained at 4 °C.

The ESI source and MS parameters were: sheath gas pressure, 50 arbitrary units; aux gas flow, 13 arbitrary units; sweep gas flow, three arbitrary units; capillary temperature, 260 °C; aux gas heater temperature, 425 °C; MS1 mass range, *m/z* 60–900; MS1 resolving power, 35,000 FWHM (*m/z* 200); number of data-dependent scans per cycle, 3; MS/MS resolving power, 17,500 FWHM (*m/z* 200). A spray voltage of 3.6 kV and −2.5 kV for ESI(+) and ESI(−), respectively, was used. A normalized collision energy of 20, 30, and 40% for all metabolomics platforms was used.

Quality control. Quality control was assured by (i) randomization of the actual samples within the sequence, (ii) injection of quality control (QC) pool samples at the beginning and the end of the sequence and between each ten actual samples, (iii) analysis of procedure blanks, (iv) serial dilution of QC sample (0, 1/16, 1/8, 1/4, 1/2, 1), (v) checking the peak shape and the intensity of spiked internal standards and the internal standard added prior to injection.

Data processing. LC-MS data from metabolomic and lipidomic profiling were processed through MS-DIAL v. 4.70 software. Metabolites were annotated using in-house retention time–*m/z* library and MS/MS libraries available from commercial and open sources (NIST20, MassBank, MoNA). Lipids were annotated using LipidBlast in-built in MS-DIAL. Traces of pioglitazone (*m/z* 355.1116) and MSDC-0602K (*m/z* 370.0749) were detected in RPLC-MS lipidomics in ESI(−) as deprotonated molecules. Raw data were filtered using blank samples, serial dilution samples, and QC pool samples with relative standard deviation (RSD) < 30% and then normalized using a locally estimated scatterplot smoothing (LOESS) approach by means of QC pool samples injected regularly between ten actual samples followed by sample-weight and injection volume normalization. Data were exported as the detector signal intensity in arbitrary units (A.U.).

Biochemical analyses of bone turnover markers. Rat/Mouse TRAP EIA for the quantitative determination of the Tartrate-resistant acid phosphatase (TRAP) for bone resorption and Rat/Mouse P1NP EIA for the determination of the N-terminal propeptide of type I procollagen (P1NP) for bone formation

(MyBioSource, San Diego, CA, USA) were measured in mouse serum samples.

Senescence-associated β-galactosidase (β-gal) activity assay. SA-β-gal Activity 96-well assay kit (Cell Biolabs, Inc-USA, Catalog Number CBA-231) was used to measure of SA-β-Gal activity coupled with cell senescence using a fluorometric substrate according to the manufacturer protocol[46]. Analyzed cells were seeded 48 h before the assay to a black 96-well plate with a clear bottom at a density of 15,000 cells/well. All reagents were freshly prepared on the day of assay. The cells were additionally treated with 50 μM TBHP (*tert*-butyl hydrogen peroxide) for 1 h at 37 °C and 5% CO_2 to induce the process of senescence. Measurements were then performed in fluorescent mode (Excitation ~360 nm/ Emission ~465 nm). Total protein concentration was determined by BCA protein assay kit (Merck) using absorbance mode (562 nm) in order to normalize the SA-β-Gal activity data. The results were expressed as a fold change of SA-β-gal activity.

Cellular Reactive Oxygen Species (ROS) detection assay. DCFDA (2,7-dichloro-dihydro-fluoroscein diacetate) (Abcam, Cambridge, United Kingdom) was used to measure the intracellular ROS production of primary BMSCs[46]. Cells were seeded to a dark, clear bottom 96-well plate at a density of 25,000 cells/well to adhere overnight. The next day, culture growth media was replaced with DCFDA Solution (25 μM) and incubated for 45 min at 37 °C and 5 % CO_2. DCFDA was removed and cells were loaded with 1x Buffer supplemented with 50 μM TBHP (*tert*-butyl hydrogen peroxide) for 1 h at 37 °C and 5% CO_2. The fluorescent intensity was detected every minute for 30 min using a fluorescent microplate reader (Excitation ~485 nm/Emission ~535 nm). The results were expressed as % of ROS production.

Statistics and reproducibility. Unless otherwise indicated, all data are collected from at least two independent experiments performed in triplicates. The statistical significance of the differences in the means of experimental groups was determined by unpaired t-test or ANOVA and Bonferroni or Tukey's post hoc tests using GraphPad Prism 5.0a software. The data are presented as means ± SEM. P value < 0.05 was considered statistically significant.

Reporting summary. Further information on research design is available in the Nature Portfolio Reporting Summary linked to this article.

Data availability

Source data for the graphs and charts are available as Supplementary Data 1 and uncropped blots are provided in Supplementary Figs. 9, 10. Any remaining information can be obtained from the corresponding author upon reasonable request.

Received: 6 April 2023; Accepted: 2 October 2023;
Published online: 14 October 2023

References

1. Bluher, M. Adipose tissue dysfunction contributes to obesity related metabolic diseases. *Best Pract. Res. Clin. Endocrinol. Metab* **27**, 163–177 (2013).
2. Benova, A. & Tencerova, M. Obesity-induced changes in bone marrow homeostasis.*Front. Endocrinol.* **11**, 294 (2020).
3. Swinburn, B. A., Caterson, I., Seidell, J. C. & James, W. P. Diet, nutrition and the prevention of excess weight gain and obesity. *Public Health Nutr.* **7**, 123–146 (2004).
4. Tencerova, M. et al. High-fat diet-induced obesity promotes expansion of bone marrow adipose tissue and impairs skeletal stem cell functions in mice. *J. Bone Miner. Res.* **33**, 1154–1165 (2018).
5. Scheller, E. L. et al. Changes in skeletal integrity and marrow adiposity during high-fat diet and after weight loss. *Front. Endocrinol.* **7**, 102 (2016).
6. Benova, A. et al. Novel thiazolidinedione analog reduces a negative impact on bone and mesenchymal stem cell properties in obese mice compared to classical thiazolidinediones. *Mol. Metab.* **65**, 101598 (2022).
7. Lecka-Czernik, B., Stechschulte, L. A., Czernik, P. J. & Dowling, A. R. High bone mass in adult mice with diet-induced obesity results from a combination of initial increase in bone mass followed by attenuation in bone formation; implications for high bone mass and decreased bone quality in obesity. *Mol. Cell Endocrinol.* **410**, 35–41 (2015).
8. Lewgood, J. et al. Efficacy of dietary and supplementation interventions for individuals with type 2 diabetes. *Nutrients* **13**, 2378 (2021).
9. Kirwan, J. P., Sacks, J. & Nieuwoudt, S. The essential role of exercise in the management of type 2 diabetes. *Cleve. Clin. J. Med.* **84**, S15–S21 (2017).
10. Saini, R. K. et al. Omega-3 Polyunsaturated Fatty Acids (PUFAs): emerging plant and microbial sources, oxidative stability, bioavailability, and health benefits-a review. *Antioxidants* **10**, 1627 (2021).
11. Sistilli, G. et al. Krill oil supplementation reduces exacerbated hepatic steatosis induced by thermoneutral housing in mice with diet-induced obesity. *Nutrients* **13**, 437 (2021).
12. Calder, P. C. Marine omega-3 fatty acids and inflammatory processes: effects, mechanisms, and clinical relevance. *Biochim. Biophys. Acta* **1851**, 469–484 (2015).
13. Flachs, P. et al. Polyunsaturated fatty acids of marine origin induce adiponectin in mice fed a high-fat diet. *Diabetologia* **49**, 394–397 (2006).
14. van Schothorst, E. M. et al. Induction of lipid oxidation by polyunsaturated fatty acids of marine origin in small intestine of mice fed a high-fat diet. *BMC Genom.* **10**, 110 (2009).
15. Kroupova, P. et al. Omega-3 phospholipids from krill oil enhance intestinal fatty acid oxidation more effectively than Omega-3 triacylglycerols in high-fat diet-fed obese mice. *Nutrients* **12**, 2037 (2020).
16. Martyniak, K. et al. Do polyunsaturated fatty acids protect against bone loss in our aging and osteoporotic population? *Bone* **143**, 115736 (2021).
17. Rossmeisl, M. et al. Omega-3 phospholipids from fish suppress hepatic steatosis by integrated inhibition of biosynthetic pathways in dietary obese mice. *Biochim. Biophys. Acta* **1841**, 267–278 (2014).
18. Salari, P., Rezaie, A., Larijani, B. & Abdollahi, M. A systematic review of the impact of n-3 fatty acids in bone health and osteoporosis. *Med. Sci. Monit.* **14**, RA37–RA44 (2008).
19. Shen, C. L., Yeh, J. K., Rasty, J., Li, Y. & Watkins, B. A. Protective effect of dietary long-chain n-3 polyunsaturated fatty acids on bone loss in gonad-intact middle-aged male rats. *Br. J. Nutr.* **95**, 462–468 (2006).
20. Bani Hassan, E. et al. The effects of dietary fatty acids on bone, hematopoietic marrow and marrow adipose tissue in a murine model of senile osteoporosis. *Aging* **11**, 7938–7947 (2019).
21. Cao, J. J., Gregoire, B. R., Michelsen, K. G. & Picklo, M. J. Increasing dietary fish oil reduces adiposity and mitigates bone deterioration in growing C57BL/6 mice fed a high-fat diet. *J. Nutr.* **150**, 99–107 (2020).
22. Levental, K. R. et al. omega-3 polyunsaturated fatty acids direct differentiation of the membrane phenotype in mesenchymal stem cells to potentiate osteogenesis. *Sci. Adv.* **3**, eaao1193 (2017).
23. Cugno, C. et al. Omega-3 fatty acid-rich fish oil supplementation prevents rosiglitazone-induced osteopenia in aging C57BL/6 mice and in vitro studies. *Sci Rep* **11**, 10364 (2021).
24. Bardova, K. et al. Additive effects of Omega-3 fatty acids and thiazolidinediones in mice fed a high-fat diet: triacylglycerol/fatty acid cycling in adipose tissue. *Nutrients* **12**, 3737 (2020).
25. Kerckhofs, G. et al. Contrast-enhanced nanofocus X-Ray computed tomography allows virtual three-dimensional histopathology and morphometric analysis of osteoarthritis in small animal models. *Cartilage* **5**, 55–65 (2014).
26. Sun, D. et al. Dietary n-3 fatty acids decrease osteoclastogenesis and loss of bone mass in ovariectomized mice. *J. Bone Miner. Res.* **18**, 1206–1216 (2003).
27. Bhattacharya, A., Rahman, M., Sun, D. & Fernandes, G. Effect of fish oil on bone mineral density in aging C57BL/6 female mice. *J Nutr Biochem* **18**, 372–379 (2007).
28. Anez-Bustillos, L. et al. Effects of dietary omega-3 fatty acids on bones of healthy mice. *Clin Nutr* **38**, 2145–2154 (2019).
29. Parahnak, Z., Freundorfer, M. T., Lavery, P. & Weiler, H. A. Dietary docosahexaenoic acid contributes to increased bone mineral accretion and strength in young female Sprague-Dawley rats. *Prostaglandins Leukot. Essent. Fatty Acids* **144**, 32–39 (2019).
30. Mollard, R. C., Gillam, M. E., Wood, T. M., Taylor, C. G. & Weiler, H. A. (n-3) fatty acids reduce the release of prostaglandin E2 from bone but do not affect bone mass in obese (fa/fa) and lean Zucker rats. *J. Nutr.* **135**, 499–504 (2005).
31. Kerckhofs, G. et al. Simultaneous three-dimensional visualization of mineralized and soft skeletal tissues by a novel microCT contrast agent with polyoxometalate structure. *Biomaterials* **159**, 1–12 (2018).

32. Scheller, E. L. et al. Use of osmium tetroxide staining with microcomputerized tomography to visualize and quantify bone marrow adipose tissue in vivo. *Methods Enzymol.* **537**, 123–139 (2014).
33. Cho, H. J., Lee, J., Yoon, S. R., Lee, H. G. & Jung, H. Regulation of hematopoietic stem cell fate and malignancy. *Int. J. Mol. Sci.* **21**, 4780 (2020).
34. Nakanishi, A. & Tsukamoto, I. n-3 polyunsaturated fatty acids stimulate osteoclastogenesis through PPARgamma-mediated enhancement of c-Fos expression, and suppress osteoclastogenesis through PPARgamma-dependent inhibition of NFkB activation. *J. Nutr. Biochem.* **26**, 1317–1327 (2015).
35. Zwart, S. R., Pierson, D., Mehta, S., Gonda, S. & Smith, S. M. Capacity of omega-3 fatty acids or eicosapentaenoic acid to counteract weightlessness-induced bone loss by inhibiting NF-kappaB activation: from cells to bed rest to astronauts. *J. Bone Miner. Res.* **25**, 1049–1057 (2010).
36. Gani, O. A. Are fish oil omega-3 long-chain fatty acids and their derivatives peroxisome proliferator-activated receptor agonists? *Cardiovasc. Diabetol.* **7**, 6 (2008).
37. McDonald, M. M. et al. Osteoclasts recycle via osteomorphs during RANKL-stimulated bone resorption. *Cell* **184**, 1330–1347.e1313 (2021).
38. Flachs, P. et al. Polyunsaturated fatty acids of marine origin upregulate mitochondrial biogenesis and induce beta-oxidation in white fat. *Diabetologia* **48**, 2365–2375 (2005).
39. Zhang, L., Mack, R., Breslin, P. & Zhang, J. Molecular and cellular mechanisms of aging in hematopoietic stem cells and their niches. *J. Hematol. Oncol.* **13**, 157 (2020).
40. Omer, M. et al. Omega-9 modifies viscoelasticity and augments bone strength and architecture in a high-fat diet-fed murine model. *Nutrients* **14**, 3165 (2022).
41. Watkins, B. A., Shen, C. L., Allen, K. G. & Seifert, M. F. Dietary (n-3) and (n-6) polyunsaturates and acetylsalicylic acid alter ex vivo PGE2 biosynthesis, tissue IGF-I levels, and bone morphometry in chicks. *J. Bone Miner. Res.* **11**, 1321–1332 (1996).
42. Raisz, L. G. Prostaglandins and bone: physiology and pathophysiology. *Osteoarthritis Cartilage* **7**, 419–421 (1999).
43. Kus, V. et al. Unmasking differential effects of rosiglitazone and pioglitazone in the combination treatment with n-3 fatty acids in mice fed a high-fat diet. *PLoS One* **6**, e27126 (2011).
44. Rossmeisl, M. et al. Differential modulation of white adipose tissue endocannabinoid levels by n-3 fatty acids in obese mice and type 2 diabetic patients. *Biochim. Biophys. Acta Mol. Cell Biol. Lipids* **1863**, 712–725 (2018).
45. Jafari, A. et al. Pharmacological inhibition of protein kinase g1 enhances bone formation by human skeletal stem cells through activation of RhoA-Akt Signaling. *Stem Cells* **33**, 2219–2231 (2015).
46. Tencerova, M. et al. Obesity-associated hypermetabolism and accelerated senescence of bone marrow stromal stem cells suggest a potential mechanism for bone fragility. *Cell Rep.* **27**, 2050–2062.e2056 (2019).
47. Halper, J., Madel, M. B. & Blin-Wakkach, C. Differentiation and phenotyping of murine osteoclasts from bone marrow progenitors, monocytes, and dendritic cells. *Methods Mol. Biol.* **2308**, 21–34 (2021).
48. Hansen, M. S. et al. GIP reduces osteoclast activity and improves osteoblast survival in primary human bone cells. *Eur. J. Endocrinol.* **188**, lvac004 (2023).
49. Ding, M., Danielsen, C. C. & Hvid, I. Age-related three-dimensional microarchitectural adaptations of subchondral bone tissues in guinea pig primary osteoarthrosis. *Calcif. Tissue Int.* **78**, 113–122 (2006).
50. Jardi, F. et al. Androgen receptor in neurons slows age-related cortical thinning in male mice. *J. Bone Miner. Res.* **34**, 508–519 (2019).
51. Callewaert, F. et al. Sexual dimorphism in cortical bone size and strength but not density is determined by independent and time-specific actions of sex steroids and IGF-1: evidence from pubertal mouse models. *J. Bone Miner. Res.* **25**, 617–626 (2010).
52. Pajuelo Reguera, D. et al. Cytochrome c oxidase subunit 4 isoform exchange results in modulation of oxygen affinity. *Cells* **9**, 443 (2020).
53. Janovska, P. et al. Dysregulation of epicardial adipose tissue in cachexia due to heart failure: the role of natriuretic peptides and cardiolipin. *J. Cachexia Sarcopenia Muscle* **11**, 1614–1627 (2020).
54. Tsugawa, H. et al. A lipidome atlas in MS-DIAL 4. *Nat. Biotechnol.* **38**, 1159–1163 (2020).

Acknowledgements

We would like to thank the Histology Core facility at CCP Biocev for their excellent work in the preparation of bone samples. We thank Kimberly Crevits at FIBEr, KU Leuven, for performing the three-point bending tests. We would like to thank Dr. Ondrej Kuda from IPHYS, CAS for his scientific input in omega-3 PUFA experiments. We are grateful for the help writing the MATLAB script for automatic histogram windowing and relative gray value normalization of CECT images to Arne Maes from KU Leuven. We are thankful for omega-3 PUFA concentrate provided by Epax Norway AS (Ålesund, Norway). The authors would like to acknowledge the Metabolomics Core Facility at the Institute of Physiology of the Czech Academy of Sciences for global metabolomic and lipidomic profiling. This work was supported by START UP Research program by the Institute of Physiology of the Czech Academy of Sciences and the Czech Science Foundation GACR 20-03586S (M.T.), GACR 19-02411S (J.K.), EFSD/NovoNordisk foundation Future leaders award (NNF20SA0066174), National Institute for Research of Metabolic and Cardiovascular Diseases (Program EXCELES, ID Project No. LX22NPO5104)—Funded by the European Union—Next Generation EU, Grant Agency of Charles University GAUK 339821 (A.B.), FRIA grant 40008717 (T.B.) and FWO G088218N (G.K. and T.B.).

Author contributions

M.T. and J.K. conceived the project. A.B., M.F., M.T., K.B., J.F., G.A., M.D., A.C., O.H., M.R. and J.K. designed in vivo experiments, performed the in vivo and in vitro experiments, collected and analyzed data. AP and TM provided material and helped interpret bioenergetic profiling results. T.C. performed and helped with the interpretation of metabolomics data. T.B. and G.K. performed BMAT measurement in bones ex vivo and helped with BMAT evaluation, and data interpretation. WW and GHL helped to perform three-point bending tests and data interpretation. J.P. and F.S. performed µCT scanning of bones ex vivo and helped with the data analysis. M.H. helped with OC experiments. R.C. helped with animal experiment and data analysis. M.T., A.B., M.R. and J.K. designed and supervised the study and wrote the manuscript. All authors revised and approved the manuscript.

Competing interests

All authors declare no competing interests.

Additional information

Supplementary information The online version contains supplementary material available at https://doi.org/10.1038/s42003-023-05407-8.

Correspondence and requests for materials should be addressed to Michaela Tencerova.

Peer review information *Communications Biology* thanks Bram van der Eerden and Eleni Douni for their contribution to the peer review of this work. Primary Handling Editors: Martina Rauner and George Inglis. A peer review file is available.

Reprints and permission information is available at http://www.nature.com/reprints

Publisher's note Springer Nature remains neutral with regard to jurisdictional claims in published maps and institutional affiliations.

3.2. AIM2: To investigate the effect of novel TZD analog MSDC-0602K on bone and BMAT metabolism in mouse model of obesity

Reference: *Benova A*, Ferencakova M, Bardova K, Funda J, Prochazka J, Spoutil F, Cajka T, Dzubanova M, Balcaen T, Kerckhofs G, Willekens W, van Lenthe GH, Alquicer G, Pecinova A, Mracek T, Horakova O, Rossmeisl M, Kopecky J, Tencerova M. Novel thiazolidinedione analog reduces a negative impact on bone and mesenchymal stem cell properties in obese mice compared to classical thiazolidinediones. Mol Metab. 2022 Nov;65:101598. doi: 10.1016/j.molmet.2022.101598. Epub 2022 Sep 11. PMID: 36103974; PMCID: PMC9508355.

Summary: To treat metabolic diseases like obesity and T2D, one of the first line medication given to the patients are insulin sensitizing drugs, including TZDs. However, the side effects associated with the first generation of TZDs (pioglitazone, rosiglitazone), such as weight gain, cardiovascular issues, increased BMA and increased bone fragility, have limited their clinical application. The negative impact of these drugs on bone health is particularly concerning, partly due to their activation of PPARγ, which promotes adipocyte differentiation and osteoclast activation both peripherally and, in the BM. This highlights the need for further research to understand the specific effects of antidiabetic treatments on bone and fat metabolism.

Thus, a new "PPARγ-sparing" TZD analog, MSDC-0602K (a second-generation TZD), was developed to minimize TZDs adverse effects on bone and fat metabolism. MSDC-0602K is designed to reduce direct PPARγ binding but maintains its inhibitory action on the MPC, which is thought to contribute to its positive effects on energy metabolism and glucose uptake. Clinical trials (phase 2b) of MSDC-0602K together with previous studies showed promising results, lowering glucose and insulin levels. Moreover, minimized negative side effect on bone parameters in aged male mice were also observed [397]. However, the effects of this novel TZD analog on bone metabolism under obesogenic conditions remain unexplored.

Therefore, in the present part of the thesis we evaluated effect of MSDC-0602K and pioglitazone on bone and BMSC characteristics in a diet-induced obesity model in male C57BL/6N mice after 2 months of treatment. Our findings demonstrated that MSDC-0602K significantly enhanced bone health in obese mice, as evidenced by an increased presence of smaller BMAds in the tibia compared to those treated with pioglitazone. Additionally, primary BMSCs isolated from mice treated with MSDC-0602K, as well as human BMSCs, showed a reduction in adipocyte differentiation and an increase in osteoblast differentiation. This was

coupled with a decrease of inflammatory response of mHSCs and senescent markers in mBMSCs compared to the same cell types treated with pioglitazone. Surprisingly, measurement of respiration of primary mBMSCs showed increased glycolysis and maximal respiration in cells obtained from MSDC-0602K treated mice compared to pioglitazone group, suggesting potential difference in cellular metabolism and nutrient utilization by MSDC-0602K compared to pioglitazone.

Our research offers novel perspectives on the efficacy of MSDC-0602K treatment in obese mice, highlighting its lack of negative impact on bone quality and BMSC metabolism in comparison to traditional TZDs. Thus, these findings emphasize the potential of MSDC-0602K in clinical use for treating both metabolic disorders and bone diseases, suggesting a promising alternative for future clinical applications.

Author's contribution: The author of this thesis was mainly involved in design of *in vivo* and *in vitro* experiments, data analysis and discussion of the results with the rest of the authors of manuscript, writing of the manuscript and performing following experiments: µCT data analysis, isolation of BMSC, measurement of assays to determine BMSC differentiation phenotype, measurement Seahorse experiments, performing glucose uptake assay to determine metabolic preference of human BMSCs, *in vitro* testing of human BMSCs differentiation phenotype and metabolic profile (Seahorse measurements) in response to pioglitazone, rosiglitazone or MSDC-0602K supplementation of differentiation media.

3.3. AIM 3: To study potential differences in the mechanism of action of classical TZDs and new analog MSDC-0602K in BMSCs

Reference: *Benova A*, Ferencakova M, Bardova K, Funda J, Prochazka J, Spoutil F, Cajka T, Dzubanova M, Balcaen T, Kerckhofs G, Willekens W, van Lenthe GH, Alquicer G, Pecinova A, Mracek T, Horakova O, Rossmeisl M, Kopecky J, Tencerova M. Novel thiazolidinedione analog reduces a negative impact on bone and mesenchymal stem cell properties in obese mice compared to classical thiazolidinediones. Mol Metab. 2022 Nov;65:101598. doi: 10.1016/j.molmet.2022.101598. Epub 2022 Sep 11. PMID: 36103974; PMCID: PMC9508355.

Summary: TZDs are insulin sensitizing drugs with dual mechanism of action. Firstly, they are PPARγ agonist and their high affinity to this transcription factor leads to increased insulin sensitivity in various tissues like muscle and AT. Second mechanism of action is coupled with binding and inhibiting of MPC proteins in mitochondria which leads to metabolic changes of the cells. However, binding of PPARγ is coupled with increased adiposity in periphery and also in the bones which consequently leads to increased fracture risk. Thus, novel TZD analog MSCD-0602K with its low affinity to PPARγ was designed to avoid the side effects caused by binding of this transcription factor and the mechanism of action via MPC inhibition should be preserved.

Following our previous results in mice where we showed comparison of the effect of two generations of TZDs on mouse bones and primary BMSCs in obesogenic conditions, we aimed to study whether these changes are caused by the same mechanism of action of these drugs as in the peripheral AT [349]. Thus, to compare the mechanism of action of these drugs in bones and in the peripheral AT, we chose two cell lines: 3T3-L1 to mimic conditions in peripheral AT and hBMSC-TERT (further just hBMSC) cell line to see how it works in bones. Moreover, to confirm the MPC inhibiting effect of the drugs we decided to use specific MPC inhibitor UK5099.

Firstly, we proved that response of hBMSCs to the TZD treatment is similar with response of primary BMSCs by measuring effect of TZDs and MSDC-0602K on differentiation potential of the cells and cellular metabolism. Further, we measured cellular metabolism, mitochondrial respiration also in 3T3-L1 cells after acute treatment with TZDs, MSDC-0602K and UK5099,

where we observed opposite effect of first generation TZDs which decreased maximal respiration in hBMSCs, while increased in 3T3-L1 cells versus MSDC-0602K similarly as by UK5099. To understand the different effect of TZD analogs in cellular metabolism between AT-MSCs and BMSCs, we tested whether different nutrient preferences after acute treatment with TZDs, MSDC-0602K and UK5099 would explain their contribution to cellular metabolism. Glucose and glutamine uptake assays showed that TZD treatment (pioglitazone) in AT-MSCs favored glucose over glutamine uptake, while MSDC-0602K-treated BMSCs preferred glutamine. These experiments confirmed different metabolic responses to TZD treatments in periphery and bone cells. These changes were also confirmed by gene expression of markers of glutamine metabolism. All these data were published together with mouse experiments with TZDs and MSDC-0602K from aim 2 in [400]. To further understand the metabolic differences behind the treatment with classical TZD pioglitazone and MSDC-0602K, we preformed fluxomic experiments in hBMSCs using ^{13}C-labeled glucose and glutamine tracers.

3.3.1. Unpublished materials and methods:

Cell transfection using siRNA system

hBMSCs were transfected with the siRNA, targeting MPC1 (ID#: s28488) as well as non-targeting siRNA (siRNA negative control, Scr cat#: AM4635) were purchased from Ambion (Life Technology Inc). siRNA was transfected to hBMSCs at a final concentration of 10 μM by Lipofectamine2000 (Invitrogen) as previously described [401] and according to the manufacturer instructions. Transfection cocktail was subsequently replaced after 7 hours with normal culture media. 48 hours post transfection culture media was replaced with adipogenic or osteogenic differentiation media and further molecular analysis after 7 days of differentiation was performed as described previously [400].

^{13}C-labeled nutrient tracing in hBMSCs

hBMSCs were seeded at the density 25 000 cells/cm^2 on 6-well plate in standard cultivation media containing minimal essential media (Thermo Fisher Scientific, Watham, MA, USA), 10% fetal bovine serum (FBS) and 1% penicillin/streptomycin (Thermo Fisher Scientific, Watham, MA, USA). Next day, cultivation media was replaced with cultivation media

containing 30 µM pioglitazone/ rosiglitazone/ MSDC-0602K or 2µM UK5099. After 24 hours, cells were washed with PBS and media containing 5,5 mM ^{13}C-labeled glucose (Cambridge Isotope laboratories- cat.n. CLM-1396-0) or 2 mM ^{13}C-labeled glutamine (Cambridge Isotope laboratories- cat.n. CLM-1822-H), 10 % dialized FBS (Gibco, cat n. A33820-01). After 72 hours, all wells were washed with 0,9 % NaCl and immediately frozen in liquid nitrogen and stored in -80°C till the subsequent analysis.

Metabolomic and lipidomic analysis

Data analysis from ^{13}C-labaled nutrient tracing of glucose and glutamine in hBMSCs was performed as described previously in the paper Lopes et al. [402].

3.3.2. Results:

To test if MPC proteins are differently expressed, we measured gene expression of MPC1 and MPC2 during hBMSC differentiation into adipocytes and osteoblasts. We observed increased MPC2 gene expression during the osteoblast differentiation, while MPC1 was slightly increased during adipo differentiation (Figure 8A-B). Also, we observed that MPC1 is more abundant in hBMSCs compared to MPC2 (Figure 8C).

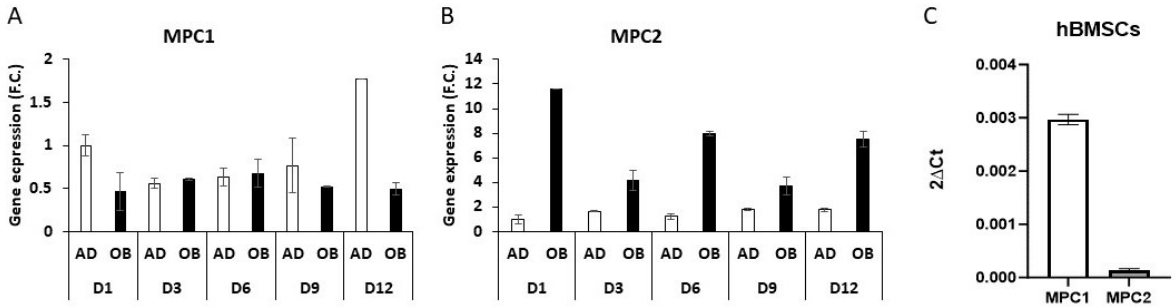

Figure 8. Differences in gene expression of MPC1 and MPC2 during hBMSC differentiation. Gene expression profile of A) MPC1 and B) MPC2 during adipo and osteo differentiation of hBMSCs in day 1, 3, 6, 9 and 12. Data are presented as fold change of gene expression normalized to AD D1; C) Relative mRNA levels of MPC1 and MPC2 in hBMSCs. Data are presented as mean of 2 CT ± SEM (n= 2).

Further, we performed hBMSC transfection using two different siRNAs (MPC1#1 and MPC1#2, see Figure 9A) to silence MPC1 subunit (MPC1 KD (knock-down)) of MPC dimer. Both MPC1 siRNAs showed high transfection efficacy, with more robust effect using siRNA MPC1#2 (more than 90%), which we chose for further *in vitro* experiments (MPC1#2, further just MPC1). Unfortunately, testing of various siRNAs targeting MPC2 did not show sufficient efficacy as showed in Figure 9B, thus we decided to exclude it from the study.

Further to test the hypothesis if MPC inactivation in hBMSCs has an effect on differentiation potential of the cells, we investigated the effect of MPC1 KD on adipocyte and osteoblast differentiation. We also measured gene expression of MPC2 in transfected cells, to show that this subunit does not compensate the effect of silencing of MPC1 and we observed just small increase of MPC2 in osteo differentiation of MPC1 KD compared to Scr OB hBMSCs (Figure 9C-D).

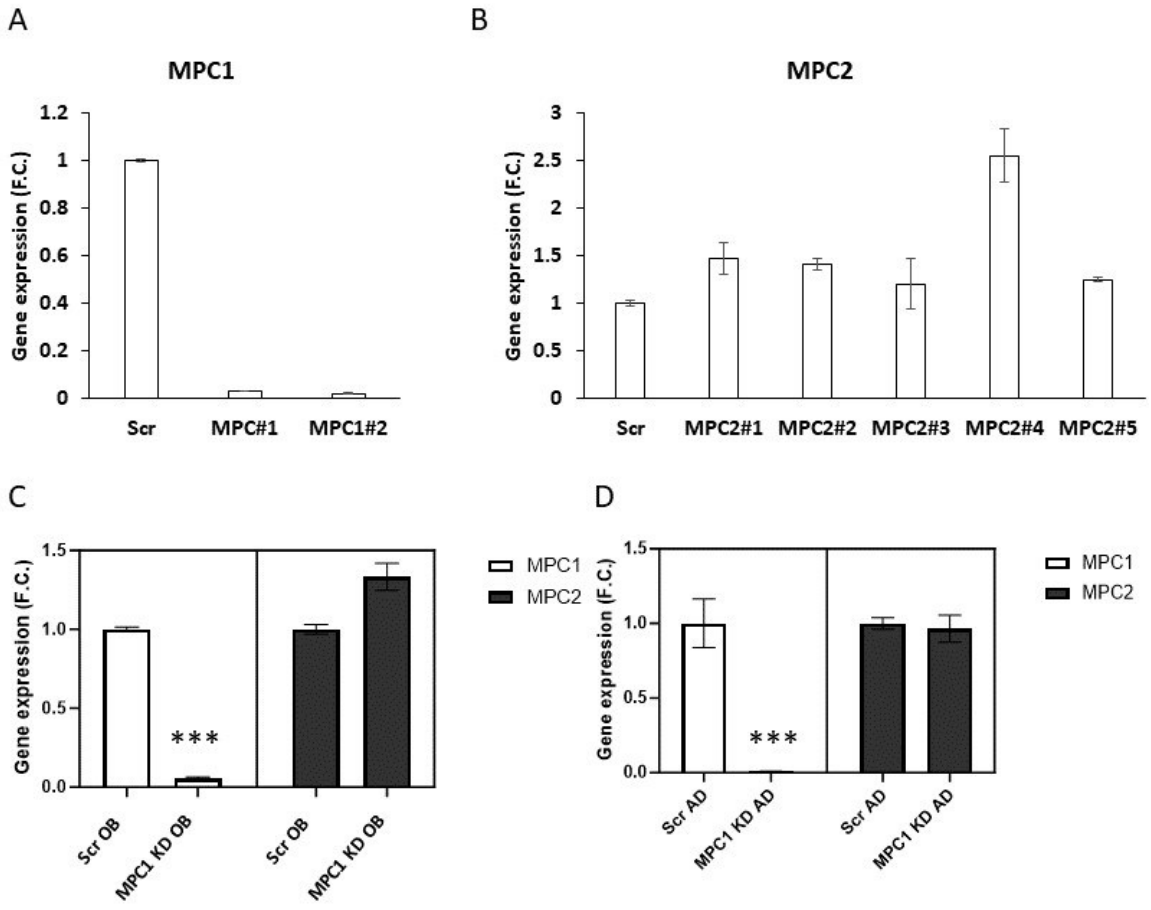

Figure 9. Efficacy of MPC transfection in hBMSCs and comparison of MPC1 and MPC2 gene expression after hBMSC cell transfection. A) Efficacy of MPC1 and B) MPC2 siRNA transfection. Analysis of gene expression of MPC1 and MPC2 in transfected hBMSCs in C) osteo and D) adipo differentiation at D7. Data are presented as mean ± SEM (n= 5 per group; 3 independent experiments); t-test: *** $p < 0.0001$.

We found that MPC1 KD increased osteoblast (Figure 10A) and decreased adipocyte differentiation in hBMSCs (Figure 10B) measured by ALP activity and Nile red after 7 days of differentiation compared to Scr hBMSCs. This was supported by the gene expression of adipogenic (*PPARG, CEBPA* and *ADIPOQ*) and osteogenic marker (*ALPL*) (Figure 10C-D).

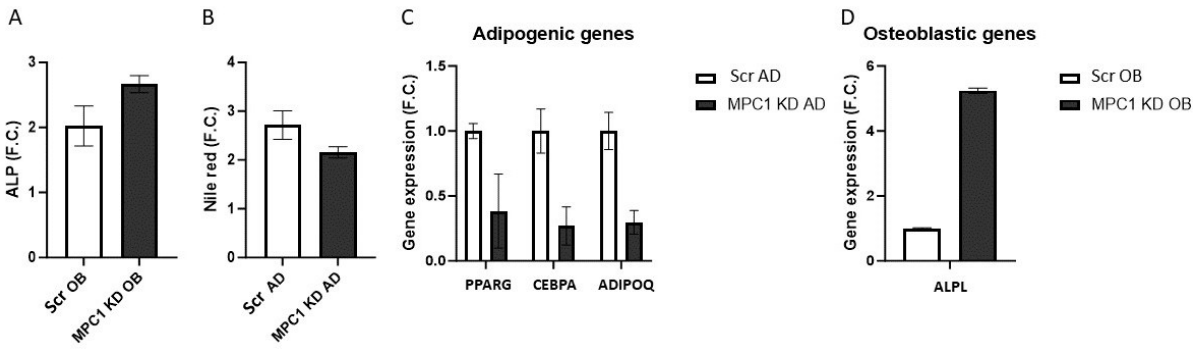

Figure 10. Effect of MPC1 KD on hBMSC differentiation. Measurement of A) ALP activity in osteo differentiated hBMSCs and B) quantification of adipogenesis of hBMSCs via Nile red staining at D7 of differentiation. Data are presented as mean fold change ALP activity in osteoblast or Nile red in adipocytes from each experimental group ± SEM (n= 3 independent experiments); t-test: ns. Gene expression analysis of C) adipogenic (*PPARG, CEBPA, ADIPOQ*) and osteogenic (*ALPL*) markers at D7 of differentiation. Data are presented as mean ± SEM (n= 2 per group).

Moreover, to test whether the effect of MPC inactivation on hBMSC differentiation (via TZD treatments or siRNA) affect also hBMSC metabolic responses, we tested insulin response of hBMSC measured by activation of AKT proteins (p-T308-AKT/totalAKT and p-S473-AKT/totalAKT). 48h-long treatment with pioglitazone and MSDC-0602K (1µM) showed upregulation of AKT signaling in pioglitazone treatment, while MSDC-0602K treatment decreased insulin response (Figure 11A-C). Further testing of hBMSC MPC1 KD cells (Figure 11D-F) confirmed similar insulin response as MSDC-0602K treated cells suggesting the mechanism of action of MSDC-0602K via MPC1 inhibition.

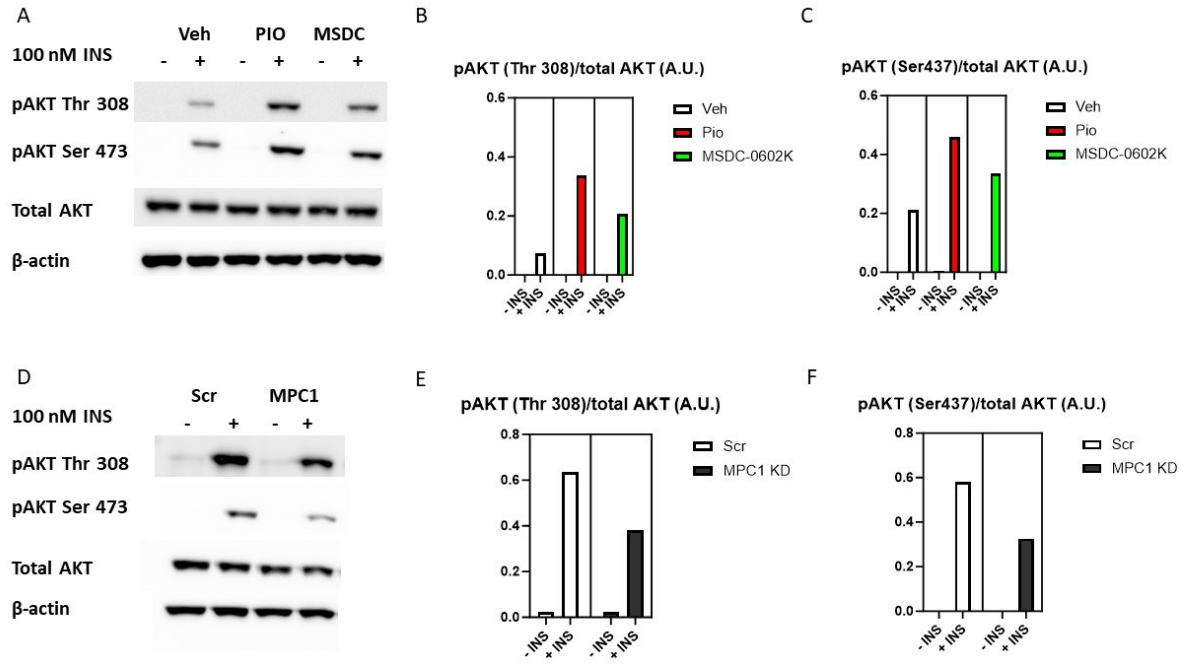

Figure 11. Comparison of pioglitazone, MSDC-0602K and MPC1 KD on insulin sensitivity of hBMSCs. A) Representative western blots and B-C) densitometry evaluation of images representing results of insulin stimulation (100 nM, 15 minutes) of p-Thr308-AKT/Total AKT and p- Ser473-AKT/Total AKT in hBMSCs treated with 1µM pioglitazone and MSDC-0602K for 48 hours. D) Representative western blots and E-F) densitometry evaluation of images representing results of insulin stimulation (100 nM, 15 minutes) of p-Thr308-AKT/Total AKT and p- Ser473-AKT/Total AKT in hBMSCs transfected with MPC1 siRNA (n= 1).

Further, based on our previous data on different nutrient preferences between pioglitazone and MSDC-0602K treatment in hBMSCs, we performed *in vitro* experiment with isotopically labeled glutamine and glucose (^{13}C-glutamine and ^{13}C-glucose) to trace metabolic fluxes of these nutrients in hBMSCs after 72h TZD treatment in order to define differences in metabolic pathways involved in nutrient utilization and downstream cellular metabolism affected by these treatments (Figure 12).

Using LC-MS measurement of isotope labeled metabolites after 72 hours long *in vitro* treatment of hBMSCs revealed that glutamine utilization via glutaminase (GLS) was increased in MSDC-0602K treatment compared to pioglitazone. On the other hand, glucose metabolic flux into pyruvate was enhanced in pioglitazone treatment. Further, MSDC-0602K treatment contributed more to production of other TCA metabolites, including acetyl-CoA by converting

citrate via ATP-citrate synthase (ACLY) compared to pioglitazone treatment in hBMSCs. ACLY is important enzyme participating in FA biosynthesis. Thus, further analysis revealed indeed that MSDC-0602K treatment further utilized acetyl-CoA and oxalacetate to form citrate in mitochondria by citrate synthase (CS) more profoundly than in pioglitazone treatment possibly contributing to lipogenesis. However, we need to perform more analysis using different tracers (e.g. palmitate) to further investigate the differences on the level of lipid utilization and contribution to *de novo* lipogenesis using different TZD treatments as our in vivo data in HFD mice also showed differences on the level of BMAd size in bones of MSDC-0602K and pioglitazone treated HFD mice. Further, increased conversion rate of alpha-ketoglutarate in mitochondria to succinate via alpha-ketoglutarate dehydrogenase (OGDH) and thus contributing to NADH production in MSDC-0602K treatment compared to pioglitazone. As NADH directly providing electrons for the respiratory chain, these findings could support our data from bioenergetics with increased respiratory rate in MSDC-0602K treated BMSCs compared to cells treated with pioglitazone.

Interestingly, fluxomic data revealed different activation of phosphoenolpyruvate carboxykinase (PEPCK), a key enzyme in gluconeogenesis (process of glucose production) in mitochondria and cytosol. While cytosolic PEPCK activity did not show any difference between MSDC-0602K and pioglitazone treatment, mitochondrial PEPCK activity was more pronounced in MSDC-0602K suggesting compensatory mechanism to inhibition of MPC1.

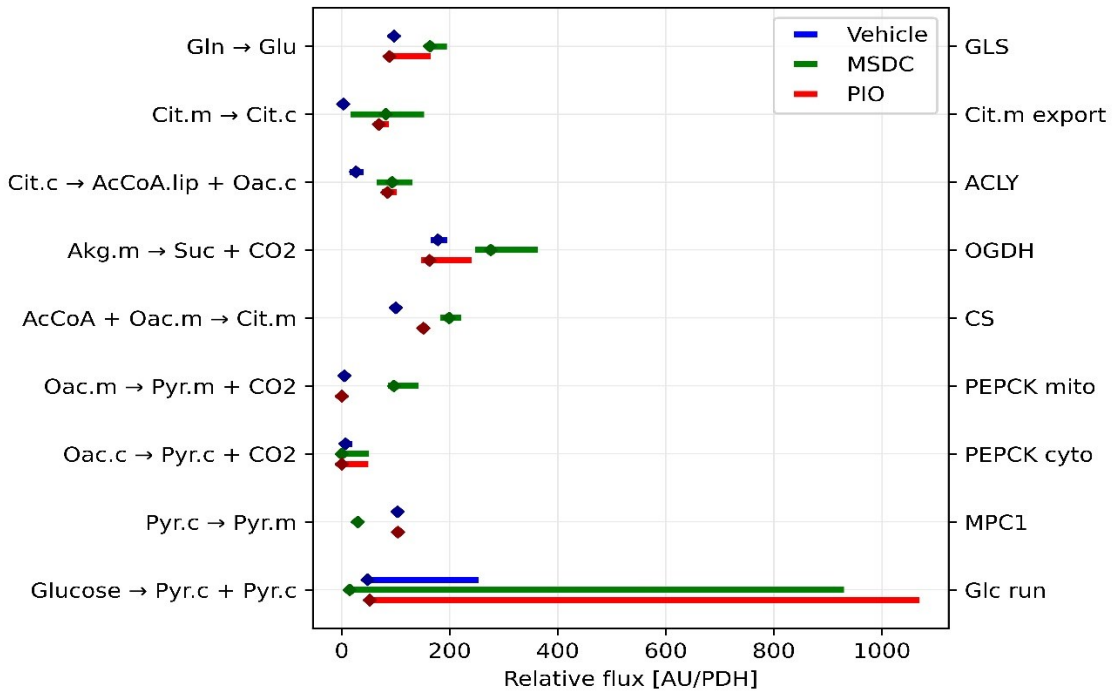

Figure 12. Analysis of ^{13}C-labeled glucose and glutamine in hBMSCs treated with MSDC-0602K and pioglitazone. The overview presents the metabolic flux values relative to the activity of PDH. Simplified metabolic reactions are listed on the left, with abbreviated names of enzymes (if available) on the right. The flux values are indicated by diamond symbols. Confidence intervals (ranging from 5% to 95%) are depicted by colored lines: blue for the control group treated with vehicle, green for the MSDC group, and red for the pioglitazone group. Data are expressed as metabolic flux values relative to the activity of PDH. (Abbreviations: Gln: glutamine, Glu: glucose, Cit: citrate, AcCoA: Acetyl-Coenzyme A, Oac: oxaloacetate, Suc: succinate, Pyr: pyruvate, GLS: glutaminase, ACLY: ATP-citrate synthase, OGDH: alpha-ketoglutarate dehydrogenase, CS: citrate synthase, PEPCK: phosphoenolpyruvate carboxykinase; MPC1: mitochondrial pyruvate carrier 1)

These preliminary results are showing different responses of bone and AT cell precursors to first and second generation of treatment. Moreover, inhibiting of MPC1 protein in hBMSCs showed similar response as MSDC-0602K treatment but not to pioglitazone suggesting differences in mechanism of action of these drugs in bones and in the periphery. Further, fluxomic analysis confirmed increased glutamine metabolism with MSDC-0602K and showed differences between MSDC-0602K and pioglitazone in activation of different enzymes used in TCA cycle. However, further research is needed to fully explain these findings.

Author's contribution: The author of this thesis designed of the *in vitro* experiments under the supervision of supervisor Dr. M. Tencerova and perform the experiments in the aim 3.

Original Article

MOLECULAR METABOLISM

Novel thiazolidinedione analog reduces a negative impact on bone and mesenchymal stem cell properties in obese mice compared to classical thiazolidinediones

Andrea Benova [1,2], Michaela Ferencakova [1], Kristina Bardova [3], Jiri Funda [3], Jan Prochazka [4], Frantisek Spoutil [4], Tomas Cajka [5], Martina Dzubanova [1,2], Tim Balcaen [6,9,10], Greet Kerckhofs [6,7,8,9], Wouter Willekens [11], G. Harry van Lenthe [12], Glenda Alquicer [1], Alena Pecinova [13], Tomas Mracek [13], Olga Horakova [3], Martin Rossmeisl [3], Jan Kopecky [3], Michaela Tencerova [1,*]

ABSTRACT

Objective: The use of thiazolidinediones (TZDs) as insulin sensitizers has been shown to have side effects including increased accumulation of bone marrow adipocytes (BMAds) associated with a higher fracture risk and bone loss. A novel TZD analog MSDC-0602K with low affinity to PPARγ has been developed to reduce adverse effects of TZD therapy. However, the effect of MSDC-0602K on bone phenotype and bone marrow mesenchymal stem cells (BM-MSCs) in relation to obesity has not been intensively studied yet.

Methods: Here, we investigated whether 8-week treatment with MSDC-0602K has a less detrimental effect on bone loss and BM-MSC properties in obese mice in comparison to first generation of TZDs, pioglitazone. Bone parameters (bone microstructure, bone marrow adiposity, bone strength) were examined by μCT and 3-point bending test. Primary BM-MSCs were isolated and measured for osteoblast and adipocyte differentiation. Cellular senescence, bioenergetic profiling, nutrient consumption and insulin signaling were also determined.

Results: The findings demonstrate that MSDC-0602K improved bone parameters along with increased proportion of smaller BMAds in tibia of obese mice when compared to pioglitazone. Further, primary BM-MSCs isolated from treated mice and human BM-MSCs revealed decreased adipocyte and higher osteoblast differentiation accompanied with less inflammatory and senescent phenotype induced by MSDC-0602K vs. pioglitazone. These changes were further reflected by increased glycolytic activity differently affecting glutamine and glucose cellular metabolism in MSDC-0602K-treated cells compared to pioglitazone, associated with higher osteogenesis.

Conclusion: Our study provides novel insights into the action of MSDC-0602K in obese mice, characterized by the absence of detrimental effects on bone quality and BM-MSC metabolism when compared to classical TZDs and thus suggesting a potential therapeutical use of MSDC-0602K in both metabolic and bone diseases.

Keywords Obesity-induced bone fragility; Bone microstructure; Bone marrow mesenchymal stem cells; Bone marrow adiposity; Thiazolidinedione analog MSDC-0602K; Pioglitazone

1. INTRODUCTION

Obesity is accompanied with ectopic fat accumulation in non-adipose organs, including bones, leading to increased bone marrow (BM) adiposity, which is associated with an increased risk of bone fractures and osteoporosis in obese and diabetic patients [1]. Several studies including our recent observations, show that obesity changes the BM microenvironment and impacts BM mesenchymal stem cell (BM-MSC) properties by increased adipogenesis, which contributes to bone fragility induced by metabolic complications [2–6].

[1]Laboratory of Molecular Physiology of Bone, Institute of Physiology of the Czech Academy of Sciences, Prague 142 20, Czech Republic [2]Faculty of Science, Charles University, Prague, Czech Republic [3]Laboratory of Adipose Tissue Biology, Institute of Physiology of the Czech Academy of Sciences, Prague 142 20, Czech Republic [4]Czech Centre for Phenogenomics & Laboratory of Transgenic Models of Diseases, Institute of Molecular Genetics of the Czech Academy of Sciences, Prague, Czech Republic [5]Laboratory of Translational Metabolism, Institute of Physiology of the Czech Academy of Sciences, Prague 142 20, Czech Republic [6]Biomechanics lab, Institute of Mechanics, Materials, and Civil Engineering, UCLouvain, Louvain-la-Neuve, Belgium [7]Department of Materials Engineering, KU Leuven, Belgium [8]Prometheus, Division of Skeletal Tissue Engineering, Katholieke Universiteit Leuven, 3000 Leuven, Belgium [9]Pole of Morphology, Institute for Experimental and Clinical Research, UCLouvain, Brussels, Belgium [10]Department of Chemistry, Molecular Design and Synthesis, KU Leuven, Leuven, Belgium [11]FIBEr, KU Leuven, Leuven, Belgium [12]Department of Mechanical Engineering, KU Leuven, Leuven, Belgium [13]Laboratory of Bioenergetics, Institute of Physiology of the Czech Academy of Sciences, Prague, Czech Republic

*Corresponding author. Molecular Physiology of Bone, Institute of Physiology of the Czech Academy of Sciences, Videnska 1083, Prague 4, 142 20, Czech Republic. E-mail: michaela.tencerova@fgu.cas.cz (M. Tencerova).

Received June 22, 2022 • Revision received September 6, 2022 • Accepted September 6, 2022 • Available online 11 September 2022

https://doi.org/10.1016/j.molmet.2022.101598

Abbreviations

ALP	Alkaline phosphatase
AT	Adipose tissue
BM	Bone marrow
BMAds	Bone marrow adipocytes
BMAT	Bone marrow adipose tissue
BM-MSCs	Bone marrow mesenchymal stem cells
CE-CT	Contrast-enhanced microCT
CESA	Contrast-enhancing staining agent
ECAR	Extracellular acidification rate
HFD	High-fat diet
HSCs	Hematopoietic stem cells
GTT	Glucose tolerance test
LPC	Lysophophatidylcholine
MPC	mitochondrial pyruvate carrier
ND	Normal diet
OCR	Oxygen consumption rate
P1NP	Procollagen type 1 N-terminal propeptide
POM	Polyoxometalate
ROS	Reactive oxygen species
TG	Triacylglycerol
TRAP	Tartrate-resistant acid phosphatase
TZDs	Thiazolidinediones

In obesity and type 2 diabetes several approaches are used to treat or prevent the detrimental effects of metabolic diseases, including physical activity, dietary or pharmacological treatment. The use of thiazolidinediones (TZDs) has been for a long time considered as an appropriate treatment for metabolic complications by improving insulin sensitivity in patients with type 2 diabetes. However, the adverse effects induced by first generation of TZDs in terms of weight gain, cardiovascular complications and bone loss have reduced their use in the clinical practice [7]. The negative effect of TZDs on bone physiology is associated with increased BM adiposity leading to bone loss [7]. The use of these insulin-sensitizing drugs usually has a secondary detrimental effect on bone physiology because of the activation of peroxisome proliferator-activated receptor-γ (PPARγ) regulating adipocyte (AD) differentiation both in the periphery and in the BM, where they also induce osteoclast activation [5,8]. Therefore, further studies are needed to dissect the molecular effects of this type of antidiabetic treatments on bone and fat physiology.

A previous study by Stechschulte et al. [9] demonstrated that changes in post-translational modification of PPARγ can reduce the negative effect on bone metabolism while maintaining the positive effect on energy metabolism. Along these lines, a novel "PPARγ-sparing" TZD analog MSDC-0602K ("second generation of TZDs") was developed to minimize the adverse side effects of TZDs on bone and fat metabolism [10–14]. MSDC-0602K was purposely designed to decrease direct binding to PPARγ [11,15], but it maintains its inhibitory effect on mitochondrial pyruvate carrier (MPC), which likely contributes to the beneficial effect on energy metabolism and glucose uptake [11,12,16]. Testing of MSDC-0602K drug in a clinical trial (phase 2b) showed promising results in terms of lowering glucose and insulin levels and improving liver steatosis without side effects in obese subjects [17]. Fukunaga et al. [13] recently reported that MSDC-0602K showed no side effects in lean mice with respect to bone parameters compared to rosiglitazone. However, the impact of this novel TZD analog on bone metabolism in obese conditions has not been studied yet. Thus, the main objective of this study was to determine whether MSDC-0602K has a less detrimental effect on bone structure and molecular properties of BM-MSCs compared to a typical TZD pioglitazone, using a model of diet-induced obesity in male C57BL/6N mice.

2. MATERIALS AND METHODS

Additional methods are described in the Supplementary Material.

2.1. Animals and dietary interventions

Male C57BL/6N mice (Charles River Laboratories, Sulzfeld, Germany) were maintained at 22 °C with 12-hour light–dark cycle (light from 6:00 a.m.). Upon arrival and before the start of the experiment all mice had free access to water and standard chow diet (ND, Ssniff Spezialdieten GmbH, Soest, Germany). At the age of 12 weeks, mice were randomly divided into 5 groups ($n = 8–10$, repeated in 3 independent experiments) and fed for 8 weeks with: i) normal diet (ND) (3.4% wt/wt as lipids; Rat/Mouse- Maintenance extrudate; Ssniff Spezialdieten GmbH, Soest, Germany); ii) high-fat diet (HFD, lipid content, ~35% wt/wt, mainly corn oil [18]; iii) HFD + P, HFD supplemented with 50 mg pioglitazone/kg diet (Actos, Takeda, Japan); iv) HFD + M, HFD supplemented with 330 mg MSDC-0602K/kg diet (Cirius Therapeutics, USA) [10]. Diets were stored at −20 °C, in sealed plastic bags filled with nitrogen. The dose of pioglitazone and MSDC-0602K was the same as in the previous studies using these compounds in mice [10,18]. Body weight and 24-hour food consumption were measured every week.

Mice were sacrificed after 8 weeks of dietary interventions in the fed-state by cervical dislocation under diethyl ether anesthesia. Tissue samples and primary isolated mBM-MSCs were used for subsequent molecular analyses. All experiments were performed according to the guideline of the Institute of Physiology of the Czech Academy of Sciences and were approved under protocol number 81/2016.

2.1.1. Glucose tolerance test

Intraperitoneal glucose tolerance test (GTT) was performed using 1 mg of glucose/g body weight in overnight fasted mice as previously published [10].

2.1.2. Biochemical analysis of plasma

Blood glucose levels were measured by OneTouch Ultra glucometers (LifeScan, Milpitas, CA, USA), and plasma insulin levels were determined by the Sensitive Rat Insulin RIA Kit (Millipore, Billerica, MA, USA).

2.2. Isolation of mBM-MSCs and mHSCs

mBM-MSCs were isolated from the bones of front and hind limbs of C57BL/6N male mice (after 8 weeks of dietary treatments) following previous protocols with the small modifications [3]. After bone crushing, collagenase digestion (StemCell, Vancouver, BC, Canada) and negative selection of CD45, CD31 and Ter119 cells (Miltenyi, Bergisch Gladbach, Germany) mBM-MSCs were obtained. mBM-MSCs were subcultured in growth medium (MEM alpha (Thermo Fisher Scientific, Waltham, MA, USA) + 20% FBS (Thermo Fisher Scientific, Waltham, MA, USA) + 1% penicillin/streptomycin (P/S) (Thermo Fisher Scientific, Waltham, MA, USA) + 0.5% Amphotericin B (Merck, Darmstadt, Germany) + 1% Glutamax (Thermo Fisher Scientific, Waltham, MA, USA) + 1% MEM NEAA (Thermo Fisher Scientific, Waltham, MA, USA) + 1% sodium pyruvate (Thermo Fisher Scientific, Waltham, MA, USA)) and cultivated for further analysis. The positive fraction with mHSCs was divided into three samples. One was

harvested for mRNA isolation with Tri-Reagent (Merck, Darmstadt, Germany), the second was harvested for proteins and the rest was seeded and cultivated in growth medium for further analysis.

2.2.1. Colony forming units-fibroblast (CFU-f) assay

After mBM-MSC isolation, cells were seeded for CFU 500 cells/60 mm Petri dish and cultivated in growth media. After 14 days in culture colonies displaying more than 50 cells were counted using Crystal Violet staining (Merck, Darmstadt, Germany).

2.2.2. Short-time proliferation assay

Isolated mBM-MSCs were plated in 24-well plate in triplicates at density of 1000 cells/well in standard growth medium. Cell number was evaluated after 1, 3, 6 and 9 days. Cells were washed with PBS, detached by trypsinization, and then manually counted using Bürker-Türk counting chamber.

2.2.3. *In vitro* differentiation of mBM-MSCs

Primary mBM-MSCs from passage 2 were used for analyzing their differentiation capacity.

2.2.3.1. Osteoblast differentiation. mBM-MSCs were seeded at a density of 20 000 cells/cm^2. When the cells reached 80% confluence MEM medium (Thermo Fisher Scientific, Waltham, MA, USA) supplemented with 10% FBS (Thermo Fisher Scientific, Waltham, MA, USA) and 1% P/S (Thermo Fisher Scientific, Waltham, MA, USA) was added to control cells and the rest of the cells were cultivated with osteoblast induction media consisting of 10 mM β-glycerophosphate (Merck, Darmstadt, Germany), 10 nM dexamethasone (Merck, Darmstadt, Germany) and 50 μg/ml Vitamin C (Wako Chemicals USA Inc., Richmond, VA, USA). The media was changed every second day for 7 days (ALP activity) and 11 days (Alizarin Red staining).

2.2.3.2. Alizarin Red staining. Mineralization of cell matrix at day 11 was measured using Alizarin Red S staining. Cells were fixed with 70% ice-cold ethanol for minimum 1 h at −20 °C after which Alizarin Red S solution (Merck, Darmstadt, Germany) was added. The cells were stained for 10 min at room temperature (RT). Excess dye was washed with distilled water followed by PBS. The amount of mineralized matrix (bound stain) was quantified by elution of the Alizarin red stain, using 20 min incubation of the cultures in 70% dH2O, 20% ethanol and 10% methanol solution on a shaker (100 rpm) at RT. The absorbance of the eluted dye was measured at 500 nm, using microplate reader according to the protocol [19].

2.2.3.3. Alkaline phosphatase (ALP) activity assay. ALP activity and cell viability assay were quantified at day 7 of OB differentiation in order to normalize the ALP activity data to the number of viable cells. Cell viability assay was performed using Cell Titer-Blue Assay Reagent (Promega, Madison, WI, USA) at fluorescence intensity ($579_{Ex}/584_{Em}$). ALP activity was determined by absorbance at 405 nm using p-nitrophenyl phosphate (Merck, Darmstadt, Germany) as substrate [2].

2.2.3.4. Adipocyte differentiation. Cells were plated at density of 30 000 cells/cm^2. For AD differentiation DMEM media (Thermo Fisher Scientific, Waltham, MA, USA) was used, containing 10% FBS (Thermo Fisher Scientific, Waltham, MA, USA), 9% horse serum (Merck, Darmstadt, Germany), 1% P/S (Thermo Fisher Scientific, Waltham, MA, USA), 100 nM dexamethasone (Merck, Darmstadt, Germany), 0.5 uM 3-isobutyl-1-methyxanthine (IBMX) (Merck, Darmstadt, Germany), 1 μM BRL (Merck, Darmstadt, Germany), 3 μg/mL Insulin (Merck, Darmstadt, Germany). The media was changed every three days for 10 days. Horse serum supplementation of media was used just for the first three days of induction.

2.2.3.5. Oil Red O staining. At day 10 of differentiation cells were rinsed with PBS and fixed in 4% paraformaldehyde (Merck, Darmstadt, Germany) for 10 min at RT. After fixation cells were briefly rinsed with 3% isopropanol solution (Merck, Darmstadt, Germany) and lipid droplets were stained with Oil Red O solution (Merck, Darmstadt, Germany) for 1 h at RT.

2.2.3.6. Nile Red staining. Nile Red Staining was performed as we previously described [20]. It is a direct stain for the detection of intracellular lipid droplets by fluorescence microscopy. Cells were cultured in polystyrene flat-bottom 96-well tissue culture-treated black microplates (BRANDplates®, cellGrade™, Brand, Wertheim, Germany). Nile Red dye (Merck, Darmstadt, Germany) working solution was prepared from a stock solution of 1 mg/ml. Cells were washed with PBS (Thermo Fisher Scientific, Waltham, MA, USA). Dye was added directly to the cells (5 μg/ml in PBS), and incubated for 10 min at room temperature in the dark, then washed twice with PBS. Fluorescent signal was measured using a Cytation 3 cell imaging multimode plate reader (BioTek, Winooski, VT, USA) using excitation of 485 nm and emission of 572 nm. The fluorescent signal of Nile Red stain was normalized to cell viability signal measured by Cell Titer-Blue Assay Reagent (Promega, Madison, WI, USA) mentioned above.

2.3. Insulin responsiveness of mHSCs

Primary mHSCs were cultured up to passage 1 and seeded for insulin and LPS stimulation. Cells were plated at a density of 300 000 cells/well in 12-well plates. After reaching the confluence, cells were starved for 4 h in serum-free MEM alpha (Thermo Fisher Scientific, Waltham, MA, USA) medium with 0.5% BSA and 1% P/S, then stimulated with 100 nM Insulin for 15 min at 37 °C and harvested for protein used in subsequent analyses.

2.4. *In vitro* differentiation of hBM-MSCs

We used well-characterized hBM-MSC-TERT cell line (as a model of hBM-MSCs) established by ectopic expression of the catalytic subunit of human telomerase, as described previously in our papers [21,22]. Cells were cultured in standard culture medium containing minimal essential medium (MEM) (Thermo Fisher Scientific, Waltham, MA, USA) supplemented with 10% fetal bovine serum (FBS) and 1% penicillin/streptomycin (P/S) (Thermo Fisher Scientific, Waltham, MA, USA) at 37 °C in a humidified atmosphere containing 5% CO_2. Cells were regularly tested for mycoplasma contamination.

For AD differentiation, cells were plated at a density of 30 000 cells/cm^2 and induced with adipogenic induction medium DMEM containing 10% FBS (Thermo Fisher Scientific, Waltham, MA, USA), 100 nM dexamethasone (Merck, Darmstadt, Germany), 500 nM insulin (Merck, Darmstadt, Germany), 1 μM BRL49653 (Merck, Darmstadt, Germany), and 0.25 mM 3-isobutyl-1-methylxanthine (Merck, Darmstadt, Germany). The medium was changed every third day up to 10 days. Oil red O/Nile Red staining of neutral lipids in mature AD was performed as mentioned above.

For OB differentiation, 20 000 cells/cm^2 were seeded and induced with OB induction medium containing 10 mM β-glycerophosphate (Merck, Darmstadt, Germany), 10 nM dexamethasone (Merck, Darmstadt, Germany), 50 μg/ml L-ascorbic acid (Wako Chemicals USA Inc., Virginia, USA), 10 nM 1,25-dihydroxyvitamin D_3 (Merck, Darmstadt, Germany) in MEM supplemented with 10% FBS and 1% P/S. The

medium was changed every third day up to 10 days. Quantification of ALP activity and Alizarin Red staining were performed as described above.

2.5. Micro-computed tomography (μCT) analysis

Proximal tibias and distal body of the 5th lumbar vertebra (L5) of mice fed for 8 weeks with ND, HFD or HFD supplemented with pioglitazone or MSDC-0602K were scanned with a high-resolution μCT SkyScan 1272 (Bruker, Billerica, MA, USA) with resolution 3 μm per voxel (voltage 80 kV, current 125 μA with 1 mm aluminum filter, exposure 1300 ms, 2time averaging, and 0.21° rotation step on 360°scanning). Reconstruction of virtual slices was performed in NRecon 1.7.3.1 (Bruker, Billerica, MA, USA) with InstaRecon 2.0.4.0 reconstruction engine (InstaRecon, Urbana, IL, USA) with 49% beam hardening correction, ring artifact correction = 9, and range of intensities 0–0.09 AU for tibia and 0–0.11 for L5. Reconstructions were reoriented in DataViewer 1.5.6 (Bruker, Billerica, MA, USA). Areas of interest were selected based on reference section and analyzed in CT Analyser 1.18.4.0 (Bruker, Billerica, MA, USA) with structure separation based on the Otsu's method. Cortical and trabecular bone were analyzed in the same area for structure volume, porosity, density, and connectivity. The region for the analyses was defined from the first slide under the growth plate to 230th slide. A detailed description for the quantification of 3D microarchitecture of trabecular and cortical bone has been presented previously [23].

2.6. Contrast-enhanced computed tomography (CECT) workflow

2.6.1. Staining procedure

The current standard for studying bone marrow adipocytes (BMAds) in 3D using CECT is osmium tetroxide (OsO_4) [24]. However, OsO_4 is highly toxic and requires decalcification of the tissue in order to obtain reliable results and does not allow subsequent colorimetric histological staining. Recently, Kerckhofs et al. introduced a polyoxometalate (POM)-based CESA, which allows the simultaneous visualization and analysis of adipocytes, bone and blood vessels [25]. However, if a researcher is only interested in adipocytes and bone, a more efficient CESA could be used. In this study, Hexabrix, a non-toxic staining agent, was used to visualize BMAT in bones. Since bone is strongly attenuating in nature, we opted to use a CESA that was unable to interact with adipocytes, but able to generally interact with other BM constituents. This would increase the contrast differences between bone, BM and adipocytes and consequently facilitate the desired BMAT analyses. Hexabrix is well-known in the field of CECT (*in vivo* and *ex vivo*), and has extensively, but not exclusively, been used in studies concerning the visualization and quantification of sulfated glycosaminoglycans (sGAGs) in cartilage tissue. Both sGAGs and Hexabrix are negatively charged at physiological pH (7.4) and will consequently repel each other [26–28]. Since adipocytes contain many types of lipid molecules (free fatty acids, TG etc.) that create a hydrophobic environment containing biomolecules bearing negatively charged functional groups (phosphate and/or carboxylate groups), we expected a similar repelling effect of this CESA towards adipocytes, rendering adipocytes darker compared to the surrounding BM in the CECT images. This combined with a computed LogD (a metric for the distribution of a molecule between a hydrophobic and a hydrophilic phase at a certain pH) at pH 7.4 of −1.52 indicates that this molecule will unlikely accumulate in hydrophobic areas (e.g. BMAds). These Hexabrix-stained CECT images of BMAT were confirmed by H&E-stained sections from the same bone area and thus validating this compound to visualize BMAT.

The staining solution was prepared by mixing commercial Hexabrix® solution (Guerbet, 10 mL, 320 mgI/mL) with a 1x PBS (phosphate-buffered saline, 40 mL, 10 mM). Formalin-fixed proximal tibias (right leg) of the mice were transferred to a 1.5 mL Eppendorf tube containing 1 mL of staining solution. These Eppendorf tubes were placed on a shaker plate (gentle shaking) at ambient temperature. The samples were stained for at least 3 days, after which they were scanned.

2.6.2. μCT image acquisition and reconstruction

For image acquisition, the samples were removed from the Eppendorf tube and wrapped in parafilm to prevent dehydration while exposed to X-rays. Samples were imaged using a Phoenix NanoTom M (GE Measurement and Control Solutions, Boston, MA, USA). A diamond-coated tungsten target was used. The system was operated with the following acquisition parameters: voltage = 60–70 kV, current = 120–140 μA, focal spot size = 1.99 μm, isotropic voxel size = 2 μm^3, exposure time = 500 ms, frame averaging = 1, image skip = 0 and scan time = 20 min. The reconstruction was performed using DatosIx GE Measurement and Control Solutions software (version 2.7.0 – RTM) with a beam hardening correction of 8 and the inline median, ROI CT filter and Filter volume algorithms, implemented in the software. Subsequently, the datasets were normalized using an in-house developed Matlab script, with air and residual Hexabrix solution as references.

2.6.3. CECT image analysis of BMAT

After consistent alignment of the datasets (DataViewer 1.5.6, Bruker MicroCT, Billerica, MA, USA), we initiated the analysis of the μCT data using CTAn (Bruker MicroCT, Billerica, MA, USA). First, we selected the volume of interest (VOI) in the proximal metaphysis of the tibia starting 250 slices below the growth plate and covering 500 slices in the distal direction. In this VOI, binarization of the dataset was performed using a global threshold (130–255). This threshold masked both cortical and trabecular bone. Based on this selection, a denoised mask for the bone marrow combined with the trabecular bone was segmented by performing a sequence of VOI shrink-wrap, closing (2–10; increments of 2) and opening (2–10; increments of 2) operations (*i.e.* everything inside the cortical bone was selected). The newly generated mask was projected on the grey value image, generating a new VOI. In this new VOI, the segmentation of adipocytes was performed using a global threshold (1–59). For the analysis of individual adipocytes, we used the Avizo 3D (version 2021.1, Thermo Fisher Scientific, Waltham, MA, USA) software. First, the adipocytes were binarized and leftover noise was removed using an interactive thresholding (1–255) and despeckle (speckle size = 7 μm × 7 μm x 7 μm) module. This was followed by the segmentation of individual adipocytes using a combination of thickness map computation and the H-extrema watershed module. Next, a border kill module was applied, which removed adipocytes that were cut by the bounding box. Then, a 3D label analysis was performed that allowed a final filtering of the data based on shape (sphericity >0.5) and volume (>4000 μm^3). Finally, sphericity, volume (μm^3), area (μm^2), thickness (μm) and number of adipocytes were computed.

2.7. Bone strength analyses

The femora isolated from C57BL/6N male mice after 8-week-long treatment with HFD or HFD supplemented with pioglitazone and MSDC-0602K were tested in a three-point bending test using an ElectroForce testing system (TestBench LM1, EnduraTEC Systems Group, Bose Corp., Minnetonka, MN, USA). A standard protocol as

described in previous work was used in this experiment [29,30]. Span length and radius of curvature of the supports were 7 mm and 2 mm, respectively. In the period between dissection and mechanical testing, the bones were fixed in 4% paraformaldehyde at 4 °C for the first 48 h after which they were stored in PBS at 4 °C. The bones were placed with the anterior surface pointing downward and were subjected to a small stabilizing preload (1 N) and two conditioning cycles before loading until failure at a rate of 0.1 mm/s. The following parameters were derived from the load—displacement curve: 1) bone strength (N), determined as the ultimate load during the three-point bending test; 2) work-to-failure (mJ), determined as the area under the load—displacement curve, representing the energy absorbed by the bone before breaking and 3) bone stiffness (N/mm), calculated as the slope of the linear proportion of the loaded-displacement curve, representing the elastic rigidity.

2.8. Bioenergetic analysis

Parallel measurement of oxygen consumption rate (OCR) and extracellular acidification rate (ECAR) was performed using the Seahorse XFe24 Analyzer (Agilent, Santa Clara, CA, USA). Primary mBM-MSCs were seeded in 24-well Agilent Seahorse XF Cell Culture Microplate in 5-plicates at a density of 20 000 cells per well in growth media the day prior the analysis. The next day, all wells were washed with 1 mL of DMEM (Merck, Darmstadt, Germany) supplemented with 10 mM glucose, 4 mM glutamine and 2 mM pyruvate (pH 7.4; 37 °C); 500 μL of the same media was pipetted and the microplate was incubated at 37 °C for 30 min. Meanwhile, an XFe24 sensor cartridge was prepared by injection of substrates according to the protocol [31] to measure metabolic rates with endogenous substrates (basal), and after subsequent additions with final concentration of 10 mM glucose (Merck, Darmstadt, Germany), 1 μM oligomycin (Oligo) (Merck, Darmstadt, Germany), 2 μM carbonyl cyanide-4-(trifluoromethoxy) phenylhydrazone (FCCP) (Merck, Darmstadt, Germany) and mixture of inhibitors of 1 μM rotenone (Rot) (Merck, Darmstadt, Germany), 1 μg/mL of antimycin A (AA) (Merck, Darmstadt, Germany) and 100 mM 2-deoxyglucose (2DG) (Merck, Darmstadt, Germany) (2DG + AA + Rot). During the measurement of acute effect of TZDs and MSDC-0602K on mitochondrial metabolism of human hBM-MSCs and 3T3-L1 cell line (ATCC, Washington, DC, USA) the protocol was adjusted by adding of vehicle (dimethyl sulfoxide (DMSO)), pioglitazone, rosiglitazone, MSDC-0602K or mitochondrial pyruvate carrier inhibitor - UK5099 (Merck, Darmstadt, Germany) instead of 10 mM glucose with the final concentration of 10—30 μM for TZDs and TZD analog and 2 μM for UK5099. The Seahorse data were analyzed using Wave Software 2.6.1. (Agilent, Santa Clara, CA, USA). The data were normalized by cell number determined by Hoechst 33342 staining of cell nuclei (final concentration 5 μg/mL) (Thermo Fisher Scientific, Waltham, MA, USA), which was performed immediately after the measurement using Cytation 3 Cell Imaging Reader (BioTek, Winooski, VT, USA) and processed by Gen5 software (BioTek, Winooski, VT, USA).

2.9. Statistical analysis

All data are representative of at least two independent experiments of similar results performed in triplicates unless otherwise indicated. The statistical significance of the differences in the means of experimental groups was determined by unpaired t-test or ANOVA and Bonferroni or Tukey post hoc tests using GraphPad Prism 5.0a software. The data are presented as means ± SEM. p value < 0.05 was considered statistically significant.

3. RESULTS

3.1. MSDC-0602K is less detrimental than pioglitazone on bone parameters in obese mice

To determine the effect of novel TZD analog, MSDC-0602K on metabolic and bone parameters in high-fat diet (HFD)-induced obesity, C57BL/6N male mice were fed for 8 weeks with HFD or HFD supplemented with first generation of TZDs, pioglitazone (HFD + P) or MSDC-0602K (HFD + M). As shown by Bardova et al. [10] and the present study, MSDC-0602K administered to HFD mice had a similar positive impact as pioglitazone on metabolic parameters, including reduction in fasting glycemia and insulinemia and improvement of glucose tolerance (Figure. S1A—D), as well as decreased adipose tissue (AT) inflammation [10], but with a more pronounced effect with respect to reduction of weight gain (Figure. S1E—F). This may indicate less severe side effects on AT function when compared to the first generation of TZDs.

As an extension of the above study with a focus on MSDC-0602K-induced impact on bone physiology, μCT analyses of proximal tibia and L5 vertebrae were performed in treated mice. While we did not observe significant changes in bone microstructure of proximal tibia (data not shown), there were more pronounced changes in L5 vertebrae (Figure 1A—E). HFD induced increased cortical porosity (Ct.Po) in L5, which was decreased in mice treated with HFD + M mice (Figure 1A). On the other hand, cortical thickness (Ct.Th) in L5 was decreased in HFD mice with a trend to increase in HFD + M group (Figure 1B). Further, trabecular number (Tb.N) in L5 was decreased in HFD + P compared to HFD mice, while HFD + M group showed a less detrimental effect on this parameter (Figure 1C). Other trabecular parameters were not changed (Figure. S1G—I). These changes are demonstrated in the representative 3D images of L5 trabecular and cortical bone in treated mice (Figure 1D—E). Further, ratio of circulating levels of bone formation marker procollagen type 1 N-terminal propeptide (P1NP) and bone resorption marker tartrate-resistant acid phosphatase (TRAP) (P1NP/TRAP) showed higher bone formation rate in HFD + M group compared to normal diet (ND) (Figure 1F). Bone strength measured by three-point bending test revealed stronger femora in HFD + M mice compared to HFD and HFD + P group (Figure 1G). Together these data showed that 8-week-long preventive treatment of HFD mice with MSDC-0602K reduced a negative impact on bone parameters with increased resistance to mechanical stress than typical TZD, pioglitazone.

3.2. BMAT composition is differently affected in obese mice treated with pioglitazone and MSDC-0602K

To further evaluate the impact of different diets on BM adiposity, the BMAT volume was analyzed using contrast-enhanced X-ray microfocus computed tomography (CECT). While μCT is unable to distinguish between distinct soft tissues due to their intrinsic low X-ray attenuation, CECT can do so by using X-ray opaque contrast-enhancing staining agents (CESAs). These CESAs enrich the X-ray attenuating atom content of the soft tissues in a specific manner. In this study, we selected Hexabrix, an anionic, iodinated CESA, which shows weaker interactions with non-adipocyte tissue constituents and is still excluded by the adipocytes. Moreover, it is a smaller molecule compared to the POM-based CESA, and thus it stains the whole tissue sample faster [26—28].

Image analysis of Hexabrix-stained BMAds confirmed an increased BM adiposity in HFD mice as in previous studies using OsO_4 [3,5]. A similar increase in BM adiposity was observed in the HFD + P and HFD + M

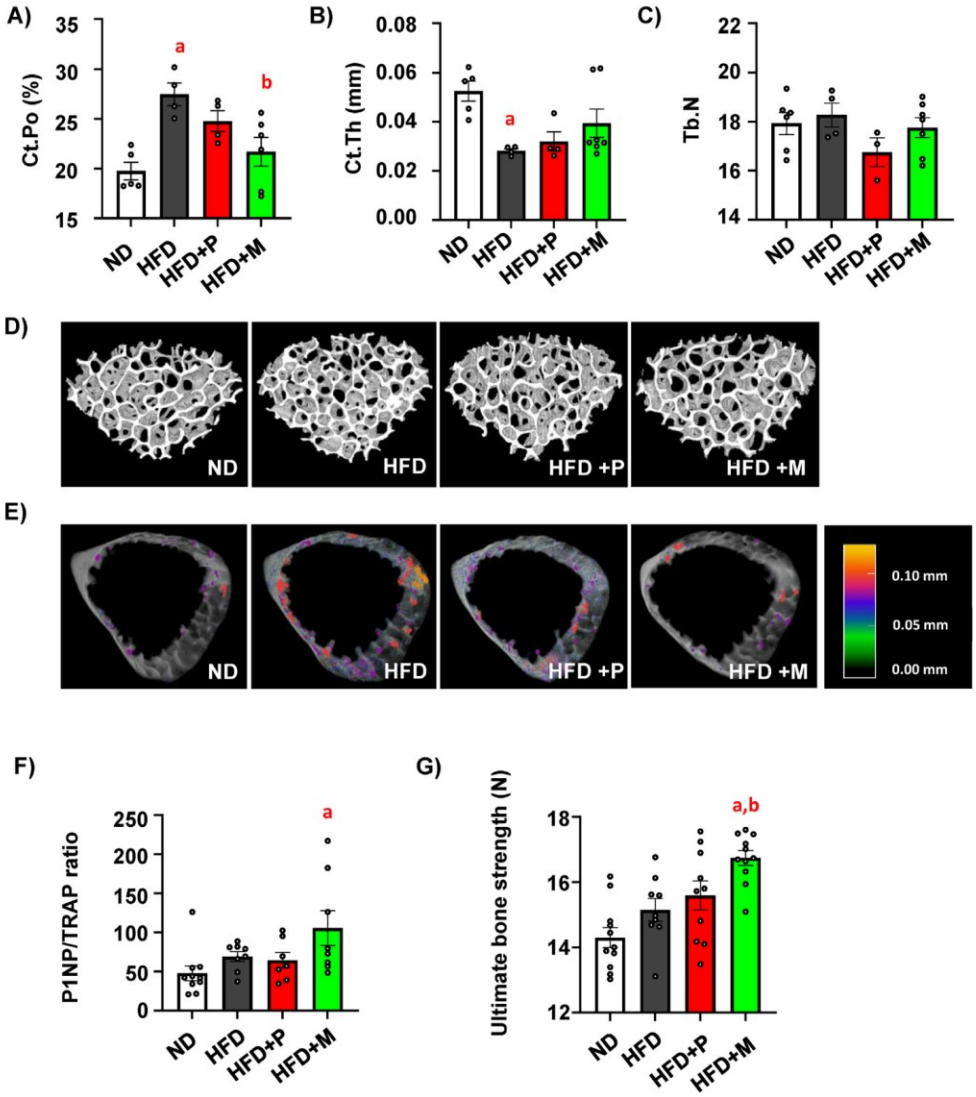

Figure 1: MSDC-0602K is less detrimental than pioglitazone on bone parameters in obese mice. (**A-E**) μCT analysis of cortical and trabecular bone in L5 vertebrae in treated mice. Cortical and trabecular parameters were calculated as (**A**) cortical porosity (Ct.Po), (**B**) cortical thickness (Ct.Th) and (**C**) trabecular number (Tb.N). Data are presented as mean ± SEM (n = 4–7 per group); one-way ANOVA, Tukey's multiple comparison test, a: ND vs other groups, b: HFD vs other groups. (**D**) Representative pictures of 3D reconstructed μCT images from trabecular and (**E**) cortical bone analysis of L5 vertebrae with colorimetric scale of pore size (scale bar 0–0.1 mm). (**F**) Analysis of the ratio of circulating markers of bone resorption (P1NP) and bone formation (TRAP) in murine plasma samples after 8 weeks of dietary intervention. Data are presented as mean ± SEM (n = 6–10 per group); one-way ANOVA, Tukey's multiple comparison test, a: ND vs other groups. (**G**) Ultimate bone strength of femurs was evaluated as first point of the plateau of the load–displacement curve measured during three-point bending test. Data are presented as mean ± SEM (n = 10–11 per group); one-way ANOVA, Tukey's multiple comparison test, a: ND vs other groups, b: HFD vs other groups. Data are presented as mean ± SEM (n = 10–11 per group); one-way ANOVA, Tukey's multiple comparison test, a: ND vs other groups.

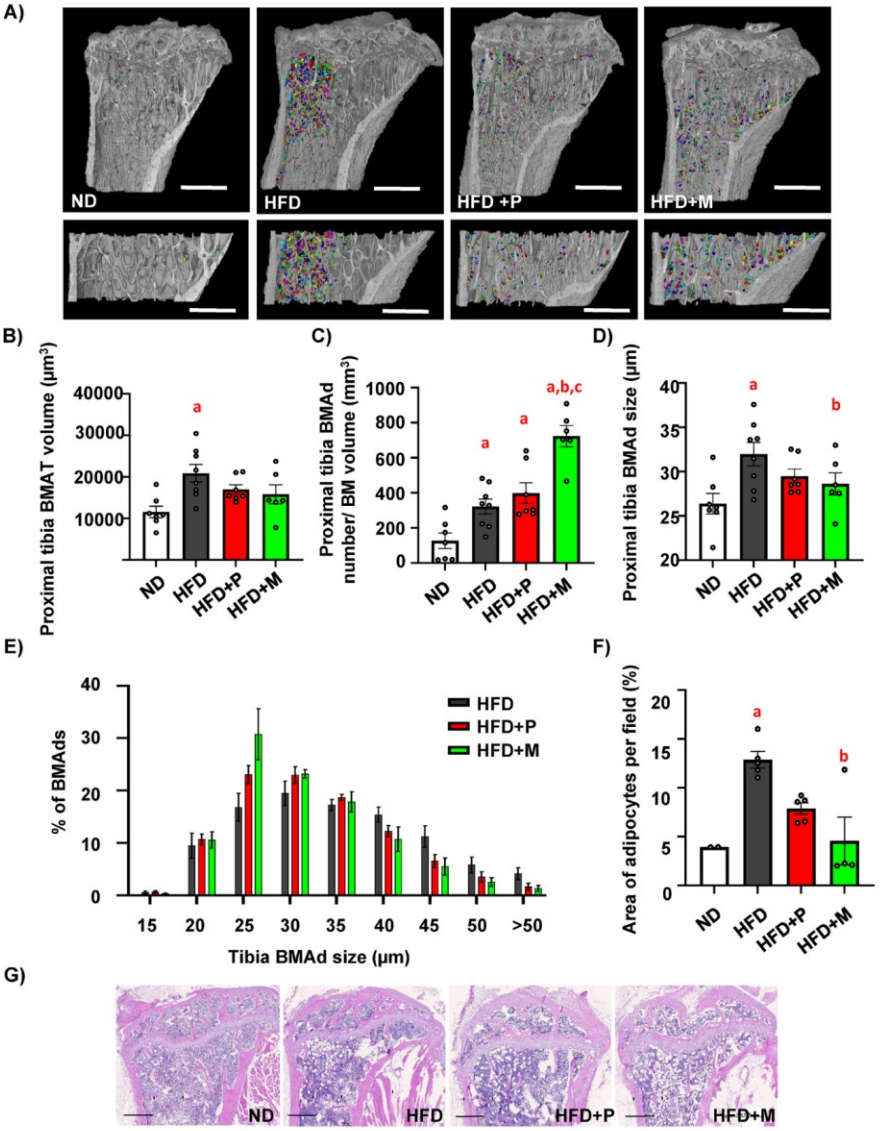

Figure 2: BMAT composition is differently affected in obese mice treated with pioglitazone and MSDC-0602K. (**A**) Representative pictures of bone marrow adipocytes (BMAds) stained with contrast agent Hexabrix in whole proximal tibia and zoomed pictures of BMAds in selected region of interest in proximal tibia (defined in Material and Methods) scanned by contrast-enhanced CT (CECT). Pictures were created using Avizo Software (scale bar 1000 µm). (**B**) Evaluation of BMAT volume in the selected region of interest in proximal tibia. (**C**) Quantification of BMAd number in the selected region of interest in proximal tibia divided by volume of selected BM region of interest (mm^3). (**D**) Quantitative evaluation of the size of Hexabrix-stained BMAds in tibia. Data are presented as mean ± SEM (n = 6–8 per group); one-way ANOVA, Tukey's multiple comparison test, a: ND vs other groups; b: HFD vs other groups. (**E**) Analysis of different distribution of BMAd size affected by TZD and TZD analog supplementation in obese mice. (**F–G**) Histomorphometric evaluation of the BMAds expressed as (**F**) area of adipocytes per field, and (**G**) Representative pictures from H&E staining of histological section of proximal tibia from mice fed with HFD supplemented with TZD and TZD analog (scale bar 500 µm). Data are presented as mean ± SEM (n = 3–11 per group); one-way ANOVA, Tukey's multiple comparison test, a: ND vs other groups, b: HFD vs other groups.

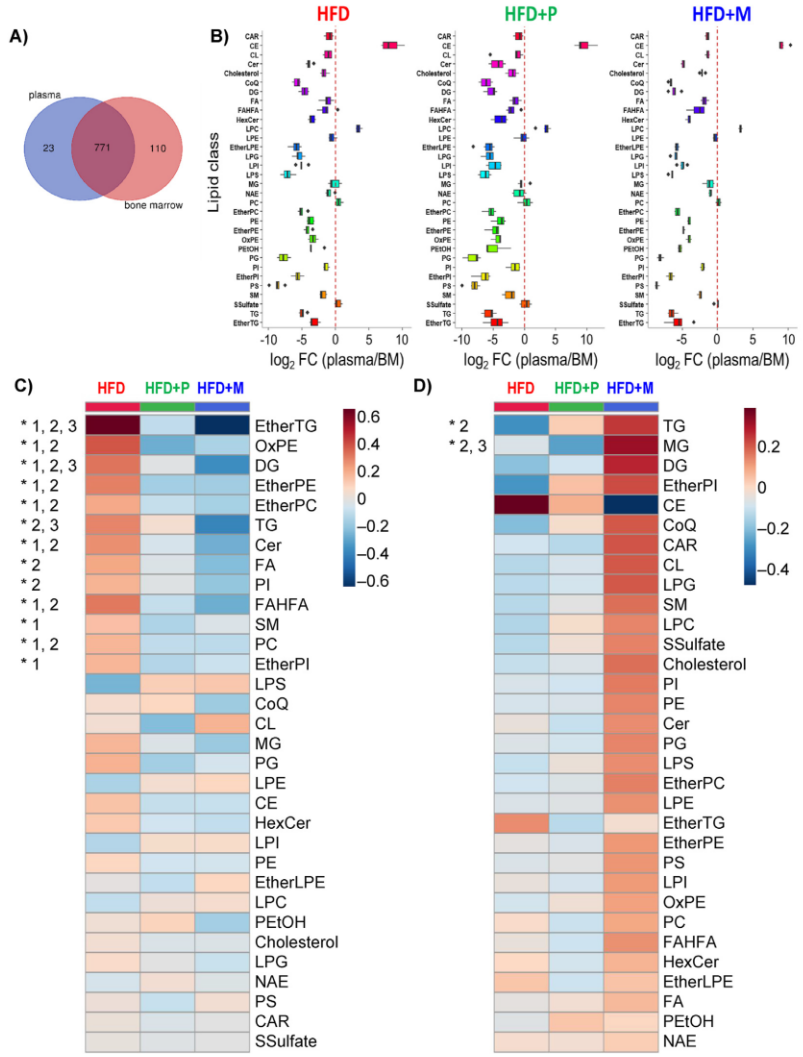

Figure 3: MSDC-0602K improves lipidome and metabolome of circulating plasma in more extend than BM composition in comparison to pioglitazone in obese mice. Global lipidomic and metabolomic analyses of plasma samples using LC–MS. **A)** Venn diagram illustrating shared and uniquely detected metabolites in plasma and BM using four LC-MS platforms. **B)** Log2-fold change of the 32 lipid classes annotated in plasma and BM in HFD, HFD + P and HFD + M groups. **(C)** Heatmap of the sum of abundances of all lipid species for each lipid class for plasma with group averages ($n = 9–10$ per group). Lipid classes statistically altered are marked by an asterisk (*) based on ANOVA with p(FDR) < 0.05. Differences between groups are marked as 1 (HFD vs. HFD + P; $p < 0.05$), 2 (HFD vs. HFD + M; $p < 0.05$) and 3 (HFD + P vs. HFD + M; $p < 0.05$). **(D)** Heatmap of the sum of abundances of all lipid species for each lipid class for BM with group averages. Lipid classes statistically altered are marked by an asterisk (*) based on ANOVA with p(FDR) < 0.05 ($n = 6$ per group). Differences between groups are marked as 2 (HFD vs. HFD + M; $p < 0.05$) and 3 (HFD + P vs. HFD + M; $p < 0.05$). (Lipid class annotation: CAR: acylcarnitine; CE: cholesteryl ester; CL: cardiolipin; Cer, ceramide; CoQ: coenzyme Q; DG: diacylglycerol; EtherPE: ether-linked phosphatidylethanolamine; EtherLPE: ether-linked lysophosphatidylethanolamine; EtherPI: ether-linked phosphatidylinositol; EtherPC: ether-linked phosphatidylcholine; EtherTG: ether-linked triacylglycerol; FA: free fatty acid; FAHFA: fatty acid ester of hydroxy fatty acid; HexCer: hexosylceramide; LPC: lysophophatidylcholine; LPE: lysophosphatidylethanolamine; LPG: lysophosphatidylglycerol; LPI: lysophosphatidylinositol; LPS: lysophosphatidylserine; MG: monoacylglycerol; NAE: N-acyl ethanolamines; OxPE: oxidized phosphatidylethanolamine; PC: phosphatidylcholine; PE: phosphatidylethanolamine; PEtOH: phosphatidylethanol; PG: phosphatidylglycerol; PI: phosphatidylinositol; PS: phosphatidylserine; SM: sphingomyelin; SSulfate: sterol sulfate; TG: triacylglycerol).

groups, as depicted on the 3D representative images of BMAds in proximal tibia and BMAT volume evaluation (Figure 2A–B). The validation of the Hexabrix-stained BMAds was confirmed by the registering a cross-section of the CECT dataset with the corresponding hematoxylin-eosin (H&E)-stained section of the same tibia (Figure S2A). Interestingly, further analyses of BMAT revealed higher number of BMAds in HFD + P and HFD + M groups compared to HFD, but with a larger proportion of smaller adipocytes in HFD + M group compared to HFD + P (Figure 2C–E).
In addition, histomorphometric analysis of H&E-stained sections of proximal tibia confirmed the data from CECT, demonstrating a sustained increase in BMAds in the HFD, HFD + P and HFD + M groups compared to ND (Figure S2B), while the size of BMAds was lower in HFD + M mice (Figure 2F–G). These data highlight that MSDC-0602K treatment in HFD mice increased the proportion of smaller BMAds in tibia compared to HFD + P.

3.3. MSDC-0602K improves lipidome and metabolome of circulating plasma in more extend than BM composition in comparison to pioglitazone in obese mice

To further examine changes in systemic and BM microenvironment in treatment with different TZDs, a global lipidomic and metabolomic analysis was performed in circulating plasma and BM samples of treated mice using LC-MS. Overall, 904 polar metabolites and simple and complex lipids were annotated in these two matrices with an overlap of 85% (Figure 3A). Partial least-squares discriminant analysis (PLS-DA) showed distinct separation of HFD + P and HFD + M groups from HFD in plasma, while less separation was observed for all three groups in case of BM (Figure S3A-B). Only a few metabolites were unique or detected at a much higher intensity in plasma compared to BM (e.g., cholesteryl esters, bile acids), while BM contained more lipid classes and polar metabolites (e.g. lysophosphatidylglycerol (LPG), lysophosphatidylinositol (LPI), phosphatidylglycerol (PG), phosphatidylserine (PS), dipeptides, nucleotides), which usually maintain low concentrations in circulating plasma [32] (Figure 3B, Table S4) suggesting that these uniquely present structural components and nutrients in BM may contribute to the fate and properties of BM-MSCs. These plasma/BM ratios were not affected by the treatment with TZD drugs apart from triacylglycerol (TG) which were reduced in HFD + P and HFD + M compared to HFD group.
Next, we examined the lipidomic data from the perspective of the sum of abundances of all lipid species for each lipid class. In plasma, 13 out of 32 lipid classes were at higher concentration in HFD compared to HFD + P and HFD + M groups (Figure 3C). Specifically, the sum of ether-linked TG was detected at 3-fold and 6.5-fold higher concentrations in HFD compared to HFD + P and HFD + M, respectively, followed by other lipid classes. On the other hand, only 2 lipid classes (TG, monoacylglycerol (MG)) were statistically altered in BM. In the case of TG, their intensity was 1.5-fold higher in HFD + M compared to HFD and HFD + P (Figure 3D). Since the use of the sum of abundances may hide useful information for data interpretation, we also examined the detailed abundance patterns of all annotated lipid species along with polar metabolites. As Figure 3C shows, the top-50 metabolites in plasma belonged to lipids in line with previous data analysis with exception of lysophosphatidylcholine (LPC). Among all annotated LPC species, 14 LPC species were statistically altered and formed two clusters (Figure S3E). In the first cluster, some LPC species (e.g. LPC 19:0, LPC 20:0, LPC 18:0) were increased in HFD and decreased with pioglitazone and MSDC-0602K treatment, which are known to be associated with oxidative stress and inflammation [33,34]. On the other hand, the second cluster showed the opposite trend, i.e. low concentration in HFD compared to HFD + P and HFD + M groups (e.g. LPC 15:0, LPC 14: 0), which have been shown to regulate glucose uptake in cells [34]. Contrary to plasma profile, BM showed mostly TG species among the top-50 metabolites changed with diet with trend towards higher levels in MSDC-0602K treated group (Figure S3D). Polar metabolites were not impacted with different interventions, besides three compounds including 3-hydroxybutyric acid, dimethylglycine, stachydrine associated with diet content, which were significantly altered in plasma, but they were not observed in BM. We also detected the parent drugs (pioglitazone and MSDC-0602K) present in both plasma and BM with higher concentrations in circulating plasma vs. BM.
Taken together, these data revealed that systemic treatment of obese mice with TZDs has a positive impact on decreasing circulating levels of lipids in HFD mice, while BM lipid content was changed differently, thus confirming data from μCT evaluation on different BMAT composition.

3.4. MSDC-0602K decreases adipocyte differentiation potential of mBM-MSCs compared to pioglitazone in obese mice

To determine cellular changes related to bone formation, primary murine BM-MSCs (mBM-MSCs) were isolated from treated mice to characterize their cellular and molecular phenotype. Stem cell properties of mBM-MSCs evaluated by colony-forming units-fibroblast (CFU-f) showed increased CFU-f in HFD + P compared to HFD mice (Figure S4A–B). The short-term proliferation rate of primary cultures did not show any differences between the groups (Figure S4C). Further, as it was previously shown [3], mBM-MSCs from the HFD group manifested increased adipocyte (AD) differentiation potential compared to mBM-MSCs from the ND group, as measured by Oil Red O staining (Figure 4A). This AD differentiation potential was further elevated in HFD + P group. However, primary mBM-MSCs derived from HFD + M did not show the same pattern as their AD differentiation potential was decreased compared to HFD + P (Figure 4A). These data were confirmed by gene expression analysis of adipogenic markers (*Pparγ2, Cebpa, Adipoq, Cd36, Fsp27, Insr*), which were more pronounced with pioglitazone treatment compared to MSDC-0602K treatment, suggesting higher PPARγ activity in HFD + P than HFD + M group (Figure 4B).
Osteoblast (OB) differentiation potential of primary mBM-MSCs measured by Alizarin staining (AZR) and alkaline phosphatase (ALP) activity (Figure 4C–E) revealed impairment in the HFD and HFD + P groups, while OB induction was improved in the HFD + M group. These data were also confirmed by gene expression analysis of osteoblastic genes (*Alpl, Oc, Col1a1, Bmp2, Dlx5, Msx2*) and genes involved in Wnt signaling, (*Ctnnb1, Lrp5*) (Figure 4F–G). Taken together, these data document that MSDC-0602K treatment in HFD-fed mice induces less AD potential and improves OB induction in primary mBM-MSCs compared to the first generation of TZD, pioglitazone, likely via lower activation of PPARγ.

3.5. MSDC-0602K increases glycolytic activity along with decreased senescence of mBM-MSCs in comparison to pioglitazone in obese mice

To further understand the impact of TZD treatment on cellular metabolism, we evaluated bioenergetic profile in primary mBM-MSCs obtained from treated mice in undifferentiated state using Seahorse

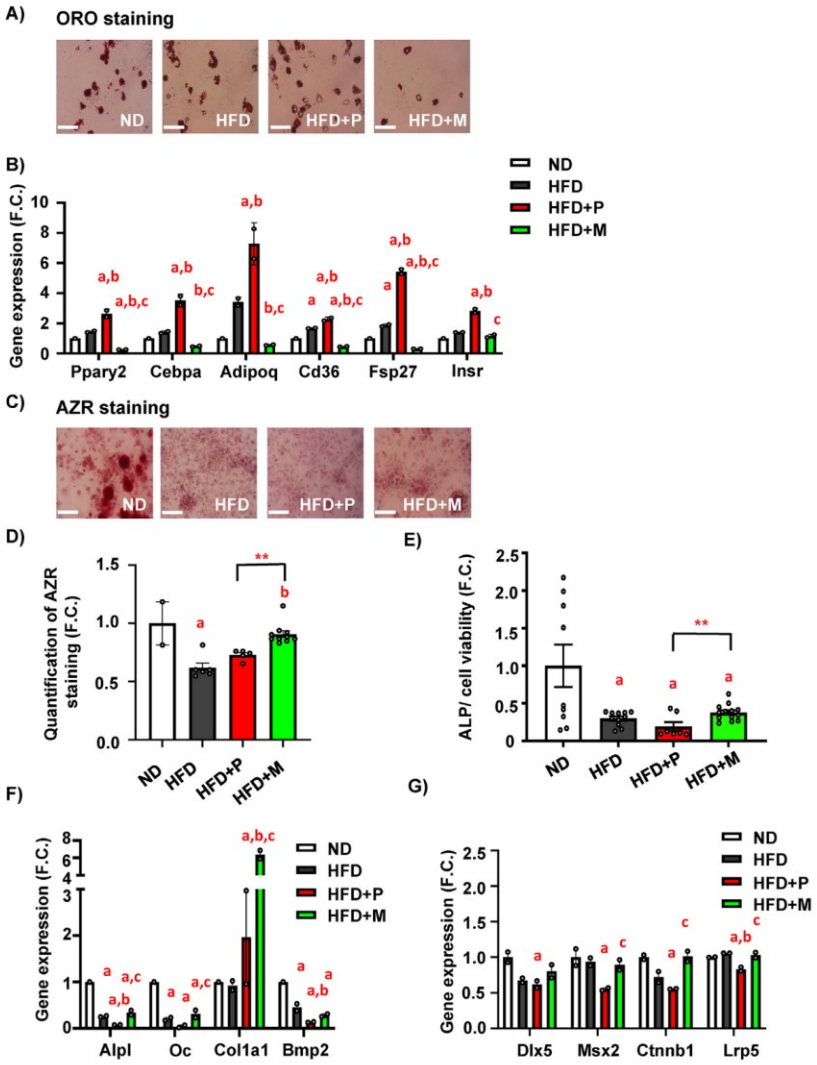

Figure 4: MSDC-0602K decreases adipocyte differentiation potential of BM-MSCs compared to pioglitazone in obese mice. (**A**) Representative picture of Oil red O (ORO) stained lipid droplets in AD differentiated mBM-MSCs (scale bar 150 μm; 20x magnification). (**B**–**C**) Gene expression profile of mBM-MSCs differentiated towards adipocytes in D10. (**B**) Gene expression of adipogenic genes (*Pparγ2, Cebpa, Adipoq, Cd36, Fsp27, Insr*). Data are presented as mean fold change (F.C.) of gene expression normalized to mBM-MSCs from ND group ± SEM (n = 2 from pooled samples); one-way ANOVA, Tukey's multiple comparison test, a: ND vs other groups; b: HFD vs other groups, c: HFD + P vs other groups. (**C**) Representative pictures of Alizarin Red (AZR) staining for calcified matrix mineralization of OB differentiated mBM-MSCs (scale bar 150 μm; 20x magnification) and (**D**) quantification of eluted AZR staining of mineralized matrix in OB differentiated mBM-MSCs in D10. Data are presented as mean fold change (F.C.) of A_{500} in OB differentiated cells (OB) normalized to mBM-MSCs from ND group ± SEM (n = 2–10); one-way ANOVA, Tukey's multiple comparison test, a: ND vs other groups; b: HFD vs other groups and unpaired t-test $^{**}p < 0.01$: HFD + P vs HFD + M. (n = 2–10). (**E**) Measurement of alkaline phosphatase (ALP) activity normalized to cell viability in OB differentiated mBM-MSCs in D7. Data are presented as mean fold change of ALP activity in OB differentiated cells (OB) from each experimental group ± SEM (n = 7–14); one-way ANOVA, Dunett's test comparing a: ND vs other groups and unpaired t-test $^{**}p < 0.01$: HFD + P vs HFD + M. (**F**) Gene expression profile of osteoblastic markers (*Alpl, Oc, Col1a1* and *Bmp2*) and (**G**) *Dlx5, Msx2, Ctnnb1, Lrp5*, in OB differentiated mBM-MSCs in D10. Data are presented as mean fold change (F.C.) of gene expression normalized to mBM-MSCs from ND group ± SEM (n = 2 from pooled samples); one-way ANOVA, Tukey's multiple comparison test, a: ND vs other groups, b: HFD vs other groups, c: HFD + P vs other groups, d: HFD + M vs other groups.

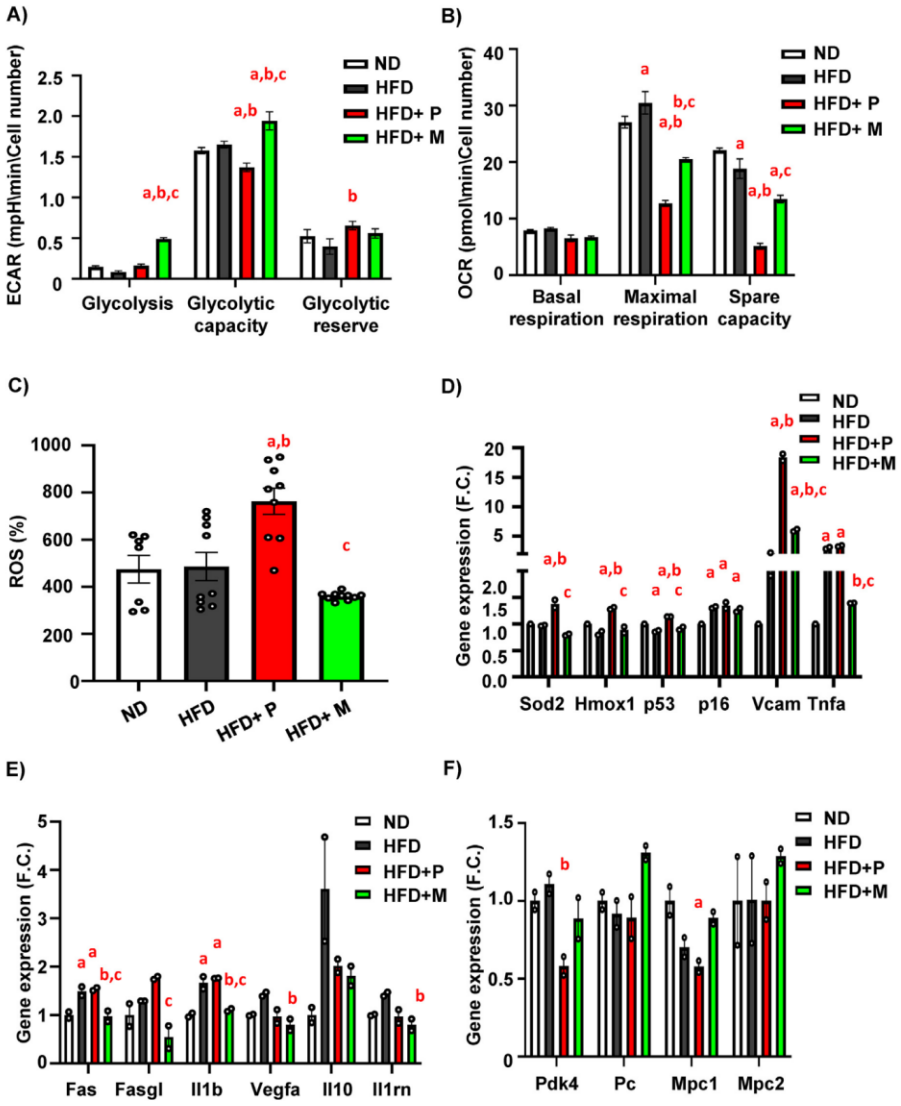

Figure 5: MSDC-0602K increases glycolytic activity along with decreased senescence of mBM-MSCs in comparison to pioglitazone in obese mice. (**A**) Glycolysis, glycolytic capacity and glycolytic reserve measured from extracellular acidification rate (ECAR) of mBM-MSCs (n = 2 independent experiments with five replicates per group). (**B**) Basal respiration, maximal respiration and spare capacity measured from oxygen consumption rate (OCR) of primary mBM-MSCs isolated from treated mice with different dietary interventions (n = 2 independent experiments with five replicates per group). Data are presented as mean ± SEM (n = 7–11 per group), one-way ANOVA, Tukey's multiple comparison test, a: ND vs other groups, b: HFD vs other groups, c: HFD + P vs other groups, d: HFD + M vs other groups. (**C**) ROS production (%) of cultivated primary mBM-MSCs isolated after 8 weeks on HFD or HFD supplemented with TZD and TZD analog. (**D**) Expression of genes associated with cell senescence (*Sod2, Hmox1, p53, p16, Vcam, Tnfα*) measured in differentiated mBM-MSCs (n = 2 per group from pooled samples). (**E**) Gene expression of SASP markers in primary mBM-MSCs obtained from treated mice exposed to 50uM H_2O_2 for 6h (*Fas, Fasgl, Il1b, Vegfa, Il10, Il1rn*) (n = 2 per group from pooled samples); (**F**) Gene expression profile of basic mitochondrial genes such as *Pdk4, Pc, Mpc1* and *Mpc2* in mBM-MSC differentiated towards osteoblasts. Data are presented as mean fold change (F.C.) of gene expression normalized to ND group ± SEM (n = 2 per group from pooled samples); one-way ANOVA, Tukey's multiple comparison test, a: ND vs other groups, b: HFD vs other groups, c: HFD + P vs other groups, d: HFD + M vs other groups.

bioanalyzer. We obtained simultaneous measurements of mitochondrial function via the oxygen consumption rate (OCR) and glycolysis via the extracellular acidification rate (ECAR) (Figure 5).

In glycolysis measurements, primary mBM-MSCs from the HFD + M group revealed higher glycolytic capacity compared to the HFD group, while HFD + P mBM-MSCs had lower glycolytic response (Figure 5A, Figure S5A). On the other hand, measurements of cellular respiration showed higher maximal respiration rate induced by carbonyl cyanide-4-(trifluoromethoxy) phenylhydrazone (FCCP) in HFD mBM-MSCs compared to ND mBM-MSCs (Figure 5B, Figure S5B). This increase in HFD-induced OCR capacity was counteracted by treatment with pioglitazone and MSDC-0602K. Surprisingly, mBM-MSCs from HFD + M group showed less reduction of maximal OCR than those from HFD + P group (Figure 5B, Figure S5B). It might indicate that glucose is in the case of HFD + M metabolized by glycolysis and cannot fully support respiratory metabolism, which prefers other substrates.

Further, measurements of reactive oxygen species (ROS) production in primary mBM-MSCs revealed increased senescent phenotype in mice from the HFD + P group compared to HFD group (Figure 5C), while mBM-MSCs obtained from HFD + M were protected from this effect. This phenotype was also confirmed by increased expression of senescent markers (e.g. *p53*) and markers of senescence-associated secretory phenotype (SASP) (e.g. *Fas, Fasgl, Vegfa, Vcam, Tnfa, Il10, Il1rn*) [35] in primary mBM-MSCs in HFD and HFD + P groups, while mBM-MSCs in HFD + M group did not show such an increase of the selected markers (Figure 5D–E). The senescent phenotype was also manifested in primary hematopoietic stem cells (mHSCs) obtained from HFD + P group, showing increased expression of *p21, p16, Vegfa, Vcam* compared to the ND and HFD groups (Figure S5C), whereas HSCs from HFD + M mice showed less senescent features. Indeed, these findings confirmed that both mBM-MSC and mHSC populations were affected by pioglitazone and MSDC-0602K treatment, which was associated with changes in BM microenvironment. In addition, gene expression of enzymes associated with mitochondrial metabolism (*Pdk4, Pc, Mpc1 and Mpc2*) (Figure 5F) were upregulated in the HFD + M group compared to HFD + P, suggesting differential activation of mitochondria in these cells.

Taken together, these data demonstrate that MSDC-0602K differently affects cellular metabolism and nutrient utilization in mBM-MSCs compared to pioglitazone with less side effects including senescence compromising their stem cell properties.

3.6. MSDC-0602K reduces insulin and inflammatory responsiveness in mHSCs in comparison to pioglitazone in obese mice

As TZD treatment under diabetic conditions is known to affect immune cell function in AT by improving insulin signaling and reducing inflammatory responses [36–38], we investigated downstream signaling pathways related to AKT and inflammatory signaling in mHSCs (as progenitors of immune cells) isolated from HFD mice and mice fed HFD supplemented with TZDs.

Insulin stimulation measured by AKT phosphorylation (pAKT S473/total AKT, and pAKT T308/total AKT) showed that insulin signaling in primary mHSCs of HFD mice was not impaired when compared to ND cells (Figure 6A–B), similarly as in primary mBM-MSCs isolated from C57BL/6J mice [3]. In addition, pioglitazone supplementation of HFD increased insulin responsiveness in the corresponding primary mHSCs compared to the HFD and HFD + M groups mostly expressed by increased pAKT T308/total AKT (Figure 6B), which was confirmed by gene expression of insulin responsive genes (*Irs1, Irs2, Insr*) (Figure 6C). This was accompanied by increased gene expression of adipogenic genes (*Pparγ2, Cebpa, Cd36*) (Figure 6D).

In addition, gene expression of inflammatory genes (*Il1β, Tnfα, RelA*) showed increased inflammatory response in mHSCs from the HFD + P group compared to the HFD + M group (Figure S5D), suggesting that TZD has a different impact on mHSCs compared to cells in peripheral tissues. These data also correlate with other data on the PPARγ upregulation in mHSCs related to osteoclast activation and bone resorption [39], which was not present in mice receiving HFD supplemented with MSDC-0602K (Figure S5E).

3.7. MSDC-0602K manifests similar beneficial effects on hBM-MSC characteristics compared to classical TZDs

Following *in vivo* experiment in HFD mice, we further evaluated the effect of novel TZD analog MSDC-0602K on stem cell properties in human BM-MSCs (hBM-MSCs). We used immortalized hBM-MSCs cell line described in previous studies [2,21,22,40]. OB differentiation measured by ALPL expression in hBM-MSCs showed inhibitory effect of pioglitazone and rosiglitazone treatment, which was improved by MSDC-0602K treatment (Figure 7A). Gene expression of MPC1 and MPC2 showed similar responses to different TZDs as in primary mBM-MSCs(Figure 7A). AD differentiation measured in hBM-MSCs by Nile Red staining confirmed a less stimulatory effect of MSDC-0602K when compared to first generation of TZDs (rosiglitazone and pioglitazone), similar to what was observed in mouse primary cells (Figure 7B). Further, measurement of cellular respiration in undifferentiated hBM-MSCs in response to TZDs and MSDC-0602K showed inhibitory effect of classical TZDs on maximal respiration compared to vehicle, while MSDC-0602K did not manifest such inhibition (Figure S6A–B), thus recapitulating the data from mBM-MSCs. These results confirmed the similar effects of MSDC-0602K treatment on hBM-MSCs as in mBM-MSCs, i.e. less detrimental effects on BM-MSC properties compared to typical TZDs.

3.8. BM-MSCs under MSDC-0602K treatment prefers glutamine over glucose utilization in comparison to AT-MSCs

Previous studies in myoblasts claimed that TZD's effect on cellular metabolism is mostly via MPC inhibition (i.e. via the inhibition of pyruvate transport) and changing substrate utilization in cells [41,42]. To further understand how TZDs and MSDC-0602K affect mitochondrial metabolism in hBM-MSCs, we analyzed how different types of TZDs affect mitochondrial function in intact cells. Our aim was to determine their inhibitory effect on the MPC pathway, the bioenergetic profile of hBM-MSCs, and the preferred energy source for mitochondrial metabolism.

Acute treatment with a lower concentration (10 μM) of TZDs and MSDC-0602K showed diminution of FCCP-induced maximal respiration compared to vehicle (Figure S7A–B), which was not present after the administration of an MPC-specific inhibitor (UK5099). This effect was even more pronounced when a higher concentration (30 μM) of tested drugs was used (Figure 7C–D). These data suggest that TZDs do not act in hBM-MSCs via inhibition of the MPC pathway as it was demonstrated in myoblasts [41].

Further, measurement of glucose uptake in hBM-MSCs after acute treatment with first generation of TZDs (pioglitazone and rosiglitazone) and MSDC-0602K revealed lower glucose uptake in cells treated with MSDC-0602K and UK5099 compared to typical TZDs (Figure 7E). On the other hand, intracellular levels of glutamate (product of glutamine metabolism after enzymatic reaction with glutaminase) were higher in MSDC-0602K-treated cells compared to pioglitazone (Figure 7F), while glutamine intracellular levels were lower (Figure 7G) suggesting

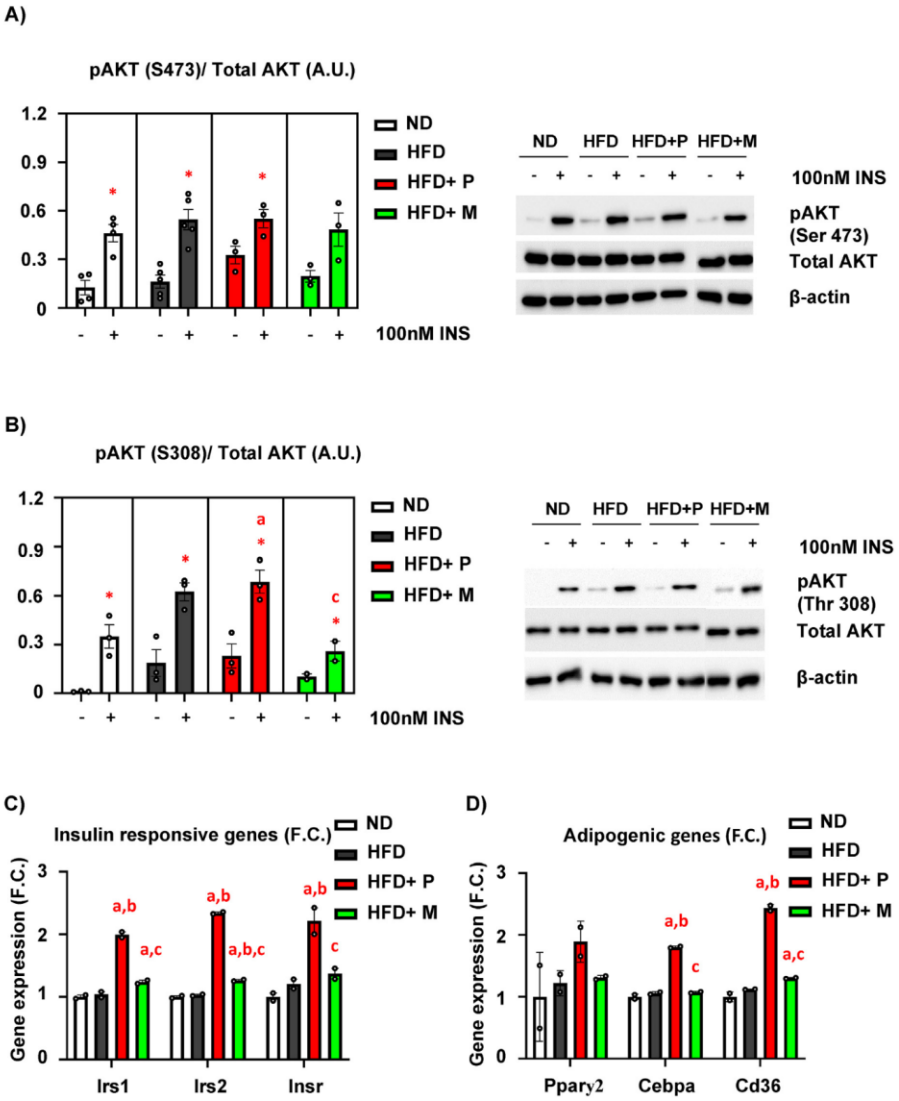

Figure 6: Pioglitazone and MSDC-0602K has a different impact on mHSC insulin and inflammatory responsiveness under HFD conditions. (**A**) Densitometry evaluation of western blot images representing the results of insulin stimulation (100 nM, 15min) of p-S473-AKT/total AKT in primary mHSCs from the ND, HFD, HFD + PIO, and HFD + M groups (n = 2–3 per group), and representative western blot images; (**B**) Densitometry evaluation of western blot images representing the results of insulin stimulation (100 nM, 15min) of p-T308-AKT/total AKT in primary mHSCs from the ND, HFD, HFD + PIO, HFD + M groups (n = 2–3 per group) and representative western blot images. Data are presented as mean densitometry ± SEM (n = 2), * significant difference between −INS vs + INS ($p \leq 0.05$, t-test), one-way ANOVA, Tukey's multiple comparison test, a: ND vs other groups; b: HFD vs other groups, c: HFD + P vs other groups. (**C**) Gene expression of insulin-responsive genes (*Irs1, Irs2, Insr*) and (**D**) adipogenic genes (*Pparγ2, Cebpa, Cd36*) in primary mHSCs (n = 2 per group from pooled samples) Data are presented as mean fold change (F.C.) of gene expression normalized to mHSC from ND ± SEM (n = 2 per group from pooled samples), one-way ANOVA, Tukey's multiple comparison test, a: ND vs other groups, b: HFD vs other groups, c: HFD + P vs other groups, d: HFD + M vs other groups.

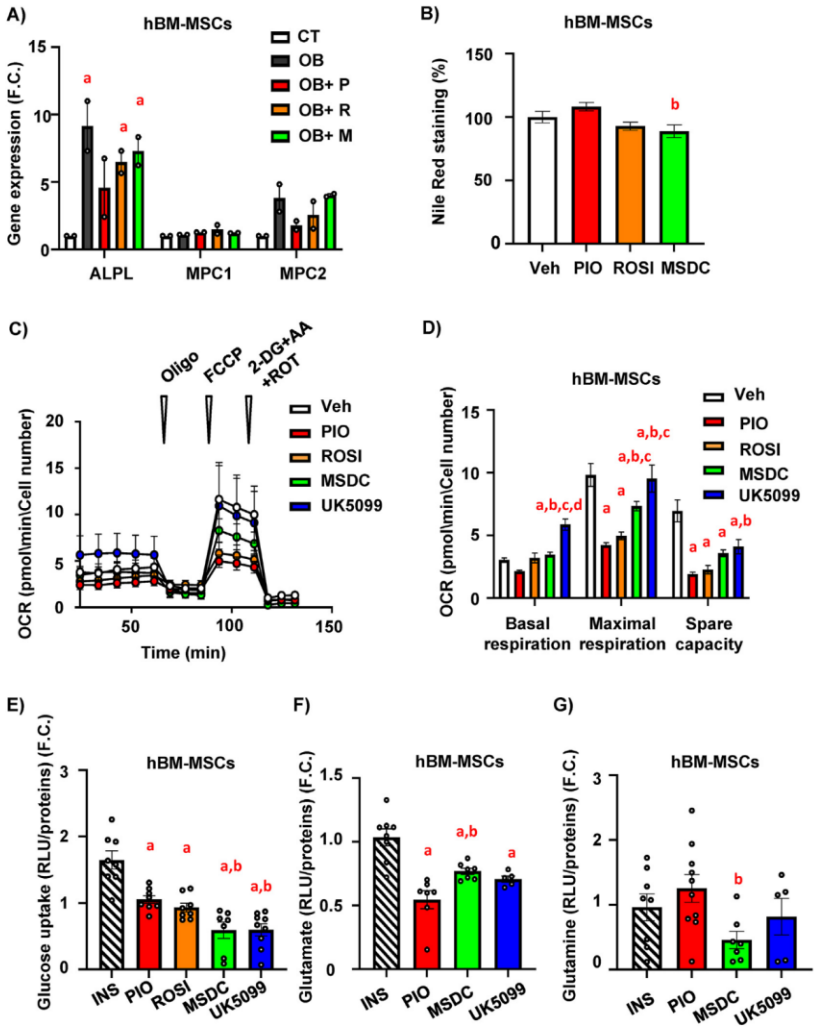

Figure 7: MSDC-0602K decreases adipocyte differentiation in hBM-MSC and differently changes cellular metabolism compared to classical TZDs. hBM-MSCs were treated for 10 days with 1 μM and 10 μM concentrations of different TZDs (rosiglitazone-ROSI, pioglitazone-PIO) or TZD analog (MSDC-0602K) together with differentiation cocktail for OB and AD differentiation. Vehicle (DMSO) was used as a control (**A**) OB differentiation of hBM-MSCs: gene expression of ALPL, MPC1, MPC2 following OB differentiation (D10) in treatment with 1uM PIO, ROSI and MSDC and vehicle (DMSO) as a control; (**B**) AD differentiation of hBM-MSCs: quantification of Nile Red staining of mature adipocytes normalized to cell viability following AD differentiation in treatment with 1 μM PIO, ROSI and MSDC and vehicle (DMSO) as a control; Data are presented as mean ± SEM from two independent experiments. One-way ANOVA, Tukey's multiple comparison test, a: Vehicle vs other groups; b: PIO vs other groups. (**C–D**) hBM-MSCs were acutely treated with 30 μM concentration of different TZDs (rosiglitazone-ROSI, pioglitazone-PIO) and TZD analog (MSDC-0602), and MPC inhibitor (UK5099) and their effect on mitochondrial respiration was analyzed. (**C–D**) Changes in oxygen consumption rate (OCR) of hBM-MSCs in response to treatment with TZDs, TZD analog and UK5099 and corresponding calculations of basal respiration, maximal respiration and spare capacity; Data are presented as mean ± SEM from at least two independent experiments with five replicates per condition; one-way ANOVA, Tukey's multiple comparison test, a: Veh vs other groups; b: PIO vs other groups, c: ROSI vs other groups, d: MSDC vs other groups. (**E**) Measurement of glucose uptake in hBM-MSC cells after 1.5-hour incubation with 1 μM INS, 30 μM PIO/ROSI/MSDC and 2 μM UK5099. Data are presented as the fold change of normalized relative light unit (RLU) value/protein of stimulated cells over non-stimulated cells. Data are presented as mean ± SEM (n = 7–11 per group); ordinary one-way ANOVA, Tukey's multiple comparison test, a: INS vs other groups; b: PIO vs other groups. Measurement of intracellular glutamate (**F**) and glutamine (**G**) in hBM-MSC cells after 3 h incubation with 1 μM INS, 30 μM PIO/MSDC and 2 μM UK5099. Data are presented as the fold change of normalized RLU value/protein of stimulated cells over non-stimulated cells. Data are presented as mean ± SEM (n = 7–11 per group); ordinary one-way ANOVA, Tukey's multiple comparison test, a: ND vs other groups.

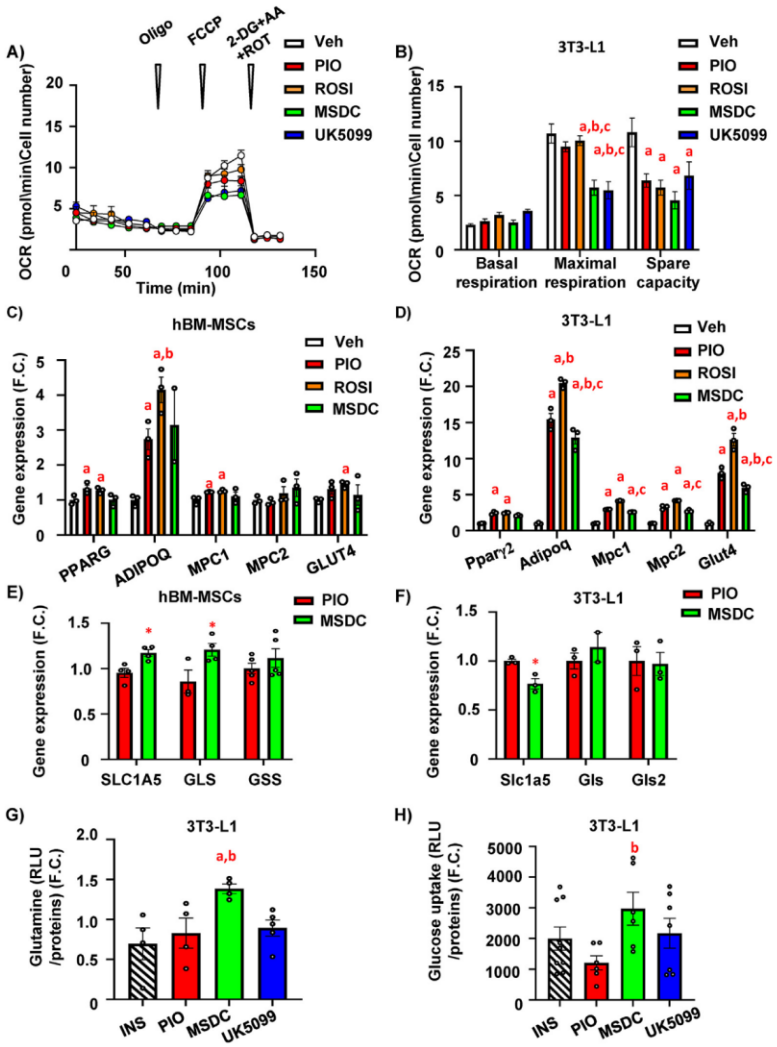

Figure 8: Differential effects of TZDs and MSDC-0602K on cellular metabolism in AT-MSCs and BM-MSCs. 3T3-L1 were acutely treated with 30 μM concentration of different TZDs (rosiglitazone-ROSI, pioglitazone-PIO) and TZD analog (MSDC-0602), and MPC inhibitor (UK5099) and their effect on mitochondrial respiration was analyzed. (**A-B**) Changes in oxygen consumption rate (OCR) of 3T3-L1 cells in response to treatment with TZDs, TZD analog and UK5099 treatment and corresponding calculations of basal respiration, maximal respiration and spare capacity. Data are presented as mean ± SEM from at least two independent experiments with five replicates per condition; one-way ANOVA, Tukey's multiple comparison test, a: Veh vs other groups; b: PIO vs other groups, c: ROSI vs other groups. (**C-D**) Gene expression profile measured in (**C**) hBM-MSC cells (*PPARG, ADIPOQ, MPC1, MPC2, GLUT4*) and (**D**) 3T3-L1 cells (*Ppary2, Adipoq, Mpc1, Mpc2, Glut4*) differentiated to AD treated with 1 μM PIO, ROSI and MSDC-0602K. Data are presented as mean ± SEM (n = 3 per condition), one-way ANOVA Tukey's multiple comparison test, a: Veh vs other groups; b: PIO vs other groups; c: ROSI vs other groups. (**E-F**) Gene expression profiling of enzymes involved in glutamine metabolism measured in (**E**) hBM-MSCs (SLC1A5, GLS, GSS) and (**F**) 3T3-L1 cells (*Slc1a5, Gls, Gls2*). Data are presented as mean of F.C. ± SEM (n = 3–5 per condition); t-test, *p < 0.05: PIO vs MSDC; (**G**) Measurement of intracellular glutamine in 3T3-L1 cells after 3 h incubation with 1 μM INS, 30 μM PIO/MSDC. Data are presented as the fold change of normalized RLU value/protein of stimulated cells over non-stimulated cells. Data are presented as mean ± SEM (n = 5 per group); ordinary one-way ANOVA, Tukey's multiple comparison test, a: INS vs other groups, b: PIO vs other groups; (**H**) Measurement of glucose uptake in 3T3-L1 cells after 1.5-hour incubation with 1 μM INS, 30 μM PIO/ROSI/MSDC and 2 μM UK5099. Data are presented as the fold change of normalized RLU value/protein of stimulated cells over non-stimulated cells. Data are presented as mean ± SEM (n = 5–7 per group); ordinary one-way ANOVA, Tukey's multiple comparison test, a: INS vs other groups, b: PIO vs other groups.

preferential utilization of glutamine in cellular metabolism after administration of novel TZD analog in comparison to the first generation of TZDs.

To understand the effect of different TZDs on bone cells compared to peripheral tissues, we also analyzed their effect on mitochondrial metabolism in AT-MSCs (i.e. 3T3-L1). Interestingly, the lower concentration of TZDs and MSDC-0602K showed a slight increase in FCCP-induced maximal respiration compared to vehicle (Figure S7C–D), while at the higher concentration (30 μM) (Figure 8A–B), there was a significant inhibition of respiration induced by MSDC-0602K and UK5099 indicating an impact on MPC function. In addition, gene expression profiling of adipogenic and metabolic genes (*Pparγ2, Cebpa, Insr, Mpc1, Mpc2*) showed differences between 3T3-L1 cells and mBM-MSCs (Figure S7E), which suggests that these cells are set up differently to respond to metabolic stimuli. AD induction assessed by gene expression profiling of adipogenic genes (*Pparγ, Adipoq*) and metabolic genes (*Mpc1, Mpc2, Glut4*) showed a stronger response to TZDs in 3T3-L1 cells than in BM-MSCs (Figure 8C–D).

Next, based on the findings of the inhibitory effect of TZDs on MPC [41], we tested the hypothesis that administration of MSDC-0602K and pioglitazone may lead to differential use of nutrients to affect cell differentiation potential under *in vitro* conditions. The gene expression of markers involved in glutamine metabolism (e.g. SLC1A5, GLS) was upregulated in response to MSDC-0602K treatment of hBM-MSCs compared to pioglitazone, suggesting a shift to increased glutamine utilization by cells (Figure 8E), while no change or decrease of glutamine metabolism genes (e.g. *Slc1a5*) was observed in 3T3-L1 cells treated with MSDC-0602K compared to pioglitazone (Figure 8F). These data were further confirmed by unchanged intracellular levels of glutamate (Figure S7F) and higher levels of glutamine in MSDC-0602K-treated 3T3-L1 cells compared to pioglitazone (Figure 8G), while glucose uptake was increased in these cells (Figure 8H).

These results indicate that the TZD analog MSDC-0602K works differently on the periphery compared to BM microenvironment. These findings are important regarding further evidence of the dual role of these drugs in different organ systems.

4. DISCUSSION

Treatment of obesity and type 2 diabetes with insulin-sensitizers such as TZDs has become a major challenge in clinical practice because of their side effects that include weight gain, cardiovascular complications, and increased risk of fractures [43]. In addition, many drugs prescribed for metabolic diseases have a negative effect on bone metabolism because the target molecules play dual roles in different organ systems. Here, we report that a novel TZD analog MSDC-0602K ("TZD of second generation or PPARγ-sparing TZD"), purposely designed to have a weak binding affinity to PPARγ, manifested less detrimental effects on metabolic and molecular properties of bone and mBM-MSCs in HFD-induced obesity in male mice compared with the classical TZD pioglitazone. Interestingly, we also found differential effects of MSDC-0602K on cellular metabolism in hBM-MSCs when compared to peripheral AT cells, thus confirming our hypothesis about the impact of systemically administered drugs on different tissues.

In our present study, we investigated the effects of 8-week-long administration of TZDs and a novel TZD analog MSDC-0602K on bone and energy metabolism in mice with HFD-induced obesity. The experimental design and doses of the tested drugs have been chosen according to previously published papers studying the metabolic flexibility of peripheral AT in response to dietary interventions in mice [10,18,44].

Even though previous studies in lean and HFD mice showed that of the classical TZDs, rosiglitazone has the most deleterious effect on bone loss in terms of inhibition of bone formation, increased osteoclastogenesis and induction of BMAT compared to pioglitazone [45–49], in our study we used pioglitazone in comparison to MSDC-0602K, as it is the only available PPARγ agonist used to treat T2D patients [50–52]. Previous studies using pioglitazone in HFD-fed male rodents (4–6 weeks) demonstrated a negative impact on vertebral bone density, decreased chondrocyte differentiation along with increased adiposity compared to non-treated animals [49,53,54]. This correlates with our data on BMAT volume, bone mechanical properties, AD differentiation potential and senescent phenotype of mBM-MSCs in HFD + P compared to HFD group. However, pioglitazone-induced detrimental effects on bone properties were not so profound compared to HFD, as in the present study we used C57BL/6N male mice and shorter dietary intervention (8 weeks vs 12–20 weeks) that did not respond to HFD administration by bone loss as is known to occur in the C57BL/6J substrain [3,5]. Nevertheless, MSDC-0602K treatment revealed a positive effect on mechanical properties in femur compared to pioglitazone treated mice, which might be explained by the changes in collagen content as OB differentiated mBM-MSCs isolated from HFD + M mice showed higher expression of *Col1a1* compared to primary cells of HFD + P mice.

Interestingly, CECT analysis of bone microstructure and BMAT content showed improved bone parameters in L5 vertebra, increased proportion of smaller BMAds in tibia along with increased mechanical properties of bones in HFD + M compared to HFD + P mice. These findings support data from Fukunaga et al. [13] demonstrating a beneficial effect of MSDC-0602K compared to rosiglitazone on bone phenotype in lean mice after 6 months of treatment.

Furthermore, our study investigated the cellular and molecular properties of primary mBM-MSCs isolated from treated mice, which has not been studied so intensively in previous reports with TZDs. Our data showed improved differentiation potential of mBM-MSCs towards OB and lower AD differentiation capacity in the HFD + M compared to HFD + P group, confirming reduced PPARγ activation in MSDC-0602K-treated mice. These changes were accompanied by less pronounced senescent and inflammatory phenotype in primary mBM-MSCs derived from mice treated with the novel TZD analog compared to the classical TZD, pioglitazone, suggesting its less detrimental effect on BM-MSC properties. Even though we did not see a decrease in lipid content measured by metabolomics in BM of HFD + M mice compared to the HFD + P and HFD group, the detailed analyses of BMAd properties by CECT revealed the impact of MSDC-0602K treatment on the distribution of smaller BMAds in the tibia, which correlated with improved bone mechanical properties. These observations may be explained by increased lipolytic activity in BMAds present in BM, which might affect the lipid cycling and using this energy to be taken by other BM-MSCs to store free fatty acids in form of small lipid droplets. This statement is further supported by decreased gene expression of metabolic genes such as *Insr, Pparγ2, Cd36* in mBM-MSCs of HFD + M mice compared to those from HFD + P, which could correspond to a higher responsiveness to lipolytic than lipogenic signals. Based on recently published data on metabolic heterogeneity of murine and human mature adipocytes in peripheral AT using spatial and single-cell transcriptomics, one can hypothesize that MSDC-0602K treatment may affect the expansion of specific BM-MSC subpopulations with different responsiveness to insulin and thus further lead to different accumulation of lipid droplets [55,56]. Indeed, our recent study documented the presence of murine BM-MSC progenitors with a distinct metabolic program, which

are differently responsive to exogenous metabolic stimuli that affect their differentiation fate [57]. However, further studies are needed to test this hypothesis using more high-throughput methods to analyze the functional heterogeneity of BM-MSCs in relation to different treatments. Regardless, our current data highlight the importance of BMAd metabolic and structural changes in response to antidiabetic drug treatment affecting bone quality.

In addition, metabolomic analysis of BM revealed the presence of unique metabolites (e.g. dipeptides, nucleotides etc.) only in BM but not in the circulation, suggesting their involvement in cellular metabolism in BM niche and affecting stem cell fate and differentiation potential. In mammals, the uptake of small peptides by the Slc15A family of oligo/dipeptide transporters provides an effective and energy-saving intracellular source of amino acids [58]. Recent study by Sharma et al. demonstrated the importance of amino acid metabolism on bone homeostasis and stem cell properties [59].

Besides MSDC-0602K, and among the novel TZDs [39,60] developed to avoid classical PPARγ transcriptional activation, Choi et al. [61] demonstrated action of a non-agonistic PPARγ ligand (SR1664) that blocks Cdk5-mediated phosphorylation at S273, thereby retaining its insulin-sensitizing effect, preventing weight gain in obese mice, and having no effect on bone formation *in vitro*. However, this compound has not been tested on bone parameters in mice with prolonged treatment. Another study by Stechschutle et al. reported that PPARγ post-translational modifications at S273 and S112 decrease PPARγ activation in resorptive osteoclasts and promote osteogenesis while maintaining its insulin-sensitizing effect [9]. Interestingly, this PPARγ agonist (SR10171) had an anabolic effect on the long bones but not on the vertebrae, whereas rosiglitazone had a negative effect in both skeletal sites explained by different cellular composition in specific skeleton sites. Our data with MSDC-0602K showed the major effect in vertebrae, which could also correlate with different cellular composition and bone turnover in vertebra vs long bones. However, we did not evaluate BMAT in vertebra site, which might have explained the different impact on bone properties.

As MSDC-0602K acts independently of PPARγ, its insulin-sensitizing effect supposes to maintain its binding affinity to mitochondria and affect cellular metabolism via MPC [11,62]. The molecular mechanism of TZD action is mainly based on the inhibition of the MPC complex (MPC1 and MPC2) [16,41]. Pyruvate uptake across the mitochondrial inner membrane is a central branch point in cellular energy metabolism with the ability to balance glycolysis and oxidative phosphorylation and control catabolic and anabolic metabolism. Transport of pyruvate into the mitochondrial matrix by the MPC is an important and rate-limiting step in its metabolism [63]. The MPC inhibition can improve cellular glucose handling, as TZDs and UK5099 increase glucose uptake in cells [41,42,64–66].

In our study we tested the effect of MSDC-0602K on cellular metabolism in primary mBM-MSCs, which could explain the changes in stem cell differentiation potential. Surprisingly, we did not observe an inhibitory effect of MSDC-0602K and UK5099 on mitochondrial respiration in primary mBM-MSCs isolated from treated animals, which was also confirmed in hBM-MSCs compared to pioglitazone. However, we found increased glycolytic activity in MSDC-0602K-treated cells compared to pioglitazone treatment, suggesting a change in the utilization of various nutrients contributing to the TCA cycle. This is an interesting finding as MSDC-0602K appears to act differently in peripheral AT-MSCs, in which we were able to detect an inhibitory effect of both drugs, MSDC-0602K and UK5099, on maximal respiration. Previous studies have shown that MPC activity determines the fuel oxidized by mitochondria, which has direct implications in terms of cellular functions and cell fate [67,68]. Recent findings in brown adipocytes showed that MPC inhibition leads to increased mitochondrial respiration, which activates lipid cycling and energy expenditure by replenishing energy from fatty acid and glutamine uptake [42]. However, these experiments were performed on isolated mitochondria compared to our data in intact cells.

We hypothesized that MSDC-0602K might affect glutamine metabolism as MSDC-0602K treatment increased OB induction in primary mBM-MSCs, which is associated with increased glutamine metabolism [69]. Interestingly, glucose uptake was decreased, and glutamate content (a product of glutamine metabolism) was increased in MSDC-0602K-treated BM-MSCs compared to pioglitazone. These changes were accompanied by upregulation of genes associated with glutamine metabolism in MSDC-treated cells compared to pioglitazone. Based on our findings we hypothesize that the beneficial effect of MSDC-0602K on BM-MSCs compared to AT-MSCs, is due to different preferences of nutrient utilization (i.e. glutamine over glucose uptake) in these cells, which affect their metabolic and stem cell properties supporting osteoblast differentiation in BM-MSCs but not in AT-MSCs. However, more data are needed to elucidate the exact mechanism behind the inhibitory effect of TZD on MPC and mitochondrial content and oxidative capacity, as well as its consequences in terms of changes in BM-MSC properties in relation to bone metabolism.

The present study brings several positive aspects. First, in contrast to previous studies investigating the impact of TZDs on bone, we performed a comprehensive analysis of bone and BMAd parameters along with cellular and molecular properties of primary mBM-MSCs from treated animals. Second, we applied a preventive strategy to investigate the effect of insulin-sensitizing drugs in the context of obesity and T2D. Third, we employed state-of-the-art methods to characterize cellular metabolism in BM-MSCs isolated from both mice and humans.

On the other hand, our study has some limitations. Dietary interventions in HFD-fed male mice lasted only 8 weeks, suggesting that longer treatment could have a much greater effect on bone properties. Moreover, we did not test the novel TZD analog in female mice, which is important for future perspective use of this drug in women with metabolic complications associated with osteoporosis.

Taken together, our study using HFD-induced obesity animal model shows that MSDC-0602K, as a novel insulin sensitizer, has reduced detrimental effects on bone parameters and BM-MSC phenotype by activation of glutamine metabolism as compared to the first generation of TZDs, i.e. pioglitazone. In addition, our findings provide novel insights on MSDC-0602K action *in vivo* and thus might further contribute to more specialized strategies in treatment of both bone and metabolic diseases.

AUTHOR CONTRIBUTIONS

MT and JK conceived the project. AB, MF, MT, KB, JF, GA, MD, MR and JK designed *in vivo* experiments, performed the *in vivo and in vitro* experiments, collected and analyzed data. AP and TM provided material and helped with interpretation of bioenergetic profiling results. TC performed and helped with interpretation of metabolomics data. TB and GK performed BMAT measurement in bones *ex vivo* and helped with BMAT evaluation, and data interpretation. WW and GHL helped performed three-point bending tests and data interpretation. JP and FS performed μCT scanning of bones *ex vivo* and helped with the data analysis. MT, AB, MR and JK designed and supervised the study and wrote the manuscript. All authors revised and approved the manuscript.

DATA AVAILABILITY

Data will be made available on request.

ACKNOWLEDGEMENTS

We would like to thank Histology Core facility at CCP Biocev for their excellent work in preparation of bone samples. We thank Kimberly Crevits at FIBEr, KU Leuven, for performing the three-point bending tests. We are grateful for help with writing of MATLAB script used for automatic histogram windowing and relative gray value normalization of CECT images to Arne Maes from KU Leuven. Further. We are grateful to Prof. Moustapha Kassem, KMEB SDU Odense for his generous gift of immortalized human cell line hBM-MSC-TERT. We thank dr. Jerry Colca from Cirius Therapeutics (Kalamazoo, USA) for providing us MSDC-0602K. We thank Dr. Siobhan Craige for the critical reading of the manuscript and discussion. The authors would like to acknowledge the Metabolomics Core Facility at the Institute of Physiology of the Czech Academy of Sciences for global metabolomic and lipidomic profiling. This work was supported by START UP Research programme by Institute of Physiology and the Czech Science Foundation GACR 20-03586S (MT), GACR 19-02411S (JK), EFSD/NovoNordisk foundation Future leaders award (NNF20SA0066174), National Institute for Research of Metabolic and Cardiovascular Diseases (Programme EXCELES, ID Project No. LX22NPO5104) - Funded by the European Union – Next Generation EU, Grant Agency of Charles University GAUK 339821 (AB) and FRIA grant 40004158 (TB).

CONFLICT OF INTEREST

All authors declare no conflict of interest.

APPENDIX A. SUPPLEMENTARY DATA

Supplementary data to this article can be found online at https://doi.org/10.1016/j.molmet.2022.101598.

REFERENCES

[1] Benova, A., Tencerova, M., 2020. Obesity-induced changes in bone marrow homeostasis. Frontiers in Endocrinology (Lausanne) 11:294. https://doi.org/10.3389/fendo.2020.00294.

[2] Tencerova, M., Frost, M., Figeac, F., Nielsen, T.K., Ali, D., Lauterlein, J.L., et al., 2019. Obesity-associated hypermetabolism and accelerated senescence of bone marrow stromal stem cells suggest a potential mechanism for bone fragility. Cell Reports 27(7):2050–2062 e2056. https://doi.org/10.1016/j.celrep.2019.04.066.

[3] Tencerova, M., Figeac, F., Ditzel, N., Taipaleenmaki, H., Nielsen, T.K., Kassem, M., 2018. High-fat diet-induced obesity promotes expansion of bone marrow adipose tissue and impairs skeletal stem cell functions in mice. Journal of Bone and Mineral Research 33(6):1154–1165. https://doi.org/10.1002/jbmr.3408.

[4] Lecka-Czernik, B., Stechschulte, L.A., Czernik, P.J., Dowling, A.R., 2015. High bone mass in adult mice with diet-induced obesity results from a combination of initial increase in bone mass followed by attenuation in bone formation; implications for high bone mass and decreased bone quality in obesity. Molecular and Cellular Endocrinology 410:35–41. https://doi.org/10.1016/j.mce.2015.01.001.

[5] Scheller, E.L., Khoury, B., Moller, K.L., Wee, N.K., Khandaker, S., Kozloff, K.M., et al., 2016. Changes in skeletal integrity and marrow adiposity during high-fat diet and after weight loss. Frontiers in Endocrinology (Lausanne) 7:102. https://doi.org/10.3389/fendo.2016.00102.

[6] Doucette, C.R., Horowitz, M.C., Berry, R., MacDougald, O.A., Anunciado-Koza, R., Koza, R.A., et al., 2015. A high fat diet increases bone marrow adipose tissue (MAT) but does not alter trabecular or cortical bone mass in C57BL/6J mice. Journal of Cellular Physiology 230(9):2032–2037. https://doi.org/10.1002/jcp.24954.

[7] Lecka-Czernik, B., 2010. Bone loss in diabetes: use of antidiabetic thiazolidinediones and secondary osteoporosis. Current Osteoporosis Reports 8(4):178–184. https://doi.org/10.1007/s11914-010-0027-y.

[8] Tornvig, L., Mosekilde, L.I., Justesen, J., Falk, E., Kassem, M., 2001. Troglitazone treatment increases bone marrow adipose tissue volume but does not affect trabecular bone volume in mice. Calcified Tissue International 69(1):46–50. https://doi.org/10.1007/s002230020018.

[9] Stechschulte, L.A., Czernik, P.J., Rotter, Z.C., Tausif, F.N., Corzo, C.A., Marciano, D.P., et al., 2016. PPARG post-translational modifications regulate bone formation and bone resorption. EBioMedicine 10:174–184. https://doi.org/10.1016/j.ebiom.2016.06.040.

[10] Bardova, K., Funda, J., Pohl, R., Cajka, T., Hensler, M., Kuda, O., et al., 2020. Additive effects of omega-3 fatty acids and thiazolidinediones in mice fed a high-fat diet: triacylglycerol/fatty acid cycling in adipose tissue. Nutrients 12(12). https://doi.org/10.3390/nu12123737.

[11] Chen, Z., Vigueira, P.A., Chambers, K.T., Hall, A.M., Mitra, M.S., Qi, N., et al., 2012. Insulin resistance and metabolic derangements in obese mice are ameliorated by a novel peroxisome proliferator-activated receptor gamma-sparing thiazolidinedione. Journal of Biological Chemistry 287(28):23537–23548. https://doi.org/10.1074/jbc.M112.363960.

[12] McCommis, K.S., Hodges, W.T., Brunt, E.M., Nalbantoglu, I., McDonald, W.G., Holley, C., et al., 2017. Targeting the mitochondrial pyruvate carrier attenuates fibrosis in a mouse model of nonalcoholic steatohepatitis. Hepatology 65(5):1543–1556. https://doi.org/10.1002/hep.29025.

[13] Fukunaga, T., Zou, W., Rohatgi, N., Colca, J.R., Teitelbaum, S.L., 2015. An insulin-sensitizing thiazolidinedione, which minimally activates PPARgamma, does not cause bone loss. Journal of Bone and Mineral Research 30(3):481–488. https://doi.org/10.1002/jbmr.2364.

[14] Colca, J.R., Scherer, P.E., 2022. The metabolic syndrome, thiazolidinediones, and implications for intersection of chronic and inflammatory disease. Molecular Metabolism 55:101409. https://doi.org/10.1016/j.molmet.2021.101409.

[15] Tanis, S.P., Colca, J.R., Parker, T.T., Artman, 3rd, G.D., Larsen, S.D., McDonald, W.G., et al., 2018. PPARgamma-sparing thiazolidinediones as insulin sensitizers. Design, synthesis and selection of compounds for clinical development. Bioorganic & Medicinal Chemistry 26(22):5870–5884. https://doi.org/10.1016/j.bmc.2018.10.033.

[16] Colca, J.R., McDonald, W.G., Cavey, G.S., Cole, S.L., Holewa, D.D., Brightwell-Conrad, A.S., et al., 2013. Identification of a mitochondrial target of thiazolidinedione insulin sensitizers (mTOT)–relationship to newly identified mitochondrial pyruvate carrier proteins. PLoS One 8(5):e61551. https://doi.org/10.1371/journal.pone.0061551.

[17] Harrison, S.A., Alkhouri, N., Davison, B.A., Sanyal, A., Edwards, C., Colca, J.R., et al., 2020. Insulin sensitizer MSDC-0602K in non-alcoholic steatohepatitis: a randomized, double-blind, placebo-controlled phase IIb study. Journal of Hepatology 72(4):613–626. https://doi.org/10.1016/j.jhep.2019.10.023.

[18] Kus, V., Flachs, P., Kuda, O., Bardova, K., Janovska, P., Svobodova, M., et al., 2011. Unmasking differential effects of rosiglitazone and pioglitazone in the combination treatment with n-3 fatty acids in mice fed a high-fat diet. PLoS One 6(11):e27126. https://doi.org/10.1371/journal.pone.0027126.

[19] Jafari, A., Siersbaek, M.S., Chen, L., Qanie, D., Zaher, W., Abdallah, B.M., et al., 2015. Pharmacological inhibition of protein kinase G1 enhances bone formation by human skeletal stem cells through activation of RhoA-akt signaling. Stem Cells 33(7):2219–2231. https://doi.org/10.1002/stem.2013.

[20] Hamam, D., Ali, D., Vishnubalaji, R., Hamam, R., Al-Nbaheen, M., Chen, L., et al., 2014. microRNA-320/RUNX2 axis regulates adipocytic differentiation of

human mesenchymal (skeletal) stem cells. Cell Death & Disease 5:e1499. https://doi.org/10.1038/cddis.2014.462.

[21] Abdallah, B.M., Haack-Sorensen, M., Burns, J.S., Elsnab, B., Jakob, F., Hokland, P., et al., 2005. Maintenance of differentiation potential of human bone marrow mesenchymal stem cells immortalized by human telomerase reverse transcriptase gene despite [corrected] extensive proliferation. Biochemical and Biophysical Research Communications 326(3):527–538. https://doi.org/10.1016/j.bbrc.2004.11.059.

[22] Simonsen, J.L., Rosada, C., Serakinci, N., Justesen, J., Stenderup, K., Rattan, S.I., et al., 2002. Telomerase expression extends the proliferative lifespan and maintains the osteogenic potential of human bone marrow stromal cells. Nature Biotechnology 20(6):592–596. https://doi.org/10.1038/nbt0602-592.

[23] Ding, M., Danielsen, C.C., Hvid, I., 2006. Age-related three-dimensional microarchitectural adaptations of subchondral bone tissues in Guinea pig primary osteoarthrosis. Calcified Tissue International 78(2):113–122. https://doi.org/10.1007/s00223-005-0028-5.

[24] Scheller, E.L., Troiano, N., Vanhoutan, J.N., Bouxsein, M.A., Fretz, J.A., Xi, Y., et al., 2014. Use of osmium tetroxide staining with microcomputerized tomography to visualize and quantify bone marrow adipose tissue in vivo. Methods in Enzymology 537:123–139. https://doi.org/10.1016/B978-0-12-411619-1.00007-0.

[25] Kerckhofs, G., Stegen, S., van Gastel, N., Sap, A., Falgayrac, G., Penel, G., et al., 2018. Simultaneous three-dimensional visualization of mineralized and soft skeletal tissues by a novel microCT contrast agent with polyoxometalate structure. Biomaterials 159:1–12. https://doi.org/10.1016/j.biomaterials.2017.12.016.

[26] Jin, L.H., Choi, B.H., Kim, Y.J., Oh, H.J., Kim, B.J., Yin, X.Y., et al., 2018. Nondestructive assessment of glycosaminoglycans in engineered cartilages using hexabrix-enhanced micro-computed tomography. Tissue Engineering and Regenerative Medicine 15(3):311–319. https://doi.org/10.1007/s13770-018-0117-y.

[27] Kerckhofs, G., Sainz, J., Marechal, M., Wevers, M., Van de Putte, T., Geris, L., et al., 2014. Contrast-enhanced nanofocus X-ray computed tomography allows virtual three-dimensional histopathology and morphometric analysis of osteoarthritis in small animal models. Cartilage 5(1):55–65. https://doi.org/10.1177/1947603513501175.

[28] Mittelstaedt, D., Xia, Y., 2015. Depth-dependent glycosaminoglycan concentration in articular cartilage by quantitative contrast-enhanced micro-computed tomography. Cartilage 6(4):216–225. https://doi.org/10.1177/1947603515596418.

[29] Jardi, F., Kim, N., Laurent, M.R., Khalil, R., Deboel, L., Schollaert, D., et al., 2019. Androgen receptor in neurons slows age-related cortical thinning in male mice. Journal of Bone and Mineral Research 34(3):508–519. https://doi.org/10.1002/jbmr.3625.

[30] Callewaert, F., Venken, K., Kopchick, J.J., Torcasio, A., van Lenthe, G.H., Boonen, S., et al., 2010. Sexual dimorphism in cortical bone size and strength but not density is determined by independent and time-specific actions of sex steroids and IGF-1: evidence from pubertal mouse models. Journal of Bone and Mineral Research 25(3):617–626. https://doi.org/10.1359/jbmr.090828.

[31] Pajuelo Reguera, D., Cunatova, K., Vrbacky, M., Pecinova, A., Houstek, J., Mracek, T., et al., 2020. Cytochrome c oxidase subunit 4 isoform exchange results in modulation of oxygen affinity. Cells 9(2). https://doi.org/10.3390/cells9020443.

[32] Bowden, J.A., Heckert, A., Ulmer, C.Z., Jones, C.M., Koelmel, J.P., Abdullah, L., et al., 2017. Harmonizing lipidomics: NIST interlaboratory comparison exercise for lipidomics using SRM 1950-Metabolites in Frozen Human Plasma. The Journal of Lipid Research 58(12):2275–2288. https://doi.org/10.1194/jlr.M079012.

[33] Yang, H., Suh, D.H., Kim, D.H., Jung, E.S., Liu, K.H., Lee, C.H., et al., 2018. Metabolomic and lipidomic analysis of the effect of pioglitazone on hepatic steatosis in a rat model of obese Type 2 diabetes. British Journal of Pharmacology 175(17):3610–3625. https://doi.org/10.1111/bph.14434.

[34] Yea, K., Kim, J., Yoon, J.H., Kwon, T., Kim, J.H., Lee, B.D., et al., 2009. Lysophosphatidylcholine activates adipocyte glucose uptake and lowers blood glucose levels in murine models of diabetes. Journal of Biological Chemistry 284(49):33833–33840. https://doi.org/10.1074/jbc.M109.024869.

[35] Farr, J.N., Fraser, D.G., Wang, H., Jaehn, K., Ogrodnik, M.B., Weivoda, M.M., et al., 2016. Identification of senescent cells in the bone microenvironment. Journal of Bone and Mineral Research 31(11):1920–1929. https://doi.org/10.1002/jbmr.2892.

[36] Ricote, M., Li, A.C., Willson, T.M., Kelly, C.J., Glass, C.K., 1998. The peroxisome proliferator-activated receptor-gamma is a negative regulator of macrophage activation. Nature 391(6662):79–82. https://doi.org/10.1038/34178.

[37] Xu, H., Barnes, G.T., Yang, Q., Tan, G., Yang, D., Chou, C.J., et al., 2003. Chronic inflammation in fat plays a crucial role in the development of obesity-related insulin resistance. Journal of Clinical Investigation 112(12):1821–1830. https://doi.org/10.1172/JCI19451.

[38] Tedesco, S., Ciciliot, S., Menegazzo, L., D'Anna, M., Scattolini, V., Cappellari, R., et al., 2020. Pharmacologic PPAR-gamma activation reprograms bone marrow macrophages and partially rescues HSPC mobilization in human and murine diabetes. Diabetes 69(7):1562–1572. https://doi.org/10.2337/db19-0640.

[39] Wu, H., Li, L., Ma, Y., Chen, Y., Zhao, J., Lu, Y., et al., 2013. Regulation of selective PPARgamma modulators in the differentiation of osteoclasts. Journal of Cellular Biochemistry 114(9):1969–1977. https://doi.org/10.1002/jcb.24534.

[40] Twine, N.A., Harkness, L., Adjaye, J., Aldahmash, A., Wilkins, M.R., Kassem, M., 2018. Molecular phenotyping of telomerized human bone marrow skeletal stem cells reveals a genetic program of enhanced proliferation and maintenance of differentiation responses. JBMR Plus 2(5):257–267. https://doi.org/10.1002/jbm4.10050.

[41] Divakaruni, A.S., Wiley, S.E., Rogers, G.W., Andreyev, A.Y., Petrosyan, S., Loviscach, M., et al., 2013. Thiazolidinediones are acute, specific inhibitors of the mitochondrial pyruvate carrier. Proceedings of the National Academy of Sciences of the United States of America 110(14):5422–5427. https://doi.org/10.1073/pnas.1303360110.

[42] Veliova, M., Ferreira, C.M., Benador, I.Y., Jones, A.E., Mahdaviani, K., Brownstein, A.J., et al., 2020. Blocking mitochondrial pyruvate import in brown adipocytes induces energy wasting via lipid cycling. EMBO Reports 21(12):e49634. https://doi.org/10.15252/embr.201949634.

[43] Pop, L.M., Lingvay, I., Yuan, Q., Li, X., Adams-Huet, B., Maalouf, N.M., 2017. Impact of pioglitazone on bone mineral density and bone marrow fat content. Osteoporosis International 28(11):3261–3269. https://doi.org/10.1007/s00198-017-4164-3.

[44] Kuda, O., Jelenik, T., Jilkova, Z., Flachs, P., Rossmeisl, M., Hensler, M., et al., 2009. n-3 fatty acids and rosiglitazone improve insulin sensitivity through additive stimulatory effects on muscle glycogen synthesis in mice fed a high-fat diet. Diabetologia 52(5):941–951. https://doi.org/10.1007/s00125-009-1305-z.

[45] Lazarenko, O.P., Rzonca, S.O., Hogue, W.R., Swain, F.L., Suva, L.J., Lecka-Czernik, B., 2007. Rosiglitazone induces decreases in bone mass and strength that are reminiscent of aged bone. Endocrinology 148(6):2669–2680. https://doi.org/10.1210/en.2006-1587.

[46] Ali, A.A., Weinstein, R.S., Stewart, S.A., Parfitt, A.M., Manolagas, S.C., Jilka, R.L., 2005. Rosiglitazone causes bone loss in mice by suppressing osteoblast differentiation and bone formation. Endocrinology 146(3):1226–1235. https://doi.org/10.1210/en.2004-0735.

[47] Ackert-Bicknell, C.L., Shockley, K.R., Horton, L.G., Lecka-Czernik, B., Churchill, G.A., Rosen, C.J., 2009. Strain-specific effects of rosiglitazone on bone mass, body composition, and serum insulin-like growth factor-I. Endocrinology 150(3):1330–1340. https://doi.org/10.1210/en.2008-0936.

[48] Liu, L., Aronson, J., Lecka-Czernik, B., 2013. Rosiglitazone disrupts endosteal bone formation during distraction osteogenesis by local adipocytic infiltration. Bone 52(1):247–258. https://doi.org/10.1016/j.bone.2012.09.038.

[49] Kyle, K.A., Willett, T.L., Baggio, L.L., Drucker, D.J., Grynpas, M.D., 2011. Differential effects of PPAR-{gamma} activation versus chemical or genetic reduction of DPP-4 activity on bone quality in mice. Endocrinology 152(2): 457–467. https://doi.org/10.1210/en.2010-1098.

[50] Pavo, I., Jermendy, G., Varkonyi, T.T., Kerenyi, Z., Gyimesi, A., Shoustov, S., et al., 2003. Effect of pioglitazone compared with metformin on glycemic control and indicators of insulin sensitivity in recently diagnosed patients with type 2 diabetes. Journal of Clinical Endocrinology and Metabolism 88(4): 1637–1645. https://doi.org/10.1210/jc.2002-021786.

[51] Alam, F., Islam, M.A., Mohamed, M., Ahmad, I., Kamal, M.A., Donnelly, R., et al., 2019. Efficacy and safety of pioglitazone monotherapy in type 2 diabetes mellitus: a systematic review and meta-analysis of randomised controlled trials. Scientific Reports 9(1):5389. https://doi.org/10.1038/s41598-019-41854-2.

[52] Wang, S., Dougherty, E.J., Danner, R.L., 2016. PPARgamma signaling and emerging opportunities for improved therapeutics. Pharmacological Research 111:76–85. https://doi.org/10.1016/j.phrs.2016.02.028.

[53] Kanda, J., Izumo, N., Kobayashi, Y., Onodera, K., Shimakura, T., Yamamoto, N., et al., 2017. Effect of the antidiabetic agent pioglitazone on bone metabolism in rats. Journal of Pharmacological Sciences 135(1):22–28. https://doi.org/10.1016/j.jphs.2017.08.004.

[54] Wu, S., Aguilar, A.L., Ostrow, V., De Luca, F., 2011. Insulin resistance secondary to a high-fat diet stimulates longitudinal bone growth and growth plate chondrogenesis in mice. Endocrinology 152(2):468–475. https://doi.org/10.1210/en.2010-0803.

[55] Lee, K.Y., Luong, Q., Sharma, R., Dreyfuss, J.M., Ussar, S., Kahn, C.R., 2019. Developmental and functional heterogeneity of white adipocytes within a single fat depot. EMBO Journal 38(3). https://doi.org/10.15252/embj.201899291.

[56] Backdahl, J., Franzen, L., Massier, L., Li, Q., Jalkanen, J., Gao, H., et al., 2021. Spatial mapping reveals human adipocyte subpopulations with distinct sensitivities to insulin. Cell Metabolism 33(9):1869–1882 e1866. https://doi.org/10.1016/j.cmet.2021.07.018.

[57] Tencerova, M., Rendina-Ruedy, E., Neess, D., Faergeman, N., Figeac, F., Ali, D., et al., 2019. Metabolic programming determines the lineage-differentiation fate of murine bone marrow stromal progenitor cells. Bone Research 7:35. https://doi.org/10.1038/s41413-019-0076-5.

[58] Naka, K., Jomen, Y., Ishihara, K., Kim, J., Ishimoto, T., Bae, E.J., et al., 2015. Dipeptide species regulate p38MAPK-Smad3 signalling to maintain chronic myelogenous leukaemia stem cells. Nature Communications 6:8039. https://doi.org/10.1038/ncomms9039.

[59] Sharma, D., Yu, Y., Shen, L., Zhang, G.F., Karner, C.M., 2021. SLC1A5 provides glutamine and asparagine necessary for bone development in mice. Elife 10. https://doi.org/10.7554/eLife.71595.

[60] Tan, Y., Muise, E.S., Dai, H., Raubertas, R., Wong, K.K., Thompson, G.M., et al., 2012. Novel transcriptome profiling analyses demonstrate that selective peroxisome proliferator-activated receptor gamma (PPARgamma) modulators display attenuated and selective gene regulatory activity in comparison with PPARgamma full agonists. Molecular Pharmacology 82(1):68–79. https://doi.org/10.1124/mol.111.076679.

[61] Choi, J.H., Banks, A.S., Kamenecka, T.M., Busby, S.A., Chalmers, M.J., Kumar, N., et al., 2011. Antidiabetic actions of a non-agonist PPARgamma ligand blocking Cdk5-mediated phosphorylation. Nature 477(7365):477–481. https://doi.org/10.1038/nature10383.

[62] Colca, J.R., McDonald, W.G., Waldon, D.J., Leone, J.W., Lull, J.M., Bannow, C.A., et al., 2004. Identification of a novel mitochondrial protein ("mitoNEET") cross-linked specifically by a thiazolidinedione photoprobe. American Journal of Physiology. Endocrinology and Metabolism 286(2): E252–E260. https://doi.org/10.1152/ajpendo.00424.2003.

[63] McCommis, K.S., Finck, B.N., 2015. Mitochondrial pyruvate transport: a historical perspective and future research directions. Biochemical Journal 466(3): 443–454. https://doi.org/10.1042/BJ20141171.

[64] Ramstead, A.G., Wallace, J.A., Lee, S.H., Bauer, K.M., Tang, W.W., Ekiz, H.A., et al., 2020. Mitochondrial pyruvate carrier 1 promotes peripheral T cell homeostasis through metabolic regulation of thymic development. Cell Reports 30(9):2889–2899. https://doi.org/10.1016/j.celrep.2020.02.042 e2886.

[65] Panic, V., Pearson, S., Banks, J., Tippetts, T.S., Velasco-Silva, J.N., Lee, S., et al., 2020. Mitochondrial pyruvate carrier is required for optimal brown fat thermogenesis. Elife 9. https://doi.org/10.7554/eLife.52558.

[66] Quansah, E., Peelaerts, W., Langston, J.W., Simon, D.K., Colca, J., Brundin, P., 2018. Targeting energy metabolism via the mitochondrial pyruvate carrier as a novel approach to attenuate neurodegeneration. Molecular Neurodegeneration 13(1):28. https://doi.org/10.1186/s13024-018-0260-x.

[67] Vacanti, N.M., Divakaruni, A.S., Green, C.R., Parker, S.J., Henry, R.R., Ciaraldi, T.P., et al., 2014. Regulation of substrate utilization by the mitochondrial pyruvate carrier. Molecular Cell 56(3):425–435. https://doi.org/10.1016/j.molcel.2014.09.024.

[68] Yang, C., Ko, B., Hensley, C.T., Jiang, L., Wasti, A.T., Kim, J., et al., 2014. Glutamine oxidation maintains the TCA cycle and cell survival during impaired mitochondrial pyruvate transport. Molecular Cell 56(3):414–424. https://doi.org/10.1016/j.molcel.2014.09.025.

[69] Yu, Y., Newman, H., Shen, L., Sharma, D., Hu, G., Mirando, A.J., et al., 2019. Glutamine metabolism regulates proliferation and lineage allocation in skeletal stem cells. Cell Metabolism 29(4):966–978. https://doi.org/10.1016/j.cmet.2019.01.016 e964.

4. Discussion

The complex interplay between metabolic diseases such as obesity and bone health is an area of significant clinical interest, particularly due to the adverse effects of obesity on bone quality and the risk of fractures [403]. Our research explores this interplay through two different but complementary approaches: the dietary supplementation with omega-3 PUFAs and the pharmacological intervention with the novel TZD analog, MSDC-0602K in mouse model of obesity. These studies aimed to elucidate the potential of these interventions in mitigating obesity-induced bone fragility and to shed light on their underlying mechanisms.

Our investigation into the non-pharmacological approach of omega-3 PUFA supplementation revealed its beneficial effects on metabolic and bone parameters in an HFD-induced obesity mouse model. Omega-3 PUFAs have been shown to modulate various aspects critical to bone health, including calcium metabolism, prostaglandin synthesis, and the balance between osteoblast and osteoclast activities [404]. Our findings indicate that omega-3 PUFA supplementation not only improves metabolic parameters but also enhances bone quality by reducing BMA, promoting osteoblast differentiation, decreasing osteoclast differentiation and senescence in BMSCs. These results underscore the potential of omega-3 PUFAs in the prevention and treatment of metabolic bone diseases, offering a non-pharmacological strategy to counteract obesity-induced bone impairment.

The pharmacological component of our research focuses on MSDC-0602K, a second-generation TZD designed to minimize the adverse effects associated with classical TZDs, such as pioglitazone [396]. This novel analog exhibited a weak affinity to PPARγ, aiming to reduce the detrimental impacts on bone health while maintaining its beneficial metabolic effects. Our study demonstrated that MSDC-0602K, in comparison to pioglitazone, had a less harmful effect on bone microarchitecture and BMSC properties in the context of diet-induced obesity. Additionally, we observed different effects of MSDC-0602K on cellular metabolism between human BMSCs and AT-MSCs, highlighting the nuanced impact of systemically administered drugs on various tissues.

Both approaches were studied *in vivo* using 12-week-old male C57BL/6N mice fed with HFD supplemented with omega-3 PUFAs (enriched with DHA and EPA), pioglitazone and MSDC-0602K during 8-week long dietary intervention. The experimental designed together with doses of the tested drugs have been chosen according to the previously published studies focusing on the effect of dietary intervention on peripheral AT [398, 405, 406]. Although,

previous research comparing lean and HFD mice indicated that among classical TZDs, rosiglitazone notably impacts bone health by suppressing bone formation, enhancing osteoclastogenesis, and promoting BMAT more than pioglitazone [368, 407-410], our study used pioglitazone in comparison to MSDC-0602K. This choice was made because pioglitazone still remains in clinical use as PPARγ agonist available for treating T2D patients [411, 412].

Previous animal studies using omega-3 PUFA diet supplementations showed ambigous results depending on the design and experimental conditions. For example, study using 1% DHA-enriched diet reported increased lumbar bone density and cortical bone volume using 10-week-long treatment in 6-week-old female Sprague-Dawley rats [413] which match our results showing improvement of cortical and trabecular parameters in L5 vertebrae with 12-week-long omega-3 PUFA dietary supplementation of HFD fed male mice. Although, administering the same treatment to 3-week-old C57BL/6J male and female mice [404] or 6-week-old male diabetic Zucker rats [414] did not result in alterations in bone phenotype as assessed by dual-energy X-ray absorptiometry (DXA) after 9 weeks of treatment. This discrepancy may be attributed to the less sensitive methodology used for evaluating bone structure and the difference in animal models of metabolic diseases. On the other hand, longer dietary treatment with omega-3 PUFAs ranging from 20 to 24-weeks consistently demonstrate the beneficial impact of omega-3 supplementation on bone phenotype, highlighting its significance in the diet [332, 415, 416]. Further, positive effect of 10-month-long omega-3 PUFA supplementation of diet in mouse model of senile osteoporosis was shown in context of age-related bone loss caused by reducing BMAT [417]. Our data using omega-3 PUFA dietary supplementation of HFD fed mice showed positive effect of this treatment by decreased BMA and improved bone microstructure and mechanical properties of bones even after 2-month intervention.

Further analysis of primary BMSC isolated from treated animals revealed decreased adipogenesis and increased osteogenesis by omega-3 PUFA supplementation. These beneficial effects of omega-3 PUFAs were also supported by decreased senescent phenotype of BMSC, decreased inflammatory response of HSCs by decreased NFκB and increased insulin signalling. These findings support results from *in vitro* studies using C3H10T1/2 and RAW264.7 cells, which showed the inhibition of RANKL and PPARγ pathways using omega-3 PUFAs [332, 418-420] and study reporting omega-3 induced changes in plasma membrane of BMSCs leading to increased osteoblast differentiation [421].

Previous studies are pointing out inhibitory effect of omega-3 PUFAs on osteoclastogenesis [332, 333, 422]. Thus, we compared osteoclastic differentiation of BM cells from HFD treated mice with HFD supplemented with omega-3 PUFAs and we observed, decreased number, TRAcP activity and size of osteoclast caused by omega-3 supplementation which showed positive effect of this diet on bone formation. However, further more detailed studies are needed to reveal resorptive activity of osteoclast depending on number of nuclei or their size.

Differentiation potential of the cells is tightly connected with cellular metabolism. Thus, testing of bioenergetics profile in primary BMSCs isolated from HFD + omega-3 PUFA treated mice showed quiescent metabolic phenotype (low glycolytic and respiratory activity) compared to HFD BMSCs with increased energetic profile, which is opposite to the response of peripheral AT to omega-3 PUFA treatment [423]. Additionally, the metabolic adjustments in BMSCs were linked to reduced ROS production and senescence, indicating that omega-3 PUFAs may protect the BM microenvironment from the detrimental impacts of an obesogenic diet by decreasing of the metabolic activity of primary BMSCs. This could facilitate the preservation of stemness and minimize epigenetic alterations within BMSCs [424]. These results were confirmed by metabolomic and lipidomic analysis of plasma and BM samples from treated mice, showing increase EPA and DHA and decreased levels of prostaglandin not only in plasma but also in BM, which supports evidence on positive effect of omega-3 PUFAs on bone homeostasis and correlates with previous studies showing increased bone formation [414, 425, 426].

Parallelly, investigation of pharmacological treatment with pioglitazone in HFD-fed rodents for 4 to 6 weeks showed negative impact on vertebrae microstructure, decreased chondrocyte differentiation and increased BMA compared to the controls [410, 427, 428]. However, 6-month long treatment of lean mice with MSDC-0602K showed beneficial effect of this analog on bone mechanical properties and microstructure compared to pioglitazone [397]. Our findings nicely correlate with previous studies [181, 298] with observations on changes in BMA, improved bone microstructure and bone mechanical properties, decreased adipogenic differentiation and cellular senescent phenotype studied in pharmacological intervention over a short 2-moth long period. However, we did not observe significant negative impact of pioglitazone on bone microstructure compared to HFD which could be caused by using C57BL/6N male mouse strain and shorter dietary intervention compared to previous studies [181, 298]. Even though, MSDC-0602K treatment demonstrated a beneficial impact on the mechanical properties of the femur when compared to mice treated with pioglitazone. This

improvement could be due to alterations in collagen content, as osteoblast-differentiated primary BMSCs from the HFD + MSDC-0602K group exhibited a higher expression of *Col1a1*, a collagen marker, than those from the HFD + pioglitazone group. Moreover, these results could be explained also by increased distribution of smaller BMAds with MSDC-0602K treatment compared to pioglitazone, analysed using contrast enhanced μCT and Hexabrix staining of BMAT within proximal tibias. This can be caused by increased lipolytic activity of BMAds which may promote lipid turnover and utilization of these lipids by BMSCs in the form of small lipid droplets. Supporting this, we observed a downregulation of metabolic gene expression, including *Insr*, *Pparγ2*, and *Cd36*, in BMSCs from the HFD + MSDC-0602K treated mice compared to the HFD + pioglitazone group, indicating a possible increased sensitivity to lipolytic rather than lipogenic signals. Also, differentiation of BMSCs from HFD + MSDC-0602K group cells towards adipocytes was decreased and osteoblastic differentiation was increased compared to pioglitazone group confirming reduced PPARγ activation with MSDC-0602K. Moreover, parameters like senescence, inflammatory or insulin response of primary BMSCs and HSCs were improved with novel TZD compared to pioglitazone suggesting less detrimental effect on bone and BM microenvironment with this treatment.

Additionally, the same analysis of cellular metabolism was performed to compare metabolism of primary BMSCs from HFD + MSDC-0602K treated mice with cells from HFD + pioglitazone treated mice. Surprisingly, cellular respiration as well as glycolysis were increased with MSDC-0602K compared to pioglitazone which was confirmed also in hBMSC cell line where we also used MPC inhibitor UK5099. These results may suggest different utilization of nutrients in these cells contributing to the mitochondrial TCA cycle, thus we compared our findings with the same experiment performed on peripheral AT-MSCs where MSDC-0602K and UK5099 inhibited respiration. Previous finding showed that activity of MPC in mitochondria are able to determine which type of nutrients mitochondria oxidize, affecting cellular function and determining cell fate [429, 430]. Recent studies in brown adipocytes have demonstrated that inhibiting MPC results in enhanced mitochondrial respiration, thereby promoting lipid cycling and energy expenditure through the uptake of fatty acids and glutamine [431]. However, these observations were made in isolated mitochondria, in contrast to our study, which examines data from intact cells.

Based on our results showing increased osteo differentiation by MSDC-0602K treatment we wondered, if it affects glutamine metabolism in hBMSCs which is usually associated with increased osteoblastogenesis [224]. Interestingly, MSDC-0602K-treated hBMSCs showed

reduced glucose uptake but increased glutamate levels, a by-product of glutamine metabolism, compared to those treated with pioglitazone. This was associated with the upregulation of genes involved in glutamine metabolism in cells treated with MSDC-0602K versus pioglitazone. Thus, experiments using peripheral AT-MSC cell line 3T3-L1 showed opposite results of increased preference of glucose over glutamine supporting the hypothesis, that positive effect of MSDC-0602K on bones may be due to metabolic changes leading to regulation of stem cell fate and increased bone formation. These metabolic changes can be caused also by mechanism of action via MPC inhibition of MSDC-0602K, which we confirmed by several experiments (Figure 8-11) using MPC1 KD hBMSCs. These results showed increased osteoblast and decreased adipocyte differentiation as well as decreased response to insulin stimulation of MPC1 KD hBMSCs, which is similar to our results from primary mouse BMSCs isolated from MSDC-0602K treated mice supporting the hypothesis that this novel analog works via MPC inhibition in bone. Moreover, inhibition of MPC dimer in inner mitochondrial membrane is well known for its effect on cellular metabolism for example in C2C12 myoblasts in terms of increased amino acid utilisation, especially glutamine, when other metabolites are abundant due to MPC inhibition [429]. Further, these results were supported by data from fluxomic analysis of ^{13}C labelled glucose and glutamine in hBMSCs showing increased glutamine utilisation with MSDC-0602K treatment compared to pioglitazone, which supported our hypothesis, that positive effect of MSDC-0602K on bones is possibly mediated by increased glutamine metabolism in bones. These data are in line with previous finding showing negative effect of GLS deletion mice by decreased bone formation and hBMSC osteo differentiation [224, 432, 433]. Further, increased glutamine utilisation can contribute to increased bone quality also by proline synthesis (synthetized from glutamine via glutamate) [434], which is important amino acid for collagen production, as proline represents 10 % of amino acids in collagen molecule [435]. Previous studies are also showing that glutamine is precursor for *de novo* synthesis of glutathione, antioxidant molecule which helps to balance redox system within cells [432]. In context of our findings, we hypothesized that MSDC-0602K treatment led to less senescent BM microenvironment compared to pioglitazone can be caused by increased glutathione synthesis with MSDC-0602K. However, further analysis of glutathione levels in BM cells (BMSCs and HSCs) treated with MSDC-0602K are needed to fully confirm this hypothesis.

Furthermore, fluxomic analysis showed also increased glucose utilisation by pioglitazone compared to MSDC-0602K treated hBMSCs supporting our previous data showing increased

glucose uptake with pioglitazone treatment. Interestingly, further analysis of glucose production by PEPCK (gluconeogenic enzyme) activity in cytosol and mitochondria revealed, that its enzymatic activity in cytosol is not changed while in mitochondria there is increased PEPCK activity in MSDC-0602K treated hBMSCs compared to pioglitazone which may compensate inhibition of MPC1 in this cells. Fluxomic analysis also showed increased production of metabolites linked with NADH production like succinate, explaining increased mitochondrial respiration measured in hBMSCs from MSDC-0602K group. Moreover, MSDC-0602K increased production of other TCA cycle related metabolites like acetyl-CoA. Further analysis showed that acetyl-CoA together with oxaloacetate were further used for citrate production in mitochondria in MSDC-0602K treated hBMSCs more profoundly than with pioglitazone treatment, which can further contribute to lipogenesis which is in line with previous results studying MPC KD in C2C12 myoblasts [429]. These results are showing potential connection with our *in vitro* data from analysis of BMAT size in proximal tibia of MSDC-0602K and pioglitazone treated HFD- fed mice. However, further analysis of the effect of TZD and novel analog MSDC-0602K on lipid metabolism and *de novo* lipid synthesis are needed to see potential difference between these treatments in bones.

To sum up, our study offers comprehensive perspective on addressing metabolic bone disease by two different approaches: non-pharmacological using omega-3 PUFAs and pharmacological with MSDC-0602K. While MSDC-0602K represents a promising pharmacological pathway with reduced skeletal risks, omega-3 PUFAs offer a dietary method with multiple positive effects on bones homeostasis. Unlike previous studies investigating effect of MSDC-0602K or omega-3 PUFAs on bone, here we conduct complex study using in vivo and in vitro analysis, including measurement of bone microstructure, BMA and cellular and molecular properties of various cell types within BM microenvironment. Our studies described the intricate mechanisms through which these interventions operate, from altering BMSC differentiation pathways to reshaping the cellular metabolism within BM niche. However, there are also some limitations in our studies, as we used 2 month-long dietary intervention in both studies using C57BL/6N male mouse model which did not manifest so pronounced negative changes in bones in obesogenic conditions compared to control. In addition, we tested this novel analog only in males, thus further study in females is needed to see future perspective of this treatment in women with metabolic complications associated with osteoporosis. Even though, we observed positive effect of omega-3 and MSDC-0602K

treatment compared to HFD which highlight their potential in treatment of metabolic bone diseases (Figure 13).

5. Conclusion and future perspective

In conclusion, this thesis provides comprehensive analysis investigating the effect of non-pharmacological and pharmacological approaches in the treatment of metabolic diseases with respect to bone homeostasis and fat metabolism. The main conclusions are:

i) Omega-3 PUFA treatment in HFD mice prevented negative side effect of obesogenic conditions on metabolic and bone health, alongside decreased BMA and enhanced differentiation potential and reduced senescence in BMSCs. Moreover, this study showed decreased osteoclastogenesis by omega-3 PUFA supplementation in HFD, which highlights a positive effect of this dietary supplement on bone remodeling. These findings emphasize the positive impact of omega-3 PUFAs on bone and cellular metabolism, suggesting their potential application in the treatment of metabolic bone disorders.

ii) Second study investigating potential of MSDC-0602K as novel analog of TZD in treatment of metabolic diseases showed reduced side effects on bone using this novel analog compared to classical TZD, pioglitazone. Moreover, this study brought detailed insight on BMAT composition using novel contrast enhanced agent Hexabrix allowing visualization both BMAT and bone microstructure by contrast enhanced μCT compared to previously used staining with osmium tetroxide (OsO_4). Additionally, detailed analysis of cellular differentiation and metabolism of primary BMSCs isolated from treated mice showed positive effect of MSDC-0602K on osteoblastogenesis showing high potential of this drug in treatment of bone related metabolic complications.

iii) Studying differences in mechanism of action of MSDC-0602K and pioglitazone in hBMSCs and AT-MSCs showed opposite metabolic responses in terms of increased preference of glutamine over glucose in hBMSCs and increased glucose uptake by AT-MSCs. These findings are showing potential of MSDC-0602K to target different metabolic pathways within distinct parts of organism. Further analysis of mechanism of MSDC-0602K in hBMSCs using MPC1 siRNA confirmed MPC inhibition effect of this treatment leading to decreased adipo differentiation and increased osteo differentiation, which is in line with our previous results from mouse study. In addition, fluxomic data analyzing different effect of MSDC-0602K and pioglitazone in hBMSCs showed increased glutamine and decreased glucose utilization with

MSDC-0602K treatment compared to pioglitazone. Thus, increasing glutamine metabolism within bones leads to improved bone homeostasis suggesting MSDC-0602K as potential drug for treatment of bone and metabolic disorders.

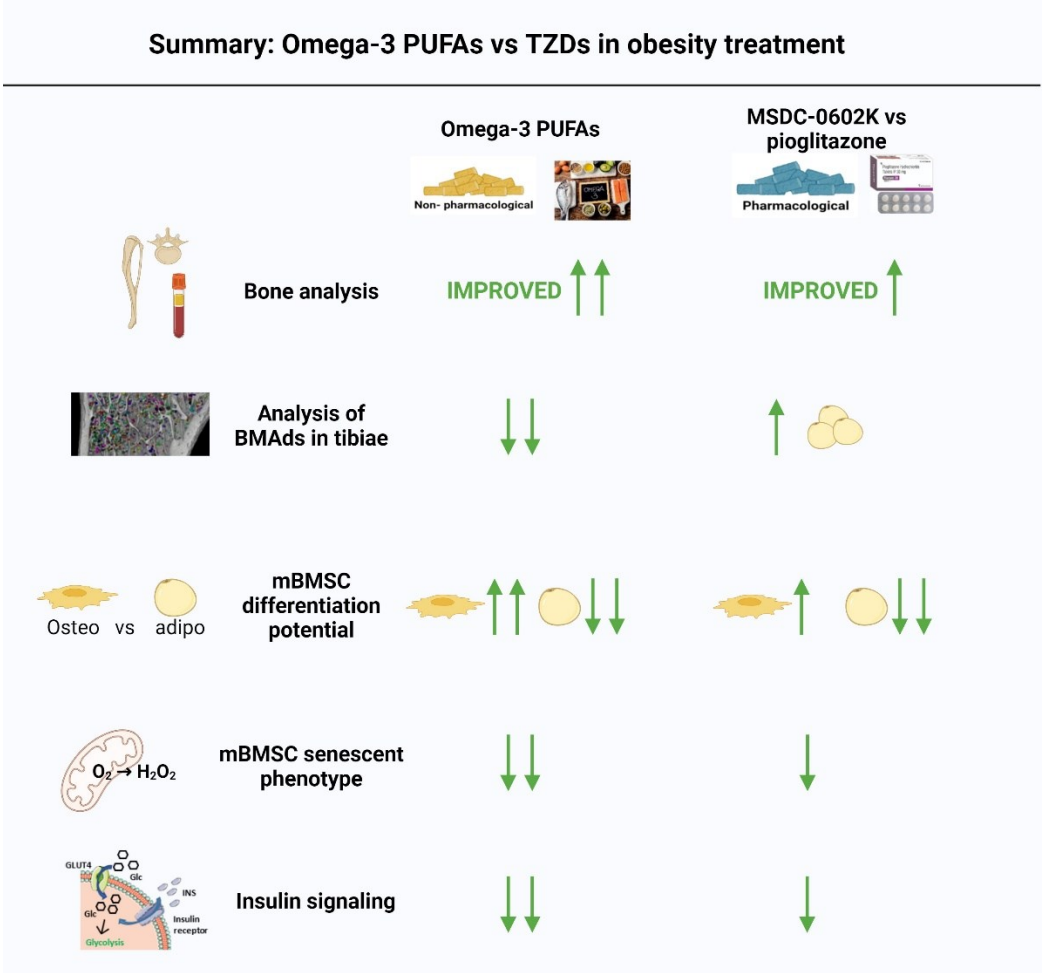

Figure 13. Concluding scheme showing main results from thesis. (Created in Biorender.com) (Abbreviations: BMAds, Bone marrow adipocytes; BMSC, Bone marrow skeletal cells; PUFAs, Polyunsaturated fatty acids; TZDs, Thiazolidinediones)

This thesis is bringing two potential strategies of treating negative effects of metabolic diseases on bones. However, further studies are needed to better understand the effect of omega-3 PUFAs on osteoclastogenesis as well as detailed steps of mechanism of MSDC-0602K in bone cells compared to AT-MSCs. Moreover, this study also opens new opportunity for further research of potential synergistic effect of these treatments in treating of metabolic bone diseases.

6. List of all author's publications

Ferencakova M, Benova A, Raska I Jr, Abaffy P, Sindelka R, Dzubanova M, Pospisilova E, Kolostova K, Cajka T, Paclik A, Zikan V, Tencerova M. Human bone marrow stromal cells: the impact of anticoagulants on stem cell properties. Front Cell Dev Biol. 2023 Sep 18;11:1255823. doi: 10.3389/fcell.2023.1255823. PMID: 37791077; PMCID: PMC10544901.

Benova A, Tencerova M. Obesity-Induced Changes in Bone Marrow Homeostasis. Front Endocrinol (Lausanne). 2020 May 12;11:294. doi: 10.3389/fendo.2020.00294. PMID: 32477271; PMCID: PMC7235195. (review)

7. References

1. Raggatt, L.J. and N.C. Partridge, *Cellular and molecular mechanisms of bone remodeling.* J Biol Chem, 2010. **285**(33): p. 25103-8.
2. Florencio-Silva, R., et al., *Biology of Bone Tissue: Structure, Function, and Factors That Influence Bone Cells.* Biomed Res Int, 2015. **2015**: p. 421746.
3. Kim, J.N., et al., *Haversian system of compact bone and comparison between endosteal and periosteal sides using three-dimensional reconstruction in rat.* Anat Cell Biol, 2015. **48**(4): p. 258-61.
4. Ralston, S.H., *Bone structure and metabolism.* 2021. **49**(9): p. 567-571.
5. Weatherholt, A.M., R.K. Fuchs, and S.J. Warden, *Specialized connective tissue: bone, the structural framework of the upper extremity.* J Hand Ther, 2012. **25**(2): p. 123-31; quiz 132.
6. Benova, A. and M. Tencerova, *Obesity-Induced Changes in Bone Marrow Homeostasis.* Front Endocrinol (Lausanne), 2020. **11**: p. 294.
7. Tencerova, M. and M. Kassem, *The Bone Marrow-Derived Stromal Cells: Commitment and Regulation of Adipogenesis.* Front Endocrinol (Lausanne), 2016. **7**: p. 127.
8. Naomi, R., P.M. Ridzuan, and H. Bahari, *Current Insights into Collagen Type I.* Polymers (Basel), 2021. **13**(16).
9. Gomez, B., Jr., et al., *Monoclonal antibody assay for free urinary pyridinium cross-links.* Clin Chem, 1996. **42**(8 Pt 1): p. 1168-75.
10. Bradshaw, A.D., *The Extracellular Matrix.* Encyclopedia of Cell Biology, 2016. **2**: p. 694-703.
11. Wu, M., G. Chen, and Y.P. Li, *TGF-beta and BMP signaling in osteoblast, skeletal development, and bone formation, homeostasis and disease.* Bone Res, 2016. **4**: p. 16009.
12. Chen, X., et al., *Osteoblast-osteoclast interactions.* Connect Tissue Res, 2018. **59**(2): p. 99-107.
13. Wang, C., et al., *Differentiation of Bone Marrow Mesenchymal Stem Cells in Osteoblasts and Adipocytes and its Role in Treatment of Osteoporosis.* Med Sci Monit, 2016. **22**: p. 226-33.
14. McDonald, M.M., et al., *New Insights Into Osteoclast Biology.* JBMR Plus, 2021. **5**(9): p. e10539.
15. Bilezikian, J.P., et al., *Principles of bone biology*. Fourth edition. ed. 2020, London, United Kingdom: Academic Press, an imprint of Elsevier.
16. Zaidi, M., *Skeletal remodeling in health and disease.* Nat Med, 2007. **13**(7): p. 791-801.
17. Cohen, M.M., Jr., *The new bone biology: pathologic, molecular, and clinical correlates.* Am J Med Genet A, 2006. **140**(23): p. 2646-706.
18. Feng, X. and J.M. McDonald, *Disorders of bone remodeling.* Annu Rev Pathol, 2011. **6**: p. 121-45.
19. Rinonapoli, G., et al., *Obesity and Bone: A Complex Relationship.* Int J Mol Sci, 2021. **22**(24).
20. Kenkre, J.S. and J. Bassett, *The bone remodelling cycle.* Ann Clin Biochem, 2018. **55**(3): p. 308-327.
21. Christensen, J. and V.P. Shastri, *Matrix-metalloproteinase-9 is cleaved and activated by cathepsin K.* BMC Res Notes, 2015. **8**: p. 322.
22. McDonald, M.M., et al., *Osteoclasts recycle via osteomorphs during RANKL-stimulated bone resorption.* Cell, 2021. **184**(5): p. 1330-1347 e13.

23. Sims, N.A. and T.J. Martin, *Coupling the activities of bone formation and resorption: a multitude of signals within the basic multicellular unit.* Bonekey Rep, 2014. **3**: p. 481.
24. Teti, A., *Mechanisms of osteoclast-dependent bone formation.* Bonekey Rep, 2013. **2**: p. 449.
25. Dirckx, N., M. Van Hul, and C. Maes, *Osteoblast recruitment to sites of bone formation in skeletal development, homeostasis, and regeneration.* Birth Defects Res C Embryo Today, 2013. **99**(3): p. 170-91.
26. Henriksen, K., M.A. Karsdal, and T.J. Martin, *Osteoclast-derived coupling factors in bone remodeling.* Calcif Tissue Int, 2014. **94**(1): p. 88-97.
27. Sims, N.A. and R. Civitelli, *Cell-cell signaling: broadening our view of the basic multicellular unit.* Calcif Tissue Int, 2014. **94**(1): p. 2-3.
28. Rucci, N., *Molecular biology of bone remodelling.* Clin Cases Miner Bone Metab, 2008. **5**(1): p. 49-56.
29. Wein, M.N. and H.M. Kronenberg, *Regulation of Bone Remodeling by Parathyroid Hormone.* Cold Spring Harb Perspect Med, 2018. **8**(8).
30. Kim, C.H., et al., *Trabecular bone response to mechanical and parathyroid hormone stimulation: the role of mechanical microenvironment.* J Bone Miner Res, 2003. **18**(12): p. 2116-25.
31. Rosenfeld, R.G., A.L. Rosenbloom, and J. Guevara-Aguirre, *Growth hormone (GH) insensitivity due to primary GH receptor deficiency.* Endocr Rev, 1994. **15**(3): p. 369-90.
32. Sjogren, K., et al., *Disproportional skeletal growth and markedly decreased bone mineral content in growth hormone receptor -/- mice.* Biochem Biophys Res Commun, 2000. **267**(2): p. 603-8.
33. Ohlsson, C. and O. Vidal, *Effects of growth hormone and insulin-like growth factors on human osteoblasts.* Eur J Clin Invest, 1998. **28**(3): p. 184-6.
34. Wang, J., et al., *Evidence supporting dual, IGF-I-independent and IGF-I-dependent, roles for GH in promoting longitudinal bone growth.* J Endocrinol, 2004. **180**(2): p. 247-55.
35. Xian, L., et al., *Matrix IGF-1 maintains bone mass by activation of mTOR in mesenchymal stem cells.* Nat Med, 2012. **18**(7): p. 1095-101.
36. Bikle, D., et al., *The skeletal structure of insulin-like growth factor I-deficient mice.* J Bone Miner Res, 2001. **16**(12): p. 2320-9.
37. Wang, Y., et al., *Role of IGF-I signaling in regulating osteoclastogenesis.* J Bone Miner Res, 2006. **21**(9): p. 1350-8.
38. Xie, J., et al., *Calcitonin and Bone Physiology: In Vitro, In Vivo, and Clinical Investigations.* Int J Endocrinol, 2020. **2020**: p. 3236828.
39. Siddiqui, J.A. and N.C. Partridge, *Physiological Bone Remodeling: Systemic Regulation and Growth Factor Involvement.* Physiology (Bethesda), 2016. **31**(3): p. 233-45.
40. Canalis, E. and A.M. Delany, *Mechanisms of glucocorticoid action in bone.* Ann N Y Acad Sci, 2002. **966**: p. 73-81.
41. Thrailkill, K.M., et al., *Is insulin an anabolic agent in bone? Dissecting the diabetic bone for clues.* Am J Physiol Endocrinol Metab, 2005. **289**(5): p. E735-45.
42. Thomas, D.M., et al., *Insulin receptor expression in bone.* J Bone Miner Res, 1996. **11**(9): p. 1312-20.
43. Hashizume, M. and M. Yamaguchi, *Stimulatory effect of beta-alanyl-L-histidinato zinc on cell proliferation is dependent on protein synthesis in osteoblastic MC3T3-E1 cells.* Mol Cell Biochem, 1993. **122**(1): p. 59-64.

44. Rosen, D.M. and R.A. Luben, *Multiple hormonal mechanisms for the control of collagen synthesis in an osteoblast-like cell line, MMB-1.* Endocrinology, 1983. **112**(3): p. 992-9.
45. Hahn, T.J., et al., *Glucose transport in osteoblast-enriched bone explants: characterization and insulin regulation.* J Bone Miner Res, 1988. **3**(3): p. 359-65.
46. Bassett, J.H. and G.R. Williams, *Role of Thyroid Hormones in Skeletal Development and Bone Maintenance.* Endocr Rev, 2016. **37**(2): p. 135-87.
47. Cawthorn, W.P., et al., *Bone marrow adipose tissue is an endocrine organ that contributes to increased circulating adiponectin during caloric restriction.* Cell Metab, 2014. **20**(2): p. 368-375.
48. Xiao, L., et al., *Disruption of the Fgf2 gene activates the adipogenic and suppresses the osteogenic program in mesenchymal marrow stromal stem cells.* Bone, 2010. **47**(2): p. 360-70.
49. Oshima, K., et al., *Adiponectin increases bone mass by suppressing osteoclast and activating osteoblast.* Biochem Biophys Res Commun, 2005. **331**(2): p. 520-6.
50. Wu, Y., et al., *Central adiponectin administration reveals new regulatory mechanisms of bone metabolism in mice.* Am J Physiol Endocrinol Metab, 2014. **306**(12): p. E1418-30.
51. Lewis, J.W., et al., *Adiponectin signalling in bone homeostasis, with age and in disease.* Bone Res, 2021. **9**(1): p. 1.
52. Ducy, P., et al., *Leptin inhibits bone formation through a hypothalamic relay: a central control of bone mass.* Cell, 2000. **100**(2): p. 197-207.
53. Cornish, J., et al., *Leptin directly regulates bone cell function in vitro and reduces bone fragility in vivo.* J Endocrinol, 2002. **175**(2): p. 405-15.
54. Borjesson, A.E., et al., *The role of estrogen receptor alpha in the regulation of bone and growth plate cartilage.* Cell Mol Life Sci, 2013. **70**(21): p. 4023-37.
55. Khosla, S., L.J. Melton, 3rd, and B.L. Riggs, *The unitary model for estrogen deficiency and the pathogenesis of osteoporosis: is a revision needed?* J Bone Miner Res, 2011. **26**(3): p. 441-51.
56. Khosla, S., M.J. Oursler, and D.G. Monroe, *Estrogen and the skeleton.* Trends Endocrinol Metab, 2012. **23**(11): p. 576-81.
57. Jackson, J.A., M.W. Riggs, and A.M. Spiekerman, *Testosterone deficiency as a risk factor for hip fractures in men: a case-control study.* Am J Med Sci, 1992. **304**(1): p. 4-8.
58. Kenny, A.M., et al., *Determinants of bone density in healthy older men with low testosterone levels.* J Gerontol A Biol Sci Med Sci, 2000. **55**(9): p. M492-7.
59. Tracz, M.J., et al., *Testosterone use in men and its effects on bone health. A systematic review and meta-analysis of randomized placebo-controlled trials.* J Clin Endocrinol Metab, 2006. **91**(6): p. 2011-6.
60. Chapuy, M.C., et al., *Vitamin D3 and calcium to prevent hip fractures in elderly women.* N Engl J Med, 1992. **327**(23): p. 1637-42.
61. Kim, J.H., et al., *Wnt signaling in bone formation and its therapeutic potential for bone diseases.* Ther Adv Musculoskelet Dis, 2013. **5**(1): p. 13-31.
62. Ke, H.Z., et al., *Sclerostin and Dickkopf-1 as therapeutic targets in bone diseases.* Endocr Rev, 2012. **33**(5): p. 747-83.
63. Westendorf, J.J., R.A. Kahler, and T.M. Schroeder, *Wnt signaling in osteoblasts and bone diseases.* Gene, 2004. **341**: p. 19-39.
64. Li, X., et al., *Sclerostin binds to LRP5/6 and antagonizes canonical Wnt signaling.* J Biol Chem, 2005. **280**(20): p. 19883-7.

65. Baron, R. and G. Rawadi, *Targeting the Wnt/beta-catenin pathway to regulate bone formation in the adult skeleton.* Endocrinology, 2007. **148**(6): p. 2635-43.
66. Li, X., et al., *Targeted deletion of the sclerostin gene in mice results in increased bone formation and bone strength.* J Bone Miner Res, 2008. **23**(6): p. 860-9.
67. Christodoulides, C., et al., *The Wnt antagonist Dickkopf-1 and its receptors are coordinately regulated during early human adipogenesis.* J Cell Sci, 2006. **119**(Pt 12): p. 2613-2620.
68. Park, J.R., et al., *The roles of Wnt antagonists Dkk1 and sFRP4 during adipogenesis of human adipose tissue-derived mesenchymal stem cells.* Cell Prolif, 2008. **41**(6): p. 859-874.
69. Colditz, J., et al., *Contributions of Dickkopf-1 to Obesity-Induced Bone Loss and Marrow Adiposity.* JBMR Plus, 2020. **4**(6): p. e10364.
70. Fairfield, H., et al., *The skeletal cell-derived molecule sclerostin drives bone marrow adipogenesis.* J Cell Physiol, 2018. **233**(2): p. 1156-1167.
71. Lewiecki, E.M., *New targets for intervention in the treatment of postmenopausal osteoporosis.* Nat Rev Rheumatol, 2011. **7**(11): p. 631-8.
72. Fei, Y., et al., *Fibroblast growth factor 2 stimulation of osteoblast differentiation and bone formation is mediated by modulation of the Wnt signaling pathway.* J Biol Chem, 2011. **286**(47): p. 40575-83.
73. Nagayama, T., et al., *FGF18 accelerates osteoblast differentiation by upregulating Bmp2 expression.* Congenit Anom (Kyoto), 2013. **53**(2): p. 83-8.
74. Takeshita, A., et al., *Central role of the proximal tubular alphaKlotho/FGF receptor complex in FGF23-regulated phosphate and vitamin D metabolism.* Sci Rep, 2018. **8**(1): p. 6917.
75. Yoshiko, Y., et al., *Mineralized tissue cells are a principal source of FGF23.* Bone, 2007. **40**(6): p. 1565-73.
76. Li, Y., et al., *FGF23 affects the lineage fate determination of mesenchymal stem cells.* Calcif Tissue Int, 2013. **93**(6): p. 556-64.
77. Charoenphandhu, N., et al., *Fibroblast growth factor-21 restores insulin sensitivity but induces aberrant bone microstructure in obese insulin-resistant rats.* J Bone Miner Metab, 2017. **35**(2): p. 142-149.
78. Wei, W., et al., *Fibroblast growth factor 21 promotes bone loss by potentiating the effects of peroxisome proliferator-activated receptor gamma.* Proc Natl Acad Sci U S A, 2012. **109**(8): p. 3143-8.
79. Yang, Q., et al., *The Multiple Biological Functions of Dipeptidyl Peptidase-4 in Bone Metabolism.* Front Endocrinol (Lausanne), 2022. **13**: p. 856954.
80. Maurizi, A., et al., *Lipocalin 2 serum levels correlate with age and bone turnover biomarkers in healthy subjects but not in postmenopausal osteoporotic women.* Bone Rep, 2021. **14**: p. 101059.
81. Kjeldsen, L., et al., *Isolation and primary structure of NGAL, a novel protein associated with human neutrophil gelatinase.* J Biol Chem, 1993. **268**(14): p. 10425-32.
82. Rucci, N., et al., *Lipocalin 2: a new mechanoresponding gene regulating bone homeostasis.* J Bone Miner Res, 2015. **30**(2): p. 357-68.
83. Gambara, G., et al., *Microgravity-Induced Transcriptome Adaptation in Mouse Paraspinal longissimus dorsi Muscle Highlights Insulin Resistance-Linked Genes.* Front Physiol, 2017. **8**: p. 279.
84. Capulli, M., et al., *A Complex Role for Lipocalin 2 in Bone Metabolism: Global Ablation in Mice Induces Osteopenia Caused by an Altered Energy Metabolism.* J Bone Miner Res, 2018. **33**(6): p. 1141-1153.

85. Cook, K.S., et al., *Adipsin: a circulating serine protease homolog secreted by adipose tissue and sciatic nerve.* Science, 1987. **237**(4813): p. 402-5.
86. Abernathy, R.P. and D.R. Black, *Healthy body weights: an alternative perspective.* Am J Clin Nutr, 1996. **63**(3 Suppl): p. 448S-451S.
87. Trayhurn, P. and I.S. Wood, *Adipokines: inflammation and the pleiotropic role of white adipose tissue.* Br J Nutr, 2004. **92**(3): p. 347-55.
88. Cannon, B. and J. Nedergaard, *Brown adipose tissue: function and physiological significance.* Physiol Rev, 2004. **84**(1): p. 277-359.
89. Park, A., W.K. Kim, and K.H. Bae, *Distinction of white, beige and brown adipocytes derived from mesenchymal stem cells.* World J Stem Cells, 2014. **6**(1): p. 33-42.
90. Scheele, C. and C. Wolfrum, *Brown Adipose Crosstalk in Tissue Plasticity and Human Metabolism.* Endocr Rev, 2020. **41**(1): p. 53-65.
91. Czech, M.P., et al., *Insulin signalling mechanisms for triacylglycerol storage.* Diabetologia, 2013. **56**(5): p. 949-64.
92. Fazeli, P.K., et al., *Marrow fat and bone--new perspectives.* J Clin Endocrinol Metab, 2013. **98**(3): p. 935-45.
93. Herrmann, M., *Marrow Fat-Secreted Factors as Biomarkers for Osteoporosis.* Curr Osteoporos Rep, 2019. **17**(6): p. 429-437.
94. Suchacki, K.J., et al., *Bone marrow adipose tissue is a unique adipose subtype with distinct roles in glucose homeostasis.* Nat Commun, 2020. **11**(1): p. 3097.
95. Young, P., J.R. Arch, and M. Ashwell, *Brown adipose tissue in the parametrial fat pad of the mouse.* FEBS Lett, 1984. **167**(1): p. 10-4.
96. Loncar, D., B.A. Afzelius, and B. Cannon, *Epididymal white adipose tissue after cold stress in rats. I. Nonmitochondrial changes.* J Ultrastruct Mol Struct Res, 1988. **101**(2-3): p. 109-22.
97. Wang, S., et al., *From white to beige adipocytes: therapeutic potential of dietary molecules against obesity and their molecular mechanisms.* Food Funct, 2019. **10**(3): p. 1263-1279.
98. Mika, A., et al., *Effect of Exercise on Fatty Acid Metabolism and Adipokine Secretion in Adipose Tissue.* Front Physiol, 2019. **10**: p. 26.
99. Kaisanlahti, A. and T. Glumoff, *Browning of white fat: agents and implications for beige adipose tissue to type 2 diabetes.* J Physiol Biochem, 2019. **75**(1): p. 1-10.
100. Ikeda, K., P. Maretich, and S. Kajimura, *The Common and Distinct Features of Brown and Beige Adipocytes.* Trends Endocrinol Metab, 2018. **29**(3): p. 191-200.
101. Giordano, A., et al., *White, brown and pink adipocytes: the extraordinary plasticity of the adipose organ.* Eur J Endocrinol, 2014. **170**(5): p. R159-71.
102. Cinti, S., *Pink Adipocytes.* Trends Endocrinol Metab, 2018. **29**(9): p. 651-666.
103. Apostoli, A.J., et al., *Loss of PPARgamma expression in mammary secretory epithelial cells creates a pro-breast tumorigenic environment.* Int J Cancer, 2014. **134**(5): p. 1055-66.
104. Tontonoz, P. and B.M. Spiegelman, *Fat and beyond: the diverse biology of PPARgamma.* Annu Rev Biochem, 2008. **77**: p. 289-312.
105. Bielczyk-Maczynska, E., *White Adipocyte Plasticity in Physiology and Disease.* Cells, 2019. **8**(12).
106. Baer, P.C. and H. Geiger, *Adipose-derived mesenchymal stromal/stem cells: tissue localization, characterization, and heterogeneity.* Stem Cells Int, 2012. **2012**: p. 812693.
107. Fraser, J.K., et al., *Adipose-derived stem cells.* Methods Mol Biol, 2008. **449**: p. 59-67.
108. Wang, W., et al., *Ebf2 is a selective marker of brown and beige adipogenic precursor cells.* Proc Natl Acad Sci U S A, 2014. **111**(40): p. 14466-71.

109. Seale, P., et al., *PRDM16 controls a brown fat/skeletal muscle switch.* Nature, 2008. **454**(7207): p. 961-7.
110. Atit, R., et al., *Beta-catenin activation is necessary and sufficient to specify the dorsal dermal fate in the mouse.* Dev Biol, 2006. **296**(1): p. 164-76.
111. Sanchez-Gurmaches, J., et al., *PTEN loss in the Myf5 lineage redistributes body fat and reveals subsets of white adipocytes that arise from Myf5 precursors.* Cell Metab, 2012. **16**(3): p. 348-62.
112. Sanchez-Gurmaches, J. and D.A. Guertin, *Adipocytes arise from multiple lineages that are heterogeneously and dynamically distributed.* Nat Commun, 2014. **5**: p. 4099.
113. Vegiopoulos, A., M. Rohm, and S. Herzig, *Adipose tissue: between the extremes.* EMBO J, 2017. **36**(14): p. 1999-2017.
114. Villarroya, F., et al., *Brown adipose tissue as a secretory organ.* Nat Rev Endocrinol, 2017. **13**(1): p. 26-35.
115. Rogers, N.H., et al., *Aging leads to a programmed loss of brown adipocytes in murine subcutaneous white adipose tissue.* Aging Cell, 2012. **11**(6): p. 1074-83.
116. Zhu, Y., et al., *Structural organization of mouse peroxisome proliferator-activated receptor gamma (mPPAR gamma) gene: alternative promoter use and different splicing yield two mPPAR gamma isoforms.* Proc Natl Acad Sci U S A, 1995. **92**(17): p. 7921-5.
117. Lehrke, M. and M.A. Lazar, *The many faces of PPARgamma.* Cell, 2005. **123**(6): p. 993-9.
118. Gross, B., et al., *PPARs in obesity-induced T2DM, dyslipidaemia and NAFLD.* Nat Rev Endocrinol, 2017. **13**(1): p. 36-49.
119. Tontonoz, P., E. Hu, and B.M. Spiegelman, *Stimulation of adipogenesis in fibroblasts by PPAR gamma 2, a lipid-activated transcription factor.* Cell, 1994. **79**(7): p. 1147-56.
120. Rosen, E.D. and O.A. MacDougald, *Adipocyte differentiation from the inside out.* Nat Rev Mol Cell Biol, 2006. **7**(12): p. 885-96.
121. Imai, T., et al., *Peroxisome proliferator-activated receptor gamma is required in mature white and brown adipocytes for their survival in the mouse.* Proc Natl Acad Sci U S A, 2004. **101**(13): p. 4543-7.
122. Wang, Q.A., et al., *Peroxisome Proliferator-Activated Receptor gamma and Its Role in Adipocyte Homeostasis and Thiazolidinedione-Mediated Insulin Sensitization.* Mol Cell Biol, 2018. **38**(10).
123. Semple, R.K., V.K. Chatterjee, and S. O'Rahilly, *PPAR gamma and human metabolic disease.* J Clin Invest, 2006. **116**(3): p. 581-9.
124. Auwerx, J., *PPARgamma, the ultimate thrifty gene.* Diabetologia, 1999. **42**(9): p. 1033-49.
125. Morrison, S.F. and C.J. Madden, *Central nervous system regulation of brown adipose tissue.* Compr Physiol, 2014. **4**(4): p. 1677-713.
126. Duncan, R.E., et al., *Regulation of lipolysis in adipocytes.* Annu Rev Nutr, 2007. **27**: p. 79-101.
127. Kersten, S., *Mechanisms of nutritional and hormonal regulation of lipogenesis.* EMBO Rep, 2001. **2**(4): p. 282-6.
128. Morral, N., et al., *Effects of glucose metabolism on the regulation of genes of fatty acid synthesis and triglyceride secretion in the liver.* J Lipid Res, 2007. **48**(7): p. 1499-510.
129. Mayes, J.S. and G.H. Watson, *Direct effects of sex steroid hormones on adipose tissues and obesity.* Obes Rev, 2004. **5**(4): p. 197-216.
130. Craft, C.S., et al., *Bone marrow adipose tissue does not express UCP1 during development or adrenergic-induced remodeling.* Sci Rep, 2019. **9**(1): p. 17427.

131. Scheller, E.L., et al., *Region-specific variation in the properties of skeletal adipocytes reveals regulated and constitutive marrow adipose tissues.* Nat Commun, 2015. **6**: p. 7808.
132. Mosialou, I., et al., *MC4R-dependent suppression of appetite by bone-derived lipocalin 2.* Nature, 2017. **543**(7645): p. 385-390.
133. Li, Z., et al., *Lipolysis of bone marrow adipocytes is required to fuel bone and the marrow niche during energy deficits.* Elife, 2022. **11**.
134. Zhou, B.O., et al., *Bone marrow adipocytes promote the regeneration of stem cells and haematopoiesis by secreting SCF.* Nat Cell Biol, 2017. **19**(8): p. 891-903.
135. Ambrosi, T.H., et al., *Adipocyte Accumulation in the Bone Marrow during Obesity and Aging Impairs Stem Cell-Based Hematopoietic and Bone Regeneration.* Cell Stem Cell, 2017. **20**(6): p. 771-784 e6.
136. Cawthorn, W.P., et al., *Expansion of Bone Marrow Adipose Tissue During Caloric Restriction Is Associated With Increased Circulating Glucocorticoids and Not With Hypoleptinemia.* Endocrinology, 2016. **157**(2): p. 508-21.
137. Scheller, E.L., et al., *Bone marrow adipocytes resist lipolysis and remodeling in response to beta-adrenergic stimulation.* Bone, 2019. **118**: p. 32-41.
138. Frayn, K.N., *Regulation of fatty acid delivery in vivo.* Adv Exp Med Biol, 1998. **441**: p. 171-9.
139. Frayn, K.N., *Adipose tissue and the insulin resistance syndrome.* Proc Nutr Soc, 2001. **60**(3): p. 375-80.
140. Zimmermann, R., et al., *Fat mobilization in adipose tissue is promoted by adipose triglyceride lipase.* Science, 2004. **306**(5700): p. 1383-6.
141. Langin, D., S. Lucas, and M. Lafontan, *Millennium fat-cell lipolysis reveals unsuspected novel tracks.* Horm Metab Res, 2000. **32**(11-12): p. 443-52.
142. Attane, C., et al., *Human Bone Marrow Is Comprised of Adipocytes with Specific Lipid Metabolism.* Cell Rep, 2020. **30**(4): p. 949-958 e6.
143. Lee, K.Y., et al., *Lessons on conditional gene targeting in mouse adipose tissue.* Diabetes, 2013. **62**(3): p. 864-74.
144. Bluher, M., et al., *Adipose tissue selective insulin receptor knockout protects against obesity and obesity-related glucose intolerance.* Dev Cell, 2002. **3**(1): p. 25-38.
145. Qiang, G., et al., *Lipodystrophy and severe metabolic dysfunction in mice with adipose tissue-specific insulin receptor ablation.* Mol Metab, 2016. **5**(7): p. 480-490.
146. Zoch, M.L., et al., *In vivo radiometric analysis of glucose uptake and distribution in mouse bone.* Bone Res, 2016. **4**: p. 16004.
147. Huovinen, V., et al., *Vertebral bone marrow glucose uptake is inversely associated with bone marrow fat in diabetic and healthy pigs: [(18)F]FDG-PET and MRI study.* Bone, 2014. **61**: p. 33-8.
148. Harasymiak-Krzyzanowska, I., et al., *Adipose tissue-derived stem cells show considerable promise for regenerative medicine applications.* Cell Mol Biol Lett, 2013. **18**(4): p. 479-93.
149. Zakrzewski, W., et al., *Stem cells: past, present, and future.* Stem Cell Res Ther, 2019. **10**(1): p. 68.
150. Kolios, G. and Y. Moodley, *Introduction to stem cells and regenerative medicine.* Respiration, 2013. **85**(1): p. 3-10.
151. Morrison, S.J. and A.C. Spradling, *Stem cells and niches: mechanisms that promote stem cell maintenance throughout life.* Cell, 2008. **132**(4): p. 598-611.
152. Hindorf, C., et al., *EANM Dosimetry Committee guidelines for bone marrow and whole-body dosimetry.* Eur J Nucl Med Mol Imaging, 2010. **37**(6): p. 1238-50.

153. Zhao, E., et al., *Bone marrow and the control of immunity.* Cell Mol Immunol, 2012. **9**(1): p. 11-9.
154. Tuckermann, J. and R.H. Adams, *The endothelium-bone axis in development, homeostasis and bone and joint disease.* Nat Rev Rheumatol, 2021. **17**(10): p. 608-620.
155. Qin, Q., et al., *Neurovascular coupling in bone regeneration.* Exp Mol Med, 2022. **54**(11): p. 1844-1849.
156. Schneider, R.K., et al., *The osteogenic differentiation of adult bone marrow and perinatal umbilical mesenchymal stem cells and matrix remodelling in three-dimensional collagen scaffolds.* Biomaterials, 2010. **31**(3): p. 467-80.
157. Zhang, Z.Y., et al., *Neo-vascularization and bone formation mediated by fetal mesenchymal stem cell tissue-engineered bone grafts in critical-size femoral defects.* Biomaterials, 2010. **31**(4): p. 608-20.
158. Yin, T. and L. Li, *The stem cell niches in bone.* J Clin Invest, 2006. **116**(5): p. 1195-201.
159. Cottler-Fox, M.H., et al., *Stem cell mobilization.* Hematology Am Soc Hematol Educ Program, 2003: p. 419-37.
160. Sahin, A.O. and M. Buitenhuis, *Molecular mechanisms underlying adhesion and migration of hematopoietic stem cells.* Cell Adh Migr, 2012. **6**(1): p. 39-48.
161. Mazo, I.B., S. Massberg, and U.H. von Andrian, *Hematopoietic stem and progenitor cell trafficking.* Trends Immunol, 2011. **32**(10): p. 493-503.
162. Oliveira, M.C., J. Vullings, and F.A.J. van de Loo, *Osteoporosis and osteoarthritis are two sides of the same coin paid for obesity.* Nutrition, 2020. **70**: p. 110486.
163. Caplan, A.I., *Mesenchymal stem cells.* J Orthop Res, 1991. **9**(5): p. 641-50.
164. Schirrmacher, V., et al., *T-cell priming in bone marrow: the potential for long-lasting protective anti-tumor immunity.* Trends Mol Med, 2003. **9**(12): p. 526-34.
165. Minges Wols, H.A., et al., *The role of bone marrow-derived stromal cells in the maintenance of plasma cell longevity.* J Immunol, 2002. **169**(8): p. 4213-21.
166. Zeng, D., et al., *Heterogeneity of NK1.1+ T cells in the bone marrow: divergence from the thymus.* J Immunol, 1999. **163**(10): p. 5338-45.
167. Banchereau, J., et al., *Immunobiology of dendritic cells.* Annu Rev Immunol, 2000. **18**: p. 767-811.
168. Terstappen, L.W. and J. Levin, *Bone marrow cell differential counts obtained by multidimensional flow cytometry.* Blood Cells, 1992. **18**(2): p. 311-30; discussion 331-2.
169. Boivin, G., et al., *Durable and controlled depletion of neutrophils in mice.* Nat Commun, 2020. **11**(1): p. 2762.
170. Rankin, S.M., *The bone marrow: a site of neutrophil clearance.* J Leukoc Biol, 2010. **88**(2): p. 241-51.
171. Itkin, T., et al., *Distinct bone marrow blood vessels differentially regulate haematopoiesis.* Nature, 2016. **532**(7599): p. 323-8.
172. Kopp, H.G., et al., *The bone marrow vascular niche: home of HSC differentiation and mobilization.* Physiology (Bethesda), 2005. **20**: p. 349-56.
173. Adler, B.J., K. Kaushansky, and C.T. Rubin, *Obesity-driven disruption of haematopoiesis and the bone marrow niche.* Nat Rev Endocrinol, 2014. **10**(12): p. 737-48.
174. Birbrair, A. and P.S. Frenette, *Niche heterogeneity in the bone marrow.* Ann N Y Acad Sci, 2016. **1370**(1): p. 82-96.
175. Rharass, T. and S. Lucas, *MECHANISMS IN ENDOCRINOLOGY: Bone marrow adiposity and bone, a bad romance?* Eur J Endocrinol, 2018. **179**(4): p. R165-R182.

176. Mendelson, A. and P.S. Frenette, *Hematopoietic stem cell niche maintenance during homeostasis and regeneration.* Nat Med, 2014. **20**(8): p. 833-46.
177. Horwitz, E.M., et al., *Clarification of the nomenclature for MSC: The International Society for Cellular Therapy position statement.* Cytotherapy, 2005. **7**(5): p. 393-5.
178. Taipaleenmaki, H., et al., *Wnt signalling mediates the cross-talk between bone marrow derived pre-adipocytic and pre-osteoblastic cell populations.* Exp Cell Res, 2011. **317**(6): p. 745-56.
179. Ali, D., et al., *The pathophysiology of osteoporosis in obesity and type 2 diabetes in aging women and men: The mechanisms and roles of increased bone marrow adiposity.* Front Endocrinol (Lausanne), 2022. **13**: p. 981487.
180. Tencerova, M., et al., *Obesity-Associated Hypermetabolism and Accelerated Senescence of Bone Marrow Stromal Stem Cells Suggest a Potential Mechanism for Bone Fragility.* Cell Rep, 2019. **27**(7): p. 2050-2062 e6.
181. Tencerova, M., et al., *High-Fat Diet-Induced Obesity Promotes Expansion of Bone Marrow Adipose Tissue and Impairs Skeletal Stem Cell Functions in Mice.* J Bone Miner Res, 2018. **33**(6): p. 1154-1165.
182. Beekman, K.M., et al., *Osteoporosis and Bone Marrow Adipose Tissue.* Curr Osteoporos Rep, 2023. **21**(1): p. 45-55.
183. Abdallah, B.M., et al., *Skeletal (stromal) stem cells: an update on intracellular signaling pathways controlling osteoblast differentiation.* Bone, 2015. **70**: p. 28-36.
184. Marie, P.J. and M. Kassem, *Extrinsic mechanisms involved in age-related defective bone formation.* J Clin Endocrinol Metab, 2011. **96**(3): p. 600-9.
185. Hata, K., et al., *A CCAAT/enhancer binding protein beta isoform, liver-enriched inhibitory protein, regulates commitment of osteoblasts and adipocytes.* Mol Cell Biol, 2005. **25**(5): p. 1971-9.
186. Tominaga, H., et al., *CCAAT/enhancer-binding protein beta promotes osteoblast differentiation by enhancing Runx2 activity with ATF4.* Mol Biol Cell, 2008. **19**(12): p. 5373-86.
187. MacDougald, O.A. and M.D. Lane, *Transcriptional regulation of gene expression during adipocyte differentiation.* Annu Rev Biochem, 1995. **64**: p. 345-73.
188. Lane, M.D., *Adipogenesis.* Encyclopedia of Biological Chemistry, 2013: p. 52-56.
189. Mueller, E., et al., *Genetic analysis of adipogenesis through peroxisome proliferator-activated receptor gamma isoforms.* J Biol Chem, 2002. **277**(44): p. 41925-30.
190. Akune, T., et al., *PPARgamma insufficiency enhances osteogenesis through osteoblast formation from bone marrow progenitors.* J Clin Invest, 2004. **113**(6): p. 846-55.
191. Tamori, Y., et al., *Role of peroxisome proliferator-activated receptor-gamma in maintenance of the characteristics of mature 3T3-L1 adipocytes.* Diabetes, 2002. **51**(7): p. 2045-55.
192. Sun, H., et al., *Osteoblast-targeted suppression of PPARgamma increases osteogenesis through activation of mTOR signaling.* Stem Cells, 2013. **31**(10): p. 2183-92.
193. Lian, J.B. and G.S. Stein, *Development of the osteoblast phenotype: molecular mechanisms mediating osteoblast growth and differentiation.* Iowa Orthop J, 1995. **15**: p. 118-40.
194. Ducy, P., et al., *Osf2/Cbfa1: a transcriptional activator of osteoblast differentiation.* Cell, 1997. **89**(5): p. 747-54.
195. Komori, T., et al., *Targeted disruption of Cbfa1 results in a complete lack of bone formation owing to maturational arrest of osteoblasts.* Cell, 1997. **89**(5): p. 755-64.
196. Chen, G., C. Deng, and Y.P. Li, *TGF-beta and BMP signaling in osteoblast differentiation and bone formation.* Int J Biol Sci, 2012. **8**(2): p. 272-88.

197. Nakashima, K. and B. de Crombrugghe, *Transcriptional mechanisms in osteoblast differentiation and bone formation.* Trends Genet, 2003. **19**(8): p. 458-66.
198. Nakashima, K., et al., *The novel zinc finger-containing transcription factor osterix is required for osteoblast differentiation and bone formation.* Cell, 2002. **108**(1): p. 17-29.
199. Fedde, K.N., et al., *Alkaline phosphatase knock-out mice recapitulate the metabolic and skeletal defects of infantile hypophosphatasia.* J Bone Miner Res, 1999. **14**(12): p. 2015-26.
200. Ross, F.P., et al., *Interactions between the bone matrix proteins osteopontin and bone sialoprotein and the osteoclast integrin alpha v beta 3 potentiate bone resorption.* J Biol Chem, 1993. **268**(13): p. 9901-7.
201. McKee, M.D., C.E. Pedraza, and M.T. Kaartinen, *Osteopontin and wound healing in bone.* Cells Tissues Organs, 2011. **194**(2-4): p. 313-9.
202. Cho, H.H., et al., *Induction of osteogenic differentiation of human mesenchymal stem cells by histone deacetylase inhibitors.* J Cell Biochem, 2005. **96**(3): p. 533-42.
203. Schroeder, T.M. and J.J. Westendorf, *Histone deacetylase inhibitors promote osteoblast maturation.* J Bone Miner Res, 2005. **20**(12): p. 2254-63.
204. Addison, W.N., et al., *Direct transcriptional repression of Zfp423 by Zfp521 mediates a bone morphogenic protein-dependent osteoblast versus adipocyte lineage commitment switch.* Mol Cell Biol, 2014. **34**(16): p. 3076-85.
205. Rauch, A., et al., *Osteogenesis depends on commissioning of a network of stem cell transcription factors that act as repressors of adipogenesis.* Nat Genet, 2019. **51**(4): p. 716-727.
206. Meyer, M.B., et al., *Epigenetic Plasticity Drives Adipogenic and Osteogenic Differentiation of Marrow-derived Mesenchymal Stem Cells.* J Biol Chem, 2016. **291**(34): p. 17829-47.
207. Tencerova, M., et al., *Metabolic programming determines the lineage-differentiation fate of murine bone marrow stromal progenitor cells.* Bone Res, 2019. **7**: p. 35.
208. Li, Z., et al., *Development, regulation, metabolism and function of bone marrow adipose tissues.* Bone, 2018. **110**: p. 134-140.
209. Morganti, C., N. Cabezas-Wallscheid, and K. Ito, *Metabolic Regulation of Hematopoietic Stem Cells.* Hemasphere, 2022. **6**(7): p. e740.
210. Wellen, K.E. and C.B. Thompson, *A two-way street: reciprocal regulation of metabolism and signalling.* Nat Rev Mol Cell Biol, 2012. **13**(4): p. 270-6.
211. Hansson, J., et al., *Highly coordinated proteome dynamics during reprogramming of somatic cells to pluripotency.* Cell Rep, 2012. **2**(6): p. 1579-92.
212. Klimmeck, D., et al., *Proteomic cornerstones of hematopoietic stem cell differentiation: distinct signatures of multipotent progenitors and myeloid committed cells.* Mol Cell Proteomics, 2012. **11**(8): p. 286-302.
213. Salazar-Noratto, G.E., et al., *Understanding and leveraging cell metabolism to enhance mesenchymal stem cell transplantation survival in tissue engineering and regenerative medicine applications.* Stem Cells, 2020. **38**(1): p. 22-33.
214. Lunt, S.Y. and M.G. Vander Heiden, *Aerobic glycolysis: meeting the metabolic requirements of cell proliferation.* Annu Rev Cell Dev Biol, 2011. **27**: p. 441-64.
215. Spencer, J.A., et al., *Direct measurement of local oxygen concentration in the bone marrow of live animals.* Nature, 2014. **508**(7495): p. 269-73.
216. Shum, L.C., et al., *Energy Metabolism in Mesenchymal Stem Cells During Osteogenic Differentiation.* Stem Cells Dev, 2016. **25**(2): p. 114-22.
217. Stegen, S., et al., *Adequate hypoxia inducible factor 1alpha signaling is indispensable for bone regeneration.* Bone, 2016. **87**: p. 176-86.

218. Ambrosi, T.H., M.T. Longaker, and C.K.F. Chan, *A Revised Perspective of Skeletal Stem Cell Biology.* Front Cell Dev Biol, 2019. **7**: p. 189.
219. Matsushita, Y., W. Ono, and N. Ono, *Skeletal Stem Cells for Bone Development and Repair: Diversity Matters.* Curr Osteoporos Rep, 2020. **18**(3): p. 189-198.
220. Martinez-Reyes, I. and N.S. Chandel, *Mitochondrial TCA cycle metabolites control physiology and disease.* Nat Commun, 2020. **11**(1): p. 102.
221. Fillmore, N., et al., *Effect of fatty acids on human bone marrow mesenchymal stem cell energy metabolism and survival.* PLoS One, 2015. **10**(3): p. e0120257.
222. van Gastel, N., et al., *Lipid availability determines fate of skeletal progenitor cells via SOX9.* Nature, 2020. **579**(7797): p. 111-117.
223. Kurmi, K. and M.C. Haigis, *Nitrogen Metabolism in Cancer and Immunity.* Trends Cell Biol, 2020. **30**(5): p. 408-424.
224. Yu, Y., et al., *Glutamine Metabolism Regulates Proliferation and Lineage Allocation in Skeletal Stem Cells.* Cell Metab, 2019. **29**(4): p. 966-978 e4.
225. Stegen, S., et al., *Glutamine Metabolism Controls Chondrocyte Identity and Function.* Dev Cell, 2020. **53**(5): p. 530-544 e8.
226. van Gastel, N. and G. Carmeliet, *Metabolic regulation of skeletal cell fate and function in physiology and disease.* Nat Metab, 2021. **3**(1): p. 11-20.
227. Lee, S.Y. and F. Long, *Notch signaling suppresses glucose metabolism in mesenchymal progenitors to restrict osteoblast differentiation.* J Clin Invest, 2018. **128**(12): p. 5573-5586.
228. Jin, Z., et al., *Nitric oxide modulates bone anabolism through regulation of osteoblast glycolysis and differentiation.* J Clin Invest, 2021. **131**(5).
229. Li, Q., et al., *The role of mitochondria in osteogenic, adipogenic and chondrogenic differentiation of mesenchymal stem cells.* Protein Cell, 2017. **8**(6): p. 439-445.
230. Shares, B.H., et al., *Active mitochondria support osteogenic differentiation by stimulating beta-catenin acetylation.* J Biol Chem, 2018. **293**(41): p. 16019-16027.
231. Pattappa, G., et al., *The metabolism of human mesenchymal stem cells during proliferation and differentiation.* J Cell Physiol, 2011. **226**(10): p. 2562-70.
232. Esen, E., et al., *WNT-LRP5 signaling induces Warburg effect through mTORC2 activation during osteoblast differentiation.* Cell Metab, 2013. **17**(5): p. 745-55.
233. Hofmann, A.D., et al., *OXPHOS supercomplexes as a hallmark of the mitochondrial phenotype of adipogenic differentiated human MSCs.* PLoS One, 2012. **7**(4): p. e35160.
234. Wellen, K.E., et al., *ATP-citrate lyase links cellular metabolism to histone acetylation.* Science, 2009. **324**(5930): p. 1076-80.
235. Guntur, A.R., et al., *Osteoblast-like MC3T3-E1 Cells Prefer Glycolysis for ATP Production but Adipocyte-like 3T3-L1 Cells Prefer Oxidative Phosphorylation.* J Bone Miner Res, 2018. **33**(6): p. 1052-1065.
236. Li, J., et al., *The Role of Bone Marrow Microenvironment in Governing the Balance between Osteoblastogenesis and Adipogenesis.* Aging Dis, 2016. **7**(4): p. 514-25.
237. Schaepe, K., et al., *ToF-SIMS study of differentiation of human bone-derived stromal cells: new insights into osteoporosis.* Anal Bioanal Chem, 2017. **409**(18): p. 4425-4435.
238. Glenske, K., et al., *Effect of long term palmitate treatment on osteogenic differentiation of human mesenchymal stromal cells - Impact of albumin.* Bone Rep, 2020. **13**: p. 100707.
239. Palomer, X., et al., *Palmitic and Oleic Acid: The Yin and Yang of Fatty Acids in Type 2 Diabetes Mellitus.* Trends Endocrinol Metab, 2018. **29**(3): p. 178-190.
240. Casado-Diaz, A., G. Dorado, and J.M. Quesada-Gomez, *Influence of olive oil and its components on mesenchymal stem cell biology.* World J Stem Cells, 2019. **11**(12): p. 1045-1064.

241. Gao, B., et al., *GPR120: A bi-potential mediator to modulate the osteogenic and adipogenic differentiation of BMMSCs.* Sci Rep, 2015. **5**: p. 14080.
242. Cruzat, V., et al., *Glutamine: Metabolism and Immune Function, Supplementation and Clinical Translation.* Nutrients, 2018. **10**(11).
243. Zhou, T., et al., *Glutamine Metabolism Is Essential for Stemness of Bone Marrow Mesenchymal Stem Cells and Bone Homeostasis.* Stem Cells Int, 2019. **2019**: p. 8928934.
244. Wang, Y., et al., *Alpha-ketoglutarate ameliorates age-related osteoporosis via regulating histone methylations.* Nat Commun, 2020. **11**(1): p. 5596.
245. Hill, J.O., H.R. Wyatt, and J.C. Peters, *Energy balance and obesity.* Circulation, 2012. **126**(1): p. 126-32.
246. Khanna, D., et al., *Body Mass Index (BMI): A Screening Tool Analysis.* Cureus, 2022. **14**(2): p. e22119.
247. Pi-Sunyer, X., *The medical risks of obesity.* Postgrad Med, 2009. **121**(6): p. 21-33.
248. American Diabetes, A., *2. Classification and Diagnosis of Diabetes: Standards of Medical Care in Diabetes-2018.* Diabetes Care, 2018. **41**(Suppl 1): p. S13-S27.
249. Hussain, A., et al., *Prevention of type 2 diabetes: a review.* Diabetes Res Clin Pract, 2007. **76**(3): p. 317-26.
250. Quesada, I., et al., *Physiology of the pancreatic alpha-cell and glucagon secretion: role in glucose homeostasis and diabetes.* J Endocrinol, 2008. **199**(1): p. 5-19.
251. Bluher, M., *Adipose tissue dysfunction in obesity.* Exp Clin Endocrinol Diabetes, 2009. **117**(6): p. 241-50.
252. Snel, M., et al., *Ectopic fat and insulin resistance: pathophysiology and effect of diet and lifestyle interventions.* Int J Endocrinol, 2012. **2012**: p. 983814.
253. Shapses, S.A., L.C. Pop, and Y. Wang, *Obesity is a concern for bone health with aging.* Nutr Res, 2017. **39**: p. 1-13.
254. Cao, J.J., *Effects of obesity on bone metabolism.* J Orthop Surg Res, 2011. **6**: p. 30.
255. Smitka, K. and D. Maresova, *Adipose Tissue as an Endocrine Organ: An Update on Pro-inflammatory and Anti-inflammatory Microenvironment.* Prague Med Rep, 2015. **116**(2): p. 87-111.
256. Shinohara, H., et al., *Double Stranded RNA-Dependent Protein Kinase is Necessary for TNF-alpha-Induced Osteoclast Formation In Vitro and In Vivo.* J Cell Biochem, 2015. **116**(9): p. 1957-67.
257. Luo, G., et al., *TNF-alpha and RANKL promote osteoclastogenesis by upregulating RANK via the NF-kappaB pathway.* Mol Med Rep, 2018. **17**(5): p. 6605-6611.
258. Shu, L., et al., *High-fat diet causes bone loss in young mice by promoting osteoclastogenesis through alteration of the bone marrow environment.* Calcif Tissue Int, 2015. **96**(4): p. 313-23.
259. Noguchi, T., et al., *TNF-alpha stimulates the expression of RANK during orthodontic tooth movement.* Arch Oral Biol, 2020. **117**: p. 104796.
260. Zhang, K., et al., *Preservation of high-fat diet-induced femoral trabecular bone loss through genetic target of TNF-alpha.* Endocrine, 2015. **50**(1): p. 239-49.
261. Marahleh, A., et al., *TNF-alpha Directly Enhances Osteocyte RANKL Expression and Promotes Osteoclast Formation.* Front Immunol, 2019. **10**: p. 2925.
262. Ye, X., et al., *Inhibition of Runx2 signaling by TNF-alpha in ST2 murine bone marrow stromal cells undergoing osteogenic differentiation.* In Vitro Cell Dev Biol Anim, 2016. **52**(10): p. 1026-1033.
263. Wang, N., et al., *TNF-alpha-induced NF-kappaB activation upregulates microRNA-150-3p and inhibits osteogenesis of mesenchymal stem cells by targeting beta-catenin.* Open Biol, 2016. **6**(3).

264. Constanze, B., et al., *Evidence that TNF-beta suppresses osteoblast differentiation of mesenchymal stem cells and resveratrol reverses it through modulation of NF-kappaB, Sirt1 and Runx2.* Cell Tissue Res, 2020. **381**(1): p. 83-98.
265. Galozzi, P., et al., *The revisited role of interleukin-1 alpha and beta in autoimmune and inflammatory disorders and in comorbidities.* Autoimmun Rev, 2021. **20**(4): p. 102785.
266. Lee, J., et al., *Stimulation of osteoclast migration and bone resorption by C-C chemokine ligands 19 and 21.* Exp Mol Med, 2017. **49**(7): p. e358.
267. Cao, Y., et al., *IL-1beta differently stimulates proliferation and multinucleation of distinct mouse bone marrow osteoclast precursor subsets.* J Leukoc Biol, 2016. **100**(3): p. 513-23.
268. Son, H.S., et al., *Benzydamine inhibits osteoclast differentiation and bone resorption via down-regulation of interleukin-1 beta expression.* Acta Pharm Sin B, 2020. **10**(3): p. 462-474.
269. Wang, Y., et al., *IL1beta and TNFalpha promote RANKL-dependent adseverin expression and osteoclastogenesis.* J Cell Sci, 2018. **131**(11).
270. Lee, W.S., et al., *Atorvastatin inhibits osteoclast differentiation by suppressing NF-kappaB and MAPK signaling during IL-1beta-induced osteoclastogenesis.* Korean J Intern Med, 2018. **33**(2): p. 397-406.
271. Moon, S.J., et al., *Temporal differential effects of proinflammatory cytokines on osteoclastogenesis.* Int J Mol Med, 2013. **31**(4): p. 769-77.
272. Ozeki, N., et al., *IL-1beta-induced matrix metalloproteinase-13 is activated by a disintegrin and metalloprotease-28-regulated proliferation of human osteoblast-like cells.* Exp Cell Res, 2014. **323**(1): p. 165-177.
273. Yang, H., et al., *Luteolin downregulates IL-1beta-induced MMP-9 and -13 expressions in osteoblasts via inhibition of ERK signalling pathway.* J Enzyme Inhib Med Chem, 2012. **27**(2): p. 261-6.
274. McKnight, Q., et al., *IL-1beta Drives Production of FGF-23 at the Onset of Chronic Kidney Disease in Mice.* J Bone Miner Res, 2020. **35**(7): p. 1352-1362.
275. Yamazaki, M., et al., *Interleukin-1-induced acute bone resorption facilitates the secretion of fibroblast growth factor 23 into the circulation.* J Bone Miner Metab, 2015. **33**(3): p. 342-54.
276. Rupp, T., et al., *High FGF23 levels are associated with impaired trabecular bone microarchitecture in patients with osteoporosis.* Osteoporos Int, 2019. **30**(8): p. 1655-1662.
277. He, B., et al., *Blockade of IL-6 alleviates bone loss induced by modeled microgravity in mice.* Can J Physiol Pharmacol, 2020. **98**(10): p. 678-683.
278. Bakker, A.D., et al., *IL-6 alters osteocyte signaling toward osteoblasts but not osteoclasts.* J Dent Res, 2014. **93**(4): p. 394-9.
279. Wang, C., et al., *Interleukin-6 gene knockout antagonizes high-fat-induced trabecular bone loss.* J Mol Endocrinol, 2016. **57**(3): p. 161-70.
280. Nagareddy, P.R., et al., *Hyperglycemia promotes myelopoiesis and impairs the resolution of atherosclerosis.* Cell Metab, 2013. **17**(5): p. 695-708.
281. Chan, M.E., et al., *Bone structure and B-cell populations, crippled by obesity, are partially rescued by brief daily exposure to low-magnitude mechanical signals.* FASEB J, 2012. **26**(12): p. 4855-63.
282. Brotfain, E., et al., *Neutrophil functions in morbidly obese subjects.* Clin Exp Immunol, 2015. **181**(1): p. 156-63.
283. Kraakman, M.J., et al., *Neutrophil-derived S100 calcium-binding proteins A8/A9 promote reticulated thrombocytosis and atherogenesis in diabetes.* J Clin Invest, 2017. **127**(6): p. 2133-2147.

284. Calixto, M.C., et al., *Obesity enhances eosinophilic inflammation in a murine model of allergic asthma.* Br J Pharmacol, 2010. **159**(3): p. 617-25.
285. Liu, A., et al., *Bone marrow lympho-myeloid malfunction in obesity requires precursor cell-autonomous TLR4.* Nat Commun, 2018. **9**(1): p. 708.
286. Trottier, M.D., et al., *Enhancement of hematopoiesis and lymphopoiesis in diet-induced obese mice.* Proc Natl Acad Sci U S A, 2012. **109**(20): p. 7622-9.
287. Naranjo, M.C., et al., *Acute effects of dietary fatty acids on osteclastogenesis via RANKL/RANK/OPG system.* Mol Nutr Food Res, 2016. **60**(11): p. 2505-2513.
288. Collins, A.T., et al., *Obesity alters the in vivo mechanical response and biochemical properties of cartilage as measured by MRI.* Arthritis Res Ther, 2018. **20**(1): p. 232.
289. JE, L.L., et al., *Induction and rescue of skeletal fragility in a high-fat diet mouse model of type 2 diabetes: An in vivo and in vitro approach.* Bone, 2022. **156**: p. 116302.
290. Patsch, J.M., et al., *Bone marrow fat composition as a novel imaging biomarker in postmenopausal women with prevalent fragility fractures.* J Bone Miner Res, 2013. **28**(8): p. 1721-8.
291. Gonnelli, S., C. Caffarelli, and R. Nuti, *Obesity and fracture risk.* Clin Cases Miner Bone Metab, 2014. **11**(1): p. 9-14.
292. Tchkonia, T., et al., *Fat tissue, aging, and cellular senescence.* Aging Cell, 2010. **9**(5): p. 667-84.
293. Ionova-Martin, S.S., et al., *Reduced size-independent mechanical properties of cortical bone in high-fat diet-induced obesity.* Bone, 2010. **46**(1): p. 217-25.
294. Patsch, J.M., et al., *Increased bone resorption and impaired bone microarchitecture in short-term and extended high-fat diet-induced obesity.* Metabolism, 2011. **60**(2): p. 243-9.
295. Lu, X.M., H. Zhao, and E.H. Wang, *A high-fat diet induces obesity and impairs bone acquisition in young male mice.* Mol Med Rep, 2013. **7**(4): p. 1203-8.
296. Fehrendt, H., et al., *Negative influence of a long-term high-fat diet on murine bone architecture.* Int J Endocrinol, 2014. **2014**: p. 318924.
297. Fujita, Y., K. Watanabe, and K. Maki, *Serum leptin levels negatively correlate with trabecular bone mineral density in high-fat diet-induced obesity mice.* J Musculoskelet Neuronal Interact, 2012. **12**(2): p. 84-94.
298. Scheller, E.L., et al., *Changes in Skeletal Integrity and Marrow Adiposity during High-Fat Diet and after Weight Loss.* Front Endocrinol (Lausanne), 2016. **7**: p. 102.
299. Gustafson, B. and U. Smith, *Regulation of white adipogenesis and its relation to ectopic fat accumulation and cardiovascular risk.* Atherosclerosis, 2015. **241**(1): p. 27-35.
300. Longo, M., et al., *Adipose Tissue Dysfunction as Determinant of Obesity-Associated Metabolic Complications.* Int J Mol Sci, 2019. **20**(9).
301. de Mello, A.H., et al., *Mitochondrial dysfunction in obesity.* Life Sci, 2018. **192**: p. 26-32.
302. Lavallard, V.J., et al., *Autophagy, signaling and obesity.* Pharmacol Res, 2012. **66**(6): p. 513-25.
303. Kawasaki, N., et al., *Obesity-induced endoplasmic reticulum stress causes chronic inflammation in adipose tissue.* Sci Rep, 2012. **2**: p. 799.
304. Ahmed, B., R. Sultana, and M.W. Greene, *Adipose tissue and insulin resistance in obese.* Biomed Pharmacother, 2021. **137**: p. 111315.
305. Boroumand, P. and A. Klip, *Bone marrow adipose cells - cellular interactions and changes with obesity.* J Cell Sci, 2020. **133**(5).
306. Yu, E.W., et al., *Marrow adipose tissue composition in adults with morbid obesity.* Bone, 2017. **97**: p. 38-42.
307. Bray, G.A., et al., *Management of obesity.* Lancet, 2016. **387**(10031): p. 1947-56.

308. Imam, K., *Management and treatment of diabetes mellitus.* Adv Exp Med Biol, 2012. **771**: p. 356-80.
309. Leitner, D.R., et al., *Obesity and Type 2 Diabetes: Two Diseases with a Need for Combined Treatment Strategies - EASO Can Lead the Way.* Obes Facts, 2017. **10**(5): p. 483-492.
310. Raveendran, A.V., E.C. Chacko, and J.M. Pappachan, *Non-pharmacological Treatment Options in the Management of Diabetes Mellitus.* Eur Endocrinol, 2018. **14**(2): p. 31-39.
311. Lingvay, I., et al., *Obesity management as a primary treatment goal for type 2 diabetes: time to reframe the conversation.* Lancet, 2022. **399**(10322): p. 394-405.
312. Shi, Z., et al., *Exercise Promotes Bone Marrow Microenvironment by Inhibiting Adipsin in Diet-Induced Male Obese Mice.* Nutrients, 2022. **15**(1).
313. Liu, W.X., et al., *Voluntary exercise prevents colonic inflammation in high-fat diet-induced obese mice by up-regulating PPAR-gamma activity.* Biochem Biophys Res Commun, 2015. **459**(3): p. 475-80.
314. Zheng, Y., et al., *Dietary intervention reprograms bone marrow cellular signaling in obese mice.* Front Endocrinol (Lausanne), 2023. **14**: p. 1171781.
315. Brown, J.D., S.P. Naples, and F.W. Booth, *Effects of voluntary running on oxygen consumption, RQ, and energy expenditure during primary prevention of diet-induced obesity in C57BL/6N mice.* J Appl Physiol (1985), 2012. **113**(3): p. 473-8.
316. Zhang, X., et al., *Effect of lifestyle interventions on cardiovascular risk factors among adults without impaired glucose tolerance or diabetes: A systematic review and meta-analysis.* PLoS One, 2017. **12**(5): p. e0176436.
317. McCabe, L.R., et al., *Exercise prevents high fat diet-induced bone loss, marrow adiposity and dysbiosis in male mice.* Bone, 2019. **118**: p. 20-31.
318. Picke, A.K., et al., *Differential effects of high-fat diet and exercise training on bone and energy metabolism.* Bone, 2018. **116**: p. 120-134.
319. Beaver, L.M., et al., *Diet composition influences the effect of high fat diets on bone in growing male mice.* Bone, 2023. **176**: p. 116888.
320. Lv, Z., W. Shi, and Q. Zhang, *Role of Essential Amino Acids in Age-Induced Bone Loss.* Int J Mol Sci, 2022. **23**(19).
321. Blais, A., et al., *Monosodium Glutamate Supplementation Improves Bone Status in Mice Under Moderate Protein Restriction.* JBMR Plus, 2019. **3**(10): p. e10224.
322. Kuda, O., M. Rossmeisl, and J. Kopecky, *Omega-3 fatty acids and adipose tissue biology.* Mol Aspects Med, 2018. **64**: p. 147-160.
323. Sistilli, G., et al., *Krill Oil Supplementation Reduces Exacerbated Hepatic Steatosis Induced by Thermoneutral Housing in Mice with Diet-Induced Obesity.* Nutrients, 2021. **13**(2).
324. Flachs, P., et al., *Polyunsaturated fatty acids of marine origin induce adiponectin in mice fed a high-fat diet.* Diabetologia, 2006. **49**(2): p. 394-7.
325. Calder, P.C., *Marine omega-3 fatty acids and inflammatory processes: Effects, mechanisms and clinical relevance.* Biochim Biophys Acta, 2015. **1851**(4): p. 469-84.
326. van Schothorst, E.M., et al., *Induction of lipid oxidation by polyunsaturated fatty acids of marine origin in small intestine of mice fed a high-fat diet.* BMC Genomics, 2009. **10**: p. 110.
327. Ruzickova, J., et al., *Omega-3 PUFA of marine origin limit diet-induced obesity in mice by reducing cellularity of adipose tissue.* Lipids, 2004. **39**(12): p. 1177-85.
328. Adamcova, K., et al., *Reduced Number of Adipose Lineage and Endothelial Cells in Epididymal fat in Response to Omega-3 PUFA in Mice Fed High-Fat Diet.* Mar Drugs, 2018. **16**(12).

329. Kunesova, M., et al., *The influence of n-3 polyunsaturated fatty acids and very low calorie diet during a short-term weight reducing regimen on weight loss and serum fatty acid composition in severely obese women.* Physiol Res, 2006. **55**(1): p. 63-72.
330. Mori, T.A., et al., *Dietary fish as a major component of a weight-loss diet: effect on serum lipids, glucose, and insulin metabolism in overweight hypertensive subjects.* Am J Clin Nutr, 1999. **70**(5): p. 817-25.
331. Martyniak, K., et al., *Do polyunsaturated fatty acids protect against bone loss in our aging and osteoporotic population?* Bone, 2021. **143**: p. 115736.
332. Cugno, C., et al., *Omega-3 fatty acid-rich fish oil supplementation prevents rosiglitazone-induced osteopenia in aging C57BL/6 mice and in vitro studies.* Sci Rep, 2021. **11**(1): p. 10364.
333. Sun, D., et al., *Dietary n-3 fatty acids decrease osteoclastogenesis and loss of bone mass in ovariectomized mice.* J Bone Miner Res, 2003. **18**(7): p. 1206-16.
334. Andreo-Lopez, M.C., et al., *The Influence of the Mediterranean Dietary Pattern on Osteoporosis and Sarcopenia.* Nutrients, 2023. **15**(14).
335. Van Gaal, L. and A. Scheen, *Weight management in type 2 diabetes: current and emerging approaches to treatment.* Diabetes Care, 2015. **38**(6): p. 1161-72.
336. Schwartz, A.V., et al., *Effect of 1 year of an intentional weight loss intervention on bone mineral density in type 2 diabetes: results from the Look AHEAD randomized trial.* J Bone Miner Res, 2012. **27**(3): p. 619-27.
337. Svendsen, O.L., C. Hassager, and C. Christiansen, *Effect of an energy-restrictive diet, with or without exercise, on lean tissue mass, resting metabolic rate, cardiovascular risk factors, and bone in overweight postmenopausal women.* Am J Med, 1993. **95**(2): p. 131-40.
338. Devlin, M.J., et al., *Caloric restriction leads to high marrow adiposity and low bone mass in growing mice.* J Bone Miner Res, 2010. **25**(9): p. 2078-88.
339. Maridas, D.E., et al., *Progenitor recruitment and adipogenic lipolysis contribute to the anabolic actions of parathyroid hormone on the skeleton.* FASEB J, 2019. **33**(2): p. 2885-2898.
340. Abildgaard, J., et al., *Effects of a Lifestyle Intervention on Bone Turnover in Persons with Type 2 Diabetes: A Post Hoc Analysis of the U-TURN Trial.* Med Sci Sports Exerc, 2022. **54**(1): p. 38-46.
341. Fu, W. and J. Fan, *Intervention effect of exercise rehabilitation therapy on patients with type 2 diabetic osteoporosis.* Am J Transl Res, 2021. **13**(4): p. 3400-3408.
342. Jenkins, D.J., et al., *Glycemic index of foods: a physiological basis for carbohydrate exchange.* Am J Clin Nutr, 1981. **34**(3): p. 362-6.
343. Greenwood, D.C., et al., *Glycemic index, glycemic load, carbohydrates, and type 2 diabetes: systematic review and dose-response meta-analysis of prospective studies.* Diabetes Care, 2013. **36**(12): p. 4166-71.
344. Keys, A., et al., *The diet and 15-year death rate in the seven countries study.* Am J Epidemiol, 1986. **124**(6): p. 903-15.
345. Panagiotakos, D.B., et al., *The epidemiology of Type 2 diabetes mellitus in Greek adults: the ATTICA study.* Diabet Med, 2005. **22**(11): p. 1581-8.
346. Ortega, E., et al., *Mediterranean diet adherence in individuals with prediabetes and unknown diabetes: the Di@bet.es Study.* Ann Nutr Metab, 2013. **62**(4): p. 339-46.
347. Bailey, C.J. and R.C. Turner, *Metformin.* N Engl J Med, 1996. **334**(9): p. 574-9.
348. Al-Saleh, Y., et al., *Sulfonylureas in the Current Practice of Type 2 Diabetes Management: Are They All the Same? Consensus from the Gulf Cooperation Council (GCC) Countries Advisory Board on Sulfonylureas.* Diabetes Ther, 2021. **12**(8): p. 2115-2132.

349. Yau, H., et al., *The future of thiazolidinedione therapy in the management of type 2 diabetes mellitus.* Curr Diab Rep, 2013. **13**(3): p. 329-41.
350. Herzig, S., et al., *Identification and functional expression of the mitochondrial pyruvate carrier.* Science, 2012. **337**(6090): p. 93-6.
351. Bricker, D.K., et al., *A mitochondrial pyruvate carrier required for pyruvate uptake in yeast, Drosophila, and humans.* Science, 2012. **337**(6090): p. 96-100.
352. Lecka-Czernik, B. and C.J. Rosen, *Energy Excess, Glucose Utilization, and Skeletal Remodeling: New Insights.* J Bone Miner Res, 2015. **30**(8): p. 1356-61.
353. Yki-Jarvinen, H., *Thiazolidinediones.* N Engl J Med, 2004. **351**(11): p. 1106-18.
354. Choi, J.H., et al., *Anti-diabetic drugs inhibit obesity-linked phosphorylation of PPARgamma by Cdk5.* Nature, 2010. **466**(7305): p. 451-6.
355. Brunmair, B., et al., *Thiazolidinediones, like metformin, inhibit respiratory complex I: a common mechanism contributing to their antidiabetic actions?* Diabetes, 2004. **53**(4): p. 1052-9.
356. Divakaruni, A.S., et al., *Thiazolidinediones are acute, specific inhibitors of the mitochondrial pyruvate carrier.* Proc Natl Acad Sci U S A, 2013. **110**(14): p. 5422-7.
357. Colca, J.R., et al., *Identification of a novel mitochondrial protein ("mitoNEET") cross-linked specifically by a thiazolidinedione photoprobe.* Am J Physiol Endocrinol Metab, 2004. **286**(2): p. E252-60.
358. Rabol, R., et al., *Opposite effects of pioglitazone and rosiglitazone on mitochondrial respiration in skeletal muscle of patients with type 2 diabetes.* Diabetes Obes Metab, 2010. **12**(9): p. 806-14.
359. Hickson, R.P., A.L. Cole, and S.B. Dusetzina, *Implications of Removing Rosiglitazone's Black Box Warning and Restricted Access Program on the Uptake of Thiazolidinediones and Dipeptidyl Peptidase-4 Inhibitors Among Patients with Type 2 Diabetes.* J Manag Care Spec Pharm, 2019. **25**(1): p. 72-79.
360. Yamanouchi, T., *Concomitant therapy with pioglitazone and insulin for the treatment of type 2 diabetes.* Vasc Health Risk Manag, 2010. **6**: p. 189-97.
361. Vieira, R., et al., *Sugar-Lowering Drugs for Type 2 Diabetes Mellitus and Metabolic Syndrome-Review of Classical and New Compounds: Part-I.* Pharmaceuticals (Basel), 2019. **12**(4).
362. Choi, S.S., J. Park, and J.H. Choi, *Revisiting PPARgamma as a target for the treatment of metabolic disorders.* BMB Rep, 2014. **47**(11): p. 599-608.
363. Juurlink, D.N., et al., *Adverse cardiovascular events during treatment with pioglitazone and rosiglitazone: population based cohort study.* BMJ, 2009. **339**: p. b2942.
364. Festuccia, W.T., et al., *Peroxisome proliferator-activated receptor-gamma-mediated positive energy balance in the rat is associated with reduced sympathetic drive to adipose tissues and thyroid status.* Endocrinology, 2008. **149**(5): p. 2121-30.
365. Garretson, J.T., et al., *Peroxisome proliferator-activated receptor gamma controls ingestive behavior, agouti-related protein, and neuropeptide Y mRNA in the arcuate hypothalamus.* J Neurosci, 2015. **35**(11): p. 4571-81.
366. Rosen, E.D., et al., *PPAR gamma is required for the differentiation of adipose tissue in vivo and in vitro.* Mol Cell, 1999. **4**(4): p. 611-7.
367. Abbas, A., et al., *PPAR- gamma agonist in treatment of diabetes: cardiovascular safety considerations.* Cardiovasc Hematol Agents Med Chem, 2012. **10**(2): p. 124-34.
368. Ali, A.A., et al., *Rosiglitazone causes bone loss in mice by suppressing osteoblast differentiation and bone formation.* Endocrinology, 2005. **146**(3): p. 1226-35.
369. Zhu, Z.N., Y.F. Jiang, and T. Ding, *Risk of fracture with thiazolidinediones: an updated meta-analysis of randomized clinical trials.* Bone, 2014. **68**: p. 115-23.

370. Bilik, D., et al., *Thiazolidinediones and fractures: evidence from translating research into action for diabetes.* J Clin Endocrinol Metab, 2010. **95**(10): p. 4560-5.
371. Tan, K.C.B., et al., *Thiazolidinedione increases serum soluble receptor for advanced glycation end-products in type 2 diabetes.* Diabetologia, 2007. **50**(9): p. 1819-1825.
372. Yamamoto, M. and T. Sugimoto, *Advanced Glycation End Products, Diabetes, and Bone Strength.* Curr Osteoporos Rep, 2016. **14**(6): p. 320-326.
373. Alikhani, M., et al., *Advanced glycation end products stimulate osteoblast apoptosis via the MAP kinase and cytosolic apoptotic pathways.* Bone, 2007. **40**(2): p. 345-53.
374. Dormuth, C.R., et al., *Thiazolidinediones and fractures in men and women.* Arch Intern Med, 2009. **169**(15): p. 1395-402.
375. Meier, C., et al., *Use of thiazolidinediones and fracture risk.* Arch Intern Med, 2008. **168**(8): p. 820-5.
376. Giovannini, P., M.J. Howes, and S.E. Edwards, *Medicinal plants used in the traditional management of diabetes and its sequelae in Central America: A review.* J Ethnopharmacol, 2016. **184**: p. 58-71.
377. Palmer, S.C., et al., *Comparison of Clinical Outcomes and Adverse Events Associated With Glucose-Lowering Drugs in Patients With Type 2 Diabetes: A Meta-analysis.* JAMA, 2016. **316**(3): p. 313-24.
378. DeFronzo, R., et al., *Metformin-associated lactic acidosis: Current perspectives on causes and risk.* Metabolism, 2016. **65**(2): p. 20-9.
379. Aloke, C., et al., *Current Advances in the Management of Diabetes Mellitus.* Biomedicines, 2022. **10**(10).
380. Hedrington, M.S. and S.N. Davis, *Considerations when using alpha-glucosidase inhibitors in the treatment of type 2 diabetes.* Expert Opin Pharmacother, 2019. **20**(18): p. 2229-2235.
381. Hinnen, D., *Glucagon-Like Peptide 1 Receptor Agonists for Type 2 Diabetes.* Diabetes Spectr, 2017. **30**(3): p. 202-210.
382. Dutta, P., et al., *Tirzepatide: A Promising Drug for Type 2 Diabetes and Beyond.* Cureus, 2023. **15**(5): p. e38379.
383. Chao, A.M., et al., *Semaglutide for the treatment of obesity.* Trends Cardiovasc Med, 2023. **33**(3): p. 159-166.
384. Dhirani, D., A. Shahid, and H. Mumtaz, *A new kind of diabetes medication approved by the FDA: is there hope for obesity?* Int J Surg, 2023. **109**(2): p. 81-82.
385. Hansen, M.S., et al., *GIP reduces osteoclast activity and improves osteoblast survival in primary human bone cells.* Eur J Endocrinol, 2023. **188**(1).
386. Scheen, A.J., *Pharmacodynamics, efficacy and safety of sodium-glucose co-transporter type 2 (SGLT2) inhibitors for the treatment of type 2 diabetes mellitus.* Drugs, 2015. **75**(1): p. 33-59.
387. Santer, R., et al., *Molecular analysis of the SGLT2 gene in patients with renal glucosuria.* J Am Soc Nephrol, 2003. **14**(11): p. 2873-82.
388. Dong, B., et al., *The Extraglycemic Effect of SGLT-2is on Mineral and Bone Metabolism and Bone Fracture.* Front Endocrinol (Lausanne), 2022. **13**: p. 918350.
389. Al-Mashhadi, Z.K., et al., *SGLT2 inhibitor treatment is not associated with an increased risk of osteoporotic fractures when compared to GLP-1 receptor agonists: A nationwide cohort study.* Front Endocrinol (Lausanne), 2022. **13**: p. 861422.
390. Hamdi, A., et al., *Development of new thiazolidine-2,4-dione hybrids as aldose reductase inhibitors endowed with antihyperglycaemic activity: design, synthesis, biological investigations, and in silico insights.* J Enzyme Inhib Med Chem, 2023. **38**(1): p. 2231170.

391. Soccio, R.E., E.R. Chen, and M.A. Lazar, *Thiazolidinediones and the promise of insulin sensitization in type 2 diabetes.* Cell Metab, 2014. **20**(4): p. 573-91.
392. Colca, J.R., et al., *Clinical proof-of-concept study with MSDC-0160, a prototype mTOT-modulating insulin sensitizer.* Clin Pharmacol Ther, 2013. **93**(4): p. 352-9.
393. Bolten, C.W., et al., *Insulin sensitizing pharmacology of thiazolidinediones correlates with mitochondrial gene expression rather than activation of PPAR gamma.* Gene Regul Syst Bio, 2007. **1**: p. 73-82.
394. Mallet, D., et al., *Re-routing Metabolism by the Mitochondrial Pyruvate Carrier Inhibitor MSDC-0160 Attenuates Neurodegeneration in a Rat Model of Parkinson's Disease.* Mol Neurobiol, 2022. **59**(10): p. 6170-6182.
395. Quansah, E., et al., *Targeting energy metabolism via the mitochondrial pyruvate carrier as a novel approach to attenuate neurodegeneration.* Mol Neurodegener, 2018. **13**(1): p. 28.
396. Chen, Z., et al., *Insulin resistance and metabolic derangements in obese mice are ameliorated by a novel peroxisome proliferator-activated receptor gamma-sparing thiazolidinedione.* J Biol Chem, 2012. **287**(28): p. 23537-48.
397. Fukunaga, T., et al., *An insulin-sensitizing thiazolidinedione, which minimally activates PPARgamma, does not cause bone loss.* J Bone Miner Res, 2015. **30**(3): p. 481-8.
398. Bardova, K., et al., *Additive Effects of Omega-3 Fatty Acids and Thiazolidinediones in Mice Fed a High-Fat Diet: Triacylglycerol/Fatty Acid Cycling in Adipose Tissue.* Nutrients, 2020. **12**(12).
399. Lecka-Czernik, B., et al., *High bone mass in adult mice with diet-induced obesity results from a combination of initial increase in bone mass followed by attenuation in bone formation; implications for high bone mass and decreased bone quality in obesity.* Mol Cell Endocrinol, 2015. **410**: p. 35-41.
400. Benova, A., et al., *Novel thiazolidinedione analog reduces a negative impact on bone and mesenchymal stem cell properties in obese mice compared to classical thiazolidinediones.* Mol Metab, 2022. **65**: p. 101598.
401. Chen, L., et al., *Actin depolymerization enhances adipogenic differentiation in human stromal stem cells.* Stem Cell Res, 2018. **29**: p. 76-83.
402. Lopes, M., et al., *Metabolomics atlas of oral 13C-glucose tolerance test in mice.* Cell Rep, 2021. **37**(2): p. 109833.
403. Pop, L.M., et al., *Impact of pioglitazone on bone mineral density and bone marrow fat content.* Osteoporos Int, 2017. **28**(11): p. 3261-3269.
404. Anez-Bustillos, L., et al., *Effects of dietary omega-3 fatty acids on bones of healthy mice.* Clin Nutr, 2019. **38**(5): p. 2145-2154.
405. Kus, V., et al., *Unmasking differential effects of rosiglitazone and pioglitazone in the combination treatment with n-3 fatty acids in mice fed a high-fat diet.* PLoS One, 2011. **6**(11): p. e27126.
406. Kuda, O., et al., *n-3 fatty acids and rosiglitazone improve insulin sensitivity through additive stimulatory effects on muscle glycogen synthesis in mice fed a high-fat diet.* Diabetologia, 2009. **52**(5): p. 941-51.
407. Lazarenko, O.P., et al., *Rosiglitazone induces decreases in bone mass and strength that are reminiscent of aged bone.* Endocrinology, 2007. **148**(6): p. 2669-80.
408. Ackert-Bicknell, C.L., et al., *Strain-specific effects of rosiglitazone on bone mass, body composition, and serum insulin-like growth factor-I.* Endocrinology, 2009. **150**(3): p. 1330-40.
409. Liu, L., J. Aronson, and B. Lecka-Czernik, *Rosiglitazone disrupts endosteal bone formation during distraction osteogenesis by local adipocytic infiltration.* Bone, 2013. **52**(1): p. 247-58.

410. Kyle, K.A., et al., *Differential effects of PPAR-gamma activation versus chemical or genetic reduction of DPP-4 activity on bone quality in mice.* Endocrinology, 2011. **152**(2): p. 457-67.
411. Pavo, I., et al., *Effect of pioglitazone compared with metformin on glycemic control and indicators of insulin sensitivity in recently diagnosed patients with type 2 diabetes.* J Clin Endocrinol Metab, 2003. **88**(4): p. 1637-45.
412. Alam, F., et al., *Efficacy and Safety of Pioglitazone Monotherapy in Type 2 Diabetes Mellitus: A Systematic Review and Meta-Analysis of Randomised Controlled Trials.* Sci Rep, 2019. **9**(1): p. 5389.
413. Farahnak, Z., et al., *Dietary docosahexaenoic acid contributes to increased bone mineral accretion and strength in young female Sprague-Dawley rats.* Prostaglandins Leukot Essent Fatty Acids, 2019. **144**: p. 32-39.
414. Mollard, R.C., et al., *(n-3) fatty acids reduce the release of prostaglandin E2 from bone but do not affect bone mass in obese (fa/fa) and lean Zucker rats.* J Nutr, 2005. **135**(3): p. 499-504.
415. Shen, C.L., et al., *Protective effect of dietary long-chain n-3 polyunsaturated fatty acids on bone loss in gonad-intact middle-aged male rats.* Br J Nutr, 2006. **95**(3): p. 462-8.
416. Cao, J.J., et al., *Increasing Dietary Fish Oil Reduces Adiposity and Mitigates Bone Deterioration in Growing C57BL/6 Mice Fed a High-Fat Diet.* J Nutr, 2020. **150**(1): p. 99-107.
417. Bani Hassan, E., et al., *The effects of dietary fatty acids on bone, hematopoietic marrow and marrow adipose tissue in a murine model of senile osteoporosis.* Aging (Albany NY), 2019. **11**(18): p. 7938-7947.
418. Nakanishi, A. and I. Tsukamoto, *n-3 polyunsaturated fatty acids stimulate osteoclastogenesis through PPARgamma-mediated enhancement of c-Fos expression, and suppress osteoclastogenesis through PPARgamma-dependent inhibition of NFkB activation.* J Nutr Biochem, 2015. **26**(11): p. 1317-27.
419. Zwart, S.R., et al., *Capacity of omega-3 fatty acids or eicosapentaenoic acid to counteract weightlessness-induced bone loss by inhibiting NF-kappaB activation: from cells to bed rest to astronauts.* J Bone Miner Res, 2010. **25**(5): p. 1049-57.
420. Gani, O.A., *Are fish oil omega-3 long-chain fatty acids and their derivatives peroxisome proliferator-activated receptor agonists?* Cardiovasc Diabetol, 2008. **7**: p. 6.
421. Levental, K.R., et al., *omega-3 polyunsaturated fatty acids direct differentiation of the membrane phenotype in mesenchymal stem cells to potentiate osteogenesis.* Sci Adv, 2017. **3**(11): p. eaao1193.
422. Bhattacharya, A., et al., *Effect of fish oil on bone mineral density in aging C57BL/6 female mice.* J Nutr Biochem, 2007. **18**(6): p. 372-9.
423. Flachs, P., et al., *Polyunsaturated fatty acids of marine origin upregulate mitochondrial biogenesis and induce beta-oxidation in white fat.* Diabetologia, 2005. **48**(11): p. 2365-75.
424. Zhang, L., et al., *Molecular and cellular mechanisms of aging in hematopoietic stem cells and their niches.* J Hematol Oncol, 2020. **13**(1): p. 157.
425. Watkins, B.A., et al., *Dietary (n-3) and (n-6) polyunsaturates and acetylsalicylic acid alter ex vivo PGE2 biosynthesis, tissue IGF-I levels, and bone morphometry in chicks.* J Bone Miner Res, 1996. **11**(9): p. 1321-32.
426. Raisz, L.G., *Prostaglandins and bone: physiology and pathophysiology.* Osteoarthritis Cartilage, 1999. **7**(4): p. 419-21.
427. Kanda, J., et al., *Effect of the antidiabetic agent pioglitazone on bone metabolism in rats.* J Pharmacol Sci, 2017. **135**(1): p. 22-28.

428. Wu, S., et al., *Insulin resistance secondary to a high-fat diet stimulates longitudinal bone growth and growth plate chondrogenesis in mice.* Endocrinology, 2011. **152**(2): p. 468-75.
429. Vacanti, N.M., et al., *Regulation of substrate utilization by the mitochondrial pyruvate carrier.* Mol Cell, 2014. **56**(3): p. 425-435.
430. Yang, C., et al., *Glutamine oxidation maintains the TCA cycle and cell survival during impaired mitochondrial pyruvate transport.* Mol Cell, 2014. **56**(3): p. 414-424.
431. Veliova, M., et al., *Blocking mitochondrial pyruvate import in brown adipocytes induces energy wasting via lipid cycling.* EMBO Rep, 2020. **21**(12): p. e49634.
432. Stegen, S., et al., *Glutamine Metabolism in Osteoprogenitors Is Required for Bone Mass Accrual and PTH-Induced Bone Anabolism in Male Mice.* J Bone Miner Res, 2021. **36**(3): p. 604-616.
433. Karner, C.M., et al., *Increased glutamine catabolism mediates bone anabolism in response to WNT signaling.* J Clin Invest, 2015. **125**(2): p. 551-62.
434. Devignes, C.S., G. Carmeliet, and S. Stegen, *Amino acid metabolism in skeletal cells.* Bone Rep, 2022. **17**: p. 101620.
435. Krane, S.M., *The importance of proline residues in the structure, stability and susceptibility to proteolytic degradation of collagens.* Amino Acids, 2008. **35**(4): p. 703-10.

8. Supplemental materials

8.1. Supplemental materials Aim 1

Following pages are consisting of Supplemental materials to publication:

Benova A, Ferencakova M, Bardova K, Funda J, Prochazka J, Spoutil F, Cajka T, Dzubanova M, Balcaen T, Kerckhofs G, Willekens W, van Lenthe GH, Charyyeva A, Alquicer G, Pecinova A, Mracek T, Horakova O, Coupeau R, Hansen MS, Rossmeisl M, Kopecky J, Tencerova M. Omega-3 PUFAs prevent bone impairment and bone marrow adiposity in mouse model of obesity. Commun Biol. 2023 Oct 14;6(1):1043. doi: 10.1038/s42003-023-05407-8. PMID: 37833362; PMCID: PMC10575870.

SUPPLEMENTARY INFORMATION

CONTENT:

Supplementary Tables: Supplementary Table 1-4

Supplementary Figures with figure legends: Supplementary Figure S1-10

SUPPLEMENTARY TABLES

Supplementary Table 1: Macronutrient composition and energy content in the experimental diets.

	ND	HFD	HFD+F
Lipids (% diet, wt/wt)	2.9	31.8	32.4
Carbohydrates (% diet, wt/wt)	64.3	47.2	47.6
Proteins (% diet, wt/wt)	16.9	11.7	11.7
Energy density (kJ/g)	13.0	20.1	20.1
Supplement:			
Epax 1050 TG (g/100g)	0.0	0.0	5.3

Supplementary Table 2: Fatty acid composition of dietary lipids

(mol %)	ND	HFD	HFD+F
12:0	0.15	0.26	-
14:0	0.14	1.22	-
16:0	12.52	13.42	12.05
16:1 (n-9)	-	-	-
16:1 (n-7)	0.32	0.26	0.31
18:0	6.00	3.34	3.84
18:1 (trans)	0.55	0.42	0.45
18:1 (n-9)	25.64	31.00	28.44
18:1 (n-7)	1.59	0.65	0.87
18:2 (n-6)	46.62	47.22	41.10
18:3 (n-6)	-	-	-
20:0	0.42	0.43	0.50
18:3 (n-3)	4.89	1.24	1.24
20:1 (n-9)	0.31	0.26	0.47
20:2 (n-6)	-	-	0.14
20:3 (n-6)	-	-	-
20:4 (n-6)	-	-	0.47
20:5 (n-3)	-	-	1.65
22:4 (n-6)	-	-	0.12
22:5 (n-6)	-	-	0.48
22:5 (n-3)	-	-	0.34
22:6 (n-3)	0.45	-	6.39
SFA	23.71	19.48	18.14
MUFA	27.92	32.26	30.18
n-6 PUFA	46.86	47.34	42.35
n-3 PUFA	0.97	0.49	8.87

Fatty acid composition in total dietary lipids was determined using gas chromatography.

SFA, saturated fatty acid; MUFA, monounsaturated fatty acid. -, <0.1 %.

Supplementary Table 3: List of mouse primers

Gene name	Gene Sequence 5'-3'
36B4 F	TCCAGGCTTTGGGCATCA
36B4 R	CTTTATCAGCTGCACATCACTCAGA
Fsp27 F	ATCAGAACAGCGCAAGAAGA
Fsp27 R	CAGCTTGTACAGGTCGAAGG
Cd36 F	ATGGGCTGTGATCGGAACTG
Cd36 R	TTTGCCACGTCATCTGGGTTT
Alpl F	GCCCTCTCCAAGACATATA
Alpl R	CCATGATCACGTCGATATCC
Bmp2 F	GGGACCCGCTGTCTTCTAGT
Bmp2 R	TCAACTCAAATTCGCTGAGGAC
Col1a1 F	GGTGAACAGGGGTTCCTGG
Col1a1 R	TTCGCACCAGGTTGCCATC
Adipoq F	GACGTTACTACAACTGAAGAGC
Adipoq R	CATTCTTTTCCTGATACTGGTC
Cebpa F	AAGCCAAGAAGTCGGTGGA
Cebpa R	CAGTTCACGGCTCAGCTGTTC
Il1β F	GCAACTGTTCCTGAACTCAACT
Il1β R	ATCTTTTGGGGTCCGTCAACT
Tnfα F	CCCTCACACTCAGATCATCTTCT
Tnfα R	GCTACGACGTGGGCTACAG
p53 F	TCTTATCCGGGTGGAAGGAAA
p53 R	GGCGAAAAGTCTGCCTGTCTT
p16 F	GGGTTTTCTTGGTGAAGTTCG
p16 R	TTGCCCATCATCATCACCT
Sod2 F	CAGACCTGCCTTACGACTATGG
Sod2 R	CTCGGTGGCGTTGAGATTGTT
Hmox1 F	AGGTACACATCCAAGCCGAGA
Hmox1 R	CATCACCAGCTTAAAGCCTTCT

Pparγ2 F	GGGTCAGCTCTTGTGAATGG
Pparγ2 R	CTGATGCACTGCCTATGAGC
Oc F	TGCGCTCTGTCTCTCTGACC
Oc R	CTGTGACATCCATACTTGCAGG
p21 F	CCTGGTGATGTCCGACCTG
p21 R	CCATGAGCGCATCGCAATC
Trap F	CAGCTCCCTAGAAGATGGATTCAT
Trap R	GTCAGGAGTGGGAGCCATATG
Rankl F	AGCCGAGACTACGGCAAGTA
Rankl R	AAAGTACAGGAACAGAGCGATG
Rela F	ACTGCCGGGATGGCTACTAT
Rela R	TCTGGATTCGCTGGCTAATGG
Opg F	CCTTGCCCTGACCACTCTTAT
Opg R	CACACACTCGGTTGTGGGT
Ctsk F	AGGCAGCTAAATGCAGAGGGTACA
Ctsk R	AGCTTGCATCGATGGACACAGAGA
Ctnnb1 F	CCCAGTCCTTCACGCAAGAG
Ctnnb1 R	CATCTAGCGTCTCAGGGAACA
Vegfa F	GTACCTCCACCATGCCAAGTG
Vegfa R	TGGGACTTCTGCTCTCCTTCTG
Vcam F	GGCTCCAGACATTTACCCAGTT
Vcam R	CATGAGCTGGTCACCCTTGAA
Fas F	CTGCACCCTGACCCAGAATAC
Fas R	ACAGCCAGGAGAATCGCAGTA
Fasgl F	CAGTCCACCCCCTGAAAAAAA
Fasgl R	CCTTGAGTTGGACTTGCCTGTT
Il10 F	CTGGACAACATACTGCTAACCG
Il10 R	GGGCATCACTTCTACCAGGTAA
Il1rn F	GCTCATTGCTGGGTACTTACAA
Il1rn R	CCAGACTTGGCACAAGACAGG

Supplementary Table 4. List of primary and secondary antibodies used for western blot

Primary antibodies	**Catalog #**	**Company**	**Dilution**
Phospho-Akt Ser473_ Rabbit	#4058 (193H12)	Cell Signaling	1:1000
Phospho-Akt Thr308_Rabbit	#13038 (D25E6)	Cell Signaling	1:1000
Total AKT_Rabbit	#9272	Cell Signaling	1:1000
β-actin_Rabbit	#4970 (13E5)	Cell Signaling	1:1000
Phospho-NF-kB p65_Rabbit	#3031	Cell Signaling	1:1000
NF-kB p65_Rabbit	#8242 (D14E12)	Cell Signaling	1:1000
Secondary HRP-conjugated antibodies			
Anti-rabbit IgG, HRP-linked Antibody	#7074	Cell Signaling	1:5000

Supplementary Fig. 1

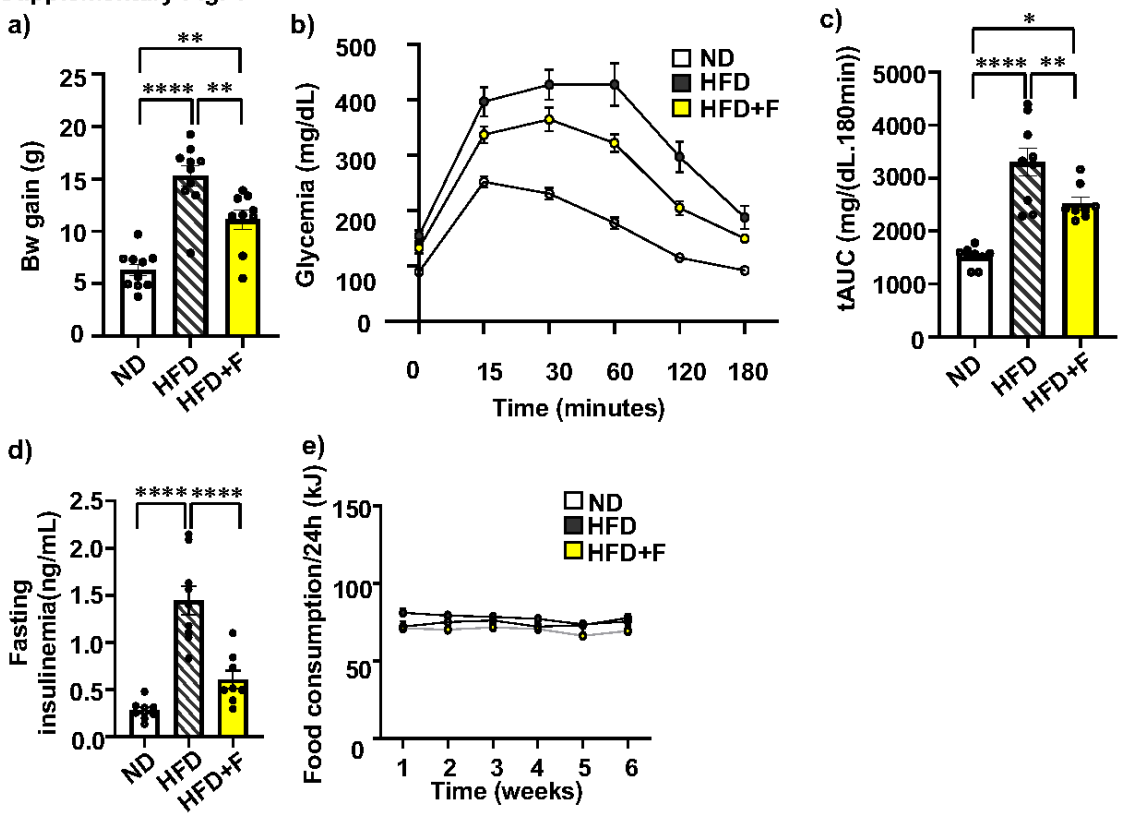

Supplementary Fig. 1 legend: Metabolic parameters of investigated mice.
(**a-d**) Omega-3 PUFAs improve metabolic parameters in HFD mice. (**a**) Body weigh gain, (**b**) measurement of intraperitoneal glucose tolerance test (GTT) in treated mice at the end of dietary intervention after overnight fasting (groups coding: white circle-ND, black circle-HFD, yellow circle-HFD+F), (**c**) area under the curve of coresponding GTT graphs; (**d**) insulinemia after overnight fasting at the end of dietary intervention in treated mice (n= 7-10). (**e**) Food intake (kJ) in treated mice during dietary intervention (n=7-10). Data are presented as mean ± SEM (n = 6-8 per group); one-way ANOVA, Tukey's multiple comparison test with * $p \leq 0.05$, ** $p \leq 0.01$, **** $p \leq 0.0001$. (groups coding: white column-ND, black line shading-HFD, yellow column-HFD+F)

Supplementary Fig. 2

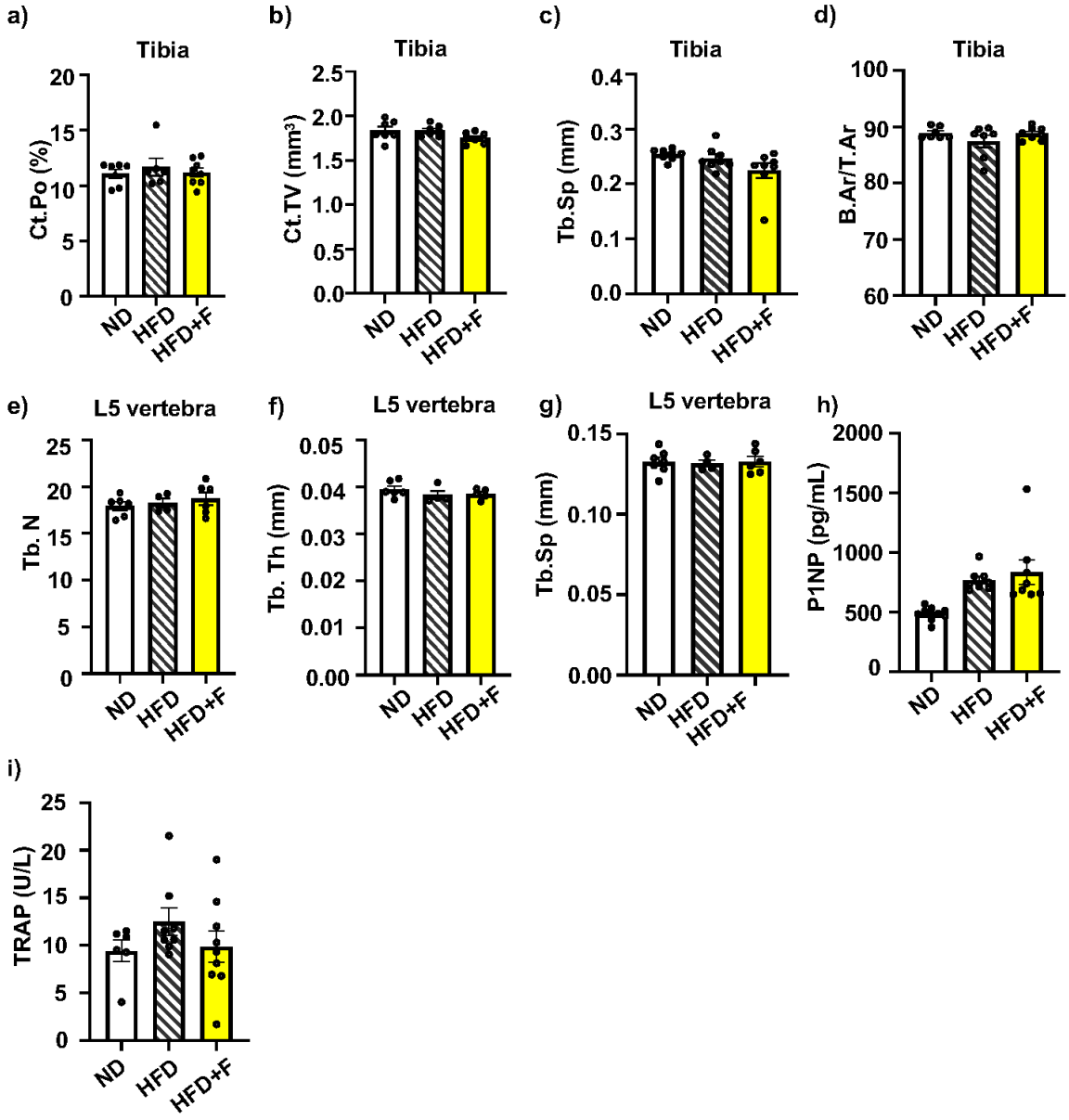

Supplementary Fig. 2 legend: Bone parameters of investigated mice.
(**a-d**) Evaluation of bone parameters in tibia: (**a**) Cortical porosity (Ct.Po), (**b**) Cortical total volume (Ct.TV); (**c**) trabecular separation (Tb.Sp) and (**d**) cortical area fraction (B.Ar/T.Ar) in treated mice (n= 7-10). (**e-g**) Evaluation of bone parameters in L5 vertebra: (**e**) Trabecular number (Tb.N), (**f**) trabecular thickness (Tb.Th), (**g**) trabecular separation (Tb.Sp). Analysis of circulating (**h**) bone formation marker P1NP (pg/mL) and (**i**) bone resorption marker TRAP (U/L). Data are presented as mean ± SEM (n = 6-8 per group); one-way ANOVA, Tukey's multiple comparison test with * $p \leq 0.05$. (groups coding: white column-ND, black line shading-HFD, yellow column-HFD+F)

Supplementary Fig. 3

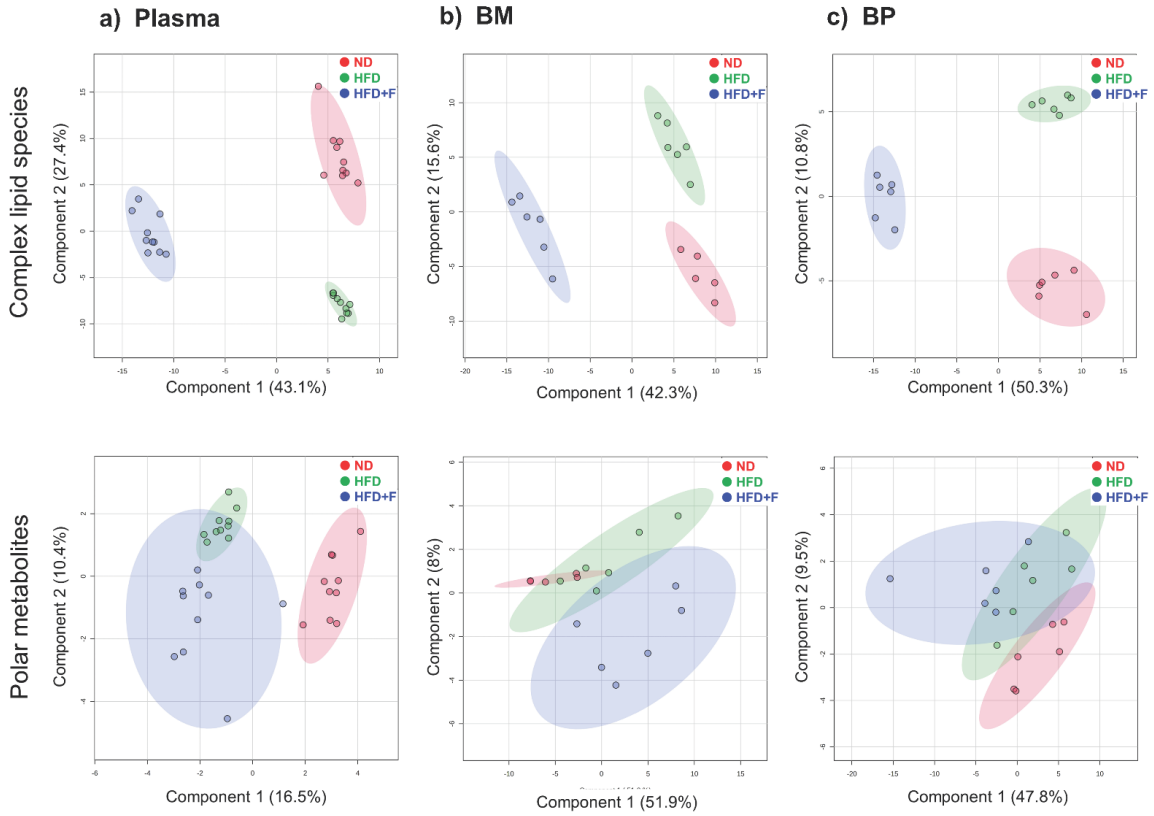

Supplementary Fig. 3 legend: Metabolomic analysis of plasma, bone marrow (BM) and bone powder samples obtained from investigated mice.
PLS-DA score plots of unique lipid species (top panels) and polar metabolites (bottom panels) for (**a**) plasma, (**b**) bone marrow, and (**c**) bone powder samples.

Supplementary Fig. 4

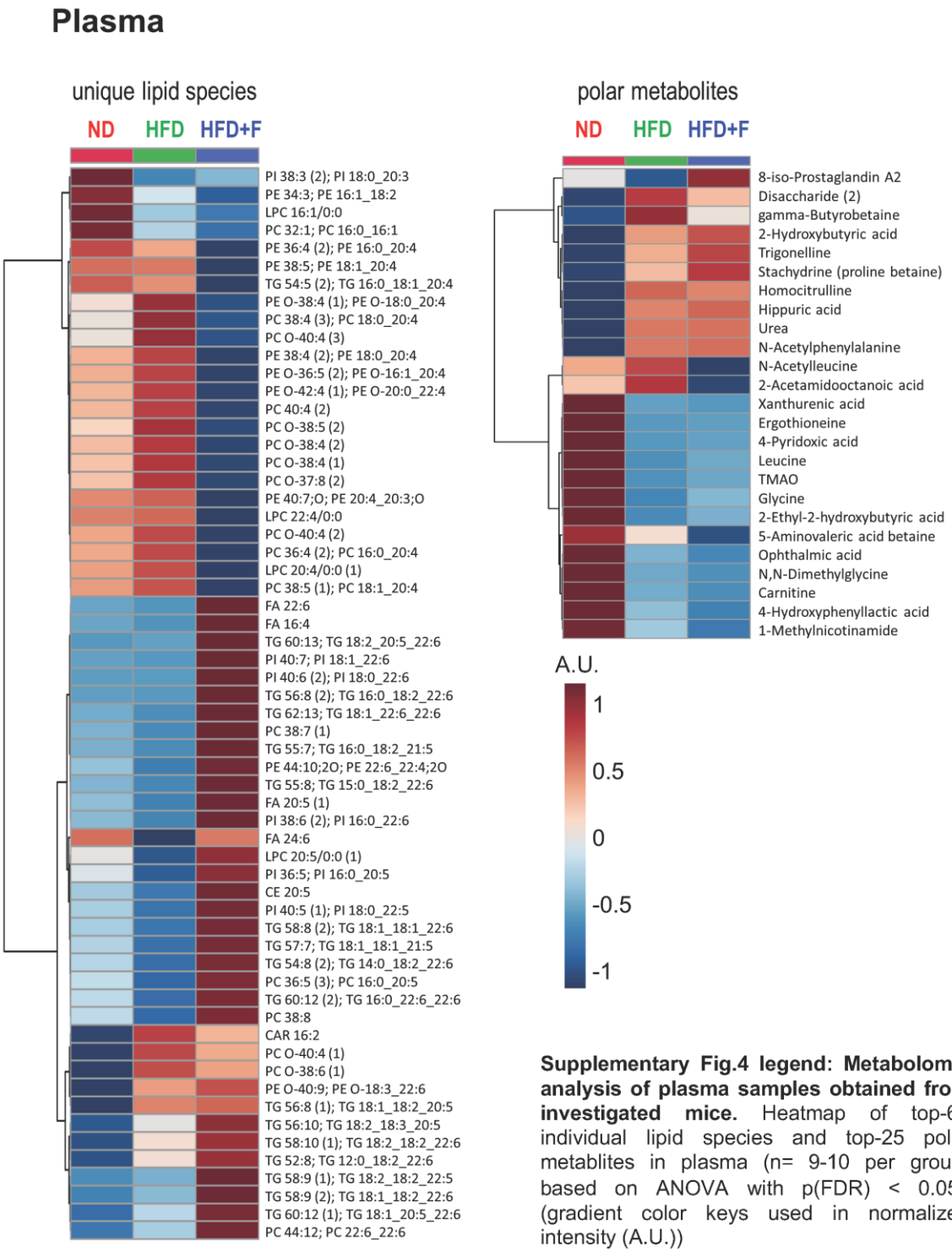

Supplementary Fig.4 legend: Metabolomic analysis of plasma samples obtained from investigated mice. Heatmap of top-60 individual lipid species and top-25 polar metablites in plasma (n= 9-10 per group) based on ANOVA with p(FDR) < 0.05,. (gradient color keys used in normalized intensity (A.U.))

Supplementary Fig. 5

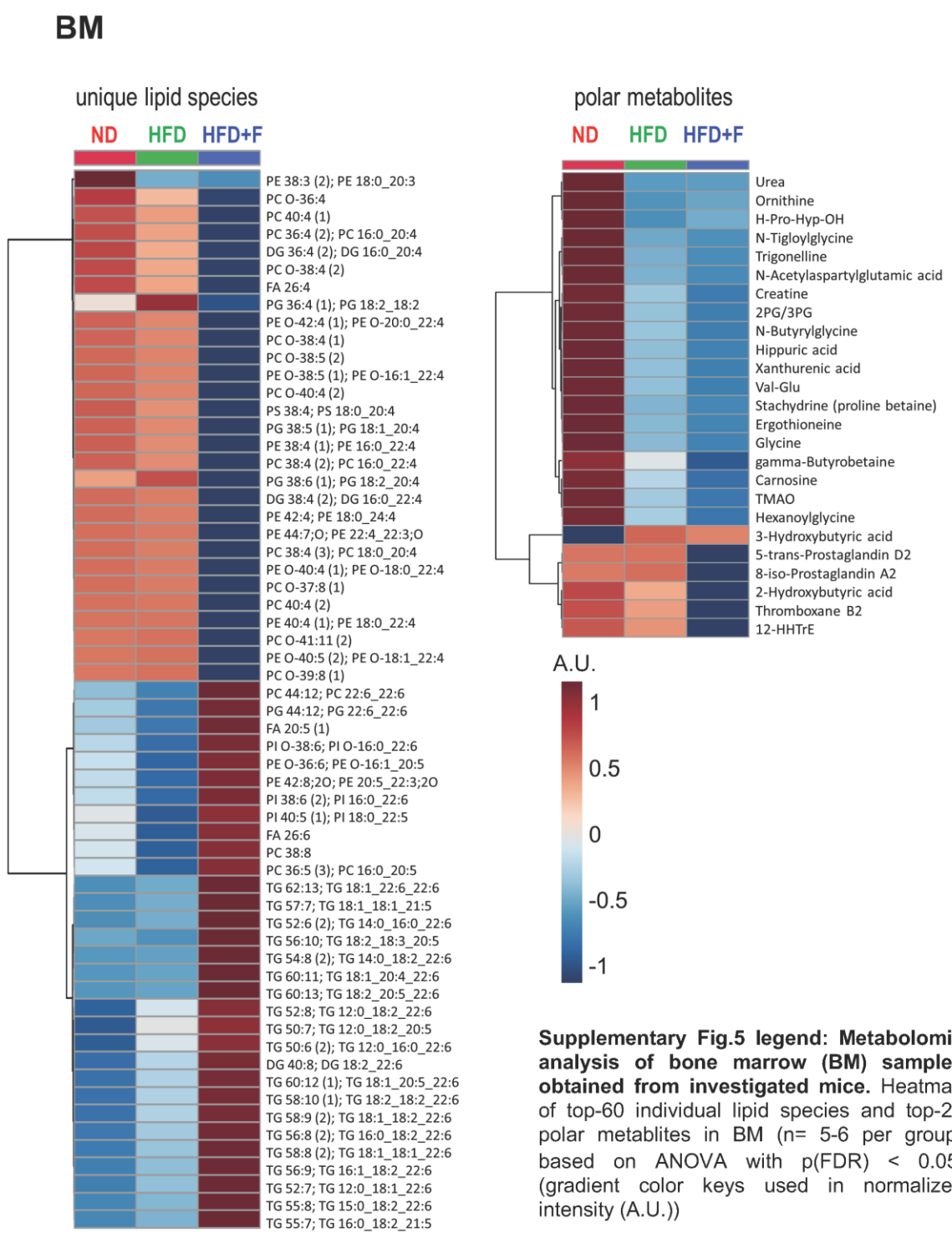

Supplementary Fig.5 legend: Metabolomic analysis of bone marrow (BM) samples obtained from investigated mice. Heatmap of top-60 individual lipid species and top-25 polar metablites in BM (n= 5-6 per group) based on ANOVA with p(FDR) < 0.05. (gradient color keys used in normalized intensity (A.U.))

Supplementary Fig. 6

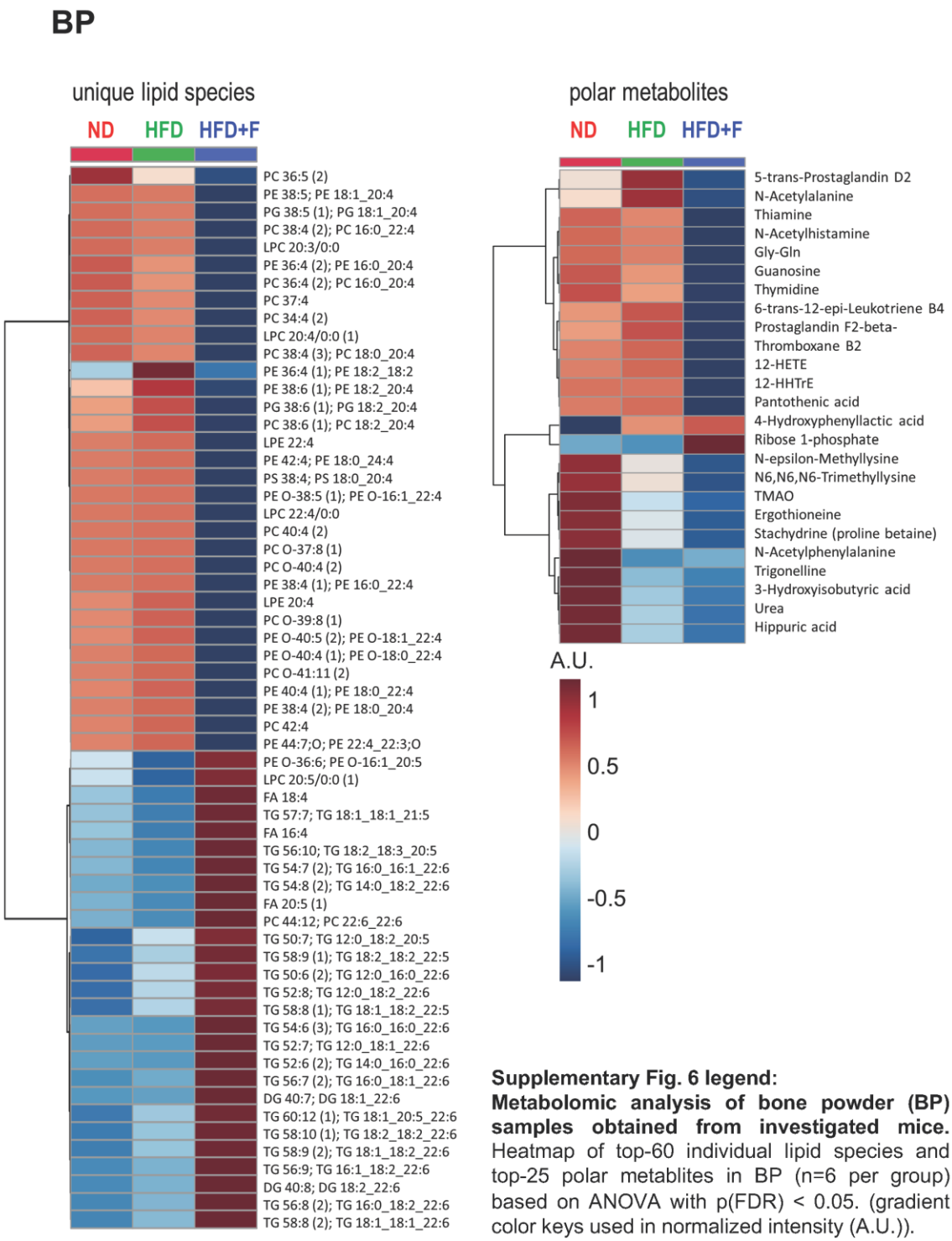

Supplementary Fig. 6 legend:
Metabolomic analysis of bone powder (BP) samples obtained from investigated mice. Heatmap of top-60 individual lipid species and top-25 polar metablites in BP (n=6 per group) based on ANOVA with p(FDR) < 0.05. (gradient color keys used in normalized intensity (A.U.)).

Supplementary Fig. 7

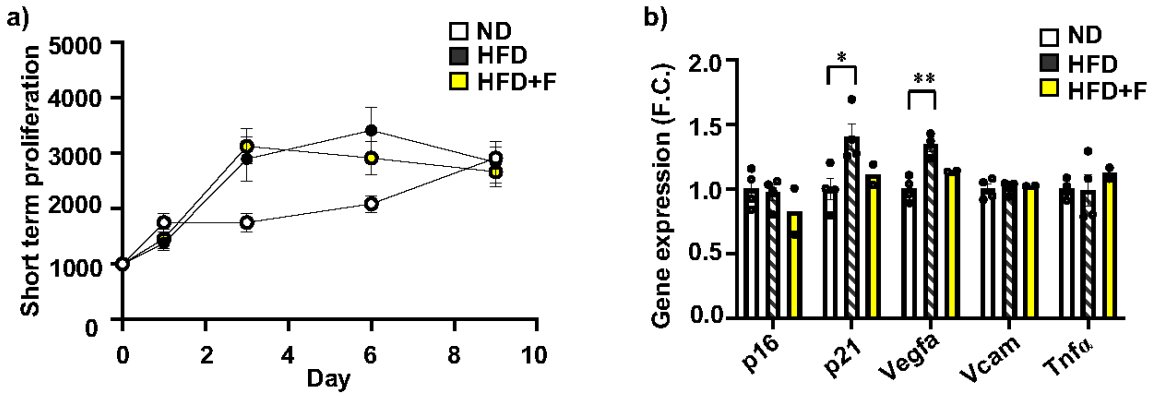

Supplementary Fig. 7 legend: Cellular characteristics of bone cells obtained from the treated mice. (**a**) Short-term proliferation assay of primary BMSCs calculated after 1, 3, 6 and 9 days in culture after seeding (n = 3 per group) (groups coding: white circle-ND, black circle-HFD, yellow circle-HFD+F). (**b**) Gene expression of senescence genes (*p16, p21, Vegfa, Vecam, Tnfα*) measured in mouse HSCs. Data are presented as mean ± SEM (n = 4 per group); one-way ANOVA, Tukey's multiple comparison test, * $p \leq 0.05$, ** $p \leq 0.01$. (groups coding: white column-ND, black line shading-HFD, yellow column-HFD+F)

Supplementary Fig. 8

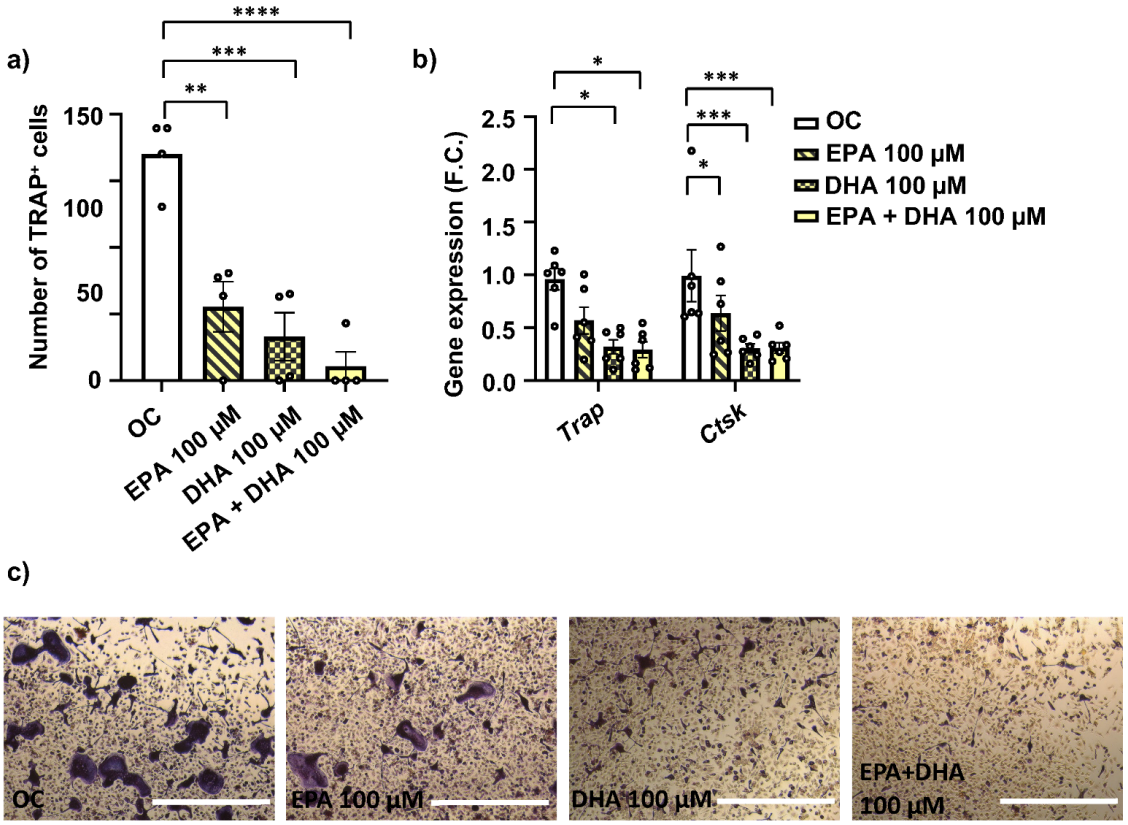

Supplementary Fig. 8 legend: The effect of omega-3 PUFA treatment in vitro on osteoclast differentiation

(**a**) Number of TRAP+ cells after 5 days of differentiation with omega-3 PUFA short term supplementation (n = 4 per group). (**b**) Gene expression of osteoclastic genes (*Trap, Ctsk*) measured in Ocs after 5 days differentiation. Data are presented as mean ± SEM (n = 6 per group); one-way ANOVA, Tukey's multiple comparison test, **p ≤ 0.01, *** p ≤ 0.001, ****p ≤ 0.0001. (**c**) Representative pictures of TRAP+ differentiated OCs after 5 days of differentiation with omega-3 PUFAs (scale bar 250 µm). (groups coding: white column-ND, black line shading-HFD, yellow column-HFD+F)

Supplementary Fig. 9

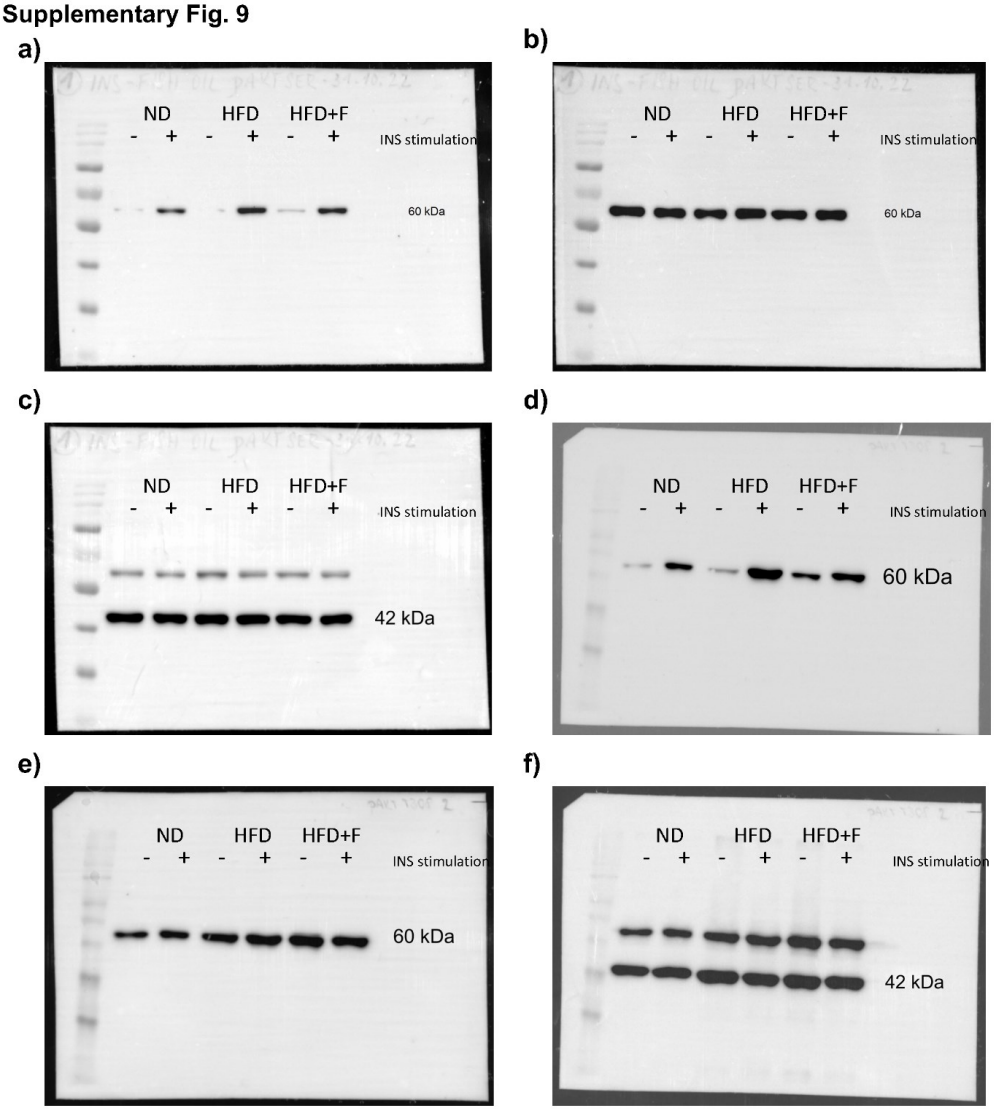

Supplementary Fig. 9 legend: Uncropped western blot membrane images corresponding to Fig.6b and Fig. 6d

(**a**) p-S473-AKT, (**b**) total AKT and corresponding (**c**) β-actin. (**e**) p-T308-AKT, (**f**) total AKT and corresponding **(g**) β-actin.

Supplementary Fig. 10

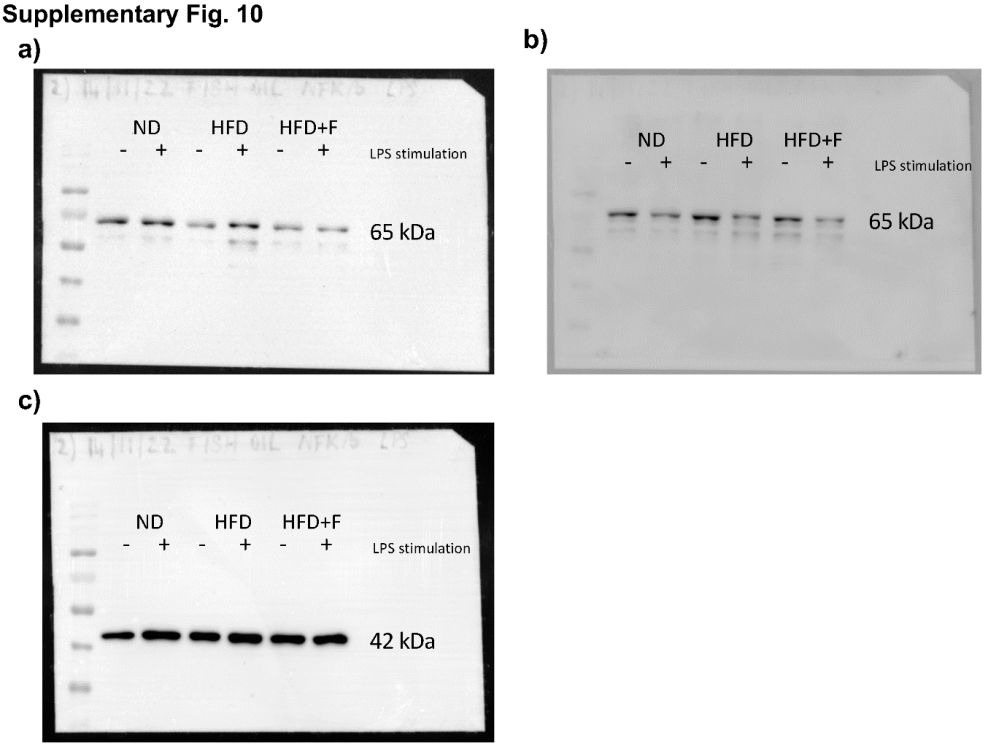

Supplementary Fig. 10 legend: Uncropped western blot membrane images corresponding to Fig. 6f. (**a**) p-NFκB, (**b**) total NFκB and corresponding (**c**) β-actin.

8.2. Supplemental materials Aim 2

Following pages are consisting of Supplemental materials to publication:

Benova A, Ferencakova M, Bardova K, Funda J, Prochazka J, Spoutil F, Cajka T, Dzubanova M, Balcaen T, Kerckhofs G, Willekens W, van Lenthe GH, Alquicer G, Pecinova A, Mracek T, Horakova O, Rossmeisl M, Kopecky J, Tencerova M. Novel thiazolidinedione analog reduces a negative impact on bone and mesenchymal stem cell properties in obese mice compared to classical thiazolidinediones. Mol Metab. 2022 Nov;65:101598. doi: 10.1016/j.molmet.2022.101598. Epub 2022 Sep 11. PMID: 36103974; PMCID: PMC9508355.

SUPPLEMENTARY MATERIAL

Supplemental Material and Methods

Supplemental Tables: Table S1-S4

Supplemental Figures with figure legends: Fig. S1-S7

Supplemental Material and Methods

Bone histology

Tibias were collected after the dissection and fixed for 48 h in 10% formalin. After formalin fixation, bones were demineralized by EDTA 12% solution for 14 days. Tissues were embedded in paraffin and sections were used for haematoxylin eosin staining as previously published [1].

Isolation of mRNA and quantitative RT-PCR

Total RNA was isolated using TRI Reagent (Merck, Darmstadt, Germany) and RNA concentration was measured using Nanodrop spectrometer. cDNA synthesis was performed from 1 μg of total RNA using High-Capacity cDNA Reverse Transcription Kit (Thermo Fisher Scientific, Waltham, MA, USA) according to the manufacturer protocol. Quantitative real-time PCR was performed using Light Cycler® 480 SYBR Green I Master (Roche, Basel, Switzerland) with specific primers (GeneriBiotech, Hradec Králové, Czech Republic) listed in **Table S1** and **Table S2**. RT-PCR data were normalized to the housekeeping gene expression (36B4 for mouse, β-ACTIN for human).

Western blot

Protein lysates from the cells were prepared using M2 lysis buffer. Protein concentration was measured using BCA assay (Thermo Fisher Scientific, Waltham, MA, USA). Proteins with a final loading concentration of 15 μg/mL were separated in sodium dodecyl sulphate polyacrylamide gels and transferred onto PVDF (polyvinylidene difluoride) membrane (Imobilon-P) by semi-dry electroblotting. Due to higher number of experimental groups, internal control was loaded into each membrane with loading concentration similar to concentration of the samples. After blotting, membranes were washed for 5 minutes in TBS (150 mM Tris-HCl, 10 mM NaCl; pH 7,4) and blocked in 5% (*w/v*) fat-free dry milk diluted in TBS-T (TBS with 1% (*v/v*) detergent Tween-20) for 1 hour. After blocking, the membranes were washed 5 x 5 minutes in TBS-T. For immunodetection, the membranes were incubated with primary antibody (diluted in 5% milk) overnight in 4 °C. Next day, membranes were washed 5 x 5 minutes. in TBS-T and then incubated with corresponding HRP-conjugated secondary antibody for 1 hour at RT. The list of WB

antibodies (Cell Signaling, Danvers, MA, USA) is presented in **Table S3**. Protein detection was performed using ECL Clarity Max detection substrate (Bio-Rad) measured by ChemiDoc imaging system (Bio-Rad, Hercules, CA, USA) and signals were calculated by Image Lab software (Bio-Rad, Hercules, CA, USA). Densitometry analysis was normalized to signals from positive control protein lysates present in each membrane.

Lipidomics and metabolomics

Global lipidomic and metabolomic profiling of BM, bone powder (BP), and plasma samples was conducted using a combined untargeted and targeted workflow for the lipidome, metabolome, and exposome analysis (LIMeX) [2-4] with some modifications. Extraction was carried out using a biphasic solvent system of cold methanol, methyl *tert*-butyl ether (MTBE), and 10% methanol. Four different liquid chromatography-mass spectrometry (LC-MS) platforms were used for profiling: (i) lipidomics of complex lipids using reversed-phase liquid chromatography with mass spectrometry (RPLC-MS) in positive ion mode, (ii) lipidomics of complex lipids in RPLC-MS in negative ion mode, (iii) metabolomics of polar metabolites using hydrophilic interaction chromatography with mass spectrometry (HILIC-MS) in positive ion mode, and (iv) metabolomics of polar metabolites using RPLC-MS in negative ion mode.

Sample extraction for metabolomic and lipidomic analyses

BM and BP samples (20–25 mg) were homogenized with 275 µL methanol containing internal standards (PE 17:0/17:0, PG 17:0/17:0, LPC 17:1, Sphingosine d17:1, Cer d18:1/17:0, SM d18:1/17:0, PC 15:0/18:1-d_7, cholesterol-d_7, TG 17:0/17:1/17:0-d_5, DG 12:0/12:0/0:0, DG 18:1/2:0/0:0, LPE 17:1, oleic acid-d_9, PI 15:0/18:1-d_7, MG 17:0/0:0/0:0, PS 17:0/17:0, HexCer d18:1/17:0, DG 18:1/0:0/18:1-d_5, TG 20:0/20:1/20:0-d_5, LPG 17:1, LPS 17:1, cardiolipin 16:0/16:0/16:0/16:0) and 275 µL 10% methanol containing internal standards (caffeine-d_9, acetylcholine-d_4, creatinine-d_3, choline-d_9, TMAO-d_9, *N*-methylnicotinamide-d_4, betaine-d_9, butyrobetaine-d_9, creatine-d_3, cotinine-d_3, glucose-d_7, succinic acid-d_4, metformin-d_6) for 1.5 min using a grinder (MM400, Retsch, Germany). Then, 1 mL of MTBE with internal standard (CE 22:1) was added, the tubes were shaken for 1 min and centrifuge at 16,000 rpm for 5 min.

Plasma samples (25 µL) were mixed with 765 µL of cold methanol/MTBE mixture (165 µL + 600 µL, respectively) containing the same mixtures of internal standards as before and shaken for 30 s. Then, 165 µL of 10% MeOH with deuterated polar metabolite internal standards was added, shaken for 30 s, and centrifuged at 16,000 rpm for 5 min.

For lipidomic profiling, 100 µL of upper organic phase was collected, evaporated and resuspended using 100 µL methanol with internal standard (12-[[(cyclohexylamino)carbonyl]amino]-dodecanoic acid, CUDA), shaken for 30 s, centrifuged at 16,000 rpm for 5 min and used for LC-MS analysis.

For metabolomic profiling, 70 µL of bottom aqueous phase was collected, evaporated, resuspended in 70 µL of an acetonitrile/water (4:1, *v*/*v*) mixture with internal standards (CUDA and Val-Tyr-Val), shaken for 30 s, centrifuged at 16,000 rpm for 5 min and analyzed using HILIC metabolomics platform. Another 70 µL aliquote of bottom aqueous phase was mixed with 210 µL of an isopropanol/acetonitrile (1:1, *v*/*v*) mixture, shaken for 30 s, centrifuged at 16,000 rpm for 5 min, and the supernatant was evaporated, resuspended in 5% methanol/0.2% formic acid with internal standards (CUDA and Val-Tyr-Val), shaken for 30 s, centrifuged at 16,000 rpm for 5 min and analyzed using RPLC metabolomics platform.

LC-MS-based lipidomics

The LC-MS systems consisted of a Vanquish UHPLC System (Thermo Fisher Scientific, Waltham, MA, USA) coupled to a Q Exactive Plus mass spectrometer (Thermo Fisher Scientific, Waltham, MA, USA).

Lipids were separated on an Acquity UPLC BEH C18 column (50 × 2.1 mm; 1.7 µm) coupled to an Acquity UPLC BEH C18 VanGuard pre-column (5 × 2.1 mm; 1.7 µm) (Waters, Milford, MA, USA). The column was maintained at 65°C at a flow-rate of 0.6 mL/min. For LC–ESI(+)-MS analysis, the mobile phase consisted of (A) 60:40 (*v*/*v*) acetonitrile:water with ammonium formate (10 mM) and formic acid (0.1%) and (B) 90:10:0.1 (*v*/*v*/*v*) isopropanol:acetonitrile:water with ammonium formate (10 mM) and formic acid (0.1%). For LC–ESI(−)-MS analysis, the composition of the solvent mixtures were the same with the exception of the addition of ammonium acetate (10 mM) and acetic acid (0.1%) as mobile-phase modifiers. Separation was

conducted under the following gradient for LC–ESI(+)-MS: 0 min 15% (B); 0–1 min 30% (B); 1–1.3 min from 30% to 48% (B); 1.3–5.5 min from 48% to 82% (B); 5.5–5.8 min from 82% to 99% (B); 5.8–6 min 99% (B); 6–6.1 min from 99% to 15% (B); 6.1–7.5 min 15% (B). For LC–ESI(−)-MS, the following gradient was used: 0 min 15% (B); 0–1 min 30% (B); 1–1.3 min from 30% to 48% (B); 1.3–4.8 min from 48% to 76% (B); 4.8–4.9 min from 76% to 99% (B); 4.9–5.3 min 99% (B); 5.3–5.4 min from 99% to 15% (B); 5.4–6.8 min 15% (B). A sample volume of 0.3 µL, 1.5 µL, and 1.5 µL was used for bone marrow, bone powder, and plasma extracts, respectively, in ESI(+). A sample volume of 5 µL for all matrices was used in ESI(–). Sample temperature was maintained at 4°C.

The ESI source and MS parameters were: sheath gas pressure, 60 arbitrary units; aux gas flow, 25 arbitrary units; sweep gas flow, 2 arbitrary units; capillary temperature, 300°C; aux gas heater temperature, 370°C; MS1 mass range, *m/z* 200–1700; MS1 resolving power, 35,000 FWHM (*m/z* 200); number of data-dependent scans per cycle, 3; MS/MS resolving power, 17,500 FWHM (*m/z* 200). For ESI(+), a spray voltage of 3.6 kV and normalized collision energy of 20% was used while for ESI(−) a spray voltage of −3.0 kV and normalized collision energy of 10, 20 and 30% were set-up.

LC-MS-based metabolomics

Polar metabolites were separated on an Acquity UPLC BEH Amide column (50 × 2.1 mm; 1.7 µm) coupled to an Acquity UPLC BEH Amide VanGuard pre-column (5 × 2.1 mm; 1.7 µm) (Waters, Milford, MA, USA). The column was maintained at 45°C at a flow-rate of 0.4 mL/min. The mobile phase consisted of (A) water with ammonium formate (10 mM) and formic acid (0.125%) and (B) acetonitrile:water (95/5) with ammonium formate (10 mM) and formic acid (0.125%). Separation was conducted under the following gradient: 0 min 100% (B); 0–1 min 100% (B); 1–3.9 min from 100% to 70% (B); 3.9–5.1 min from 70% to 30% (B); 5.1–6.4 min from 30% to 100%(B); 6.4–8.0 min 100% (B). A sample volume of 0.5 µL, 0.5 µL, and 1.5 µL was used for bone marrow, bone powder, and plasma extracts, respectively, in ESI(+). Sample temperature was maintained at 4°C.

Polar metabolites were also separated on an Acquity UPLC HSS T3 column (50 × 2.1 mm; 1.8 µm) coupled to an Acquity UPLC HSS T3 VanGuard pre-column (5 × 2.1 mm; 1.8 µm) (Waters,

Milford, MA, USA). The column was maintained at 45°C using a ramped flow-rate. The mobile phase consisted of (A) water with formic acid (0.2%) and (B) methanol with formic acid (0.1%). Separation was conducted under the following gradient: 0 min 1% (B) 0.3 mL/min; 0–0.5 min 1% (B) 0.3 mL/min; 0.5–2 min from 1% to 60% (B) 0.3 mL/min; 2–2.3 min from 60% to 95% (B) from 0.3 mL/min to 0.5 mL/min; 2.3–3.0 min 95% (B) 0.5 mL/min; 3.0–3.1 min from 95% to 1% (B) 0.5 mL/min; 3.1–4.5 min 1% (B) 0.5 mL/min; 4.5–4.6 min 1% (B) from 0.5 mL/min to 0.3 mL/min; 4.6–5.5 min 1% (B) 0.3 mL/min. A sample volume of 5 µL was used for the injection in ESI(–). Sample temperature was maintained at 4°C.

The ESI source and MS parameters were: sheath gas pressure, 50 arbitrary units; aux gas flow, 13 arbitrary units; sweep gas flow, 3 arbitrary units; capillary temperature, 260°C; aux gas heater temperature, 425°C; MS1 mass range, *m/z* 60–900; MS1 resolving power, 35,000 FWHM (*m/z* 200); number of data-dependent scans per cycle, 3; MS/MS resolving power, 17,500 FWHM (*m/z* 200). A spray voltage of 3.6 kV and −2.5 kV for ESI(+) and ESI(–), respectively, was used. For all metabolomics platforms a normalized collision energy of 20, 30 and 40% was used.

Quality control

Quality control was assured by (i) randomization of the actual samples within the sequence, (ii) injection of quality control (QC) pool samples at the beginning and the end of the sequence and between each 10 actual samples, (iii) analysis of procedure blanks, (iv) serial dilution of QC sample (0, 1/16, 1/8, 1/4, 1/2, 1), (v) checking the peak shape and the intensity of spiked internal standards and the internal standard added prior to injection.

Data processing

LC-MS data from metabolomic and lipidomic profiling were processed through MS-DIAL v. 4.70 software. Metabolites were annotated using in-house retention time–*m/z* library and using MS/MS libraries available from commercial and open sources (NIST20, MassBank, MoNA). Lipids were annotated using LipidBlast in-built in MS-DIAL. Traces of pioglitazone (*m/z* 355.1116) and MSDC-0602K (*m/z* 370.0749) were detected in RPLC-MS lipidomics in ESI (–) as deprotonated molecules. Raw data were filtered using blank samples, serial dilution samples, and QC pool samples with relative standard deviation (RSD) <30%, and then normalized using locally estimated scatterplot smoothing (LOESS) approach by means of QC pool samples injected regularly between

10 actual samples followed by sample-weight and injection volume normalization. Data were exported as the detector signal intensity in arbitrary units (A.U.).

Biochemical analyses of bone turnover markers

Rat/Mouse TRAP EIA for the quantitative determination of the Tartrate-resistant acid phosphatase (TRAP) for bone resorption and Rat/Mouse P1NP EIA for the determination of the N-terminal propeptide of type I procollagen (P1NP) for bone formation (MyBioSource, San Diego, CA, USA) were measured in mouse serum samples.

Cellular Reactive Oxygen Species (ROS) Detection assay

DCFDA (2,7-dichloro-dihydro-fluoroscein diacetate) (Abcam, Cambridge, United Kingdom) was used to measure the intracellular ROS production of primary mBM-MSCs [5]. Cells were seeded to a dark, clear bottom 96-well plate at a density of 25000 cells/well to adhere overnight. The next day, culture growth media was replaced with DCFDA Solution (25 µM) and incubated for 45 minutes at 37 °C and 5 % CO_2. DCFDA was removed and cells were loaded with 1x Buffer supplemented with 50 µM TBHP (tert-butyl hydrogen peroxide) for 1 hour at 37 °C and 5 % CO_2. The fluorescent intensity was detected every minute for 30 minutes using a fluorescent microplate reader (Excitation ~485 nm/Emission ~535 nm). The results were expressed as % of ROS production.

Glucose uptake assay

The Glucose Uptake-Glo Assay (Promega, Madison, WI, USA) was used to measure glucose uptake in hBM-MSC and 3T3-L1 cells after short term treatment with insulin, TZDs, TZD analog MSDC-0602K and MPC inhibitor UK5099. Cells were seeded at the density of 10 000 cells per well in 96-well black plate with clear bottom. Following day, cells were washed with PBS and cultured with serum-free MEM alpha (Thermo Fisher Scientific, Waltham, MA, USA) medium with 0.5 % BSA overnight. Next day, media was replaced with basal DMEM media (Thermo Fisher Scientific, Waltham, MA, USA) with 0.5 % BSA supplemented with 1 µM insulin (+INS), 30 µM PIO, ROSI and MSDC-0602K and 2 µM UK5099. After 1.5-hour incubation media was replaced with 1 mM 2-deoxyglucose (2DG). The reaction was stopped after 15 minutes incubation, and samples were prepared for measurement of luminescence according to the manufacturer

protocol. Luminescence signal was detected using Tecan infinity M200 reader (Tecan, Männedorf, Switzerland) and relative light units (RLU) were normalized to protein content of samples measured by BCA assay (Thermo Fisher Scientific, Waltham, MA, USA). The data are expressed as the fold change of the normalized RLU values/ protein of non-stimulated cells.

Glutamine/Glutamate assay

The Glutamine-Glutamate-Glo Assay (Promega, Madison, WI, USA) was used to detect glutamine and glutamate in hBM-MSC and 3T3-L1 cells after short-term treatment with 1μM insulin, 30 μM PIO, and 30 μM TZD analog MSDC-0602K. Cells were seeded at the density of 15 000 cells per well in 96-well plate. Following day, cells were washed with PBS and cultured with serum-free MEM alpha (Thermo Fisher Scientific, Waltham, MA, USA) medium with 0.5 % BSA (Merck, Darmstadt, Germany) overnight. Next day, starvation media was replaced with basal DMEM media (Thermo Fisher Scientific, Waltham, MA, USA) with 2mM glutamine, 5mM glucose supplemented with 1 μM insulin (+INS), 30 μM PIO, ROSI and MSDC-0602K and 2 μM UK5099. After 3 hours incubation, the cells were washed twice with PBS and then processed with PBS containing Inactivation solution followed by Tris solution. Cell lysates were transferred to the white 96-well plate for the measurement of glutamine/glutamate according to the manufacturer protocol. Luminescent signal was detected using Tecan infinity M200 reader (Tecan, Männedorf, Switzerland) and relative light units (RLU) were normalized to protein content of samples measured by BCA assay (Thermo Fisher Scientific, Waltham, MA, USA). The data are expressed as the fold change of the normalized RLU values/ protein of non-stimulated cells.

References

[1] Tencerova M, Figeac F, Ditzel N, Taipaleenmaki H, Nielsen TK, Kassem M (2018) High-Fat Diet-Induced Obesity Promotes Expansion of Bone Marrow Adipose Tissue and Impairs Skeletal Stem Cell Functions in Mice. J Bone Miner Res 33(6): 1154-1165. 10.1002/jbmr.3408

[2] Sistilli G, Kalendova V, Cajka T, et al. (2021) Krill Oil Supplementation Reduces Exacerbated Hepatic Steatosis Induced by Thermoneutral Housing in Mice with Diet-Induced Obesity. Nutrients 13(2). 10.3390/nu13020437

[3] Janovska P, Melenovsky V, Svobodova M, et al. (2020) Dysregulation of epicardial adipose tissue in cachexia due to heart failure: the role of natriuretic peptides and cardiolipin. J Cachexia Sarcopenia Muscle 11(6): 1614-1627. 10.1002/jcsm.12631

[4] Tsugawa H, Ikeda K, Takahashi M, et al. (2020) A lipidome atlas in MS-DIAL 4. Nat Biotechnol 38(10): 1159-1163. 10.1038/s41587-020-0531-2
[5] Tencerova M, Frost M, Figeac F, et al. (2019) Obesity-Associated Hypermetabolism and Accelerated Senescence of Bone Marrow Stromal Stem Cells Suggest a Potential Mechanism for Bone Fragility. Cell Rep 27(7): 2050-2062 e2056. 10.1016/j.celrep.2019.04.066

SUPPLEMENTAL TABLES

Table S1: List of mouse primers

Gene name	**Gene Sequence 5'-3'**
36B4 F	TCCAGGCTTTGGGCATCA
36B4 R	CTTTATCAGCTGCACATCACTCAGA
Fsp27 F	ATCAGAACAGCGCAAGAAGA
Fsp27 R	CAGCTTGTACAGGTCGAAGG
Cd36 F	ATGGGCTGTGATCGGAACTG
Cd36 R	TTTGCCACGTCATCTGGGTTT
Alp F	GCCCTCTCCAAGACATATA
Alp R	CCATGATCACGTCGATATCC
Bmp2 F	GGGACCCGCTGTCTTCTAGT
Bmp2 R	TCAACTCAAATTCGCTGAGGAC
Col1a1 F	GGTGAACAGGGGTTCCTGG
Col1a1 R	TTCGCACCAGGTTGCCATC
Adipoq F	GACGTTACTACAACTGAAGAGC
Adipoq R	CATTCTTTTCCTGATACTGGTC

Cebpa F	AAGCCAAGAAGTCGGTGGA
Cebpa R	CAGTTCACGGCTCAGCTGTTC
Il1β F	GCAACTGTTCCTGAACTCAACT
Il1β R	ATCTTTTGGGGTCCGTCAACT
Tnfα F	CCCTCACACTCAGATCATCTTCT
Tnfα R	GCTACGACGTGGGCTACAG
Mpc1 F	TCATTCAGGGAGGACGACTTATC
Mpc1 R	TGTTTTCCCTTCAGCACGACTAC
Mpc2 F	CTCCCACCCTGCTGCTGTCG
Mpc2 R	GGCCTGCCGGGTGGTTGTA
p53 F	TCTTATCCGGGTGGAAGGAAA
p53 R	GGCGAAAAGTCTGCCTGTCTT
p16 F	GGGTTTTCTTGGTGAAGTTCG
p16 R	TTGCCCATCATCATCACCT
Sod2 F	CAGACCTGCCTTACGACTATGG
Sod2 R	CTCGGTGGCGTTGAGATTGTT
Hmox1 F	AGGTACACATCCAAGCCGAGA
Hmox1 R	CATCACCAGCTTAAAGCCTTCT
Pparγ2 F	GGGTCAGCTCTTGTGAATGG
Pparγ2 R	CTGATGCACTGCCTATGAGC
Pdk4 F	GGCTTGCCAATTTCTCGTCTCTA

10

Pdk4 R	TTCGCCAGGTTCTTCGGTTCC
Pc F	CCCCTGGATAGCCTTAATACTCGT
Pc R	TGGCCCTTCACATCCTTCAAA
Oc F	TGCGCTCTGTCTCTCTGACC
Oc R	CTGTGACATCCATACTTGCAGG
p21 F	CCTGGTGATGTCCGACCTG
p21 R	CCATGAGCGCATCGCAATC
Trap F	CAGCTCCCTAGAAGATGGATTCAT
Trap R	GTCAGGAGTGGGAGCCATATG
Rankl F	AGCCGAGACTACGGCAAGTA
Rankl R	AAAGTACAGGAACAGAGCGATG
Opg F	CCTTGCCCTGACCACTCTTAT
Opg R	CACACACTCGGTTGTGGGT
Ctsk F	AGGCAGCTAAATGCAGAGGGTACA
Ctsk R	AGCTTGCATCGATGGACACAGAGA
RelA F	ACTGCCGGGATGGCTACTAT
RelA R	TCTGGATTCGCTGGCTAATGG
Irs1 F	TCTACACCCGAGACGAACACT
Irs1 R	TGGGCCTTTGCCCGATTATG
Irs2 F	CTGCGTCCTCTCCCAAAGTG
Irs2 R	GGGGTCATGGGCATGTAGC

Insr F	ATGGGCTTCGGGAGAGGAT
Insr R	CTTCGGGTCTGGTCTTGAACA
Slc1a5 F	CAGGCAGGCTGACACTGGAT
Slc1a5 R	TGGAGATGAAAGACGTCCGC
Slc2a4 /Glut4 F	CTCATGGGCCTAGCCAATGC
Slc2a4/ Glut4 R	CCCTGATGTTAGCCCTGAGTA
Gls F	AGGGTGAAGTCGGTGATAAAC
Gls R	GGGCTGTTCTGGAGTCATAAT
Gls2 F	CAACTTCAATGTGCCCTTCAG
Gls2 R	CTGCATATAGTGGAGATGTCTCG
Ctnnb1 F	CCCAGTCCTTCACGCAAGAG
Ctnnb1 R	CATCTAGCGTCTCAGGGAACA
Dlx5 F	CACCACCCGTCTCAGGAATC
Dlx5 F	GCTTTGCCATAAGAAGCAGAGG
Lrp5 F	CCGAGGGAGCCTTTCTACTC
Lrp5 R	CCCTGTCTTGCACGTCTTG
Msx2 F	CTAAAGGCGGTGACTTGTTTTCG
Msx2 R	CGGCTTCTTGTCGGACATGAG
Vegfa F	GTACCTCCACCATGCCAAGTG
Vegfa R	TGGGACTTCTGCTCTCCTTCTG
Vcam F	GGCTCCAGACATTTACCCAGTT

Vcam R	CATGAGCTGGTCACCCTTGAA
Fas F	CTGCACCCTGACCCAGAATAC
Fas R	ACAGCCAGGAGAATCGCAGTA
Fasgl F	CAGTCCACCCCCTGAAAAAAA
Fasgl R	CCTTGAGTTGGACTTGCCTGTT
Il10 F	CTGGACAACATACTGCTAACCG
Il10 R	GGGCATCACTTCTACCAGGTAA
Il1rn F	GCTCATTGCTGGGTACTTACAA
Il1rn R	CCAGACTTGGCACAAGACAGG

Table S2. List of human primers

Gene name	**Gene Sequence 5'-3'**
β-ACTIN F	ATTGGCAATGAGCGGTTCCG
β-ACTIN R	AGGGCAGTGATCTCCTTCTG
ALPL F	ACGTGGCTAAGAATGTCATC
ALPL R	CTGGTAGGCGATGTCCTTA
MPC 1 F	TCATGAGTACGCACTTCTGGGGC
MPC 1 R	GCCAGTTCCGAGGCTGTACCT
MPC 2 F	CTCTAGGCGGCGACCTCAGC
MPC 2 R	GGAAAAGGTCCCTCGGGCTGG
PPARG F	CTCCTATTGACCCAGAAAGCGA

PPARG R	TGCCATGAGGGAGTTGGAAG
CEBPA F	AACCTTGTGCCTTGGAAATG
CEBPA R	CTGTAGCCTCGGGAAGGAG
INSR F	TACTTGGCCACTATCGACTGG
INSR R	GCCGTGTGACTTACAGATGGT
IRS1 F	CCCAGGACCCGCATTCAAA
IRS1 R	GGCGGTAGATACCAATCAGGT
ADIPOQ F	GGGCCCCAGGCCGTGATGGCA
ADIPOQ R	TCGGGGACCTTCAGCCCCGGGTA
SLC1A5 F	TCATGTGGTACGCCCCTGT
SLC1A5 R	GCGGGCAAAGAGTAAACCCA
GLS F	AGGGTCTGTTACCTAGCTTGG
GLS R	ACGTTCGCAATCCTGTAGATTT
GSS F	GGGAGCCTCTTGCAGGATAAA
GSS R	GAATGGGGCATAGCTCACCAC

Table S3. List of primary and secondary antibodies used for western blot

Primary antibodies	**Company**	**Dilution**
Phospho-Akt Ser473_ Rabbit	Cell Signaling	1:1000
Phospho-Akt Thr308_Rabbit	Cell Signaling	1:1000
Total AKT_Rabbit	Cell Signaling	1:1000

β-actin_Rabbit	Cell Signaling	1:1000
Secondary HRP-conjugated antibodies		
Anti-rabbit IgG, HRP-linked Antibody	Cell Signaling	1:5000

Table S4. List of plasma and BM unique metabolites.

Plasma unique metabolites	**BM unique metabolites**
CE 16:0; [M+NH4]+	CAR 16:0-OH; [M]+
CE 18:1; [M+NH4]+	CAR 18:2 (2); [M+H]+
CE 18:3; [M+NH4]+	CL 72:7; CL 18:1_18:2_18:2_18:2; [M-H]-
CE 20:3; [M+NH4]+	CL 72:8; CL 18:2_18:2_18:2_18:2; [M-H]-
CE 20:5; [M+NH4]+	Cer 36:0;2O; Cer 18:0;2O/18:0; [M+CH3COO]-
CE 22:5; [M+NH4]+	Cer 42:2;2O (1); Cer 18:0;2O/24:2; [M+CH3COO]-
CE 22:6; [M+NH4]+	Cer 34:2;2O; Cer 18:2;2O/16:0; [M+CH3COO]-
FA 25:1; [M-H]-	Cer 36:2;2O; Cer 18:2;2O/18:0; [M+CH3COO]-
LPC 20:5/0:0 (1); [M+H]+	DG 32:1; DG 16:0_16:1; [M+NH4]+
LPC 22:5/0:0 (1); [M+H]+	DG 38:4 (2); DG 16:0_22:4; [M+NH4]+
LPC 22:5/0:0 (2); [M+H]+	DG 40:5; DG 18:1_22:4; [M+NH4]+
PC 39:6; [M+H]+	FA 21:2; [M-H]-
PC 39:7; [M+H]+	FA 24:3; [M-H]-
PC 42:6; [M+H]+	FA 26:2; [M-H]-
SM 42:5;2O; [M+CH3COO]-	FA 26:4; [M-H]-
TG 58:10 (2); TG 16:0_20:4_22:6; [M+NH4]+	FA 26:5; [M-H]-
TG O-58:1; TG O-20:0_18:0_20:1; [M+NH4]+	FA 26:6; [M-H]-
4-Hydroxyhippuric acid; [M-H]-	HexCer 36:1;2O; [M+CH3COO]-
4-Pyridoxic acid; [M-H]-	LPG 16:0; [M-H]-
Cholic acid; [M+NH4]+	LPG 18:1; [M-H]-
H-Pro-Hyp-OH; [M+H]+	LPI 18:1; [M-H]-
Suberylglycine; [M-H]-	LPS 18:0; [M-H]-

Taurocholic acid; [M+H]+	LPS 20:4; [M-H]-
	LPS 22:6; [M-H]-
	PE 32:0; PE 16:0_16:0; [M-H]-
	PE 32:1; PE 16:0_16:1; [M-H]-
	PE 38:3 (2); PE 18:0_20:3; [M-H]-
	PE 40:7 (1); PE 18:2_22:5; [M-H]-
	PE 40:9; PE 18:3_22:6; [M-H]-
	PE 42:9; PE 20:3_22:6; [M-H]-
	PE 42:10; PE 20:4_22:6; [M-H]-
	PE 44:10; PE 22:4_22:6; [M-H]-
	PE O-32:0; PE O-16:0_16:0; [M-H]-
	PE O-36:6; PE O-16:1_20:5; [M-H]-
	PE O-40:7 (1); PE O-20:3_20:4; [M-H]-
	PE O-40:7 (2); PE O-18:2_22:5; [M-H]-
	PE O-42:9; PE O-20:3_22:6; [M-H]-
	PE 44:8;2O; PE 22:5_22:3;2O; [M-H]-
	PE 44:10;2O; PE 22:6_22:4;2O; [M-H]-
	PEtOH 34:1; PEtOH 16:0_18:1; [M-H]-
	PEtOH 38:6; PEtOH 16:0_22:6; [M-H]-
	PEtOH 40:6; PEtOH 18:0_22:6; [M-H]-
	PG 36:1; PG 18:0_18:1; [M-H]-
	PG 36:4 (2); PG 18:2_18:2; [M-H]-
	PG 36:4 (3); PG 16:0_20:4; [M-H]-
	PG 38:4; PG 18:0_20:4; [M-H]-
	PG 38:5 (1); PG 18:1_20:4; [M-H]-
	PG 38:5 (2); PG 18:1_20:4; [M-H]-
	PG 38:6 (2); PG 16:0_22:6; [M-H]-
	PG 40:6; PG 18:1_22:5; [M-H]-
	PG 40:7; PG 18:1_22:6; [M-H]-
	PG 40:8; PG 18:2_22:6; [M-H]-
	PG 42:10; PG 20:4_22:6; [M-H]-
	PG 44:11; PG 22:5_22:6; [M-H]-
	PG 44:12; PG 22:6_22:6; [M-H]-

	PI 40:5 (2); PI 18:0_22:5; [M-H]-
	PI O-38:6; PI O-16:0_22:6; [M-H]-
	PS 34:1; PS 16:0_18:1; [M-H]-
	PS 36:1; PS 18:0_18:1; [M-H]-
	PS 36:2; PS 18:0_18:2; [M-H]-
	PS 36:3; PS 18:1_18:2; [M-H]-
	PS 36:4; PS 16:0_20:4; [M-H]-
	PS 38:3; PS 18:0_20:3; [M-H]-
	PS 38:5; PS 18:1_20:4; [M-H]-
	PS 38:6; PS 16:0_22:6; [M-H]-
	PS 40:5 (2); PS 18:0_22:5; [M-H]-
	PS 40:8; PS 20:4_20:4; [M-H]-
	SM 42:0;2O; [M+CH3COO]-
	SM 44:2;2O; [M+CH3COO]-
	TG 50:7; TG 12:0_18:2_20:5; [M+NH4]+
	TG 57:7; TG 18:1_18:1_21:5; [M+NH4]+
	TG 60:12 (2); TG 16:0_22:6_22:6; [M+NH4]+
	TG O-56:7; TG O-16:0_18:1_22:6; [M+NH4]+
	12-HETE; [M-H]-
	12-HHTrE; [M-H]-
	5-trans-Prostaglandin D2; [M-H]-
	6-trans-12-epi-Leukotriene B4; [M-H]-
	Ala-Lys; [M+H]+
	Arg-Ala; [M+H]+
	Arg-Val; [M+H]+
	Asp-Leu; [M-H]-
	Cytidine 3'-monophosphate; [M-H]-
	Cytidine 5'-diphosphocholine; [M+H]+
	Gly-Gln; [M+H]+
	Gly-His; [M+H]+
	Guanosine 5'-monophosphate; [M-H]-
	Guanosine; [M+H]+
	His-Ala; [M+H]+

	His-Asn; [M+H]+
	His-Gln; [M+H]+
	His-Gly; [M+H]+
	His-Leu; [M+H]+
	His-Ser; [M+H]+
	His-Thr; [M+H]+
	His-Tyr; [M+H]+
	His-Val; [M+H]+
	Leu-Ala; [M-H]-
	Lys-Ile; [M+H]+
	Lys-Phe; [M+H]+
	Phe-Gly; [M-H]-
	Prostaglandin F2-beta-; [M-H]-
	Ribose 1-phosphate; [M-H]-
	Thr-Lys; [M+H]+
	Thr-Tyr; [M-H]-
	Uridine 5'-diphosphoacetylglucosamine; [M+H]+
	Val-Arg; [M+H]+
	Val-Gly; [M-H]-
	Val-Leu; [M-H]-
	Val-Val; [M-H]-
	Xanthine; [M+H]+

Fig. S1

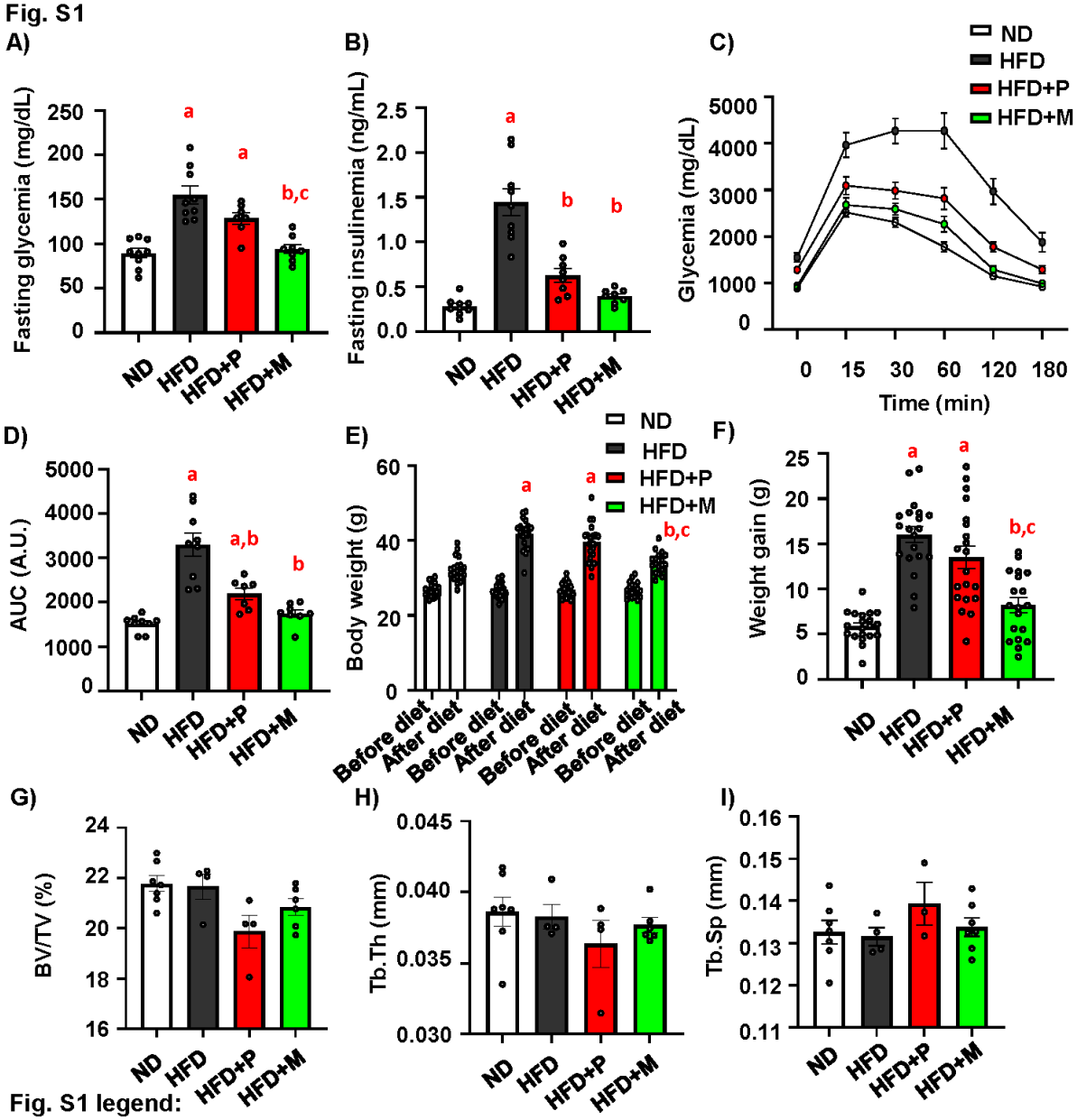

Fig. S1 legend:
(**A-F**) MSDC-0602K improves metabolic phenotype in HFD-fed mice. (**A**) Glycemia and (**B**) insulinemia after overnight fasting at the end of dietary intervention in treated mice (n= 7-9). (**C**) Measurement of intraperitoneal glucose tolerance test (GTT) in treated mice at the end of dietary intervention after overnight fasting; (**D**) Area under the curve of coresponding GTT graphs (n= 7-9). (**E**) Body weight before and after two months of dietary intervention (n= 19-20 per group), (**F**) Weight gain after 2 months of dietary intervention in mice fed with ND, HFD and HFD supplemented with pioglitazone and MSDC-0602K (n= 19-20 per group). (**G-I**) Evaluation of trabecular parameters in L5 vertebra. (G) trabecular volume per total volume (BV/TV), (**H**) trabecular thickness (Tb.Th), (**I**) trabecular separation (Tb.Sep.); Data are presented as mean ± SEM (n = 7-8 per group); one-way ANOVA, Tukey's multiple comparison test, a: ND vs other groups; b: HFD vs other groups, c: HFD+P vs other groups, d: HFD+M vs other groups.

Fig. S2

A)

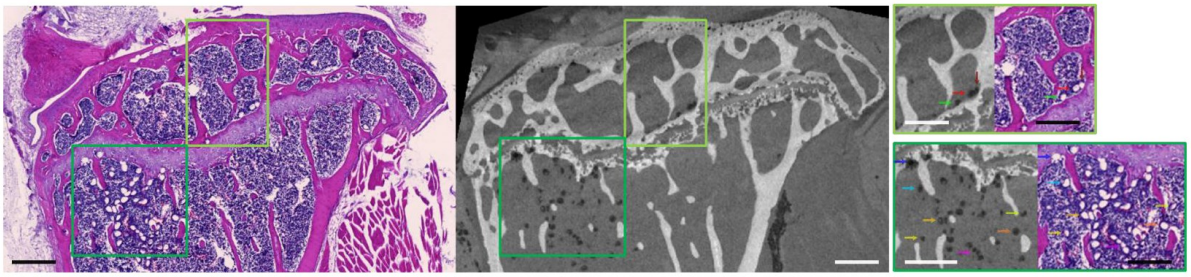

B)

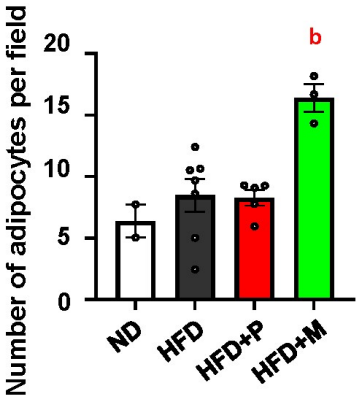

Fig. S2 legend:
(**A**) Registration of a H&E-stained section and a CECT image from the same tibia for BMAT evaluation (scale bar 250 µm); (**B**) Histological evaluation of BMAd number expressed as adipocyte number per section. Data are presented as mean ± SEM (n = 3-8 per group); one-way ANOVA, Tukey's multiple comparison test, a: ND vs other groups; b: HFD vs other groups, c: HFD+P vs other groups, d: HFD+M vs other groups.

Fig. S3

A) plasma

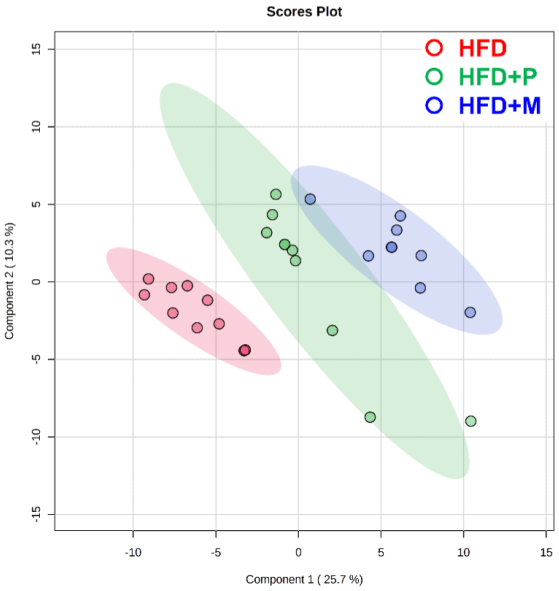

B) BM

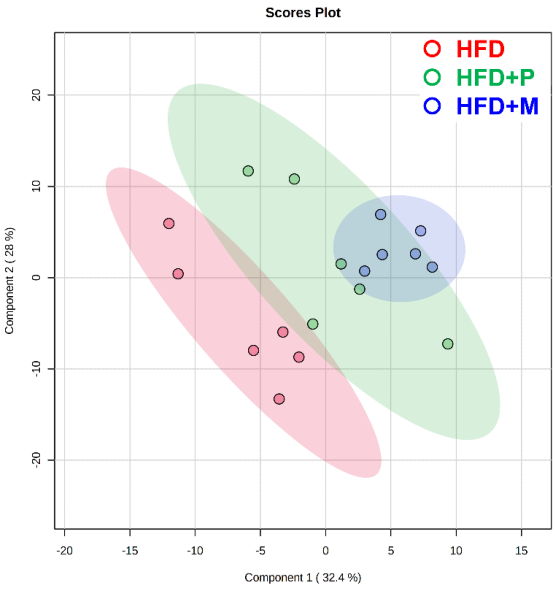

Fig. S3

C) PLASMA

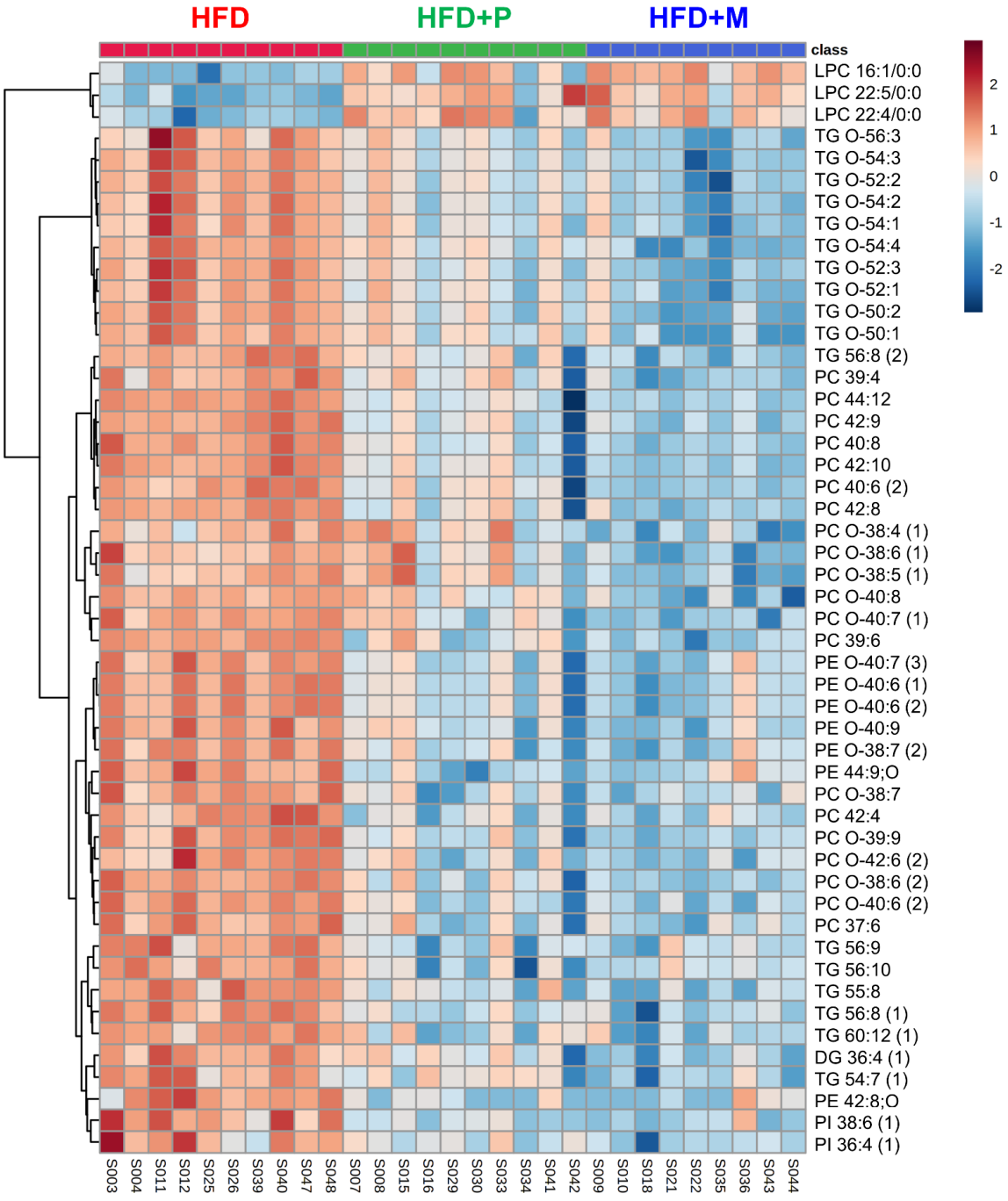

Fig. S3

D) BM

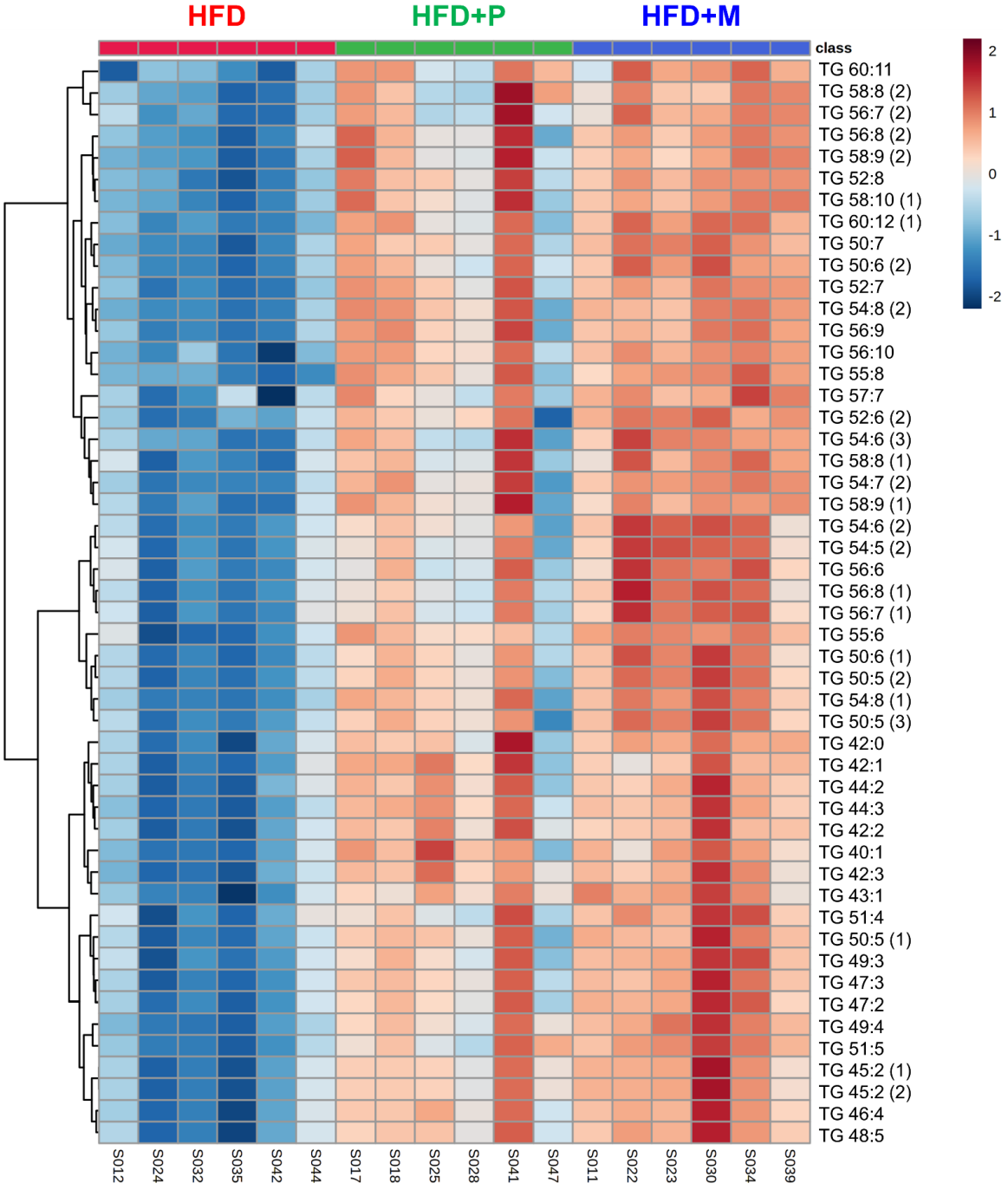
HFD
HFD+P
HFD+M
class
TG 60:11
TG 58:8 (2)
TG 56:7 (2)
TG 56:8 (2)
TG 58:9 (2)
TG 52:8
TG 58:10 (1)
TG 60:12 (1)
TG 50:7
TG 50:6 (2)
TG 52:7
TG 54:8 (2)
TG 56:9
TG 56:10
TG 55:8
TG 57:7
TG 52:6 (2)
TG 54:6 (3)
TG 58:8 (1)
TG 54:7 (2)
TG 58:9 (1)
TG 54:6 (2)
TG 54:5 (2)
TG 56:6
TG 56:8 (1)
TG 56:7 (1)
TG 55:6
TG 50:6 (1)
TG 50:5 (2)
TG 54:8 (1)
TG 50:5 (3)
TG 42:0
TG 42:1
TG 44:2
TG 44:3
TG 42:2
TG 40:1
TG 42:3
TG 43:1
TG 51:4
TG 50:5 (1)
TG 49:3
TG 47:3
TG 47:2
TG 49:4
TG 51:5
TG 45:2 (1)
TG 45:2 (2)
TG 46:4
TG 48:5
S012
S024
S032
S035
S042
S044
S017
S018
S025
S028
S041
S047
S011
S022
S023
S030
S034
S039
2
1
0
-1
-2

Fig. S3

E) PLASMA

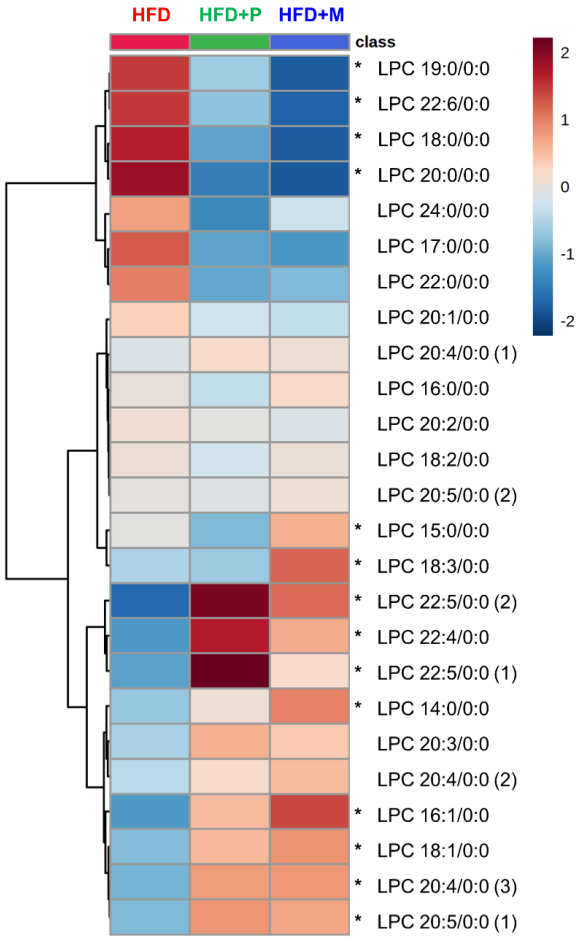

Fig. S3 legend:
(**A)** PLS-DA score plot for plasma samples; (**B**) PLS-DA score plot for BM samples; (**C**) Heatmap of top-50 individual lipid species in plasma based on ANOVA with p(FDR)<0.05, (n = 9-10 per group). (**D**) Heatmap of top-50 individual lipid species in BM based on ANOVA with p(FDR)<0.05 (n = 6 per group). **(E)** Heatmap of LPC species detected in plasma. LPC species statistically altered are marked by an asterisk (*) based on ANOVA with p(FDR)<0.05.

Fig. S4

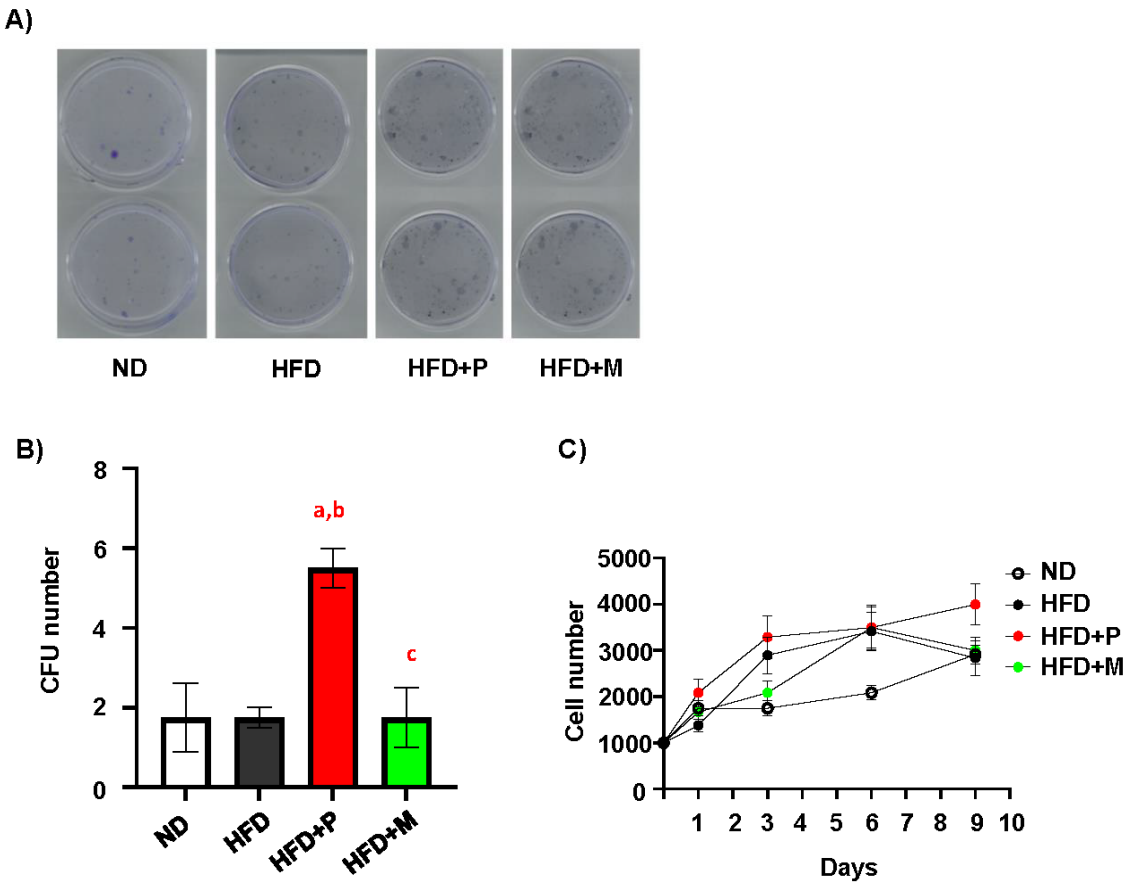

Fig. S4 legend:
(**A**) Representative pictures and (**B**) calculation of colony forming unit (CFU) analysis of mBM-MSCs isolated from treated mice, seeded directly after cell isolation and cultivated 14 days in growth media. Data are presented as mean ± SEM (n = 2-4 per group), Tukey's multiple comparison test, a: ND vs other groups, b: HFD vs other groups, c: HFD+P vs other groups. (**C**) Short-term proliferation assay of primary mBM-MSCs calculated after 1, 3, 6 and 9 days in culture after seeding (n = 3 per group).

Fig. S5

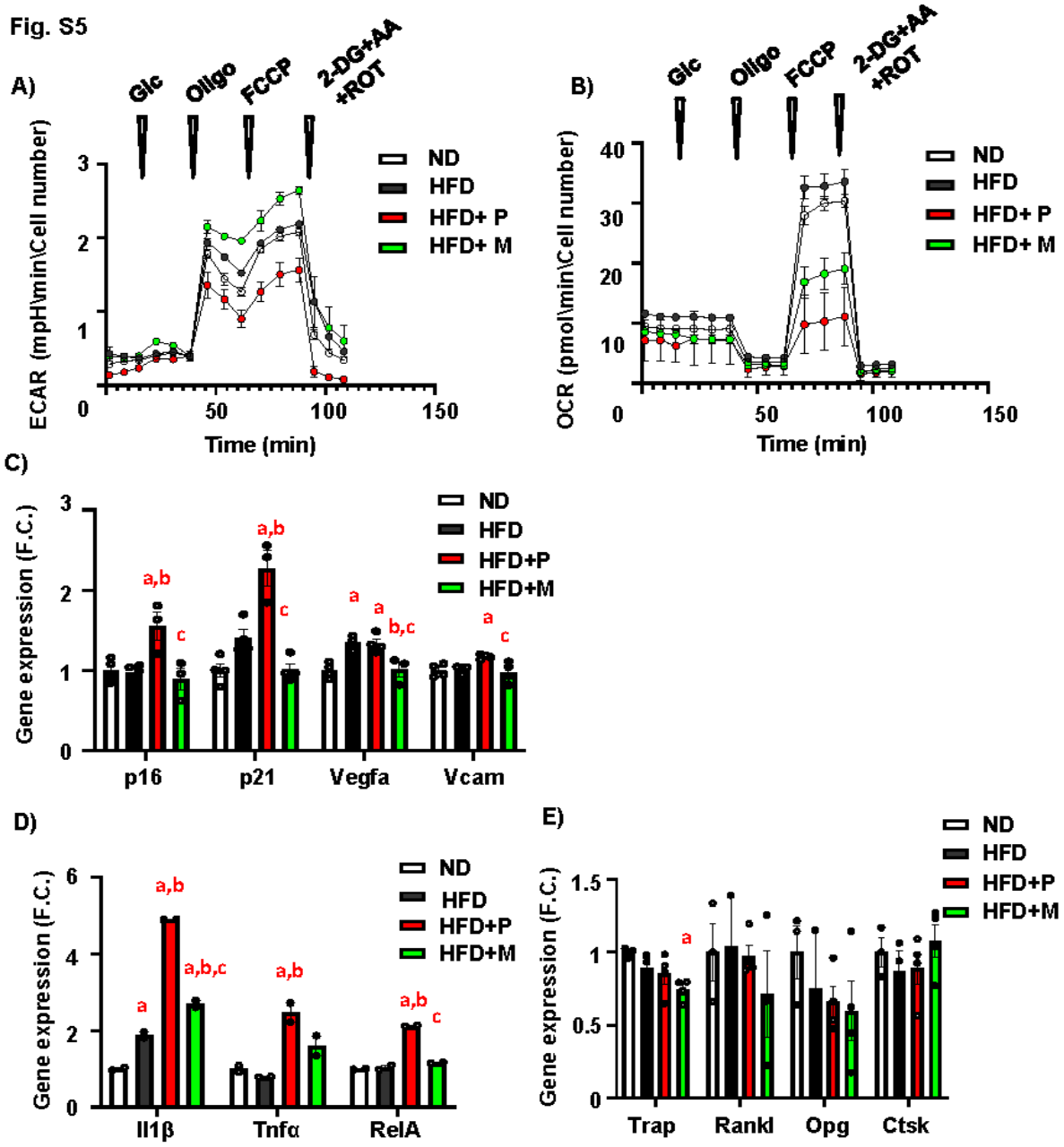

Fig. S5 legend:

A) Measurement of extracellular acidification rate (ECAR) and (**B**) oxygen consumption rate (OCR) of primary mBM-MSCs from mice treated with different dietary interventions (n = 2 independent experiments with five replicates per group). (**C**) Gene expression of senescence genes (*p16*, *p21*, *Vegfa*, *Vcam*); (**D**) Gene expression of inflammatory genes (*Il1β*, *Tnfa*, *RelA*) and (**E**) bone resorption genes (*Trap*, *Rankl*, *Opg*, *Ctsk*) in primary mHSCs obtained from treated mice. Data are presented as mean ± SEM (n = 2-4 per group); one-way ANOVA, Tukey's multiple comparison test, a: ND vs other groups; b: HFD vs other groups, c: HFD+P vs other groups, d: HFD+M vs other groups.

Fig. S6

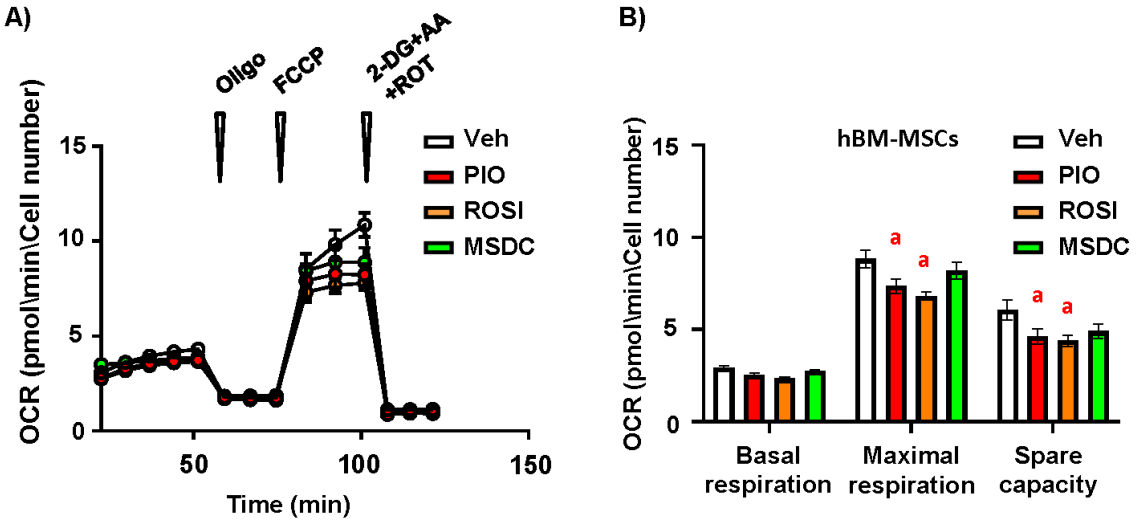

Fig. S6 legend:

(**A**) Changes in oxygen consumption rate (OCR) of hBM-MSCs in response to acute treatment with 10 µM PIO, ROSI and MSDC and vehicle (DMSO) as a control and (**B**) corresponding calculations of basal respiration, maximal respiration and spare capacity (n= 2 independent experiments with five replicates per condition). Data are presented as mean ± SEM from two independent experiments. one-way ANOVA, Tukey's multiple comparison test, a: Vehicle vs other groups;

Fig. S7

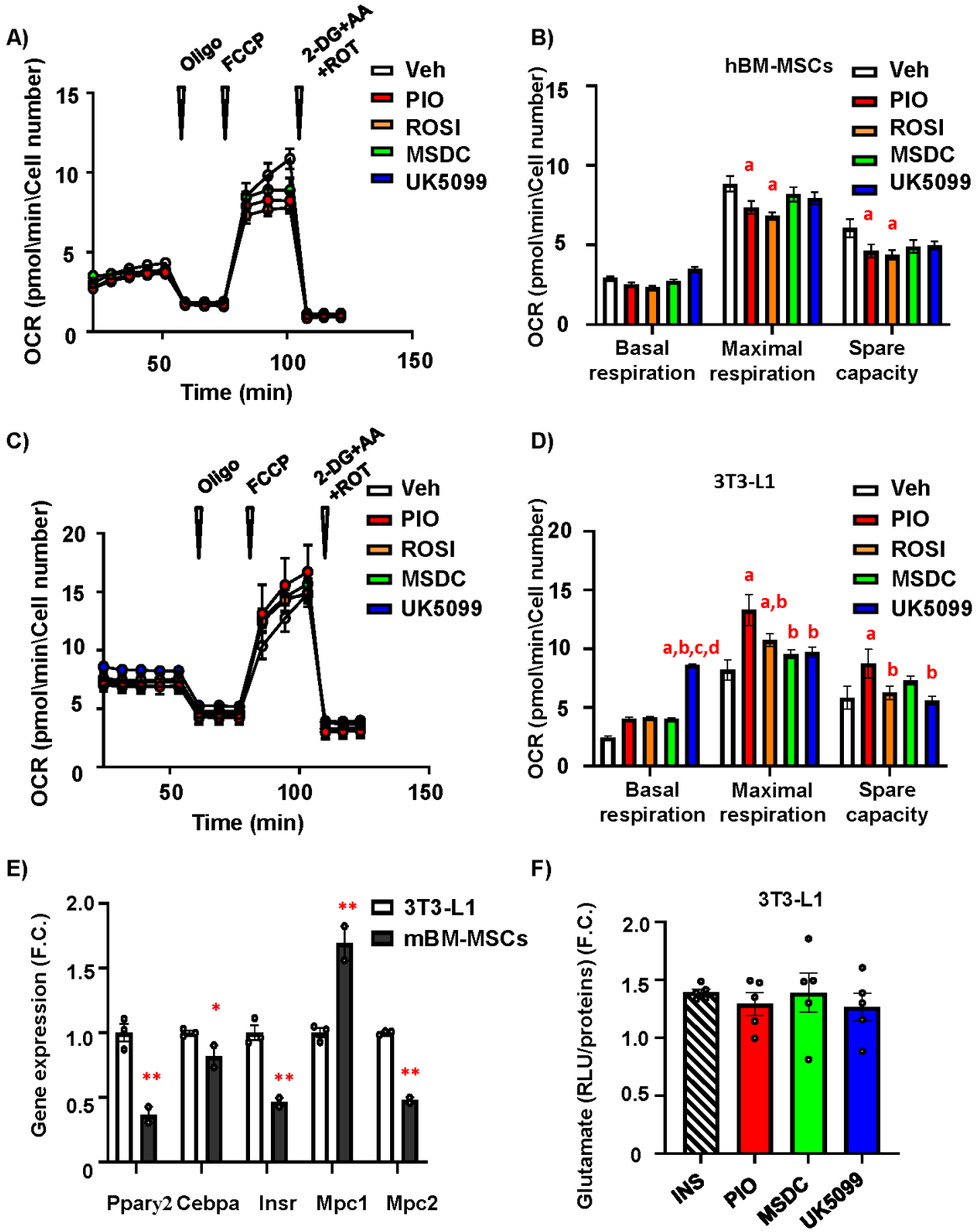
A)
Oligo
FCCP
2-DG+AA +ROT
Veh
PIO
ROSI
MSDC
UK5099
OCR (pmol\min\Cell number)
Time (min)
B)
hBM-MSCs
Basal respiration
Maximal respiration
Spare capacity
C)
D)
3T3-L1
E)
3T3-L1
mBM-MSCs
Gene expression (F.C.)
Ppary2
Cebpa
Insr
Mpc1
Mpc2
F)
Glutamate (RLU/proteins) (F.C.)
INS
PIO
MSDC
UK5099

Fig. S7 legend:
(**A-D**) hBM-MSCs and 3T3-L1 cells were acutely treated with 10 µM concentration of ROSI, PIO and MSDC-0602K, and MPC inhibitor UK5099. The effect on their mitochondrial respiration was measured by Seahorse. (**A**) Oxygen consumption rate (OCR) measured in hBM-MSCs and (**B**) corresponding calculations of basal respiration, maximal respiration and spare capacity. (**C**) OCR measured in 3T3-L1 and (**D**) corresponding calculations of basal respiration, maximal respiration and spare capacity. Data are presented as mean ± SEM from two independent measurements with five replicates per condition, a: Veh vs other groups, b: PIO vs other groups, c: ROSI vs other groups; (**E**) Gene expression of adipogenic and metabolic genes (*Pparγ2*, *Cebpa*, *Insr*, *Mpc1*, *Mpc2*) in 3T3-L1 and mBM-MSCs. Data are presented as mean ± SEM (n = 2-3 per group); t-test, 3T3-L1 vs mBM-MSC; *$p < 0.05$, **$p < 0.01$: 3T3-L1 vs mBM-MSCs. (**F**) Measurement of intracellular glutamate in 3T3-L1 cells after 3 hours incubation with 1 µM INS, 30 µM PIO/MSDC. Data are presented as the fold change of normalized RLU value/protein of stimulated cells over non-stimulated cells. Data are presented as mean ± SEM (n = 5 per group);